Regulation of Stem Cell Identity and Function in Moss

A Thesis

Presented to the Faculty of the Graduate School

of Cornell University

In Partial Fulfillment of the Requirements for the Degree of

Doctor of Philosophy

By

Joseph Thomas Cammarata

May 2021

Regulation of Stem Cell Identity and Function in Moss

Joseph Thomas Cammarata, Ph.D.
Cornell University 2021

All plants grow from stem cells or a collection of stem cells organized at meristems. The activity and function of these meristems determine plant morphology. In shoots, development at the Shoot Apical Meristem (SAM) determines the rate and position of lateral organ formation, the transition from vegetative to reproductive growth, and the overall branching architecture. SAMs accomplish these functions while maintaining themselves and simultaneously producing cells incorporated into lateral organs.

Decades of research in the model plant *Arabidopsis thaliana* has revealed numerous mechanisms at play regulating meristem function. A negative feedback loop between the indeterminacy promoting transcription factor WUSCHEL (WUS), the secreted peptide CLAVATA3 (CLV3), and a series of LEUCINE-RICH REPEAT RECEPTOR-LIKE KINASEs (LRR-RLKs) that inhibit WUS comprises the canonical network governing SAM maintenance. *WUS* is induced by the phytohormone cytokinin, which is in turn regulated by crosstalk from another phytohormone: auxin. Altogether, a complex regulatory network composed of *WUS*, *CLV3*, LRR-RLKs, cytokinin, and auxin regulates the function of the SAM.

Our understanding of SAM function is limited outside of Arabidopsis and a few crops. However, even anatomically and evolutionarily disparate SAMs must perform the same functions as those in angiosperms. For example, whereas diploid flowering plant SAMs are multicellular structures organized into distinct clonal layers and different functional domains, the haploid shoot of the moss *Physcomitrium patens* is derived from a single tetrahedral apical cell. This apical cell nonetheless produces leaves (phyllids) in a spiral phyllotactic pattern while maintaining itself until it establishes the site of reproductive organ formation. In my dissertation

work, I sought to elucidate whether the mechanisms regulating the function of this single celled meristem parallel those in the flowering plant SAM.

I took a reverse-genetics approach and assessed the function of moss *LRR-RLK* genes *CLAVATA1a* (*CLV1a*), *CLV1b*, and *RECEPTOR-LIKE PROTEIN KINASE2* (*RPK2*), which are orthologs of *LRR-RLKs* that inhibit *WUS* in Arabidopsis. I found that these *LRR-RLK* genes performed the same developmental function in moss as in flowering plants, namely the inhibition of stem cell specification. Fascinatingly, published data suggest that *WUSCHEL-RELATED HOMEOBOX* (*WOX*) genes do not function in regulation of the moss SAM, leading me to ask how *CLV1* and *RPK2* function in moss if not by inhibiting *WUS*.

In both moss and flowering plants, cytokinin promotes SAM specification and function while CLV1 and RPK2 inhibit them. Given the absence of a *WOX* gene from moss stem cell regulation I tested whether there is crosstalk between cytokinin and CLV1/RPK2. Using a combination of genetics, hormone treatments, and mathematical modeling, I provide support for a model where CLV1 acts upstream of cytokinin-mediated SAM specification while RPK2 acts in a distinct pathway. Next, by combinatorically increasing and decreasing auxin and cytokinin signaling, I show that the ratio of auxin to cytokinin signaling also governs moss shoot morphogenesis.

Overall, this work supports the conclusion that similar mechanisms support SAM function in mosses and flowering plants, despite the independent evolution of these shoots over four hundred million years ago. To support future evolutionary and developmental work on this topic, my final contribution is a phylogenetic analysis and functional summary of stem cell-regulating LRR-RLKs. In total, I hope that this work contributes to a general understanding of the developmental mechanisms at play across the land plant tree of life.

Biographical Sketch

Joe Cammarata was born and raised in Queens, New York. He attended the Macaulay Honors College at Hunter College for his bachelor's education. During his freshman year, Joe began conducting scientific research in the laboratory of Dr. Diana Bratu. There, he studied the mechanisms required for RNA transport and silencing during *Drosophila* oogenesis. As there were no plant biologists or plant biology courses at Hunter College, Joe was first exposed to the field of plant development when he was selected for the Undergraduate Research Program at Cold Spring Harbor Laboratory. There he worked in the laboratory of Dr. Zachary Lippman, who taught him to see the ubiquitous modular patterns that give rise to plant morphologies. After finishing his undergraduate studies with several awards including a Goldwater Scholarship and being selected Valedictorian of his graduating class, Joe wanted to pursue his newfound fascination with the evolution of plant forms. To do so, he completed a Master of Philosophy (MPhil) degree at the University of Cambridge, where he completed his dissertation research on the role of *RECEPTOR-LIKE PROTEIN KINASE 2* (*RPK2*) in moss development. After returning to the United States and a brief time as a volunteer at the New York Botanic Garden, Joe began his graduate studies at Cornell University under the mentorship of Dr. Michael Scanlon and Dr. Adrienne Roeder. There, Joe's research has focused on the regulation of moss shoot stem cell identity and function by genetic and physical mechanisms.

Dedicated

To Anthony, Elizabeth, Marc, and Ryan

for their lifelong love and support

To Celine

Without whom life would be no fun at all

Acknowledgements

I would like to first and foremost acknowledge Mike Scanlon and Adrienne Roeder. Their combined enthusiasm and expertise helped me from the first. I also want to thank them for mostly letting me do whatever I wanted, but also knowing when to stop me.

To Fay-Wei Li, thank you for sharing your infectious enthusiasm, your wealth of knowledge, and your generosity.

I want to thank all the members, current and past, of the Scanlon and Roeder labs. I was constantly astounded by the patience and work ethic of my lab mates, whom I tried to emulate in these respects but probably failed.

To my collaborators and friends: especially Chris Whitewoods, Yoan Coudert, Richard Smith, and my former advisor Jill Harrison. Thank you for helping me grow as a scientist.

I would like to thank all of the undergraduate students I had the pleasure of teaching. They inspired me, energized me, and constantly forced me to understand Biology in new ways.

I would also like to acknowledge the pivotal role that the FASEB Mechanisms in Plant Development meetings played in shaping my time as a graduate student. At these meetings, I felt I became part of a global community of experts, most of whom were astoundingly welcoming to a young graduate student. These conferences were the highlights of my PhD, even if I sometimes made a fool of myself.

Lastly, I would like to acknowledge the various sources of funding that have allowed me to conduct my research for these past years, including the grants NSF IOS-1238142 to M.J.S. and NSF IOS-1553030 to A.H.K.R., the Schmittau-Novak Small (SNIPS) Grant, the Cornell Provost Diversity Dissertation Completion Fellowship, funding from the Weill Institute for Cell and Molecular Biology, and TAships supported by Plant Biology and Biology.

Contents

Chapter 1: Cytokinin and CLE signaling are highly intertwined developmental regulators across tissues and species.

Foreword

This chapter presents the final version of the review article I wrote for Current Opinion in Plant Biology, published in October 2019.

This review stemmed from my interest in crosstalk between CLE and cytokinin signaling, and the knowledge I gained by writing it served as the basis for my experiments in Chapter 3.

The article in its published form can be found at: https://doi.org/10.1016/j.pbi.2019.05.006

Cammarata, J., Roeder, A.H., and Scanlon, M.J. (2019). Cytokinin and CLE signaling are highly intertwined developmental regulators across tissues and species. Curr. Opin. Plant Biol. *51*, 96–104.

Cytokinin and CLE signaling are highly intertwined developmental regulators across tissues and species.

Joseph Cammarata[1,2], Adrienne H.K. Roeder[1,2], Michael J. Scanlon[1]

Affiliations

1. Cornell University School of Integrative Plant Sciences, Section of Plant Biology
2. Weill Institute for Cell and Molecular Biology

Highlights

- CLE peptide ligands and the hormone cytokinin comprise potent, interactive regulators of plant development.
- Comparative analyses support a model for the evolution of conserved, developmental interactions of CLE and cytokinin signaling across wide, phylogenetic distance.
- CLE and cytokinin signaling confer antagonistic developmental functions in shoot development but act synergistically during root development.

Abstract

The control of cell identity and differentiation is critical for proper development. In plants, cell identity is largely determined by a cell's spatial context, which is communicated in the form of varying abundances of hormones. Two classes of hormones: the classical phytohormone cytokinin and the small CLE peptide hormones, are potent regulators of cell division and cell differentiation. While a relationship between these two classes of hormones is well-established at developing shoot tips, recent evidence suggests that CLE and cytokinin signaling converge on the same developmental processes across many different contexts and in widely divergent species. Here we review evidence predominately from *Arabidopsis thaliana* and the moss *Physcomitrella patens* that supports a general model where CLE and cytokinin signaling are highly intertwined developmental regulators with antagonistic functions in shoots and synergistic functions in roots.

Main Text

Plants have the ability to maintain indeterminate postembryonic growth, by reserving pools of slowly dividing stem cells at key developmental and organogenic regions such as the shoot apical meristem (SAM) at the tip of the shoot; the procambium in the primary vasculature; and the root apical meristem (RAM) at the root tip. Additionally, development of specialized cell types or organs often involves transient meristematic cells, such as the meristemoid during stomatagenesis. Function of these meristems requires a strict balance between stem cell identity and cell differentiation.

Many pathways regulating plant stem cell identity have been discovered across diverse organs and species. Recent data suggest that two such pathways, one consisting of CLAVATA3/EMBRYO SURROUNDING REGION (CLE) peptide ligands and their membrane bound kinase receptors, and the other comprising the signaling pathway of the phytohormone cytokinin, converge on regulating common developmental processes across land plants (Figure 1). Specifically, evidence suggests that CLEs and cytokinin act antagonistically in shoots and cooperatively in roots. While cytokinin and CLE signaling during plant development have been reviewed recently[•1–•4]; this review will focus on recent evidence of functional overlaps between these two pathways.

A brief overview of cytokinin and CLE signaling

The phytohormone cytokinin signals through a two-component phosphor-relay similar to bacterial signaling systems[5]. The Arabidopsis cytokinin receptors are encoded by the *ARABIDOPSIS HISTIDINE KINASE* (*AHK*) genes, and similar histidine kinases have been shown to perceive and relay cytokinin signaling in other species[6–8]. The histidine kinases phosphorylate ARABIDOPSIS HISTIDINE PHOSPHOTRANSFER

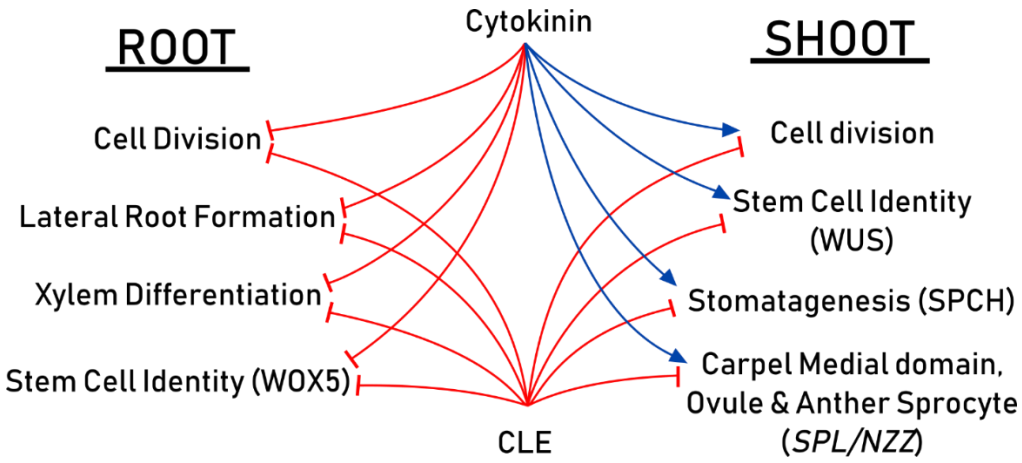

Figure 1. CLE and cytokinin signaling are antagonistic in the shoot, but cooperative in the root. Schematic outlining convergence of CLE and cytokinin signaling in *Arabidopsis.* Where possible, known transcriptional hubs that these signaling pathways center around are included. Red lines indicate inhibition; blue arrows induction.

(AHP) proteins, which relay the phosphate onto the class B ARABIDOPSIS RESPONSE REGULATOR (B-ARR) transcription factors that activate the downstream genetic response[9–12]. One set of genes activated by B-ARRs are the class *A ARABIDOPSIS RESPONSE REGULATORs* (*A-ARRs*), which resemble *B-ARR*s except that the encoded proteins lack DNA binding domains[13]. These A-ARRs are inhibitors of B-ARRs; thus, cytokinin signaling includes a negative feedback loop. Other inhibitors of cytokinin signaling include the pseudo-histidine phosphotransfer protein, AHP6[14]. Crosstalk between cytokinin and other developmental regulators such as auxin can influence cytokinin signaling independently of cytokinin concentration, e.g. by inhibiting *A-ARR* expression[15–18].

CLEs are small peptide hormones that are produced in many developing and mature contexts[19]. CLEs can act non-cell autonomously, and influence cell division and differentiation. The mechanisms of CLE perception are poorly understood, but broadly, CLEs signal through transmembrane LEUCINE RICH-REPEAT RECEPTOR-LIKE KINASEs (LRR/RLKs). Plants contain large *LRR/RLK* gene families with genes from diverse evolutionary clades implicated in CLE signaling, making elucidation of CLE-receptor relationships difficult[20]. While downstream CLE signaling is even less well understood, a number of cell signaling intermediates including MITOGEN-ACTIVATED PROTEIN KINASEs (MAPKs) and

heterotrimeric G-proteins have been implicated[21,22]. Overlaps and general trends in CLE signaling responses through different receptors have been difficult to identify. Indeed, recent evidence suggests that a given CLE receptor can transmit different intracellular signals depending on the CLE ligand[•22]. Adding another layer of complexity, many LRR/RLKs such as BARELY ANY MERISTEM (BAM) are implicated both in development and immunity[24]. This review does not consider TRACHEARY ELEMENT DIFFERENTIATION INHIBITORY FACTOR (TDIF)-like CLEs, which elicit a different set of responses from CLV3-like peptides[25,26].

CLEs antagonize Cytokinin in the SAM to suppress stem cell identity.

Primary shoot growth occurs at the SAM, a dome-shaped structure that balances the maintenance of an undifferentiated pool of stem cells with the patterning and allocation of those cells for lateral organ production. Cytokinin promotes SAM formation and identity[27], and the expression of the homeobox transcription factor-encoding gene *WUSCHEL. WUS* is expressed early during SAM formation and is necessary for SAM maintenance[28,29]. Cytokinin directly promotes *WUS* expression in the organizing center in the middle of the SAM, and WUS specifies stem cell identity in the cell layers of the central zone above the organizing center[30,31]. WUS also stabilizes cytokinin response by inhibiting the expression of *A-ARRs*, thus replacing the cytokinin negative feedback loop with a positive feedback loop[18]. Cytokinin signaling, *WUS* expression, and the stem cell population do not expand unchecked however, as WUS establishes a new negative feedback loop by inducing the production of the CLE peptide CLV3 in the central zone[32,33]. Secreted CLV3 signals via a series of LRR-RLKs including CLAVATA1 (CLV1)[34], BAM[35], CLAVATA2 (CLV2)[36], CORYNE (CRN)[37], and RECEPTOR-LIKE PROTEIN KINASE 2/TOADSTOOL 2 (RPK2/TOAD2)[38,39] to repress *WUS*[40,41]. Altogether, CLE and cytokinin antagonism establish a bi-stable state where above a certain threshold concentration of cytokinin, *WUS* expression and downstream cytokinin signaling are maintained. Below that threshold concentration, CLE signaling inhibits *WUS* and stem cell identity is lost (Figure 2B)[42]. This exquisite regulation of stem cell identity to maintain a meristem with a consistent size is conserved in diverse angiosperms[2,43].

CLEs inhibit cytokinin-induced stomatagenesis

During stomatal development, a transient stem cell called the meristemoid forms from the protoderm and divides asymmetrically, giving rise to another meristemoid and a stomatal lineage ground cell (SLGC). Entry into the stomatal lineage and meristemoid identity is promoted by the bHLH transcription factor SPEECHLESS (SPCH)[44,45]. The total number of stomata formed on a leaf is tightly regulated, and recently, roles for CLEs and cytokinin were discovered in regulating stomatal number[44••,45••]. As in the SAM, CLEs and cytokinin have antagonistic functions, here converging on expression of *SPCH* (Figure 2C).

Cytokinin induces the expression of *SPCH*, thus increasing the number of meristemoids formed[44••]**.** While SPCH is inherited by both daughter cells after asymmetric cell division of the meristemoid, it is usually rapidly degraded in the SLGC. To inhibit persistence of SPCH in the SLGC daughter, SPCH in the meristemoid daughter promotes the expression of CLE10. CLE10 signals through the LRR/RLK HEASA-LIKE1 (HSL1) to ensure degradation of SPCH in the SLGC, thus reducing the likelihood that another meristemoid will be formed by that SLGC. Inhibition of SPCH by HSL1 requires intact residues on SPCH associated with MAPK-dependent phosphorylation and degradation[45••]. Unexpectedly, other mutations affecting MAPK regulation of SPCH produce clustered stomata[48], whereas *cle9/10* and *hsl1* mutants do not, suggesting a more nuanced inhibition of SPCH by HSL1 that might include MAPK. Interestingly, time appears to be an essential factor in this feedback loop; continued division of the SLGC depends on the speed of SPCH turnover. As in the SAM, CLEs function downstream of cytokinin signaling as part of a negative feedback loop to repress cytokinin effects during stomatagenesis.

Pieces of a puzzle: CLE and cytokinin signaling oppose each other during reproductive development

During early carpel development, internal tissues are produced by a meristematic medial domain. While cytokinin promotes meristematic activity in the medial domain at least in part by inducing expression of *SPOROCYTELESS/NOZZLE* (*SPL/NZL*), CLE pathway loss of function mutants including *clv1*, *clv2*, and *rpk2* exhibit enhanced meristematic activity, indicating a role for CLEs inhibiting medial domain growth[49].

This interaction between CLEs, cytokinin, and *SPL/NZZ* might be indirect and mediated by *WUS*, which also functions in the medial domain[50–53].

While both CLE and cytokinin signaling are demonstrated regulators of early carpel development, thus far only a role for cytokinin has been identified in the developing ovule (Figure 2D). Exogenous cytokinin treatment during ovule development induces ectopic *SPL/NZZ* expression. This response requires intact cytokinin receptors[51]. As in the medial domain during early carpel development, *WUSCHEL* is also expressed in and required for ovule development[50]. Additionally, *wus* and *spl/nzz* loss of function mutants each produce similar finger-like ovules, making it difficult to disentangle the contributions of these two transcription factors.

While cytokinin promotes *SPL/NZZ* expression during ovule development with no known role for CLEs there, CLE signaling inhibits *SPL/NZZ* in the anther with no known contribution from cytokinin signaling (Figure 2D). Early Arabidopsis anther development requires strict control of cell division and cell identity to produce four concentric cell layers[54,55]. First, cells derived from the second cell layer of the floral meristem differentiate into archesporial initials. Two more rounds of periclinal divisions produce, from outside in, the endothecium, the middle layer, the tapetum, and the sporogenous cells (Figure 2D). The CLE receptors RPK2/TOAD2 and (BAM) and their *CLAVATA3* INSENSITIVE RECEPTOR KINASEs (CIK) co-receptors are required for proper anther development[54-58••,59••]. CLE receptor mutants misspecify cell identity and fail to undergo the stereotypical periclinal cell divisions that produce the layers of the anther. Instead, *rpk2, bam,* and *cik* mutant anthers have overly abundant sporogenous cells and swollen tapetum cells[54–56]. This misspecification is concurrent with ectopic and higher expression of the transcription factor *SPL/NZZ* (Figure 2D).

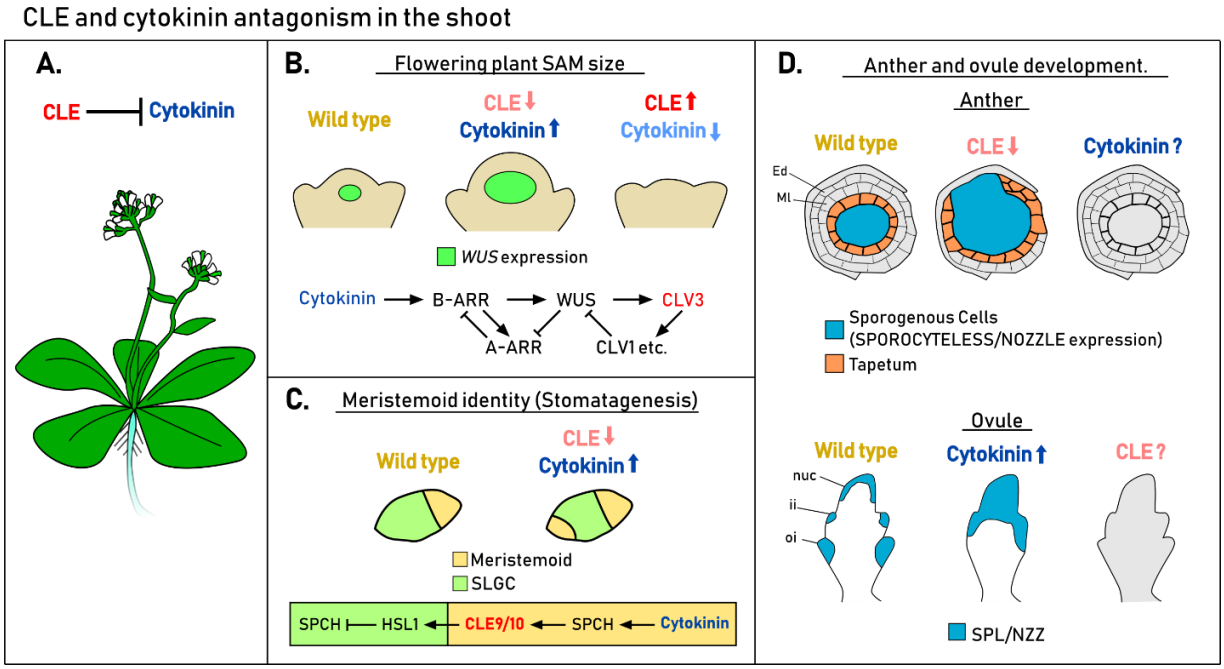

Figure 2. CLE and Cytokinin interactions during development in the Arabidopsis shoot. A) In each case, CLEs inhibit processes induced by cytokinin in the Arabidopsis shoot. B) In the SAM, cytokinin induces *WUS*, which sustains cytokinin signaling. WUS then promotes the expression of CLV3, which inhibits *WUS* through a series of receptors including CLV1. C) The meristemoid is a transient stem cell established during stomatagenesis. *SPCH*, the master regulator of meristemoid identity, is promoted by cytokinin; SPCH then promotes synthesis of CLE9/10, which acts through HSL1 to promote SPCH degradation and prevent the formation of additional meristemoids. D) CLE signaling inhibits *SPL/NZZ* expression during anther development, while cytokinin promotes *SPL/NZZ* expression during ovule development. However, roles for cytokinin in the anther or CLEs in the ovule are not well established.

These data leave us with pieces of a puzzle. Cytokinin promotes whereas CLE signaling inhibits *SPL/NZZ* in the carpel medial domain, but this interaction could be another instance of signaling through *WUS*. Meanwhile, cytokinin induces *SPL/NZZ* in ovules while CLE signaling represses *SPL/NZZ* in anthers, but roles for CLEs in ovule development and cytokinin in anther development are unknown. It will be interesting to see whether these data from the anther and ovule represent pieces of a whole network regulating *SPL/NZZ*, or whether regulation of *SPL/NZZ* is in fact distinct between anthers and ovules.

Cytokinin gain of function resembles CLE loss of function in the early embryo

While direct interactions between CLE and cytokinin signaling have not been found in the Arabidopsis embryo, evidence suggests that similarly to the shoot, CLE and cytokinin signaling act antagonistically there. Putative CLE receptor RPK2 and its paralog RPK1 have redundant functions in the embryo. In *rpk1*;*rpk2*

double loss of function embryos, cells swell and become disorganized, epidermal and ground tissue identity are lost, *PIN-FORMED* (*PIN*) expression is reduced, cotyledons fail to form, and vascular initial markers expand throughout the embryo[60,61].These embryos morphologically resemble Arabidopsis embryos in which *B-ARRs* are overexpressed or *A-ARRs* are repressed at early developmental stages, thus boosting cytokinin signaling[62]. This resemblance includes changes in gene expression: in both *rpk1;rpk2* and hyperactive cytokinin signaling embryos, expression of ground tissue marker gene *SCARECROW (SCR)* and of RAM marker *WUSCHEL RELATED HOMEOBOX 5* (*WOX5*) is reduced and diffuse[60–62]. However, a convincing connection between CLE and cytokinin signaling will require more careful comparisons of gene expression changes through embryo development of *rpk1*; *rpk2/+* and high-cytokinin signaling embryos.

CLE and cytokinin signaling are antagonistic in the moss, Physcomitrella

In addition to the examples from *Arabidopsis thaliana* above, CLE and cytokinin signaling have antagonistic functions in the distantly related moss *Physcomitrella patens* (Figure 3A). In Physcomitrella, juvenile filamentous tissue called protonema branches to produce additional filaments or an asymmetrically dividing bud that establishes a SAM and gives rise to a leafy shoot[63]. Physcomitrella *clavata1, rpk2,* or *amiRNA-CLE* lines all produce greater numbers of buds than wild type plants – indicating a higher propensity to initiate asymmetrically dividing SAMs (Figure 3B) – and display ectopic meristems along the lengths of their shoots (Figure 3C) – indicating an inability to maintain differentiation[62••]. Cytokinin treatment also increases bud number and can induce ectopic SAMs on shoots (Figure 3B, C)[65–67], and cytokinin receptor mutants form very few and delayed buds[68], demonstrating that these two pathways antagonistically regulate SAM initiation and maintenance of differentiation (Figure 3B).

In Physcomitrella, an additional link between CLE signaling and cytokinin signaling exists in the control of leaf cell proliferation. Physcomitrella grown on CLE peptides have smaller leaves and shoots, and this reduction in leaf size is caused by a reduction in cell number (Figure 3D)[62••]. Similarly, cytokinin receptor loss of function mutants have small leaves with fewer cells[68], while treatment with low concentrations of cytokinin promotes cell division in the leaf and results in larger leaves (Figure 3D)[69]. Collectively, these

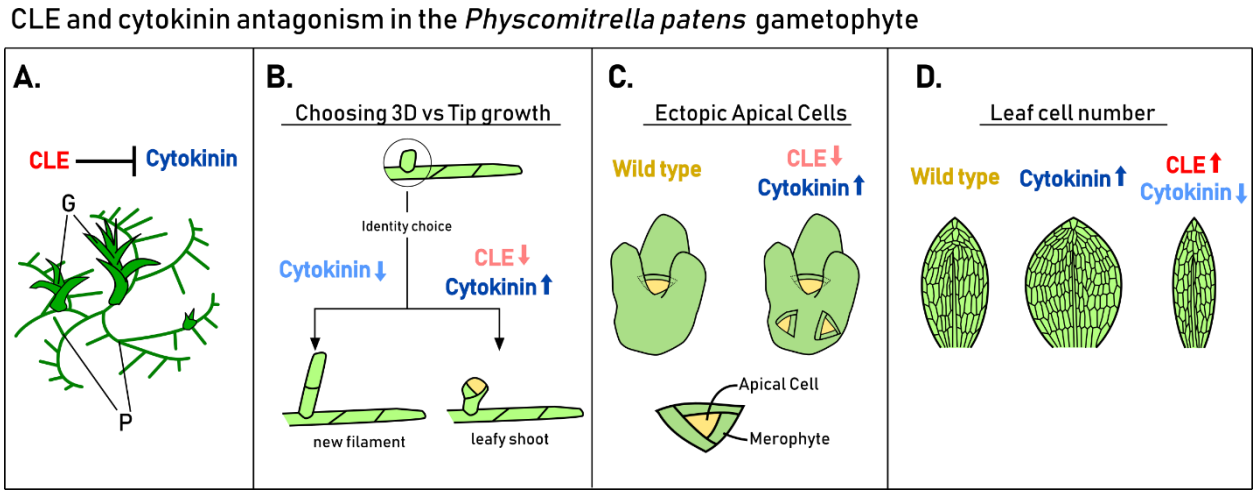

Figure 3. CLE and Cytokinin regulation of cell identity and division are conserved in moss. A) The basic body plan of *Physcomitrella patens* consists of protonema filaments (P) and leafy gametophores (G). In each tissue, CLEs appear to inhibit effects elicited by cytokinin. B) Filament initials either persist as new filaments or differentiate into 3D-growing buds; bud production is promoted by cytokinin and inhibited by CLE signaling. C) Treatment with exogenous cytokinin or mutating CLE signaling pathway components induces ectopic apical meristem formation on moss shoots. D) Treatment with low levels of cytokinin promotes cell division and results in wider leaves, while cytokinin receptor mutants and CLE treatment each result in narrower leaves with fewer cells

two lines of evidence suggest that the opposing roles of CLE and cytokinin signaling in regulating meristem function and cell division are more generally conserved in the moss Physcomitrella.

Intriguingly, while the roles of CLEs in regulating the SAM are conserved, the role for *WUS* in this process is not. The *WUSCHEL-LIKE HOMEOBOX* (*WOX*) gene family contains three major clades: the *WUS*-like clade, the intermediate clade, and the ancient clade[70]. The Physcomitrella genome contains only members of the ancient clade of WOX genes. Loss of *WOX* gene function results in tip growth defects and arrest of the zygote, but had no effect on SAM or shoot development in moss[71]. This implies that CLV receptors were an important component of ancestral SAM signaling that pre-dated the addition of *WOX* genes to this network. This points to a fascinatingly open area of research, as *WOX*-independent functions of CLV1 and its cohort of seemingly redundant LRR-RLKs in the SAM are largely unexplored.

CLEs and Cytokinin act cooperatively in the root

While in each case from the Arabidopsis and Physcomitrella shoots discussed above CLEs and cytokinin antagonistically regulate the same processes, this pattern is reversed in the Arabidopsis root (Figure 4A). Here

we describe how CLE and cytokinin signaling both reduce the overall size of the RAM, inhibit stem cell identity in the RAM center, and inhibit protoxylem formation.

CLEs and Cytokinin both promote meristem to transition zone differentiation

Whereas cytokinin promotes meristem maintenance and expansion in the shoot, in the root it promotes differentiation from the meristem zone, where cells divide abundantly, to the transition zone, where cells elongate (Figure 4B). Transition zone identity is induced by repression of auxin signaling by cytokinin-mediated expression of *SHORT HYPOCOTYL 2* (*SHY2*), which encodes an AUX/IAA inhibitor of auxin response[72]. Diverse CLEs also shorten the meristem and promote transition zone identity. In one proposed mechanism, CLE signaling in the developing protophloem is responsible for shortening the meristematic zone (Figure 4B)[71•]. Mutants of the CLE pathway pseudo-kinase CRN are insensitive to CLE-induced meristem shortening, but *CRN* expression solely in the protophloem restores RAM-shortening sensitivity to CLEs[71•]. These data suggest that CLE action in developing protophloem is sufficient to shorten the RAM. Because cytokinin is transported through the phloem, it is appealing to think that CLEs alter the distribution of cytokinin by inhibiting protophloem development, thus indirectly inducing *SHY2* and promoting transition zone identity[74]. However, directly reducing the cytokinin content of the phloem by inducing cytokinin degradation there does not change the RAM size[74]. This suggests that cytokinin abundance in the phloem (as opposed to in the cortex) does not directly influence *SHY2*-mediated differentiation. However, inhibition of protophloem development may result in a more drastic redistribution of cytokinin or its downstream signaling than could be alleviated by inducing cytokinin degradation in the phloem. It would be interesting to investigate how cytokinin response and *SHY2* expression are altered upon CLE addition.

CLEs and cytokinin antagonize the root stem cell niche

Stem cell differentiation in the RAM is inhibited by the close relative of *WUS*, *WOX5*, which acts non-cell autonomously to maintain stem cells around the Quiescent Center (QC)[75]. In a network reminiscent of the CLV3-WUS feedback loop in the SAM, CLE40 acts through CLV1 and ARABIDOPSIS CRINKLEY 4 (ACR4) to restrict *WOX5* expression and promote cell differentiation (Figure4B)[76]. Treatment with CLE40 results in a loss of the QC and a shift of *WOX5* expression away from the columella, where ACR4 and CLV1

are present[76,77]. In contrast to the SAM where *CLV1* and *WUS* are expressed in overlapping domains, however, *CLV1* and *ACR4* are expressed in non-overlapping domains with *WOX5*, suggesting that CLE40-mediated regulation of *WOX5* is indirect. Similarly, Cytokinin also inhibits *WOX5* expression (Figure4B)[10,78]. While CLEs exert a stronger effect on the QC than cytokinin, there are likely robust mechanisms limiting cytokinin response there, which is consistent with a strong auxin response maximum in the QC. QC-specific induction of genes that circumvent such feedback loops or inhibitory effects, such as constitutively active B-ARRs or *CKI*, could reveal whether downstream effects of cytokinin signaling in the RAM are similar to those of CLEs. Also, it is not clear whether CLEs and cytokinin inhibit *WOX5* independently, or whether they act through overlapping signaling pathways.

CLEs support cytokinin function to inhibit xylem and promote procambial identity in the root

The Arabidopsis root is bisymmetrical, possessing two poles of phloem cells, a line of xylem cells through the center, and procambial cells between the xylem and phloem. To produce this bisymmetric pattern, cytokinin inhibits auxin transport in the procambium and phloem while focusing auxin transport through the xylem

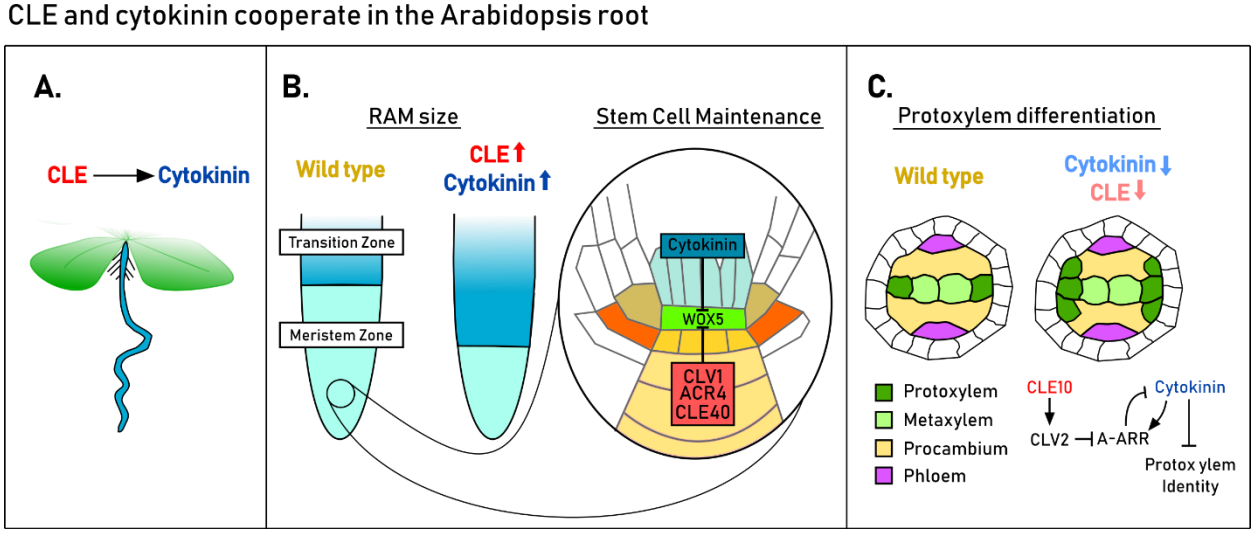

Figure 4. CLE and Cytokinin signaling promote overlapping processes in the Arabidopsis root. A) Throughout the Arabidopsis root, CLEs either support cytokinin signaling or converge by promoting the same downstream targets. B) Both CLE and cytokinin signaling promote transition zone identity and inhibit meristem identity. Within the stem cell niche, CLE and cytokinin signaling inhibit *WOX5* expression and QC function; it is currently unclear whether they act together or independently. C) CLE signaling directly promotes cytokinin signaling in procambial cells adjacent to the xylem poles in the root. Together, these pathways inhibit protoxylem identity and ensure proper vascular patterning.

poles[79]. High auxin abundance in those xylem poles promotes xylem identity and acts through the bHLH transcription factors TARGET OF MONOPTEROS 5 and LONESOME HIGHWAY (TMO5 and LHW) to activate *LONELY GUY* (*LOG*) genes, which synthesize active cytokinin Auxin also promotes the expression of *AHP6*, a cytokinin response inhibitor[79]. In neighboring cells, active cytokinin prevents xylem cell identity and promotes periclinal divisions, while AHP6 inhibits cytokinin response in the xylem poles[77,78•,79]. Intriguingly, *clv2* mutants display a spread of *AHP6* expression and xylem cell identity from the xylem poles to adjacent procambial cells, indicating a reduction of cytokinin signaling (Figure 4C)[82]. Meanwhile, treatment with CLE10 similarly inhibits protoxylem development. The relationship between CLE and cytokinin signaling here is one of the best established. B-ARR double mutants *arr10;arr12*, which are insensitive to cytokinin-mediated inhibition of protoxylem[82], are also insensitive to CLE10-mediated protoxylem inhibition, indicating that CLE10 functions through the cytokinin pathway[82]. CLE10 signals through CLV2 to repress the inhibitory *ARR5* and *ARR6***,** allowing for sustained cytokinin signaling and inhibition of protoxylem identity (Figure 4C).

Conclusion

Here we have described numerous contexts where CLE and cytokinin signaling seem to converge on the same developmental processes. In a few cases, this interaction appears direct, such as CLE-mediated inhibition of *A-ARRs* in root procambium or of cytokinin-induced *WUS* in the SAM. However, the downstream signaling pathways of CLE receptors are still very poorly understood, making it difficult to tell whether the apparent convergence of CLE and cytokinin signaling presented here is mechanistically direct or indirect. Additionally, both cytokinin and CLE signaling are influenced by crosstalk with numerous other developmental signaling pathways, including auxin and brassinosteroids, which play important roles in many of the developmental processes discussed in this review[83–86]. It is thus possible that the apparent high degree of overlap between CLE and cytokinin signaling owes to our incomplete understanding of this highly interconnected and complex system. However, recent evidence of overlap between CLE and cytokinin signaling is abundant and extends across tissues and distantly related plant lineages, suggesting that this is a connection worth investigating.

Acknowledgements

The authors would like to thank Josh Strable, Celine Cammarata, Kate Harline, and Mingyuan Zhu for their comments on the manuscript and Jack Satterlee and Brianne Conlon for comments on figures. The authors would also like to thank the National Science Foundation, the Weill Institute for Cell and Molecular Biology, and School of Integrative Plant Science at Cornell for funding and support.

References

1. • Wybouw B, De Rybel B: **Cytokinin – A Developing Story**. *Trends Plant Sci* 2019, **24**:177–185.

   This recent review covers the roles of cytokinin signlaing in development in more depth than we could provide here, where we focus on the interactions of CLEs and cytokinins.

2. Somssich M, Je B Il, Simon R, Jackson D: **CLAVATA-WUSCHEL signaling in the shoot meristem**. *Development* 2016, **143**:3238–3248.

3. Soyars CL, James SR, Nimchuk ZL: **Ready, aim, shoot: Stem cell regulation of the shoot apical meristem**. *Curr Opin Plant Biol* 2016, **29**:163–168.

4. • Kieber JJ, Schaller GE: **Cytokinin signaling in plant development.** *Development* 2018, **145**:dev149344.

   This review provides an excellent account of cytokinin perception, signaling, and response components, and ties them into a developmental context.

5. Stock AM, Robinson VL, Goudreau PN: **Two-Component Signal Transduction**. *Annu Rev Biochem* 2000, **69**:183–215.

6. Inoue T, Higuchi M, Hashimoto Y, Seki M, Kobayashi M, Kato T, Tabata S, Shinozaki K, Kakimoto T: **Identification of CRE1 as a cytokinin receptor from Arabidopsis**. *Nature* 2001, **409**:1060–1063.

7. Nishimura C, Ohashi Y, Sato S, Kato T, Tabata S, Ueguchi C: **Histidine kinase homologs that act as cytokinin receptors possess overlapping functions in the regulation of shoot and root growth in Arabidopsis.** *Plant Cell* 2004, **16**:1365–77.

8. Du L, Jiao F, Chu J, Jin G, Chen M, Wu P: **The two-component signal system in rice (Oryza sativa L.): A genome-wide study of cytokinin signal perception and transduction**. *Genomics* 2007, **89**:697–707.

9. Hutchison CE, Li J, Argueso C, Gonzalez M, Lee E, Lewis MW, Maxwell BB, Perdue TD, Schaller GE, Alonso JM, et al.: **The Arabidopsis histidine phosphotransfer proteins are redundant positive regulators of cytokinin signaling.** *Plant Cell* 2006, **18**:3073–87.

10. Zhang W, Swarup R, Bennett M, Schaller GE, Kieber JJ: **Cytokinin induces cell division in the quiescent center of the Arabidopsis root apical meristem.** *Curr Biol* 2013, **23**:1979–89.

11. Argyros RD, Mathews DE, Chiang Y-H, Palmer CM, Thibault DM, Etheridge N, Argyros DA, Mason MG, Kieber JJ, Schaller GE: **Type B Response Regulators of Arabidopsis Play Key Roles in Cytokinin Signaling and Plant Development**. *PLANT CELL ONLINE* 2008, **20**:2102–2116.

12. Ishida K, Yamashino T, Yokoyama A, Mizuno T: **Three Type-B Response Regulators, ARR1, ARR10 and ARR12, Play Essential but Redundant Roles in Cytokinin Signal Transduction Throughout the Life Cycle of Arabidopsis thaliana**. *Plant Cell Physiol* 2008, **49**:47–57.

13. Brandstatter I, Kieber JJ: **Two genes with similarity to bacterial response regulators are rapidly and specifically induced by cytokinin in Arabidopsis.** *Plant Cell* 1998, **10**:1009–19.

14. Schaller GE, Kieber JJ, Shiu S-H: **Two-Component Signaling Elements and Histidyl-Aspartyl Phosphorelays** †. *Arab B* 2008, **6**:e0112.

15. Zhao Z, Andersen SU, Ljung K, Dolezal K, Miotk A, Schultheiss SJ, Lohmann JU: **Hormonal control of the shoot stem-cell niche**. *Nature* 2010, **465**:1089–1092.

16. Marhavý P, Duclercq J, Weller B, Feraru E, Bielach A, Offringa R, Friml J, Schwechheimer C, Murphy A, Benková E: **Cytokinin controls polarity of PIN1-dependent auxin transport during lateral root organogenesis.** *Curr Biol* 2014, **24**:1031–7.

17. El-Showk S, Ruonala R, Helariutta Y: **Crossing paths: cytokinin signalling and crosstalk.** *Development* 2013, **140**:1373–83.

18. Leibfried A, To JPC, Busch W, Stehling S, Kehle A, Demar M, Kieber JJ, Lohmann JU: **WUSCHEL controls meristem function by direct regulation of cytokinin-inducible response regulators.** *Nature* 2005, **438**:1172–1175.

19. Jun J, Fiume E, Roeder AHK, Meng L, Sharma VK, Osmont KS, Baker C, Ha CM, Meyerowitz EM, Feldman LJ, et al.: **Comprehensive Analysis of CLE Polypeptide Signaling Gene Expression and Overexpression Activity in Arabidopsis**. *Plant Physiol* 2010, **154**:1721–1736.

20. Liu P-L, Du L, Huang Y, Gao S-M, Yu M: **Origin and diversification of leucine-rich repeat receptor-like protein kinase (LRR-RLK) genes in plants**. *BMC Evol Biol* 2017, **17**:47.

21. Betsuyaku S, Takahashi F, Kinoshita A, Miwa H, Shinozaki K, Fukuda H, Sawa S: **Mitogen-activated protein kinase regulated by the CLAVATA receptors contributes to shoot apical meristem homeostasis**. *Plant Cell Physiol* 2011, **52**:14–29.

22. Bommert P, Je B Il, Goldshmidt A, Jackson D: **The maize Gα gene COMPACT PLANT2 functions in CLAVATA signalling to control shoot meristem size.** *Nature* 2013, **502**:555–8.

23. • Je B Il, Xu F, Wu Q, Liu L, Meeley R, Gallagher JP, Corcilius L, Payne RJ, Bartlett ME, Jackson D: **The CLAVATA receptor FASCIATED EAR2 responds to distinct CLE peptides by signaling through two downstream effectors**. *Elife* 2018, **7**.

    The LRR/RLKs CLV2 and CRN are typically thought to act as a single signaling unit. Je et al. provide interesting genetic evidence that FEA2, the maize homolog of CLV2, can transmit a downstream signal either through ZmCRN or through a heterotrimeric G-protein depending on the CLE ligand.

24. Rosas-Diaz T, Zhang D, Fan P, Wang L, Ding X, Jiang Y, Jimenez-Gongora T, Medina-Puche L, Zhao X, Feng Z, et al.: **A virus-targeted plant receptor-like kinase promotes cell-to-cell spread of RNAi.** *Proc Natl Acad Sci U S A* 2018, **115**:1388–1393.

25. Kondo Y, Fukuda H: **The TDIF signaling network**. *Curr Opin Plant Biol* 2015, **28**:106–110.

26. Etchells JP, Smit ME, Gaudinier A, Williams CJ, Brady SM: **A brief history of the TDIF-PXY signalling module: balancing meristem identity and differentiation during vascular development.** *New Phytol* 2015, doi:10.1111/nph.13642.

27. Skoog F, Miller CO, Folke K. Skoog and Carlos O. Miller: **Chemical regulation of growth and organ formation in plant tissue cultured in vitro.** *Symp Soc exp Biol* 1957, doi:10.1093/pcp/pcp176.

28. Gordon SP, Heisler MG, Reddy G V., Ohno C, Das P, Meyerowitz EM: **Pattern formation during de novo assembly of the Arabidopsis shoot meristem**. *Development* 2007, **134**:3539–3548.

29. Laux T, Mayer KF, Berger J, Jürgens G: **The WUSCHEL gene is required for shoot and floral meristem integrity in Arabidopsis.** *Development* 1996, **122**:87–96.

30. Meng W, Cheng ZJ, Sang YL, Zhang MM, Rong XF, Wang ZW, Tang YY, Zhang XS: **Type-B ARABIDOPSIS RESPONSE REGULATORs Is Critical to the Specification of Shoot Stem Cell Niche by Dual Regulation of WUSCHEL**. *Plant Cell* 2017, **29**:tpc.00640.2016.

31. Yadav RK, Tavakkoli M, Reddy G V.: **WUSCHEL mediates stem cell homeostasis by regulating stem cell number and patterns of cell division and differentiation of stem cell progenitors**. *Development* 2010, **137**:3581–3589.

32. Yadav RK, Perales M, Gruel J, Girke T, Jönsson H, Venugopala Reddy G: **WUSCHEL protein movement mediates stem cell homeostasis in the Arabidopsis shoot apex**. *Genes Dev* 2011, **25**:2025–2030.

33. Daum G, Medzihradszky A, Suzaki T, Lohmann JU: **A mechanistic framework for noncell autonomous stem cell induction in Arabidopsis**. *Proc Natl Acad Sci* 2014, **111**:14619–14624.

34. Clark SE, Williams RW, Meyerowitz EM: **The CLAVATA1 gene encodes a putative receptor kinase that controls shoot and floral meristem size in Arabidopsis.** *Cell* 1997, **89**:575–585.

35. Nimchuk ZL, Zhou Y, Tarr PT, Peterson B a., Meyerowitz EM: **Plant stem cell maintenance by transcriptional cross-regulation of related receptor kinases**. *Development* 2015, **142**:1043–1049.

36. Kayes JM, Clark SE: **CLAVATA2, a regulator of meristem and organ development in Arabidopsis.** *Development* 1998, **125**:3843–3851.

37. Müller R, Bleckmann A, Simon R: **The receptor kinase CORYNE of Arabidopsis transmits the stem cell-limiting signal CLAVATA3 independently of CLAVATA1.** *Plant Cell* 2008, **20**:934–946.

38. Sawa S, Tabata R: **RPK2 functions in diverged CLE signaling.** *Plant Signal Behav* 2011, **6**:86–88.

39. Kinoshita A, Betsuyaku S, Osakabe Y, Mizuno S, Nagawa S, Stahl Y, Simon R, Yamaguchi-Shinozaki K, Fukuda H, Sawa S: **RPK2 is an essential receptor-like kinase that transmits the CLV3 signal in Arabidopsis.** *Development* 2010, **137**:3911–3920.

40. Brand U, Fletcher JC, Hobe M, Meyerowitz EM, Simon R: **Dependence of Stem Cell Fate in Arabidopsis on a Feedback Loop Regulated by CLV3 Activity**. *Science (80-)* 2000, **289**:617–619.

41. Mayer KFX, Schoof H, Haecker A, Lenhard M, Jürgens G, Laux T: **Role of< i> WUSCHEL</i> in Regulating Stem Cell Fate in the< i> Arabidopsis</i> Shoot Meristem**. *Cell* 1998, **95**:805–815.

42. Gordon SP, Chickarmane VS, Ohno C, Meyerowitz EM: **Multiple feedback loops through cytokinin signaling control stem cell number within the Arabidopsis shoot meristem.** *Proc Natl Acad Sci U S A* 2009, **106**:16529–16534.

43. Galli M, Gallavotti A: **Expanding the Regulatory Network for Meristem Size in Plants**. *Trends Genet* 2016, **32**:372–383.

44. MacAlister CA, Ohashi-Ito K, Bergmann DC: **Transcription factor control of asymmetric cell divisions that establish the stomatal lineage**. *Nature* 2007, **445**:537–540.

45. Pillitteri LJ, Sloan DB, Bogenschutz NL, Torii KU: **Termination of asymmetric cell division and differentiation of stomata**. *Nature* 2007, **445**:501–505.

46. •• Vatén A, Soyars CL, Tarr PT, Nimchuk ZL, Bergmann DC: **Modulation of Asymmetric Division Diversity through Cytokinin and SPEECHLESS Regulatory Interactions in the Arabidopsis**

Stomatal Lineage. *Dev Cell* 2018, **47**:53–66.e5.

Vaten et al. show that cytokinin promotes entry into meristemoid identity by the induction of SPCH. The meristemoid undergoes an asymmetric cell division, and SPCH in the meristemoid daughter induces CLE9/10 to inhibit continued SPCH expression in the adjacent, differentiating SLGC. Here a novel and exciting link between CLE and cytokinin signaling in a transient meristematic cell is identified.

47. •• Qian P, Song W, Yokoo T, Minobe A, Wang G, Ishida T, Sawa S, Chai J, Kakimoto T: **The CLE9/10 secretory peptide regulates stomatal and vascular development through distinct receptors**. *Nat Plants* 2018, **4**:1071–1081.

Qian et al. provide evidence that the LRR/RLK HEASA LIKE 1 transmits the CLE9/10 signal in developing leaves to induce degredation of SPCH in the differnetiating SLGC via MAPK signaling. The authors show that HSL1 acts in conjunction with SERK co-receptors. Meanwhile in the root, the same CLE peptides act through BAM receptors to inhibit protoxylem formation. This work interestingly demonstrates a role for CLEs in stomatagensis, and shows in vivo a CLE acting through different receptors to accomplish different functions in two contexts.

48. Bergmann DC, Lukowitz W, Somerville CR: **Stomatal development and pattern controlled by a MAPKK kinase.** *Science* 2004, **304**:1494–1497.

49. Durbak AR, Tax FE: **CLAVATA signaling pathway receptors of Arabidopsis regulate cell proliferation in fruit organ formation as well as in meristems.** *Genetics* 2011, **189**:177–94.

50. Gross-Hardt R, Lenhard M, Laux T: **WUSCHEL signaling functions in interregional communication during Arabidopsis ovule development.** *Genes Dev* 2002, **16**:1129–38.

51. Bencivenga S, Simonini S, Benková E, Colombo L: **The Transcription Factors BEL1 and SPL Are Required for Cytokinin and Auxin Signaling During Ovule Development in Arabidopsis**. *Plant Cell* 2012, **24**:2886–2897.

52. Ostria-Gallardo E, Ranjan A, Chitwood DH, Kumar R, Townsley BT, Ichihashi Y, Corcuera LJ, Sinha NR: **Transcriptomic analysis suggests a key role for SQUAMOSA PROMOTER BINDING PROTEIN LIKE, NAC and YUCCA genes in the heteroblastic development of the temperate rainforest tree Gevuina avellana (Proteaceae)**. *New Phytol* 2016, **210**:694–708.

53. Schiefthaler U, Balasubramanian S, Sieber P, Chevalier D, Wisman E, Schneitz K: **Molecular analysis of NOZZLE, a gene involved in pattern formation and early sporogenesis during sex organ development in Arabidopsis thaliana.** *Proc Natl Acad Sci U S A* 1999, **96**:11664–9.

54. Sanders PM, Bui AQ, Weterings K, McIntire KN, Hsu Y-C, Lee PY, Truong MT, Beals TP, Goldberg RB: **Anther developmental defects in Arabidopsis thaliana male-sterile mutants**. *Sex Plant Reprod* 1999, **11**:297–322.

55. Walbot V, Egger RL: **Pre-Meiotic Anther Development: Cell Fate Specification and Differentiation**. *Annu Rev Plant Biol* 2016, **67**:365–395.

56. Mizuno S, Osakabe Y, Maruyama K, Ito T, Osakabe K, Sato T, Shinozaki K, Yamaguchi-Shinozaki K: **Receptor-like protein kinase 2 (RPK 2) is a novel factor controlling anther development in Arabidopsis thaliana**. *Plant J* 2007, **50**:751–766.

57. Hord CLH, Chen C, Deyoung BJ, Clark SE, Ma H: **The BAM1/BAM2 receptor-like kinases are important regulators of Arabidopsis early anther development.** *Plant Cell* 2006, **18**:1667–80.

58. •• Cui Y, Hu C, Zhu Y, Cheng K, Li X, Wei Z, Xue L, Lin F, Shi H, Yi J, et al.: **CIK Receptor Kinases Determine Cell Fate Specification during Early Anther Development in Arabidopsis**. *Plant Cell* 2018, **30**:2383–2401.

Roles for RPK2 and BAM LRR/RLKs in anther development have bene previously described, but in addition to providing an in-depth characterization of anther defects in mutants of these genes, Cui et al. identify their co-receptors. These CIK co-receptors act with BAM and RPK2 in the anther, and complete loss of CIK function encompasses both bam and rpk2 phenotypes. This work provides an important step in understanding redundancy between developmental LRR/RLKs, and in elucidating the functional unit of signal percetpion and transmission in different cellular contexts.

59. •• Hu C, Zhu Y, Cui Y, Cheng K, Liang W, Wei Z, Zhu M, Yin H, Zeng L, Xiao Y, et al.: **A group of receptor kinases are essential for CLAVATA signalling to maintain stem cell homeostasis**. *Nat Plants* 2018, **4**:205–211.

Here Hu et al present the discovery a group of SERK-like (low number of LRR repeats) LRR/RLKs that act as co-receptors for known putative CLE receptors (except FEA3) in the SAM. This represents an important step in understanding the basis of CLE signaling, and the convincing evidence that these co-receptors act in conjunction with such a wide range of LRR/RLKs is very promising.

60. Nodine MD, Yadegari R, Tax FE: **RPK1 and TOAD2 Are Two Receptor-like Kinases Redundantly Required for Arabidopsis Embryonic Pattern Formation**. *Dev Cell* 2007, **12**:943–956.

61. Nodine MD, Tax FE: **Two receptor-like kinases required together for the establishment of Arabidopsis cotyledon primordia**. *Dev Biol* 2008, **314**:161–170.

62. Müller B, Sheen J: **Cytokinin and auxin interaction in root stem-cell specification during early embryogenesis.** *Nature* 2008, **453**:1094–1097.

63. Cove DJ: **The moss Physcomitrella patens.** *Annu Rev Genet* 2005, **39**:339–358.

64. •• Whitewoods CD, Cammarata J, Nemec Venza Z, Sang S, Crook AD, Aoyama T, Wang XY, Waller M, Kamisugi Y, Cuming AC, et al.: **CLAVATA Was a Genetic Novelty for the Morphological Innovation of 3D Growth in Land Plants**. *Curr Biol* 2018, doi:10.1016/j.cub.2018.05.068.

Whitewoods et al investigate the role of CLE and putative CLE receptor genes in the develpoment of the three-dimensional body of the Physcomitrella patens gametophyte. The authors find a conserved role for CLE signaling in inhibiting shoot stem cell identity, and a novel role for CLV1 in the orientation of cell division planes that is conserved in Arabidopsis.

65. Reski R, Abel WO: **Induction of budding on chloronemata and caulonemata of the moss,Physcomitrella patens,using isopentenyladenine**. *Planta* 1985, **165**:354–358.

66. Ashton NW, Grimsley N, Cove DJ: **Analysis of gametopytic development in the moss, Physcomitrella patens, using auxin and cytokinn resistants mutants.** *Planta* 1979, **144**:427–435.

67. Coudert Y, Palubicki W, Ljung K, Novak O, Leyser O, Harrison CJ: **Three ancient hormonal cues co-ordinate shoot branching in a moss**. *Elife* 2015, doi:10.7554/eLife.06808.

68. von Schwartzenberg K, Lindner A-C, Gruhn N, Šimura J, Novák O, Strnad M, Gonneau M, Nogué F, Heyl A, Schwartzenberg K Von, et al.: **CHASE domain-containing receptors play an essential role in the cytokinin response of the moss Physcomitrella patens**. *J Exp Bot* 2015, **67**:erv479.

69. Barker EI, Ashton NW: **Heteroblasty in the moss, *Aphanoregma patens* (*Physcomitrella patens*), results from progressive modulation of a single fundamental leaf developmental programme**. *J Bryol* 2013, **35**:185–196.

70. Nardmann J, Werr W: **The invention of WUS-like stem cell-promoting functions in plants predates leptosporangiate ferns**. *Plant Mol Biol* 2012, **78**:123–134.

71. Sakakibara K, Reisewitz P, Aoyama T, Friedrich T, Ando S, Sato Y, Tamada Y, Nishiyama T, Hiwatashi Y, Kurata T, et al.: **WOX13-like genes are required for reprogramming of leaf and protoplast cells into stem cells in the moss Physcomitrella patens**. *Development* 2014, **141**:1660–1670.

72. Dello Ioio R, Nakamura K, Moubayidin L, Perilli S, Taniguchi M, Morita MT, Aoyama T, Costantino P, Sabatini S: **A genetic framework for the control of cell division and differentiation in the root meristem.** *Science* 2008, **322**:1380–1384.

73. • Hazak O, Brandt B, Cattaneo P, Santiago J, Rodriguez-Villalon A, Hothorn M, Hardtke CS: **Perception of root-active CLE peptides requires CORYNE function in the phloem vasculature**. *EMBO Rep* 2017, **18**:1367–1381.

The mechanism by which many CLEs shorten the root meristem zone is unknown. Here, Hazak et al. show that at least a part of the CLE signaling machinery - the psuedokinase CRN - need only be present in the protophloem to accomplish this CLE-induced meristem shortening function.

74. Bishopp A, Lehesranta S, Vatén A, Help H, El-Showk S, Scheres B, Helariutta K, Mähönen APPP, Sakakibara H, Helariutta Y: **Phloem-Transported Cytokinin Regulates Polar Auxin Transport and Maintains Vascular Pattern in the Root Meristem**. *Curr Biol* 2011, **21**:927–932.

75. Zhou Y, Liu X, Engstrom EM, Nimchuk ZL, Pruneda-Paz JL, Tarr PT, Yan A, Kay SA, Meyerowitz EM: **Control of plant stem cell function by conserved interacting transcriptional regulators**. *Nature* 2015, **517**:377–380.

76. Stahl Y, Wink RH, Ingram GC, Simon R: **A Signaling Module Controlling the Stem Cell Niche in Arabidopsis Root Meristems**. *Curr Biol* 2009, **19**:909–914.

77. Stahl Y, Grabowski S, Bleckmann A, Kühnemuth R, Weidtkamp-Peters S, Pinto KG, Kirschner GK, Schmid JB, Wink RH, Hülsewede A, et al.: **Moderation of arabidopsis root stemness by CLAVATA1 and ARABIDOPSIS CRINKLY4 receptor kinase complexes**. *Curr Biol* 2013, **23**:362–371.

78. •• Pernisova M, Grochova M, Konecny T, Plackova L, Harustiakova D, Kakimoto T, Heisler MG, Novak O, Hejatko J: **Cytokinin signalling regulates organ identity via the AHK4 receptor in Arabidopsis.** *Development* 2018, **145**:dev.163907.

TMO5 and LHW have an intriguing role as organizers - they induce formation of cytokinin in a cell type that is inhibited by cytokinin signaling. Of course, cytokinin signlaning is prevented in this cell type (protoxylem), and functions in procambial cells to promote periclinal cell divisions. With a great display of interesting biology and powerful methodology, Smet et al. use high temporal sensitivity RNA seq to identify a transcriptional hub downstream of cytokinin signaling that is sufficient to induce periclinal cell divisions.

79. Bishopp A, Help H, El-Showk S, Weijers D, Scheres B, Friml J, Benková E, Mähönen AP, Helariutta Y: **A mutually inhibitory interaction between auxin and cytokinin specifies vascular pattern in roots.** *Curr Biol* 2011, **21**:917–26.

80. Smet W, Sevilem I, de Luis Balaguer MA, Wybouw B, Mor E, Miyashima S, Blob B, Roszak P,

Jacobs TB, Boekschoten M, et al.: **DOF2.1 Controls Cytokinin-Dependent Vascular Cell Proliferation Downstream of TMO5/LHW**. *Curr Biol* 2019, **29**:520–529.e6.

81. Smet W, De Rybel B: **Genetic and hormonal control of vascular tissue proliferation**. *Curr Opin Plant Biol* 2016, **29**:50–56.

82. Kondo Y, Hirakawa Y, Kieber JJ, Fukuda H: **CLE Peptides can Negatively Regulate Protoxylem Vessel Formation via Cytokinin Signaling**. *Plant Cell Physiol* 2011, **52**:37–48.

83. Mandel T, Candela H, Landau U, Asis L, Zelinger E, Carles CC, Williams LE: **Differential regulation of meristem size, morphology and organization by the ERECTA, CLAVATA and class III HD-ZIP pathways.** *Development* 2016, **143**:1612–22.

84. Galinha C, Bilsborough G, Tsiantis M: **Hormonal input in plant meristems: A balancing act**. *Semin Cell Dev Biol* 2009, **20**:1149–1156.

85. Ho C-MK, Paciorek T, Abrash E, Bergmann DC: **Modulators of Stomatal Lineage Signal Transduction Alter Membrane Contact Sites and Reveal Specialization among ERECTA Kinases**. *Dev Cell* 2016, **38**:345–357.

86. Kimura Y, Tasaka M, Torii KU, Uchida N: **ERECTA-family genes coordinate stem cell functions between the epidermal and internal layers of the shoot apical meristem.** *Development* 2018, **145**:dev156380.

Chapter 2: *CLAVATA* was a genetic novelty for the morphological innovation of 3D growth in land plants

Foreword

This chapter presents a large set of work with contributions from many people. It was published in this final form in Current Biology on my birthday in August 2018. I began this project as a master's student at the University of Cambridge, where I initially generated the *rpk2* mutant line and made the initial observations of ectopic leafy growths in those lines.

During my PhD, my contribution to this work constituted the generation and phenotypic analysis of *clv1a*, *clv1b*, and *clv1a;clv1b* double mutant lines. During my PhD I also re-analyzed the *rpk2* mutants. For my contributions, I was listed as co-first author together with Chris Whitewoods.

The project was independently conceived of by Chris Whitewoods and Jill Harrison at the University of Cambridge, and by Margaret Frank and Mike Scanlon at Cornell University. I feel lucky to have conducted research on this project in both laboratories.

The published version in Current Biology can be found at: https://doi.org/10.1016/j.cub.2018.05.068

Whitewoods, C.D., Cammarata, J., Nemec Venza, Z., Sang, S., Crook, A.D., Aoyama, T., Wang, X.Y., Waller, M., Kamisugi, Y., Cuming, A.C., et al. (2018). CLAVATA Was a Genetic Novelty for the Morphological Innovation of 3D Growth in Land Plants. Curr. Biol. *28*, 1–12.

CLAVATA was a genetic novelty for the morphological innovation of 3D growth in land plants

Authors: Chris D. Whitewoods[1,2*], Joseph Cammarata[1,3,4*], Zoe Nemec Venza[5], Stephanie Sang[5,6], Ashley D. Crook[7], Tsuyoshi Aoyama[1,5,8], Manuel Waller[9], Yasuko Kamisugi[10], Andrew C. Cuming[10], Peter Szövényi[9], Zachary L. Nimchuk[7,11], Adrienne H. K. Roeder[3,4], Michael J Scanlon[3] and C. Jill Harrison[1,5,†].

[*]Equal contribution as first author

[†]**Lead contact:** jill.harrison@bristol.ac.uk

Affiliations: [1]Plant Sciences Department, Cambridge University, Downing Street, Cambridge, CB2 3EA, UK.

[2]Present address: John Innes Centre, Norwich Research Park, Colney Lane, Norwich, NR4 7UH, UK.

[3]Plant Biology Section, School of Integrative Plant Science, Cornell University, Tower Road, Ithaca, NY 14853, USA.

[4]Weill Institute for Cell and Molecular Biology, Cornell University, Ithaca, NY 14853, USA.

[5]School of Biological Sciences, University of Bristol, 24 Tyndall Avenue, Bristol, BS8 1TQ, UK.

[6]Present address: Department of Organismal Biology and Anatomy, The University of Chicago, 1027 E. 57th St., Chicago, IL 60637

[7]Department of Biology, University of North Carolina at Chapel Hill, Chapel Hill, North Carolina, 27599, USA.

[8]Present address: National Institute for Basic Biology, Nishigonaka 38, Myodaiji, Okazaki, 444-8585, Aichi, Japan.

[9]Department of Systematic and Evolutionary Botany, University of Zurich, Zollikerstrasse 107, 8008 Zurich, Switzerland.

[10]Centre for Plant Sciences, Faculty of Biological Sciences, University of Leeds, Leeds, LS2 9JT, UK.

[11]Curriculum in Genetics and Molecular Biology, University of North Carolina at Chapel Hill, Chapel Hill, North Carolina, 27599, USA.

Summary:

How genes shape diverse plant and animal body forms is a key question in biology. Unlike animal cells, plant cells are confined by rigid cell walls, and cell division plane orientation and growth rather than cell movement determine overall body form. The emergence of plants on land coincided with a new capacity to rotate stem cell divisions through multiple planes, and this enabled three-dimensional (3D) forms to arise from ancestral forms constrained to 2D growth. The genes involved in this evolutionary innovation are largely unknown. The evolution of 3D growth is recapitulated during the development of modern mosses when leafy shoots arise from a filamentous (2D) precursor tissue. Here we show that a conserved, CLAVATA peptide/receptor-like kinase pathway originated with land plants and orients stem cell division planes during the transition from 2D to 3D growth in a moss, *Physcomitrella*. We find that this newly identified role for CLAVATA in regulating cell division plane orientation is shared between *Physcomitrella* and *Arabidopsis*. We report that roles for CLAVATA in regulating cell proliferation and cell fate are also shared, and that CLAVATA-like peptides act via conserved receptor components in *Physcomitrella*. Our results suggest that *CLAVATA* was a genetic novelty enabling the morphological innovation of 3D growth in land plants.

Introduction:

The conquest of land was enabled by a series of innovations that allowed plant forms to radiate and occupy new volumes of space in the sub-aerial environment [1]. Amongst these, the innovation of shooting systems with organs positioned radially around an upright stem stands out as a primer for massively increased plant productivity and diversity [1]. Such three-dimensional (3D) growth forms first arose as a consequence of a novel stem cell function gained by land plants, namely the capacity to rotate stem cell divisions through multiple plane orientations [1-3]. The algal sister lineages of land plants are unable to rotate stem cell divisions through multiple planes and are therefore generally constrained to smaller filamentous or mat-like (2D) growth forms [1, 3]. The evolutionary transition from 2D to 3D growth is recapitulated during the development of modern

mosses when a branching, filamentous (protonemal) precursor tissue (2D) gives rise to 3D gamete-producing leafy shoots (gametophores) [4]. Previous studies have shown that gametophores and filament branches initiate similarly as hemispherical outgrowths from parent filaments, and that their divergent 2D or 3D fates are specified stochastically by APETALA2-type (APB) transcription factor activity [5]. During a single-celled stage of outgrowth development, persistent APB activity and cell swelling mark a switch to gametophore fate (3D), whereas loss of APB activity marks filament fate (2D) [4, 5]. A strongly oblique cell division is the first reliable morphological marker of gametophore development [4, 5]. A second oblique apical cell division subsequently occurs and is approximately perpendicular to the first, and then division planes rotate during two successive rounds of division to establish a tetrahedral apical stem cell [4]. This tetrahedral apical cell divides in spiraling planes to replace itself and produce daughter cells that generate the 3D gametophore axis and leaves [4]. The mechanisms regulating such novel and rotating stem cell division plane orientations during evolutionary and developmental transitions to 3D growth are unknown.

In *Arabidopsis*, the *CLAVATA (CLV)* and *WUSCHEL (WUS)* pathways act in a feedback loop to regulate many aspects of stem cell function including cell fate [6, 7], proliferation [7-9] and growth [10]. *CLV3* encodes a small, secreted peptide that is expressed in the upper cell layers of the central zone and can move throughout the meristem [11-13]. *CLV1* is expressed in the underlying cell layers of the central zone and encodes a receptor-like kinase which acts as a receptor for CLV3 [9, 14] in conjunction with CLV2, CORYNE (CRN), RECEPTOR-LIKE PROTEIN KINASE 2 (RPK2) and BARELY ANY MERISTEM (BAM) [15, 16]. *WUS* activity promotes meristem cell proliferation [17], and CLV signaling restricts the size of the *WUS* expression domain [11]. WUS acts non-cell autonomously, moving from the organizing center to the uppermost meristem cell layers where it promotes *CLV3* expression [18], thereby closing the feedback loop that maintains meristem size.

Results

The CLAVATA pathway originated in the last common ancestor of land plants

To determine how the CLV pathway evolved and identify potential roles for CLV in *Physcomitrella* stem cell function, we first queried publicly accessible genome and transcriptome databases from a wide range of green algae and land plants for *CLV3*-like (*CLE*), *CLV1/BAM*, *RPK2*, *CLV2* and *CRN* homologues (Fig. 1B, Tables S1-S5). We found no CLV pathway homologues in the chlorophyte or charophyte algae sampled, but found at least one *CLE* homologue and one *CLV1*/*BAM* homologue in each early-diverging bryophyte lineage and all other land plants, suggesting that the core CLV signaling module comprises at least one CLE peptide and a CLV/BAM receptor-like kinase. *RPK2* homologues were present in all land plants except the hornwort, *Anthoceros agrestis*. In *Physcomitrella*, we identified seven genes with a conserved *CLE* domain encoding a

A

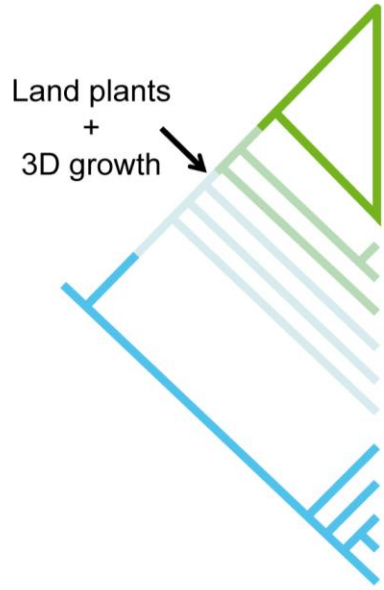

B

Clade	Species	*CLE*	*TDIF*	*CLV1/BAM*	*RPK2*	*CLV2*	*CRN*
VP	*Arabidopsis thaliana* (G)	32	5	4	1	1	1
	Glycine max (G)	38	6	10	5	2	2
	Oryza sativa (G)	36	3	4	2	1	1
	Amborella trichopoda (G)	8	1	5	2	1	1
	Picea abies (G)	52	17	4	3	1	1
	Diplazium wichurae (T)	2	0	2	2	0	0
	Selaginella moellendorfii (G)	15	4	3	1	0	0
L	*Marchantia polymorpha* (G)	2	1	1	1	0	0
M	*Physcomitrella patens* (G)	7	0	2	1	0	0
H	*Anthoceros agrestis* (G)	1	1	1	0	0	0
Cha	*Coleochaete nitellarum* (T)	0	0	0	0	0	0
	Spirogyra sp. (G)	0	0	0	0	0	0
	Chara braunii (G)	0	0	0	0	0	0
Chl	*Ostreococcus tauri* (G)	0	0	0	0	0	0
	Chlorella vulgaris (G)	0	0	0	0	0	0
	Volvox carteri (G)	0	0	0	0	0	0
	Chlamydomonas reinhardtii (G)	0	0	0	0	0	0
	Ulva spp. (T)	0	0	0	0	0	0

Fig. 1: The CLV pathway originated in the last common ancestor of land plants, concomitantly with 3D growth. See also Figs. S1-S3 and Tables S1-S5. (A) Phylogenetic relationships amongst land plants and their freshwater algal sister lineages redrawn from [19, 40] respectively. Whilst chlorophytes and charophytes undergo stem cell divisions in a single orientation (2D growth), land plants undergo stem cell divisions in multiple orientations to generate elaborate three-dimensional forms (3D growth). (B) The number of CLV pathway homologues was determined by BLAST against genome/draft genome (G) and transcriptome (T) databases as described in SI Methods. VP indicates vascular plants, L indicates liverworts, M indicates mosses, H indicates hornworts**,** Cha indicates charophytes, and Chl indicates chlorophytes.

12 amino acid peptide motif similar to CLV3 (Fig. 1, Table S1). Whilst *PpCLE*s *1*, *2* and *3* encode the peptide motif RMVPTGPNPLHN, *PpCLE4* encodes the motif RMVPSGPNPLHN, *PpCLE*s *5* and *6* encode the motif RLVPTGPNPLHN, and *PpCLE7* encodes the motif RVVPTGPNPLHN, but sequences outside the conserved CLE domain are divergent. Neighbour joining phylogenetic reconstructions showed that whilst hornworts and liverworts have *CLE*s resembling the Tracheary Element Differentiation Inhibitory Factor (TDIF)-like *CLE*s that regulate vascular development in *Arabidopsis*, *Physcomitrella* does not, consistent with an evolutionary loss in mosses (Fig. S1, Supplementary Dataset 1). Instead, the *Physcomitrella* genome encodes four CLV3-like peptides. Receptor kinase phylogenies were reconstructed by maximum likelihood analysis using amino acids from the conserved kinase domain (Fig. S2, Fig. S3, Supplementary dataset 2, Supplementary dataset 3). Clades encompassing *CLV1*/*BAM*-like sequences from each land plant lineage, or containing *RPK2*-like sequences from each lineage except hornworts were resolved. Both *CLV1*/*BAM* and *RPK2* phylogenies were broadly congruent with current hypotheses of land plant evolution [19, 20], thereby indicating orthology. Two *Physcomitrella* genes were incorporated in the *CLV1*/*BAM* clade, and these were named *Physcomitrella CLAVATA1a* and *1b* (*PpCLV1a* and *PpCLV1b*). One *RPK2* homologue was found and named *PpRPK2*, but no *CLV2* or *CRN* homologues were found. These sequence data indicate that the CLV pathway first arose in the last common ancestor of land plants, alongside the evolutionary innovation of 3D growth [21].

Physcomitrella CLAVATA pathway components are expressed during the 3D growth phase

To investigate *Physcomitrella* CLV activity, we first analyzed gene expression patterns in relation to the transition between 2D filamentous and 3D gametophore growth (Fig. 2, Fig. 5, Figs. S4, S5). By RT-PCR we detected *PpCLE1*, *2* and *7* peptide-encoding gene expression in gametophores (Fig. S4). We were unable to detect expression of *PpCLE*s *3*, *4* and *5*, but we found *PpCLE6* expression in protonemal filaments. Receptor encoding-genes *PpRPK2*, *PpCLV1a* and *PpCLV1b* were co-expressed in gametophores, although *PpRPK2* expression was evident earlier than *PpCLV1a* and *PpCLV1b* in day 10 filamentous tissues (Fig. S4). These results were broadly consistent with reports from transcriptome data (Fig. S5, [22, 23]). We also constructed *promoter::NLSGUSGFP* (*promoter::NGG*) fusion lines for *PpCLE1*, *PpCLE2*, *PpCLE7*, *PpCLV1a*, *PpCLV1b* and *PpRPK2* as RT-PCR showed that these 6 genes were up-regulated at around the time of gametophore

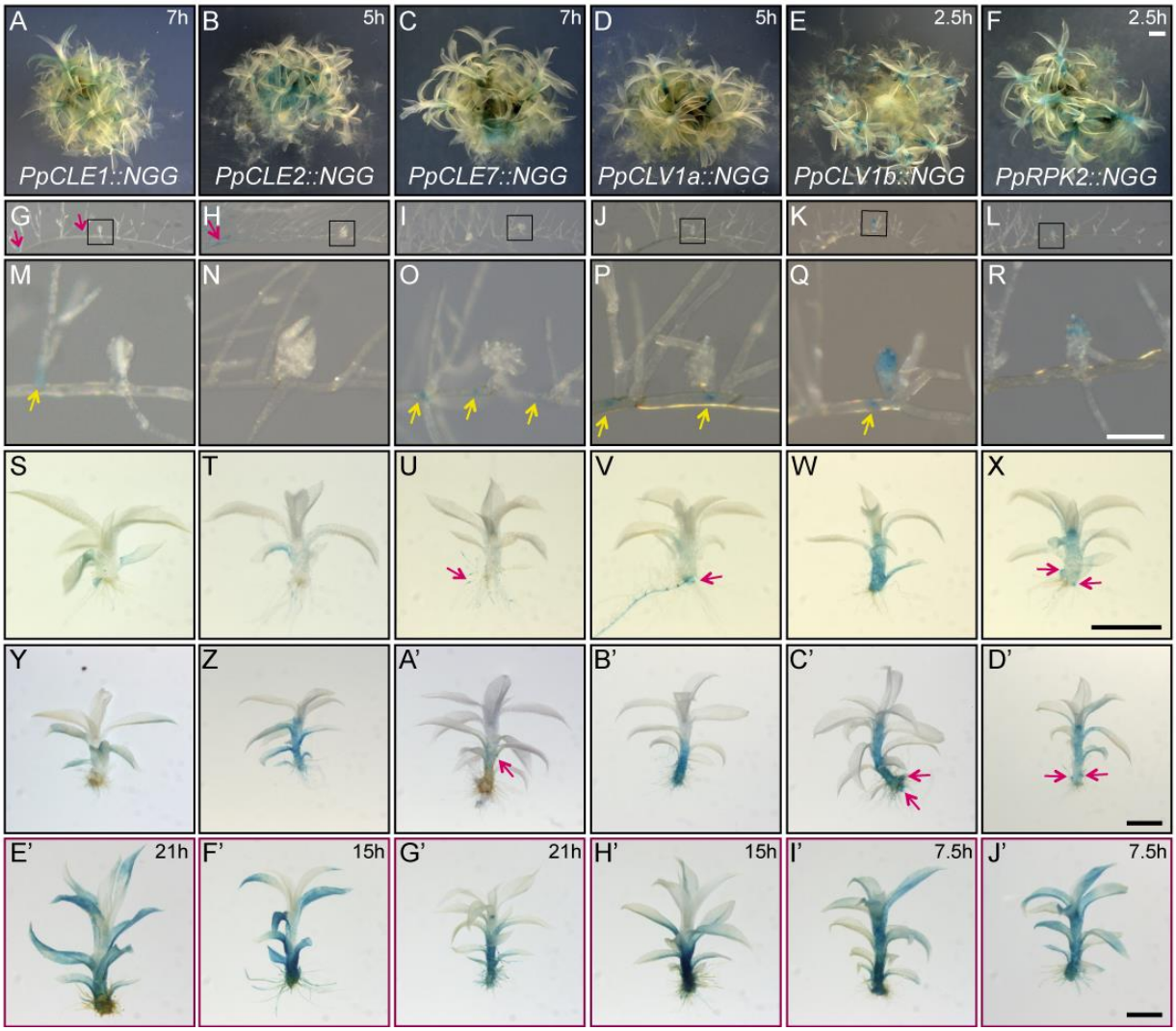

Fig. 2: CLV pathway components are expressed in *Physcomitrella* protonemata and gametophores. See also Methods Fig. 1 and Figs. S4 and S5. GUS staining of *PpCLE1::NGG* (A, G, M, S, Y, E'), *PpCLE2::NGG* (B, H, N, T, Z, F'), *PpCLE7::NGG* (C, I, O, U, A', G'), *PpCLV1a::NGG* (D, J, P, V, B', H'), *PpCLV1b::NGG* (E, K, Q, W, C', I') and *PpRPK2::NGG* (F, L, R, X, D' J') lines revealed complex expression dynamics. Whilst *PpCLE::NGG* and *PpCLV1a::NGG* signal accumulated in protonemal tissues close to buds (G-J and M-P; arrows indicate signal in protonemata), *PpCLV1b::NGG* and *PpRPK2::NGG* signal accumulated mainly in the apical region of buds (Q, R). At later stages of gametophore development (S-J') all promoters were active in gametophores, although the patterns and intensity of activity varied between reporters. *PpCLE1::NGG* lines stained most strongly in leaves (S, Y, E'), *PpCLE2::NGG* lines stained most strongly in leaves and gametophore bases (T, Z, F'), and *PpCLE7::NGG* lines accumulated stain in rhizoid tips (arrow in U), leaf bases (arrow in A'), hairs around the apex and the gametophore axis (G'). *PpCLV1a::NGG* lines did not stain intensely at early stages of gametophore development (P, V), but accumulated signal in gametophore axes and leaves at later stages. In contrast, *PpCLV1b::NGG* and *PpRPK2::NGG* lines accumulated signal in gametophore axes and leaves from early stages of development (W, X), and strong signal was detected in branches initiating at gametophore bases (arrows in X, C', and D'). All tissues in A-D' were stained in a solution containing 0.5 mM FeCN for times specified in A-F, and gametophores in E'-J' were stained three times longer in a solution containing 2 mM FeCN. Scale bar in A-F = 1 mm, scale bar in M-R = 100 µm, insets in G-L indicate position of buds in M-R. Scale bars in S-J' = 1 mm.

initiation (Methods Fig. 1, Fig. 2). In 3 week-old spot cultures (Fig. 2A-F), *PpCLE1::NGG*, *PpCLE2::NGG*, *PpCLE7::NGG* and *PpCLV1a::NGG* lines accumulated local signal in various protonemal cell types around the buds (Fig.

2G-J, M-P). *PpCLV1b::NGG* and *PpRPK2::NGG* lines accumulated signal in buds, and the signal was strongest towards the apex (Fig. 2K, L, Q, R). Whilst all lines accumulated signal in gametophore axes and leaves (Fig. 2S-J'), there was variation in the pattern, timing and intensity of signal accumulation between lines. Notably, *PpCLE1::NGG*, *PpCLE2::NGG*, *PpCLE7::NGG* and *PpCLV1a::NGG* signal accumulation in gametophores was delayed with respect to *PpCLV1b::NGG* and *PpRPK2::NGG* lines (Fig. 2M-X). These GUS accumulation patterns suggest highly dynamic foci of expression for *PpCLE*s *1*, *2* and *7* and *PpCLV1a*, *PpCLV1b* and *PpRPK2* in *Physcomitrella*, and they prompted us to investigate roles for CLV pathway components in gametophore initiation and development i.e. during the transition to 3D growth.

Physcomitrella mutants with defective CLAVATA function have a defective 2D to 3D growth transition

To identify the functions of CLV pathway components, we used AmiRNAs to silence expression of *PpCLEs 1, 2* and *3* and *PpCLEs 4*, 5, 6 and *7* (Methods Fig. 2). We used a CRISPR-Cas9 approach to disrupt the function of *PpCLV1* paralogues (Methods Fig. 3), and gene targeting was used to abrogate *PpRPK2* function (Methods Fig. 4). *PpcleAmiR1-3*, *PpcleAmiR4-7*, *Ppclv1a1b* and *Pprpk2* lines were able to form dense protonemal tissues and thus had a relatively normal 2D growth phase (Fig. 3A-E). However, all four mutant classes had defective development during the 3D growth phase, with a reduction in the overall number of mature gametophores and defects in gametophore development (Fig. 3A-E and U). Further examination revealed many more gametophore buds with 1 or fewer leaves in *PpcleAmiR1-3*, *PpcleAmiR4-7* and *Pprpk2* mutants than in WT plants (Fig. 3U), and *Ppclv1a1b* mutants had many small gametophores arrested at a later stage of development (Fig. 3U). These data suggested early defects in gametophore development with potential feedback onto the gametophore initiation process. To determine how WT and mutant phenotypes diverged during development, we imaged gametophore buds at 2-cell, 4-cell and a later stage of bud development [4] (Fig. 3F-T). Whilst WT gametophores initiated normally and showed characteristic oblique cell division plane orientations, the plane

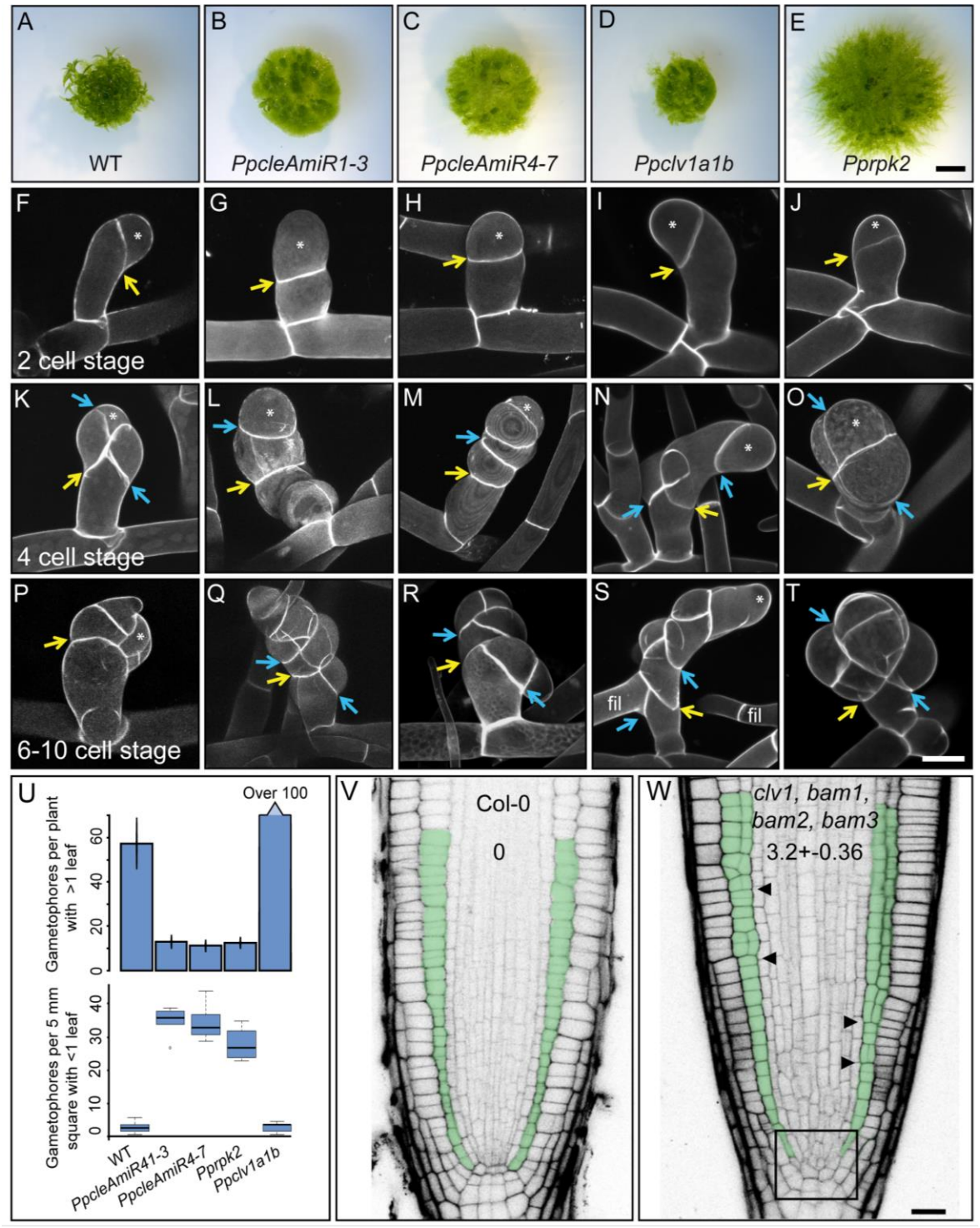
A
WT
B
PpcleAmiR1-3
C
PpcleAmiR4-7
D
Ppclv1a1b
E
Pprpk2
F
G
H
I
J
2 cell stage
K
L
M
N
O
4 cell stage
P
Q
R
S
T
fil
fil
6-10 cell stage
U
Over 100
Gametophores per plant with >1 leaf
0
20
40
60
Gametophores per 5 mm square with <1 leaf
0
10
20
30
40
WT
PpcleAmiR41-3
PpcleAmiR4-7
Pprpk2
Ppclv1a1b
V
Col-0
0
W
clv1, bam1, bam2, bam3
3.2+-0.36

Fig. 3. The CLV pathway regulates cell division plane orientations during 3D growth in *Physcomitrella* and *Arabidopsis*. See also Fig. S6 and Methods Figs. 2-4. (A-E) Whilst WT plants developed many normal gametophores, *PpcleAmiR1-3*, *PpcleAmiR4-7*, *Ppclv1a1b* and *Pprpk2* mutants had no obvious gametophores. Scale bars = 0.35 cm. (F-T) *PpcleAmiR1-3*, *PpcleAmiR4-7, Ppclv1a1b* and *Pprpk2* mutants have cell division plane defects at the onset of 3D morphogenesis. (F-J) The first division of each bud is indicated by a yellow arrow, and is set at a strongly oblique angle in WT plants, but is weakly oblique in (G) *PpcleAmiR1-3* and (H) *PpcleAmiR4-7* mutants. (K-O) Whereas (K) the second division (blue arrow) from the apical cell (asterisk) is normally oblique and roughly perpendicular to the first, in (L) *PpcleAmiR1-3*, (M) *PpcleAmiR4-7* and (N) *Ppclv1a1b* mutants it is roughly parallel to the first. (O) *Pprpk2* mutant (P) The stereotypical divisions that normally generate the tetrahedral shape of the gametophore apical cell at the 6-10 celled stage of development are mis-set in (Q) *PpcleAmiR1-3*, (R) *PpcleAmiR4-7* and *(*S) *Ppclv1a1b* and (T) *Pprpk2* mutants. Scale bar = 30 μm. (U) Bar chart and box plot showing that gametophore initiation was disrupted in *PpcleAmiR1-3*, *PpcleAmiR4-7, PpCLV1a1b* and *Pprpk2* mutants. The number of gametophores with > 1 leaf was counted in 5 WT and mutant plants from a single line representing each mutant class. Gametophore buds with < 1 leaf were counted from a 5 mm^2 area in 3 WT and mutant plants from a single line representing each mutant class. ANOVA, Tukey's HSD $p < 0.005$. (V, W) Confocal micrographs of WT (Col-0) and *clv1*/*bam1*/*bam2*/*bam3* mutant root tips showing disordered cell division plane orientations in the meristem and ground tissue layers. The box in (W) indicates the meristem and arrowheads indicate the developmental onset of

of the first division was strongly disrupted in *PpcleAmiR1-3* and *PpcleAmiR4-7* mutants, and it was set at a shallow angle relative to the main growth axis (compare Fig. 3F to Fig. 3G, H). A second round of cell division from the apical cell also had misset division planes that were frequently parallel rather than perpendicular to the first division plane, and a subset of gametophores therefore formed finger like projections in place of gametophores (compare Fig. 3K to Fig. 3L, M). At developmental stages where the tetrahedral shape of the apical cell is normally established [4], mutants also had defects indicating problems with growth and cell fate specification, appearing to reiterate divisions normally characteristic of the first gametophore initial (compare Fig. 3P to Fig. 3Q-R). *Ppclv1a1b* mutant phenotypes diverged from WT after the 2-cell stage, subsequently showing a similar pattern of division to *PpcleAmiR1-3* and *PpcleAmiR4-7* mutants (Fig. 3K, P-R), and some cells reverted to filament identity (Fig. 3S). *Pprpk2* mutant defects were less severe than *Ppcle* and *Ppclv1a1b* defects at the earliest developmental stages, and at later stages swollen cell shapes suggested growth defects as well as division plane defects (Fig. 3T). The mutant phenotypes above suggest key roles for the *Physcomitrella* CLV pathway in modulating cell division planes, cell fate, growth and proliferation during the 2D-3D developmental transition. The formation of long projections of swollen cells in *Ppcle* mutants (e.g. Fig. 3L, M)

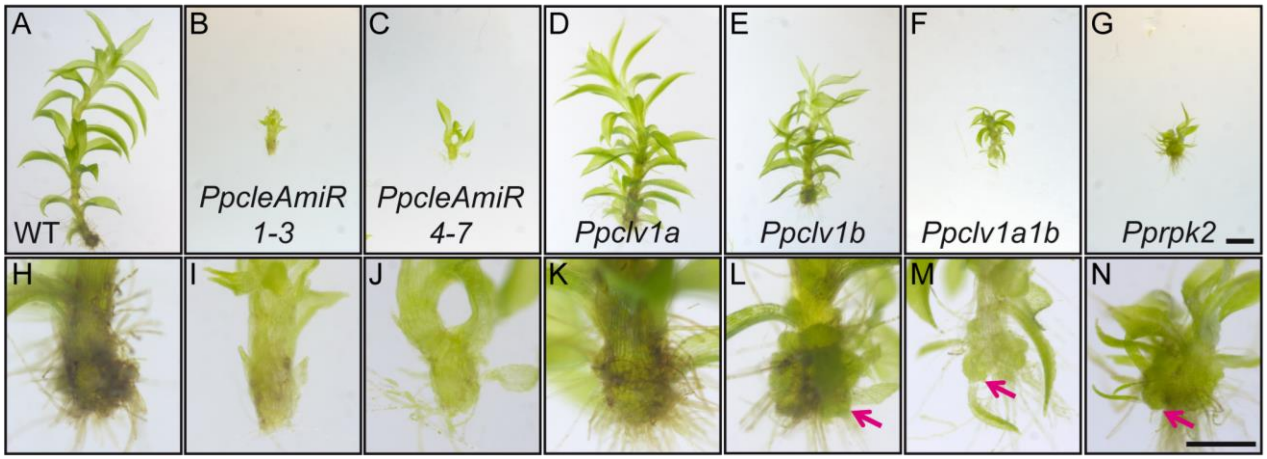

Fig. 4. Gametophore phenotypes in *PpAmiRcle*, *Ppclv1* and *Pprpk2* mutants. See also Methods Figs. 2-4. (A-G) Light micrographs of the largest gametophore dissected from 1 month-old plants showing height differences. Scale bar = 1 mm. (H-N) Light micrographs of gametophore bases showing overproliferation in *Ppclv1b*, *Ppclv1a1b* and *Pprpk2* mutants. Scale bar = 0.5 mm.

suggests that gametophore identity is attained normally, as cell swelling is a characteristic of gametophore rather than filament initials. The manifestation of plane orientation defects in the first division suggests that WT and mutant gametophore development diverge at the single-celled stage, after cell fate is specified. As roles for CLV in cell division plane orientation were previously unreported, we sought to identify conservation of function with *Arabidopsis*. To this end we examined *Arabidopsis clv1*/*bam1*/*bam2*/*bam3* quadruple mutant meristems in which the function of the entire *CLV*/*BAM* gene clade is lost [24]. Whereas division plane orientations are normally stereotypic in root meristems, we detected strongly disordered planes in the stem cell niche and ground tissue layers of *clv1/bam1/bam2/bam3* mutant roots (Fig. 3V, W, Fig. S6). Thus, a newly identified role for CLV in cell division plane orientation is conserved between *Physcomitrella* and *Arabidopsis*.

Loss-of-function data suggest that CLAVATA suppresses cell proliferation in Physcomitrella.

In *Arabidopsis* and other flowering plants, the CLV pathway is known for its role in maintaining cell proliferation at a constant level in the meristematic stem cell pool [25], and increases in the number of stem cells lead to highly-enlarged meristems in both *clv1* and *clv3* (*cle*) mutants. However, *Physcomitrella* does not fit the *Arabidopsis* paradigm of meristem function because the shoot apex comprises a single apical stem cell. The apical cell cleaves merophyte daughter cells in a spiral pattern, and merophytes subsequently divide to generate leaf initials and stem tissues [4]. To investigate whether roles for CLV in regulating stem cell

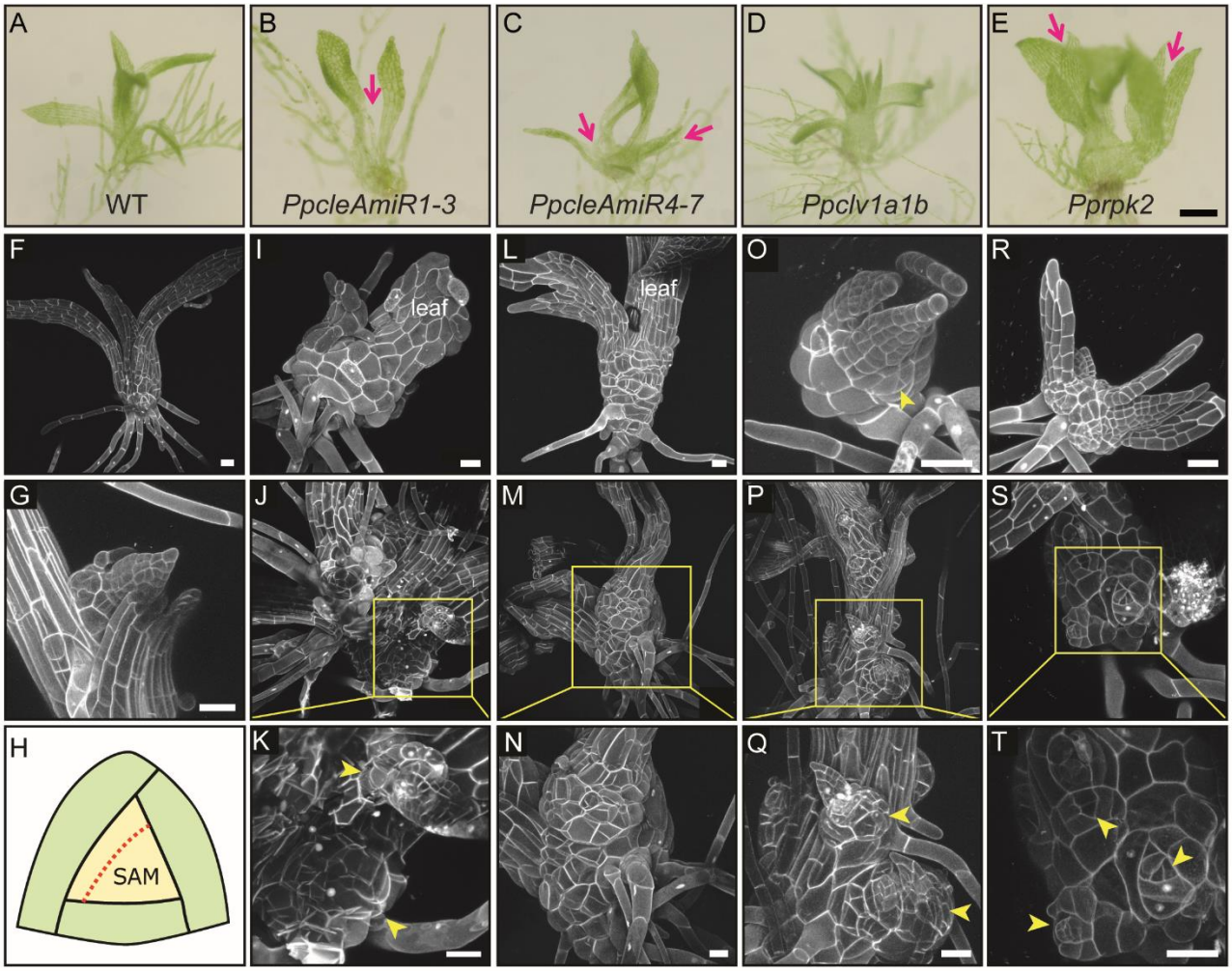

Fig. 5. Overproliferation phenotypes in *PpAmiRcle*, *Ppclv1* and *Pprpk2* mutants. See also Methods Figs. 2-4. (A-E) Light micrographs of mutant gametophore morphology showing that gametophores (B) arrest, (C and E) develop multiple axes and (C-E) develop swollen bases relative to (A) WT plants. Scale bar = 200 µm. (F, G) Confocal micrograhs showing (F) overall gametophore morphology and (G) a branch initiating in a leaf axil. (H) Schematic showing *Physcomitrella* gametophore apex organization with an apical cell (pale yellow) and rotating division plane orientations. (I-T) Confocal micrograhs showing (I-K) *PpcleAmiR1-3* mutant gametophore morphologies, with (I) overproliferation at the gametophore base and (J, K) disorganized growth with ectopic meristems. (L-N) *PpcleAmiR4-7* mutant gametophore morphologies with (L) split leaf phenotypes and (M, N) meristem overproliferation and termination. (O-Q) *Ppclv1a1b* mutant gametophore morphology, with multiple growth axes and multiple meristems at the gametophore base. (R-T) *Pprpk2* mutant gametophore morphology with multiple growth axes and multiple meristems at the gametophore base. Yellow arrowheads indicate regions of over proliferation or ectopic meristems. Yellow boxes show regions magnified in (J, M, P, S). Scale bars = 50 µm.

proliferation are conserved between *Physcomitrella* and *Arabidopsis*, we imaged the largest gametophores of 1 month-old WT and mutant plants using light and confocal microscopy and found that mutant gametophores were dwarfed to different degrees (Fig. 4). Whilst *PpcleAmiR1-3*, *PpcleAmiR4-7* and *Pprpk2* mutants were

most severely dwarfed (Fig. 4B, C, G), *Ppclv1a* and *Ppclv1b* mutants had milder defects (Fig. 4D, E). In contrast, *Ppclv1b*, *Ppclv1a1b* and *Pprpk2* mutants had strong proliferation and/or cell fate defects, developing a callus like mass at the gametophore base (Fig. 4L-N). Closer inspection revealed that these masses arose by the activity of many ectopic apical cells at the gametophore base (Fig. 5). These loss-of-function data suggest that CLV has roles in regulating stem cell proliferation and fate that are conserved between *Physcomitrella* and *Arabidopsis*.

CLE peptides can suppress cell proliferation in Physcomitrella gametophores.

To further assay conservation in CLV function, we undertook a gain-of-function approach by applying synthetic CLE peptides to growing plants (Fig. 6, Fig. S7). After 4 weeks of growth we found that treatment with a 1 μM concentration of CLE had no appreciable effect on plant spread or the number of gametophores initiating, indicating that protonemal development is normal (Fig. S7). However, whilst solute controls, a randomized peptide and CLE41 have no appreciable effect on gametophore development, CLV3 and all of the *Physcomitrella* CLEs cause gametophore dwarfing and a strong reduction in leaf size correlating with a reduction in leaf cell number (Fig. 6). Whilst this phenotype superficially resembles the stunted gametophore phenotypes of *PpcleAmiR1-3* and *PpcleAmiR4-7* mutants (Fig. 4B, C), we found no evidence of developmental arrest or meristematic over-proliferation following CLE application and no difference in the number of gametophores initiating was detected following CLE treatment (data not shown). These data show that CLEs act through a conserved signaling module to regulate cell proliferation specifically during the 3D growth phase in *Physcomitrella*.

CLE peptides can act through receptor components that are conserved between Physcomitrella and Arabidopsis

Previous studies in *Arabidopsis* have shown that application of CLV3-like but not TDIF-like CLEs to roots can arrest meristem function [26]. To assay conservation in peptide function, we germinated *Arabidopsis* seeds on MS plates containing solute or peptides at a 1 μM concentration. Whilst solute controls, a randomized peptide and CLE41 (a TDIF CLE) caused no arrest of root development, CLV3 and all of the *Physcomitrella* CLEs caused a significant reduction in root length in *Arabidopsis* resulting from collapse of the root meristem (Fig.

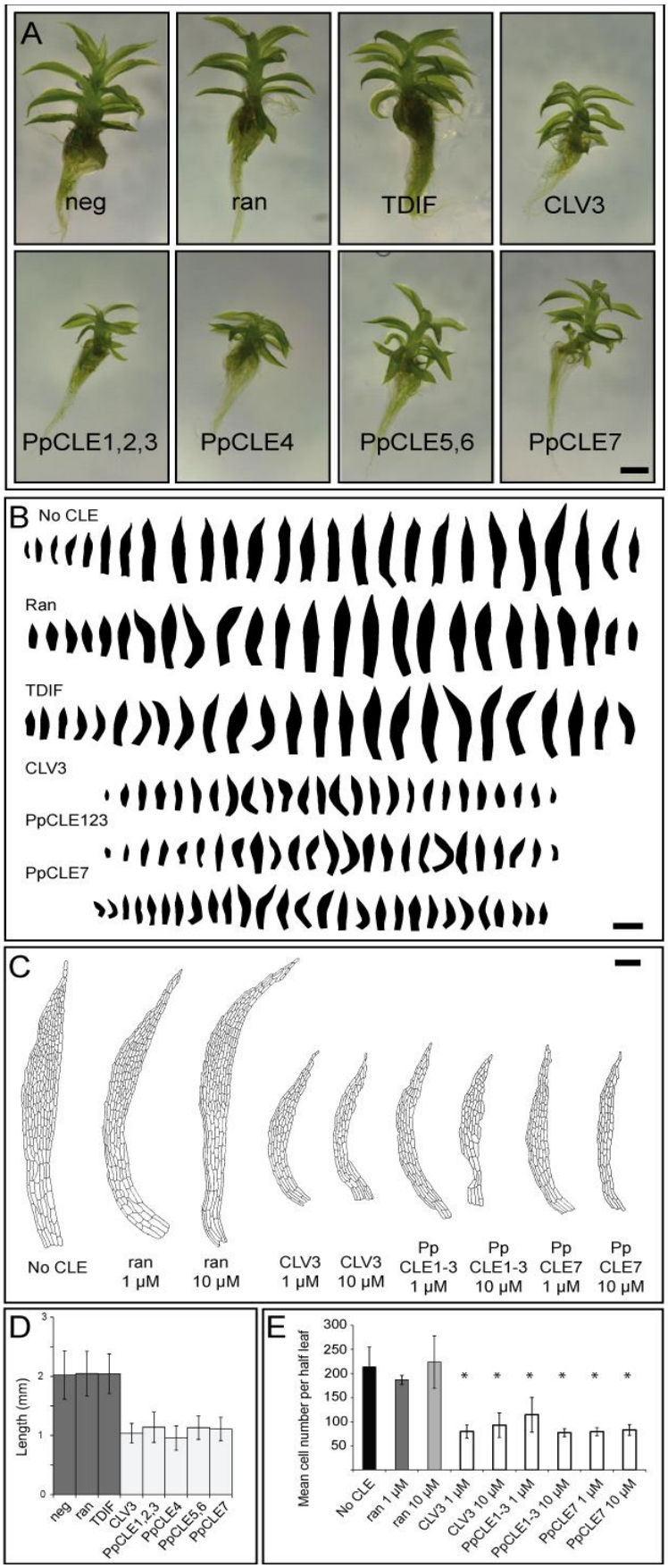

Fig. 6. *Physcomitrella* CLEs suppress cell proliferation. See also Fig. S7. (A) Treatment of *Physcomitrella* plants with 1 µM CLV3-like CLEs from *Arabidopsis* and *Physcomitrella*, but not TDIF-like CLEs, causes gametophore and leaf stunting. Scale bar = 100 µm. (B) Leaf series from gametophores treated with CLEs expressed during gametophore development. Scale bar = 1 mm. (C) Cell outlines of half leaves in CLE-treated gametophores (leaf 9 was used). Scale bar = 100 µm. (D) Height measured from ≥ 25 gametophores treated with CLEs ($n \geq 25$, ANOVA, Tukey's HSD $p < 0.005$). (E) Leaf 9 cell numbers in CLE treated half leaves ($n = 3$, ANOVA, Tukey's HSD $p<0.05$).

7A, B, E). *Physcomitrella* CLEs therefore regulate growth and proliferation in a similar manner to CLV3 in *Arabidopsis*. To confirm that PpCLEs can act through a conserved receptor machinery we used peptide treatment assays on *Arabidopsis* and *Physcomitrella rpk2* mutants (Fig. 7). Whilst treatment of WT *Arabidopsis* plants with CLV3-like peptides strongly inhibited root growth, *rpk2* mutants showed less growth inhibition when treated with *Arabidopsis* and *Physcomitrella* peptides (Fig. 7A, B). These data are in line with previously published results showing that RPK2 acts amongst other receptors to contribute to CLV signaling in *Arabidopsis* [15], and show that *Physcomitrella* CLEs can also act via RPK2 in *Arabidopsis*. To determine whether *Physcomitrella*

CLEs act via PpRPK2, we performed similar experiments in WT, *Ppcle* and *Pprpk2* mutant backgrounds. *Ppcle* mutant gametophores are roughly the same size as *Pprpk2* mutant gametophores and we reasoned that if PpCLEs act via PpRPK2 we should detect a response in *Ppcle* mutants but not *Pprpk2* mutants. As in previous experiments, we found strong inhibition of gametophore development in WT plants (Fig. 7C). Potentially due to lack of positional information, treatment of *Ppcle* mutants with CLE peptides did not rescue developmental defects, but nevertheless induced a gametophore dwarfing response, consistent with an intact receptor machinery (Fig. 7D, G-J). In contrast, *Pprpk2* mutants showed no morphological response to CLE application suggesting that PpCLEs act via PpRPK2 in regulating 3D growth (Fig. 7D, G-J).

Discussion

How might CLV pattern cell division plane orientation?

We propose that the CLV pathway regulates the 2D to 3D developmental transition in *Physcomitrella* by orienting gametophore cell division planes and regulating growth and fate. How ligands and receptors act together do this is not yet clear. One possibility is that CLE ligands diffuse to create a concentration gradient that division planes are patterned against, and a similar mechanism involving CLEs patterns cambial meristems in *Arabidopsis* [27]. CLE41 is synthesized in the phloem and diffuses to bind PXY receptors in neighboring procambial cells, thereby imparting spatial information for periclinal division [27]. Constitutive or ectopic expression of *CLE41* disrupts this positional information, resulting in disordered cambial division planes [27].

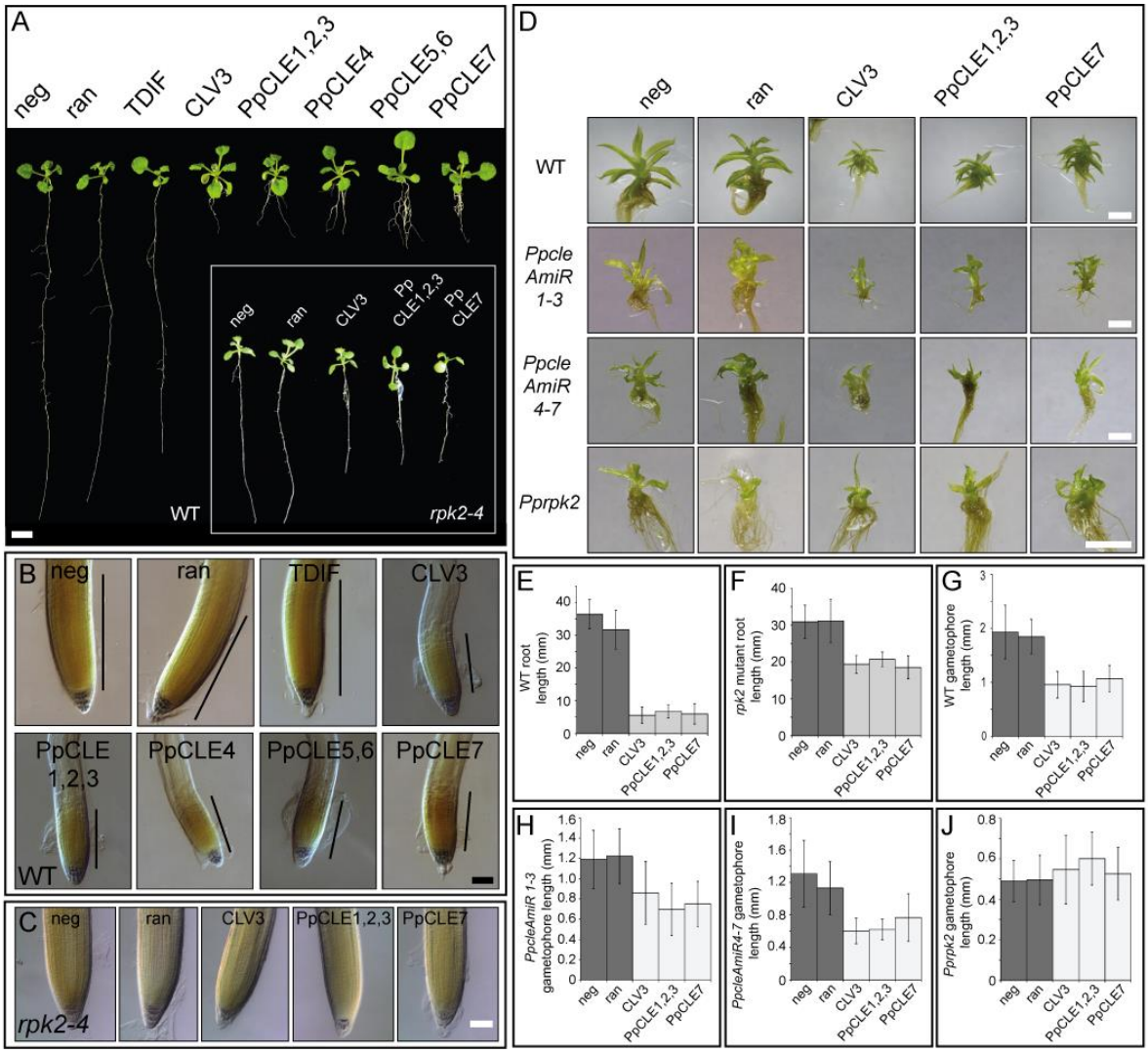

Fig. 7. *Physcomitrella* CLE peptides act via a conserved receptor machinery. (A and B) Treatment of *Arabidopsis* seedlings with 1µM CLV3-like CLEs from *Arabidopsis* and *Physcomitrella*, but not TDIF-like CLEs suppresses root meristem proliferation in WT *Arabidopsis* (n = 30, ANOVA, Tukey's HSD p<0.0005). Scale bar (A) = 1 cm, scale bars (B) = 100 µm, black bars in (B) represent approximate position and extent of root meristem. Inset in (A), and (C), *Arabidopsis rpk2-4* mutants are resistant to treatment with 1 µM CLE peptides, n ≥ 15, ANOVA, Tukey's HSD p < 0.0005. (D) Gametophores in plants treated with 10 µM CLEs are stunted in WT, *PpcleAmiR1-3* and *PpcleAmiR4-7* mutants but not *Pprpk2* mutants (n ≥ 20, ANOVA, Tukey's HSD p < 0.0005). (E, F) Quantitative data supporting inferences about root length images shown in (B). (G-J) Quantitative data supporting inferences about gametophore images shown in (D).

In *Physcomitrella*, similar patterning could be achieved by sub-cellular localization of receptors to create a graded CLV response in bud initials, or at later stages of development, patterning could be provided by receptor expression in different portions of buds. It is also possible that CLV signaling does not directly modulate cell division planes, but that CLV influences cell division planes via hormone signaling, cell geometry, and/or cell echanics. Auxin signaling and the activity of microtubule interacting proteins such as CLASPs are known to specify cell division planes in *Arabidopsis* embryos (Yoshida and new 3D MT paper)[28], and auxin signaling modulates the activity of previously identified factors necessary for correct division plane orientation in *Physcomitrella* buds including *DEK1* and *NOG1* [29, 30]. There appears to be a complex interplay between auxin cytokinin in *Physcomitrella* [31-33], and several phenotypes suggest that this interplay is disrupted in *Ppcle*, *Ppclv* and *Pprpk2* mutants. For instance, protonemal spread is perturbed in mutants (Fig. 3), cell fate and proliferation at the gametophore base are perturbed (Fig. 4, Fig. 5) and leaf cell proliferation is perturbed in plants treated with CLEs (Fig. 6), and these aspects of development are all auxin/cytokinin-regulated [31-33]. Linking CLV signaling to the hormone pathways regulating growth and fate will be important in unravelling mechanisms of cell division plane specification during 3D growth.

CLAVATA-regulated stem cell function is an ancestral feature of land plants

The data we present are important in two evolutionary contexts. First, they show that the CLV pathway originated with land plants, and that CLV-regulated stem cell proliferation and function is likely to be an ancestral feature of land plants. The acquired capacity of land plants to orient stem cell divisions in multiple planes enabled diversification by permitting plants to develop upright axes with organs arranged in multiple orientations, a crucial step in shoot evolution [1]. Stem cell division plane defects in *Ppcle* mutants specifically affect the transition to 3D growth and the 3D growth phase, and morphological responses to peptide application are also specific to the 3D growth phase. Thus, in an ancient land plant group, CLV regulates a developmental transition that mirrors an evolutionary transition. The data suggest that CLV was a genetic novelty for a key morphological innovation of land plants.

CLAVATA-regulated meristem functions originated prior to WOX- and KNOX-regulated meristem functions

Second, the data are important in the context of evolving gene regulatory networks for land plant meristem function. Whilst the first land plant meristems comprised a single gametophytic stem cell, the multicellular sporophyte meristems of vascular plants combine stem cell and more generally proliferative capacities [1]. Class I *KNOX* genes regulate meristematic proliferation in vascular plants [34, 35], but these roles are not shared between bryophytes and vascular plants. Moss *KNOX* (*MKN*) genes are primarily expressed in sporophyte tissues [23, 36], and whilst loss-of-function *mkn2* mutants have elongation defects in sporophytes, they have normal gametophytes [36]. *WOX* genes are key regulators of stem cell proliferation in *Arabidopsis* [17]. However, this function was acquired by the recently derived *WUS* gene clade [37, 38] and the downstream pathways regulated by CLV in *Physcomitrella* are likely to be distinct from those in *Arabidopsis* as *Ppwox13L* mutant gametophores develop normally [39]. Thus, Class I *KNOX*- and *WOX*-regulated meristem functions were both acquired after the bryophyte-vascular plant divergence. CLV was important in the origin of land plant meristem functions in the gametophyte stage of the life cycle, and we speculate that CLV was recruited to regulate stem cell function in the sporophyte stage of the life cycle prior to the origin of *KNOX*- and *WOX*-regulated meristem functions.

Acknowledgements:

CJH thanks the Gatsby Charitable Foundation (GAT2962) and the Royal Society for funding. JC thanks Santander and the Cambridge Overseas Trust for funding his Masters research. ZNV thanks the Gatsby Charitable Foundation for funding. ZLN and ADC thank NIH (R35GM119614-01) for funding. PS and MW thank the Swiss National Science Foundation (160004 and 131726 to PS), the URPP Evolution in Action (to PS) and Georges und Antoine Claraz-Schenkung (to PS and MW) for funding. We thank Takashi Ishida for *rpk2* mutant seed. We thank Christophe Dunand, Liam Dolan and Takayuchi Kohchi for access to *Spirogyra* and *Marchantia* genome data. We thank Tomoaki Nishiyama and Stefan Rensing for searching *Chara* genome data on our behalf. We thank Jon Hughes and Maureen Liu for preliminary expression analyses and Xiao Wang for help with plant transformation and screening.

Author contributions

Database searches (CDW, MW, PS, CJH), phylogenetic analyses (CDW, CJH), RT-PCR (CDW, CJH), *promoter::NGG* line generation and characterization (CDW, TA, YK, AC, SS, ZNV, CJH), *AmiRcle1-3* and *AmiRcle4-7* line generation and characterization (CDW, CJH), *Ppclv1a1b* mutant generation and characterization (JC, AHKR, MJS, CJH), *Pprpk2* mutant generation and characterization (JC, CDW, TA, AHKR, MJS, CJH), peptide application experiments (CDW, CJH), *Arabidopsis clv1/bam1/bam2/bam3* mutant analysis (ADC, ZLN), writing the manuscript (CJH) and editing the manuscript (CJH, CDW, JC, ZNV, TA, MJS, AHKR).

References

1. Harrison, C.J. (2017). Development and genetics in the evolution of land plant body plans. Philosophical Transactions of the Royal Society B *372*, e20150490.
2. Zimmermann, W. (1952). Main results of the 'Telome Theory'. The Palaeobotanist *1*, 456-470.
3. Graham, L.E., Cook, M.E., and Busse, J.S. (2000). The origin of plants: body plan changes contributing to a major evolutionary radiation. PNAS *97*, 4535-4540.
4. Harrison, C.J., Roeder, A.H.K., Meyerowitz, E.M., and Langdale, J.A. (2009). Local cues and asymmetric cell divisions underpin body plan transitions in the moss *Physcomitrella patens*. Current Biology *19*, 461-471.
5. Aoyama, T., Hiwatashi, Y., Shigyo, M., Kofuji, R., Kubo, M., Ito, M., and Hasebe, M. (2012). AP2-type transcription factors determine stem cell identity in the moss *Physcomitrella patens*. Development *139*, 3120-3129.
6. Brand, U., Grunewald, M., Hobe, M., and Simon, R. (2002). Regulation of CLV3 expression by two homeobox genes in *Arabidopsis*. Plant Physiology *129*, 565-575.
7. Reddy, G.V., and Meyerowitz, E.M. (2005). Stem-cell homeostasis and growth dynamics can be uncoupled in the *Arabidopsis* shoot apex. Science *310*, 663-667.
8. Ito, Y., Nakanomyo, I., Motose, H., Iwamoto, K., Sawa, S., Dohmae, N., and Fukuda, H. (2006). Dodeca-CLE peptides as suppressors of plant stem cell differentiation. Science *313*, 842-845.
9. Clark, S.E., Williams, R.W., and Meyerowitz, E.M. (1997). The *CLAVATA1* gene encodes a putative receptor kinase that controls shoot and floral meristem size in *Arabidopsis*. Cell *89*, 575-585.
10. Milani, P., Mirabet, V., Cellier, C., Rozier, F.d.r., Hamant, O., Das, P., and Boudaoud, A. (2014). Matching patterns of gene expression to mechanical stiffness at cell resolution through quantitative tandem epifluorescence and nanoindentation. Plant physiology *165*, 1399-1408.
11. Schoof, H., Lenhard, M., Haecker, A., Mayer, K.F., Jurgens, G., and Laux, T. (2000). The stem cell population of *Arabidopsis* shoot meristems in maintained by a regulatory loop between the *CLAVATA* and *WUSCHEL* genes. Cell *100*, 635-644.
12. Fletcher, J.C., Brand, U., Running, M.P., Simon, R., and Meyerowitz, E.M. (1999). Signalling of cell fate decisions by CLAVATA3 in *Arabidopsis* shoot meristems. Science *283*, 1911-1914.

13. Nimchuk, Z.L., Tarr, P.T., Ohno, C., Qu, X., and Meyerowitz, E.M. Plant stem cell signaling involves ligand-dependent trafficking of the CLAVATA1 receptor kinase. Current Biology *21*, 345-352.
14. Ogawa, M., Shinohara, H., Sakagami, Y., and Matsubayashi, Y. (2008). *Arabidopsis* CLV3 peptide directly binds CLV1 ectodomain. Science *319*, 294.
15. Kinoshita, A., Betsuyaku, S., Osakabe, Y., Mizuno, S., Nagawa, S., Stahl, Y., Simon, R., Yamaguchi-Shinozaki, K., Fukuda, H., and Sawa, S. (2010). RPK2 is an essential receptor-like kinase that transmits the CLV3 signal in *Arabidopsis*. Development *137*, 3911-3920.
16. Nimchuk, Z.L. (2017). CLAVATA1 controls distinct signaling outputs that buffer shoot stem cell proliferation through a two-step transcriptional compensation loop. PLOS Genetics *13*, e1006681.
17. Laux, T., Mayer, k.F.X., Berger, J., and Jurgens, G. (1996). The *WUSCHEL* gene is required for shoot and floral meristem integrity in *Arabidopsis*. Development *122*, 87-96.
18. Yadav, R.K., Perales, M., Gruel, J., Girke, T., Jönsson, H., and Reddy, G.V. (2011). WUSCHEL protein movement mediates stem cell homeostasis in the *Arabidopsis* shoot apex. Genes and Development *25*, 2025-2030.
19. Wickett, N.J., Mirarab, S., Nguyen, N., Warnow, T., Carpenter, E., Matascie, N., Ayyampalayam, S., Barker, M.S., Burleigh, J.G., Gitzendanner, M.A., et al. (2014). Phylotranscriptomic analysis of the origin and early diversification of land plants. PNAS *111*, E4859–E4868.
20. Cox, C.J., Li, B., Foster, P.G., Embley, M., and Civáň, P. (2014). Conflicting phylogenies for early land plants are caused by composition biases among synonymous substitutions. Systematic Biology *63*, 272-279.
21. Bowman, J.L., Kohchi, T., Yamato, K.T., Jenkins, J., Shu, S., Ishizaki, K., Yamaoka, S., Nishihama, R., Nakamura, Y., Berger, F., et al. (2017). Insights into land plant evolution garnered from the *Marchantia polymorpha* genome. Cell *171*, 287-304.
22. Ortiz-Ramírez, C., Hernandez-Coronado, M., Thamm, A., Catarino, B., Wang, M., Dolan, L., Feijó, J.A., and Becker, J.D. (2016). A transcriptome atlas of *Physcomitrella patens* provides insights into the evolution and development of land plants. Molecular Plant *9*, 205-220.
23. Frank, M.H., and Scanlon, M.J. (2015). Cell-specific transcriptomic analyses of three-dimensional shoot development in the moss *Physcomitrella patens.* Plant Journal *83*, 743-751.
24. Nimchuk, Z.L., Zhou, Y., Tarr, P.T., Peterson, B.A., and Meyerowitz, E.M. (2015). Plant stem cell maintenance by transcriptional cross-regulation of related receptor kinases. Development *142*, 1043-1049.
25. Somssich, M., Je, B.I., Simon, R.d., and Jackson, D. (2016). CLAVATA-WUSCHEL signaling in the shoot meristem. Development *143*, 3238-3248.
26. Fiers, M., Golemiec, E., Xu, J., van der Geest, L., Heidstra, R., Stiekema, W., and Liu, C.M. (2005). The 14-amino acid CLV3, CLE19, and CLE40 peptides trigger consumption of the root meristem in *Arabidopsis* through a CLAVATA2-dependent pathway. Plant Cell *17*, 2542–2553.
27. Etchells, J.P., and Turner, S.R. (2010). The PXY-CLE41 receptor ligand pair defines a multifunctional pathway that controls the rate and orientation of vascular cell division. Development *137*, 767-774.
28. Yoshida, S., Barbier¬†de¬†Reuille, P., Lane, B., Bassel, G.W., Prusinkiewicz, P., Smith, R.S., and Weijers, D. (2014). Genetic Control of Plant Development by Overriding a Geometric Division Rule. Developmental Cell *29*, 75-87.
29. Perroud, P.F., Demko, V., Johansen, W., Wilson, R.C., Olsen, O.A., and Quatrano, R.S. (2014). Defective Kernel 1 (DEK1) is required for three-dimensional growth in *Physcomitrella patens*. New Phytologist *203*, 794-804.

30. Moody, L.A., Kelly, S., Rabbinowitsch, E., and Langdale, J.A. (2018). Genetic regulation of the 2D to 3D growth transition in the moss *Physcomitrella patens*. Current Biology *28*, 473-478.e475.
31. Ashton, N.W., Grimsley, N.H., and Cove, D.J. (1979). Analysis of gametophytic development in the moss, *Physcomitrella patens*, using auxin and cytokinin resistant mutants. Planta *144*, 427-435.
32. Jang, G., Dolan, L. (2011). Auxin promotes the transition from chloronema to caulonema in moss protonema by positively regulating *PpRSL1* and *PpRSL2* in *Physcomitrella patens*. New Phytologist *192*, 319-327.
33. Coudert, Y., Palubicki, W., Ljung, K., Novak, O., Leyser, O., and Harrison, C.J. (2015). Three ancient hormonal cues co-ordinate shoot branching in a moss. eLIFE *4*, e06808.
34. Long, J.A., Moan, E.I., Medford, J.I., and Barton, M.K. (1996). A member of the KNOTTED class of homeodomain proteins encoded by the *STM* gene of *Arabidopsis*. Nature *379*, 66-69.
35. Harrison, C.J., Corley, S.B., Moylan, E.C., Alexander, D.L., Scotland, R.W., and Langdale, J.A. (2005). Independent recruitment of a conserved developmental mechanism during leaf evolution. Nature *434*, 509-514.
36. Sakakibara, K., Nishiyama, T., Deguchi, H., and Hasebe, M. (2008). Class 1 *KNOX* genes are not involved in shoot development in the moss *Physcomitrella patens* but do function in sporophyte development. Evolution and Development *10*, 555-566.
37. Nardmann, J., and Werr, W. (2012). The invention of *WUS*-like stem cell-promoting functions in plants predates leptosporangiate ferns. Plant Molecular Biology *78*, 123-124.
38. Dolzblasz, A., Nardmann, J., Clerici, E., Causier, B., van der Graaff, E., Chen, J., Davies, B., Werr, W., and Laux, T. (2016). Stem cell regulation by *Arabidopsis WOX* genes. Molecular Plant *9*, 1028-1039.
39. Sakakibara, K., Reisewitz, P., Aoyama, T., Friedrich, T., Ando, S., Sato, Y., Tamada, Y., Nishiyama, T., Hiwatashi, Y., Kurata, T., et al. (2014). *WOX13*-like genes are required for reprogramming of leaf and protoplast cells into stem cells in the moss *Physcomitrella patens*. Development *141*, 1660-1670.
40. Leliaert, F., Smith, D.R., Moreau, H., Herron, M.D., Verbruggen, H., Delwiche, C.F., and De Clerck, O. (2012). Phylogeny and molecular evolution of the green algae. Critical Reviews in Plant Sciences *31*, 1-46.
41. Ishikawa, M., Murata, T., Sato, Y., Nishiyama, T., Hiwatashi, Y., Imai, A., Kimura, M., Sugimoto, N., Akita, A., Oguri, Y., et al. (2011). *Physcomitrella* Cyclin-Dependent Kinase A links cell cycle reactivation to other cellular changes during reprogramming of leaf cells. The Plant Cell *23*, 2924-2938.
42. Ossowski, S., Schwab, R., and Weigel, D. (2008). Gene silencing in plants using artificial microRNAs and other small RNAs. The Plant Journal *53*, 674-690.
43. Eshed, Y., Baum, S.F., Perea, J.V., and Bowman, J.L. (2001). Establishment of polarity in lateral organs of plants. Current Biology *11*, 1251-1260.
44. Hellens, R.P., Edwards, E.A., Leyland, N.R., Bean, S., and Mullineaux, P.M. (2000). pGREEN: a versatile and flexible binary Ti vector for *Agrobacterium*-mediated plant transformation. Plant Molecular Biology *42*, 819-832.
45. Lopez-Obando, M., Hoffmann, B., Géry, C., Guyon-Debast, A., Téoulé, E., Rameau, C., Bonhomme, S., and Nogué, F. (2016). Simple and efficient targeting of multiple genes through CRISPR-Cas9 in *Physcomitrella patens*. G3: Genes|Genomes|Genetics *6*, 3647-3653.
46. Schaefer, D.G., Delacote, F., Charlot, F., Vrielynck, N., Guyon-Debast, A., Le Guin, S., Neuhaus, J.M., Doutriaux, M.P., and Nogué, F. (2010). RAD51 loss of function abolishes gene targeting and de-represses illegitimate integration in the moss *Physcomitrella patens*. DNA Repair *9*, 526–533.

47. Moody, L., Kelly, S., Coudert, Y., Nimchuk, Z., Harrison, C.J. and Langdale, J. (2018). Somatic hybridization provides segregating populations for the identification of causative mutations in sterile mutants of the moss *Physcomitrella patens*. New Phytologist *218*, 1270-1277.
48. Altschul, S.F., Gish, W., Miller, W., Myers, E.W., and Lipman, D.J. (1990). Basic local alignment search tool. Journal of molecular biology *215*, 403-410.
49. Petersen, T.N., Brunak, S.r., von Heijne, G., and Nielsen, H. (2011). SignalP 4.0: discriminating signal peptides from transmembrane regions. Nature Methods *8*, 785.
50. Kumar, S., Stecher, G., and Tamura, K. (2016). MEGA7: Molecular Evolutionary Genetics Analysis Version 7.0 for Bigger Datasets. Molecular Biology and Evolution *33*, 1870-1874.
51. Haeussler, M., Schönig, K., Eckert, H., Eschstruth, A., Mianné, J., Renaud, J.-B., Schneider-Maunoury, S., Shkumatava, A., Teboul, L., Kent, J., et al. (2016). Evaluation of off-target and on-target scoring algorithms and integration into the guide RNA selection tool CRISPOR. Genome Biology *17*, 148.
52. Murashige, T., and Skoog, F. (2006). A revised medium for rapid growth and bioassays with tobacco tissue cultures. Physiologica Plantarum *15*, 473-497.
53. Ashton, N.W., and Cove, D.J. (1977). The isolation and preliminary characterisation of auxotrophic and analogue resistant mutants of the moss, *Physcomitrella patens*. Molecular and General Genetics *154*, 97-95.
54. Kinoshita, A., Nakamura, Y., Sasaki, E., Kyozuka, J., Fukuda, H., and Sawa, S. (2007). Gain-of-function phenotypes of chemically synthetic CLAVATA3/ESR-related (CLE) peptides in *Arabidopsis thaliana* and *Oryza sativa*. Plant and Cell Physiology *48*, 1821-1825.
55. Miwa (2009). Evolution of CLE signaling. Plant Signalling and Behaviour *4*, 477-481.
56. Mortier, V., Den Herder, G., Whitford, R., Van de Velde, W., Rombauts, S., D'Haeseleer, K., Holsters, M., and Goormachtig, S. (2010). CLE peptides control *Medicago truncatula* nodulation locally and systemically. Plant Phsiology *153*, 222-237.
57. Schmutz, J., Cannon, S.B., Schlueter, J., Ma, J., Mitros, T., Nelson, W., Hyten, D.L., Song, Q., Thelen, J.J., Cheng, J., et al. (2010). Genome sequence of the palaeopolyploid soybean. Nature *463*, 178-183.
58. Strabala, T.J., Phillips, L., West, M., and Stanbra, L. (2014). Bioinformatic and phylogenetic analysis of the CLAVATA3/EMBRYO-SURROUNDING REGION (CLE) and the CLE-LIKE signal peptide genes in the Pinophyta. BMC Plant Biology *14*.
59. Rensing, S.A. (2008). The *Physcomitrella* genome reveals evolutionary insights into the conquest of land by plants. Science *319*, 64-68.
60. Rojo, E., Sharma, V.K., Kovalev, V., Raikhel, N.V., and Fletcher, J.C. (2002). CLV3 is localized to the extracellular space, where it activates the *Arabidopsis* CLAVATA stem cell signaling pathway. Plant Cell *14*, 969-977.
61. Nielsen, H., Engelbrecht, J., Brunak, S., and von Heijne, G. (1997). Identification of prokaryotic and eukaryotic signal peptides and prediction of their cleavage sites. Protein Engineering *10*, 1-6.
62. Goad, D.M., Zhu, C., and Kellogg, E.A. (2017). Comprehensive identification and clustering of *CLV3/ESR*-related (CLE) genes in plants finds groups with potentially shared function. New Phytologist *216*, 605-616.
63. Lang, D., Ullrich, K.K., Murat, F., Fuchs, J., Jenkins, J., Haas, F.B., Piednoel, M., Gundlach, H., Van Bel, M., Meyberg, R., et al. The *P. patens* chromosome-scale assembly reveals moss genome structure and evolution. The Plant Journal, *93* 525-533.
64. Oelkers, K., Goffard, N., Weiller, G.F., Gresshoff, P.M., Mathesius, U. and Frickey, T. (2008). Bioinformatic analysis of the CLE signaling peptide family. BMC Plant Biology *8*, 1

65. Ran, F.A., Hsu, P.D., Wright, J., Agarwala, V., Scott, D.A., and Zhang, F. (2013). Genome engineering using the CRISPR-Cas9 system. Nature Protocols *8*, 2281.
66. Schaefer, D., Zryd, J.P., Knight, C.D., and Cove, D.J. (1991). Stable transformation of the moss *Physcomitrella patens*. Mol Gen Genet *226*, 418-424.
67. Abràmoff, M.D., Magalhães, P.J., and Ram, S.J. (2004). Image processing with ImageJ. Biophotonics International *11*, 26-42.
68. Barker, E.I., and Ashton, N.W. (2013). Heteroblasty in the moss, *Aphanoregma patens* (*Physcomitrella patens*), results from progressive modulation of a single fundamental leaf developmental programme. Journal of Bryology *35*, 185-196.
69. Willemsen, V., Wolkenfelt, H., de Vrieze, G., Weisbeek, P., and Scheres, B. (1998). The *HOBBIT* gene is required for formation of the root meristem in the *Arabidopsis* embryo. Development *125*, 521-531.

STAR METHODS

KEY RESOURCES TABLE

REAGENT or RESOURCE	SOURCE	IDENTIFIER
Bacterial and Virus Strains		
E. coli strain DH5α	Widely distributed	N/A
E. coli strain DB3.1	Widely distributed	N/A
E. coli strain DH10B	Widely distributed	N/A
Chemicals, Peptides, and Recombinant Proteins		
Taq polymerase	Widely available	N/A
Phusion High-Fidelity DNA polymerase	ThermoFisher	Cat#F530S
Novagen KOD Hot Start polymerase	Sigma-Aldrich	Cat#71086
Superscript II reverse transcriptase	ThermoFisher	Cat#18064022
Restriction enzymes for cloning	New England Biolabs	N/A
DNase	Fermentas	Cat#EN0525
MS medium	Melford	Cat#M0221
Plant agar	Duchefa	Cat#P1001
Driselase (basidiomycetes sp.)	Sigma-Aldrich	Cat#8037
Polyethylene glycol (PEG) 6000	Sigma-Aldrich	Cat#81255
G418 disulphate	Melford	Cat#G0175
Hygromycin B	Melford	Cat#H7502
Blasticidin S	Melford	Cat#B1220
α-32P dCTP	GE Healthcare	Cat#PB10205
X-GlcA	Melford	Cat#MB1021
Propidium iodide	Sigma-Aldrich	Cat#P4864
Synthetic CLE peptides (95% purity)	Genecust	N/A
Lugol's stain	Fisher Scientific	Cat#12801823
Critical Commercial Assays		
RNeasy RNA extraction kit	QIAGEN	Cat#74104
Plasmid Plus Midi kit	QIAGEN	Cat#12943
Amersham Rediprime II DNA labelling kit	GE Healthcare	Cat#RPN1633
Dig-High Prime DNA labeling and detection starter kit	Sigma-Aldrich	Cat#11585614910
Dig Easy Hyb	Sigma-Aldrich	Cat#11585762001
Experimental Models: Organisms/Strains		
Physcomitrella patens Gransden	Widely available	N/A
PpCLE1::NGG line	This study	N/A
PpCLE2::NGG line	This study	N/A
PpCLE7::NGG line	This study	N/A
PpCLV1a::NGG line	This study	N/A
PpCLV1b::NGG line	This study	N/A
PpRPK2::NGG line	This study	N/A
PpcleamiR1-3 mutant	This study	N/A
PpcleamiR4-7 mutant	This study	N/A
Ppclv1a mutant	This study	N/A
Ppclv1b mutant	This study	N/A
Ppclv1ab double mutant	This study	N/A

Pprpk2 mutant	This study	N/A
Arabidopsis thaliana Col-0	Widely available	N/A
Arabidopsis thaliana rpk2-4 mutant	[15]	N/A
Arabidopsis thaliana clv1,bam1,bam2,bam3 mutant	[24]	N/A
Oligonucleotides		
A list of oligonucleotides is given in Table S6	N/A	N/A
Recombinant DNA		
PIG1NGGII construct	[41]	N/A
PpCLE1::NGG construct	This study	N/A
PpCLE2::NGG construct (NptII)	This study	GenBank: 310732, MH310732
PpCLE7::NGG construct	This study	N/A
PpCLV1a::NGG construct	This study	N/A
PpCLV1b::NGG construct	This study	N/A
PpRPK2::NGG construct (AphIV)	This study	GenBank: MH310733
pRS300	[42]	N/A
pGREEN (Hyg)	pgreen.ac.uk	N/A
pGREEN (Kan)	pgreen.ac.uk	N/A
pBJ36	[43]	N/A
pBRACT211	[44]	N/A
pJH125	This study	N/A
pJH131	This study	N/A
PpcleAmiR1-3 construct	This study	N/A
PpcleamiR4-7 construct	This study	N/A
U3::Ppclv1a sgRNA5 construct	This study	N/A
U3::Ppclv1a sgRNA7 construct	This study	N/A
U6::Ppclv1b sgRNA construct	This study	N/A
pACT::Cas9 construct	[45]	N/A
pNRF	[46]	N/A
pBHRF108	[47]	N/A
pDONR2.1®	Invitrogen	N/A
pGEMT-EASY®	Promega	Cat#A1360
Software and Algorithms		
tBLASTn	[48]	N/A
SignalP	[49]	v4.0
MEGA	[50]	v7.0.26
Figtree	tree.bio.ed.ac.uk/software/	v1.4.3
AmiR design software	wmd3.weigelworld.org	N/A
CRISPR design software	[51]	crispor.tefor.net/
ImageJ	Imagej.net	V1.4.8
Adobe Photoshop	Adobe	N/A
Adobe Illustrator	Adobe	N/A

CONTACT FOR REAGENT AND RESOURCE SHARING

Further information and requests for resources and reagents should be directed to and will be fulfilled by the Lead Contact, Jill Harrison (jill.harrison@bristol.ac.uk). Please note that the transfer of transgenic materials will be subject to MTA and any relevant import permits.

EXPERIMENTAL MODELS AND SUBJECT DETAILS

Arabidopsis plant growth

Columbia (Col-0), *rpk2-4* (*cli*) or *clv1*/*bam1*/*bam2*/*bam3* mutants [15, 24] were used for *Arabidopsis* experiments. Homozygous *rpk2-4* mutants were confirmed using a BamHI dCAPs screen with a PCR fragment amplified using primers AtRPK2-BamHIF and AtRPK2-BamHIR (see primer list). Seeds were surface sterilised in 5 % (v/v) sodium hypochlorite for 10 minutes and washed three times with sterile de-ionised water. They were then stratified at 4 °C in darkness for 48 hours and sown on 0.5 X MS plates containing 0.8 % agar [52]. Plants were grown vertically for 7 days at 25 °C in a 16 hour light/ 8 hour dark cycle prior to observation (*rpk2* experiments) or at 22 °C under continuous light (*clv1*/*bam1*/*bam2*/*bam3* experiments).

Physcomitrella plant growth

The Gransden strain of *Physcomitrella patens* [53] was used for all experiments. Plants were grown in sterile culture on BCDAT plates at 23 °C in continuous light at 30-50 µmols^{-1} in Sanyo MLR-351 growth cabinets. BCDAT medium comprises 250mg/L $MgSO_4.7H_2O$, 250mg/L KH_2PO_4 (pH6.5), 1010mg/L KNO_3, 12.5mg/L, $FeSO_4.7H_2O$, 0.001% Trace Element Solution (0.614mg/L H_3BO_3, 0.055mg/L $AlK(SO_4)2.12H_2O$, 0.055mg/L $CuSO_4.5H_2O$, 0.028mg/L KBr, 0.028mg/L LiCl, 0.389mg/L $MnCl_2.4H_2O$, 0.055mg/L $CoCl_2.6H_2O$, 0.055mg/L $ZnSO_4.7H_2O$, 0.028mg/L KI and 0.028mg/L $SnCl_2.2H_2O$), 0.92g/L $C_4H_{12}N_2O_6$ and 8g/L agar with $CaCl_2$ added to a 1mM concentration after autoclaving. Protonemal cultures for transformation were grown on BCDAT plates overlaid with autoclaved cellophane disks and molecular and phenotypic analyses were undertaken using 1 mm spot cultures unless otherwise stated.

METHOD DETAILS

Sequence retrieval

CLE genes

Previously described *Arabidopsis thaliana* and *Oryza sativa CLE* sequences were respectively retrieved from TAIR and RAP-DB [54]. *Selaginella moelendorffii* [55], *Glycine max* [56, 57] and *Picea abies* [58] *CLE*s were retrieved from NCBI. To extend taxon sampling within land plants and identify previously unknown *CLE*s, the CLE domains of *Arabidopsis thaliana* CLV3 and CLE41 were used as tBLASTn queries with an e-value cutoff of e^{-100} to screen transcriptome or draft genome assemblies of a basal angiosperm (*Amborella trichopoda*), a fern (*Diplazium wichurae*), a hornwort (*Anthoceros agrestis*), a moss (*Physcomitrella patens* v1.6 [59]) and a liverwort (*Marchantia polymorpha*). Positive hits were used in reciprocal BLASTs until no new sequences were retrieved. All sequences retrieved were checked for the presence of a signal peptide [60] using SignalP [49, 61]. Newly identified CLE sequences were named with a two-letter prefix denoting the genus and species and numbered (Table S1). A recent cluster analysis [62] succeeded our analyses with slight variation in CLE numbers between species for reasons explained in Goad *et al*. (2017). An updated version of the *Physcomitrella* genome (v 3.1 [63]) also succeeded our analyses, and this includes two further *PpCLE*s that encode the same CLE motif as PpCLEs 1, 2 and 3. Whilst these were not included in this study, V3 gene IDs including *PpCLE8* and *PpCLE9* are listed in Table S5. Transcriptomes and draft or complete genomes of charophyte (*Coleochaete nitellarum, Spirogyra* sp., *Chara braunii*) and chlorophyte algae (*Ulva linza, Chlamydomonas reinhardtii*, *Volvox carteri*, *Ostreoscoccus tauri* and *Chlorella vulgaris*) were also searched but no *CLE*s were found. A previously annotated *Chlamydomonas reinhardtii CLE* [64] was re-analysed and discarded due to lack of similarity to other *CLE*s and a premature in-frame stop codon. A full list of taxa and databases searched is given in Table S4.

CLV1/RPK2 genes

Arabidopsis CLV1 and RPK2 sequences were used to query the databases listed above using tBLASTn searches with an e-value cut-off of e^{-1000}. As the LRR-Receptor kinase family is large, only sequences that retrieved *CLV1* or *RPK2* as a top hit in reciprocal BLASTs to *Arabidopsis* were used in further analyses. Newly identified *CLV1*-like and *RPK2*-like genes were named with a two-letter prefix denoting the genus and species and given an alphabetical epithet (Table S2 and Table S3 respectively). A list of taxa searched is given in Table S4.

Phylogenetic reconstruction

To infer CLE relationships, the conserved 12 amino acid CLE motif from 193 *CLE*s was used in neighbour joining reconstructions compiled with the JTT model in MEGA7.0.26 [50] (Fig. S1, Supplementary dataset 1). This approach was taken because there is little conservation in CLE structure outside the CLE motif, and so few characters can only yield limited phylogenetic signal (see [62]). To infer CLV/BAM relationships, 525 conserved amino acid residues from 36 genes were used in maximum likelihood reconstructions with the JTT model in MEGA7.0.26 [50] (Fig. S2, Supplementary dataset 2). To infer RPK2 relationships, 782 conserved amino acid residues from 18 genes were used in maximum likelihood reconstructions with the JTT model in MEGA7.0.26 [50] (Fig. S3, Supplementary dataset 3). For all analyses 100 bootstrap replicates were performed and support values over 50 % (CLE tree) or 70 % (CLV1/BAM and RPK2 trees) are represented above the branches.

Molecular biology

RT-PCR

Total RNA was isolated from 4 day-old protonemal cultures and 10, 21 or 28 day old spot cultures using the QIAGEN RNeasy™ method. RNA was DNase treated prior to reverse transcription with SuperScript® II following manufacturer's guidelines. Semi-quantitative RT-PCR was undertaken using *UBIQUITIN* (Pp1s56_52V6.1) as a loading control. Where possible, primers were designed to span introns to detect genomic contamination, and sequences are listed in Table S6.

Genomic DNA extraction

Genomic DNA was extracted from protonemal cultures using a CTAB (Hexadecyltrimethylammonium bromide) protocol. Snap-frozen tissue was ground in liquid nitrogen and transferred to tubes containing prewarmed extraction buffer (2 % CTAB, 1.4 M NaCl, 100 mM Tris pH8.0, 20 mM EDTA pH8.0, 2 % PVP), with no more than 100 mg of tissue per mL of buffer. Samples were incubated for 10 minutes at 65 ˚C and an equal volume of 24:1 chloroform:isoamyl alcohol was added and mixed with each sample to form an emulsion. The tubes were centrifuged at high speed (>10,000 rpm) for 10 minutes, and the aqueous phase was transferred to a fresh tube prior to DNA precipitation with an equal volume of isopropanol and repeated centrifugation.

DNA was washed with 70 % ethanol and dissolved in water, 10 mM Tris pH 8.0 or 10 mM Tris pH 8.0 with 1 mM Na_2EDTA.

Generation of promoter::NGG constructs

Promoter sequences from *PpCLE1* (2.1 kbp), *PpCLE2* (2.1 kbp), *PpCLE7* (2 kbp), *PpCLV1a* (2 kbp), *PpCLV1b* (2.8 kbp) and *PpRPK2* (1.4 kbp) were PCR amplified using a proof-reading Taq polymerase and primers listed elsewhere and cloned directly or via pGEMT® Easy into the SmaI site of PIG1NGGII [41] or derivatives with alternative selection cassettes and sequenced prior to linearization and transformation as illustrated in Methods Fig. 1.

Generation of AmiR constructs

To generate *PplcleAmiR1-3* and *PplcleAmiR4-7* constructs, resistance cassettes from pGREEN [44] were first inserted into a blunt-ended HindII site of pBJ36 [43]. A soybean *UBIQUITIN* promoter from pBRACT211 [44] was inserted into the SmaI site to drive AmiRNA expression and the resultant plasmids were named pJH125 (KanR) and pJH131 (HygR). AmiRNAs were designed according to [42], generated by degenerate PCR using a proof-reading Taq polymerase and the pRS300 plasmid as a template, cloned into pGEMT-EASY® and transferred as XmaI/BamHI fragments into pJH125 or pJH131. Silencing constructs were checked by sequencing and digested with SacI for transformation as illustrated in Methods Fig. 2.

Generation of CRISPR constructs

Small cassettes containing two BsaI restriction sites and sgRNAs [65] driven by the moss U3 or U6 promoter and flanked by *attB* sites were synthesized and cloned into pDONR™201. sgRNA sequences were selected and screened for off target hits in the *Physcomitrella* V3 genome using crispor.tefor.net/. To clone guide RNAs into expression cassettes, two primers consisting of guide sequences with overhangs for U3 and U6 promoters were annealed and ligated into U3 or U6 expression vectors pre-digested with BsaI. Constructs were checked by sequencing and co-transformed with *pACT::Cas9* [45] to engineer mutants as illustrated in Methods Fig. 3.

Generation of RPK2 KO construct

5' and 3' flanking regions were PCR amplified with a proof-reading Taq polymerase and cloned sequentially into pGEMT-EASY® using primers listed in Table S6. The resultant plasmid was digested with PmeI and AscI,

and the AphIV cassette from pBHRF-108 [47] was ligated between *PpRPK2* flanking regions. This plasmid was checked by sequencing and linearized for transformation as illustrated in Methods Fig. 4.

Transgenic line generation and phenotype analyses

Moss transformation and line authentication

For gene targeting and AmiR approaches, 10-20 µg of plasmid DNA was isolated using the QIAGEN Plasmid Plus Midi™ system and linearized as illustrated in Methods Figs. 1, 2 and 4. For CRISPR approaches, 5-7 µg of Cas9 and pNRF, and 2-3 µg of each gRNA-expressing construct were purified and pooled for transformation [45] at a concentration of at least 1 µg per µL. All solutions for the transformation procedure were prepared prior to commencing transformation [66]. First, a polyethylene glycol (PEG) solution was prepared by adding 10 mL of mannitol/$CaNO_3$ solution (8 % mannitol, 0.1 M $Ca(NO_3)$, 10 mM Tris pH7.2) to 2 g of molten PEG 6000, and the tube containing the solution was left in a water bath at 45 ˚C. To isolate protoplasts, homogoenous protonemal cultures were grown for 5 days to a week post passage. A 1 % driselase solution was prepared in 25 mL 8 % mannitol, and the supernatant was removed and filter sterilized into to a clean 50 mL falcon tube following centrifugation. Tissue from 4-6 plates was transferred into the driselase solution and the tissue suspension was left for 30-40 minutes with intermittent mixing to allow cell wall digestion. The mixture was then transferred into a fresh tube through a 50 µm filter to remove cell and cell wall debris. Protoplasts were sedimented by centrifugation for 3 minutes at 120 g, resuspended and washed three times in 10 mL of 8.0 % mannitol prior to counting with a haematocytometer. Protoplasts were then sedimented and resuspended to a density of 1.2 x 10^6 per mL in MMM solution (0.5 M mannitol, 0.15 M $MgCl_2$ and 0.1 % MES pH5.6). 300 µL aliquots of protoplasts were dispensed into falcon tubes prior to addition of DNA and 300 µL PEG solution, and cells were then heat shocked for 5 minutes at 45 ˚C. Transformation mixtures were progressively diluted with 1 mL of 8 % mannitol solution and washed. Protoplasts were then sedimented by centrifugation as above and washed four more times. After the final wash and spin, protoplasts were resuspended in 5 mL liquid BCD medium (constituents as specified above but without ammonium tartrate or agar) with 8 % mannitol, 10 mM $CaCl_2$ and 0.5 % glucose, wrapped in aluminium foil and left at 23 ˚C overnight. The next day, the protoplast suspension was plated onto BCDAT plates overlain with cellophane and containing 8 % mannitol and 5 g/L

glucose, using c.1 mL per plate. Plants were grown under standard conditions until regenerants comprised 10-20 cells. Cellophane discs were then transferred onto BCDAT plates containing antibiotics for selection (25 µg/ml Hyg, 50 µg/ml G418, 100µg/ml BSD). Plants were grown for 2 weeks on selection plates prior to transfer onto BCDAT plates lacking antibiotic for 2 weeks and then back on to selection plates for a further 2 weeks. All lines were screened by PCR, RT-PCR, Southern analysis or sequencing as illustrated in Methods Figs. 1-4. PCR conditions were standard and primer sequences are listed in Table S6.

Southern hybridization

For *PpcleAmiR* Southerns, 10-15 µg genomic DNA was digested with EcoRV and fractionated in 0.8 % agarose by gel electrophoresis. DNA in each gel was depurinated with 0.2 M HCl for 20 minutes and denatured with 0.4 M NaOH for 20 minutes prior to neutralisation for 20 minutes in a solution containing 3 M NaCl and 1 M Tris pH 7.5. Gels were inverted onto a Whatman paper wick inserted into a bath of 20 X SSC solution, and DNA was transferred onto a nitrocellulose membrane by overnight Southern blotting. DNA was UV crosslinked to the membrane and the membrane was rinsed in water prior to immersion in pre-hybridisation solution (3 X SSC, 1 % SDS, 0.1 % sodium pyrophosphate, 5 X Denhardt's and 200 µg per mL sheared salmon sperm DNA). The probe template was excised with EcoRV and BamHI from the *PpcleAmiR1-3* construct and the probe was synthesized using an Amersham Rediprime II DNA labelling kit as per manufacturer's instructions. Hybridization was undertaken in a 3 X SSC buffer at 58 ˚C and this was followed by two 20 minute washes at 58 ˚C in 3 X SSC and 2 X SSC buffers respectively. Membranes were wrapped in Saran Wrap and used to expose X-ray film, and film was then developed using a film processor. For *promoter::NGG* and *Pprpk2* Southerns, 2.5-3 µg genomic DNA was digested as illustrated in Methods Fig. 1 and Methods Fig. 4. Probe templates comprising *PIG1* flanking sequence, *PpRPK2* coding sequence or a hygromycin resistance cassette were PCR amplified and labeled using the Roche DIG High Prime™ system. Hybridization was undertaken overnight at 42 ˚C using the Roche DIG Easy Hyb™ system. Washing and detection were performed using the manufacturer's protocol from the Roche DIG High Prime DNA labeling and Detection Starter kit II™.

Physcomitrella plant imaging

To assess whole plant and gametophore phenotypes, 4 to 5 week-old spot cultures were imaged using a Keyence VHX-1000E digital microscope with a 20-50 X or 50-200 X objective. To analyse leaf phenotypes, leaves were removed form gametophores, arranged in heteroblastic series, cleared in 1% chloral hydrate overnight, washed in deionised water and treated with 2M NaOH for two hours. They were then washed with water and stained with 0.05% toluidine blue for two minutes before destaining for 10 minutes in water. The stained leaves were then mounted on a slide under a coverslip and imaged to visualise cell outlines. Adobe Illustrator™was used to trace leaf outlines to produce silhouettes for illustration purposes (Fig. 6). Quantitative analyses of leaf size were performed using ImageJ, and cell numbers were evaluated using the 'analyze particles' option [67]. Leaf size comparisons were undertaken using leaves from the same point in the heteroblastic leaf series [68] as stipulated in figure legends.

Arabidopsis *plant imaging*

Root length was scored from scanned images of plants grown on ½ X MS plates using ImageJ [67]. To visualise *rpk2* meristems, roots were stained with Lugol's stain, cleared, and imaged using a 20 X objective on a Leica DMRXA microscope with DIC [69]. *clv1*/*bam1*/*bam2*/*bam3* roots were stained with 15 mM propidium iodide and imaged using a C-Apochromat 40 X/1.20 W Korr objective on a Zeiss LSM710 microscope. Excitation and emission windows for propidium iodide were 560 nm and 566-719 nm respectively. Confocal images were analyzed and processed using ImageJ and Adobe Photoshop™.

GUS staining and imaging

Moss plants grown on BCDAT were cut out of plates with agar and incubated at 37 ºC in a 100 mM phosphate buffer with 10 mM Tris pH8.0, 1 mM EDTA pH8.0, 0.05 % Triton X100, 1 mg/mL X-GlcA (5-Bromo-4-chloro-3-indolyl-ß-D-glucuronic acid) and potassium ferri/ferrocyanide using concentrations and times indicated in Fig. 2 and legend. Plants were bleached in 70% ethanol and dissected and mounted in 0.3 % low melting point agarose prior to imaging with a Keyence VHX-1000 digital microscope with a 0-50 X or 50-200 X objective.

CLE peptide application

Synthetic CLE peptides (Genecust, >95% purity) were dissolved in phosphate buffer (50 μm, pH6.8) to stock concentrations of 1 mM and 10 mM. Plants were grown on BCDAT plates containing peptides diluted to concentrations specified in the main text.

QUANTIFICATION AND STATISTICAL ANALYSIS

Quantification and statistical analyses were undertaken as stipulated in main text and SI figures and figure legends.

DATA AND SOFTWARE AVAILABILITY

Genome and transcriptome data were searched as described in Method details and details of data repositories are listed in Table S4.

Methods Figures

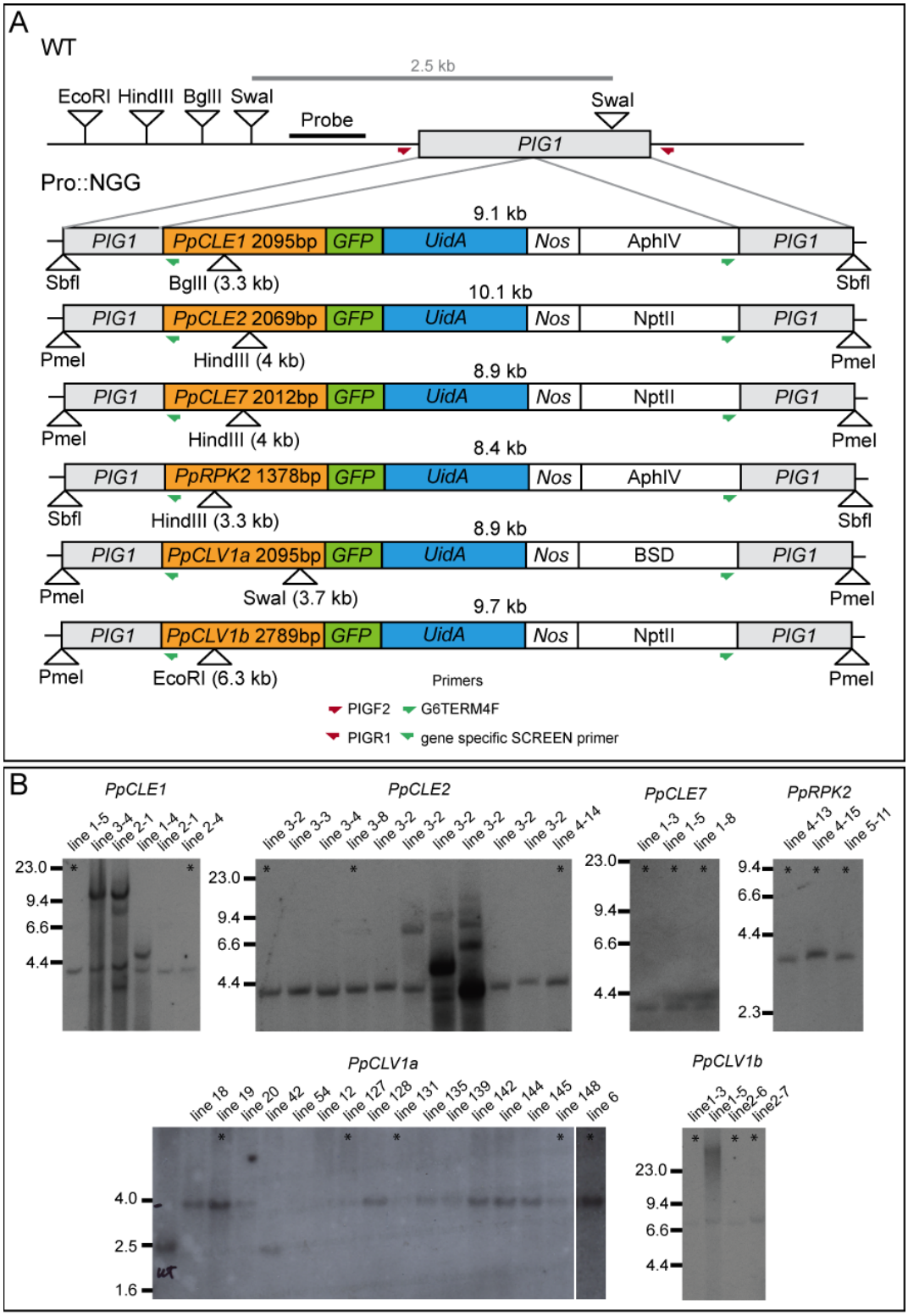

Methods Fig. 1 related to Fig. 2: Strategy for generation of *promoter::NLSGUSGFP* reporter lines. (A) Promoter fragments of *PpCLE1*, *PpCLE2*, *PpCLE7*, *PpRPK2*, *PpCLV1a* and *PpCLV1b* of varying lengths were PCR amplified and cloned into the SmaI site of the PIG1NGGII [41] vector with or without replacement of the BSD casette with an NptII casette or an AphIV cassette, and transgenes were delivered into plants as PmeI or SbfI fragments. Lines were screened first by PCR using PIGF2 and gene specific SCREEN primers, and PIGR2 and G6TERMF primers. (B) Subsequent screening was undertaken by Southern analysis with a 5' PIG locus-specific probe following BglII, HindIII, SwaI or EcoRI digestion. Targeted single insertant lines were used in expression analyses.

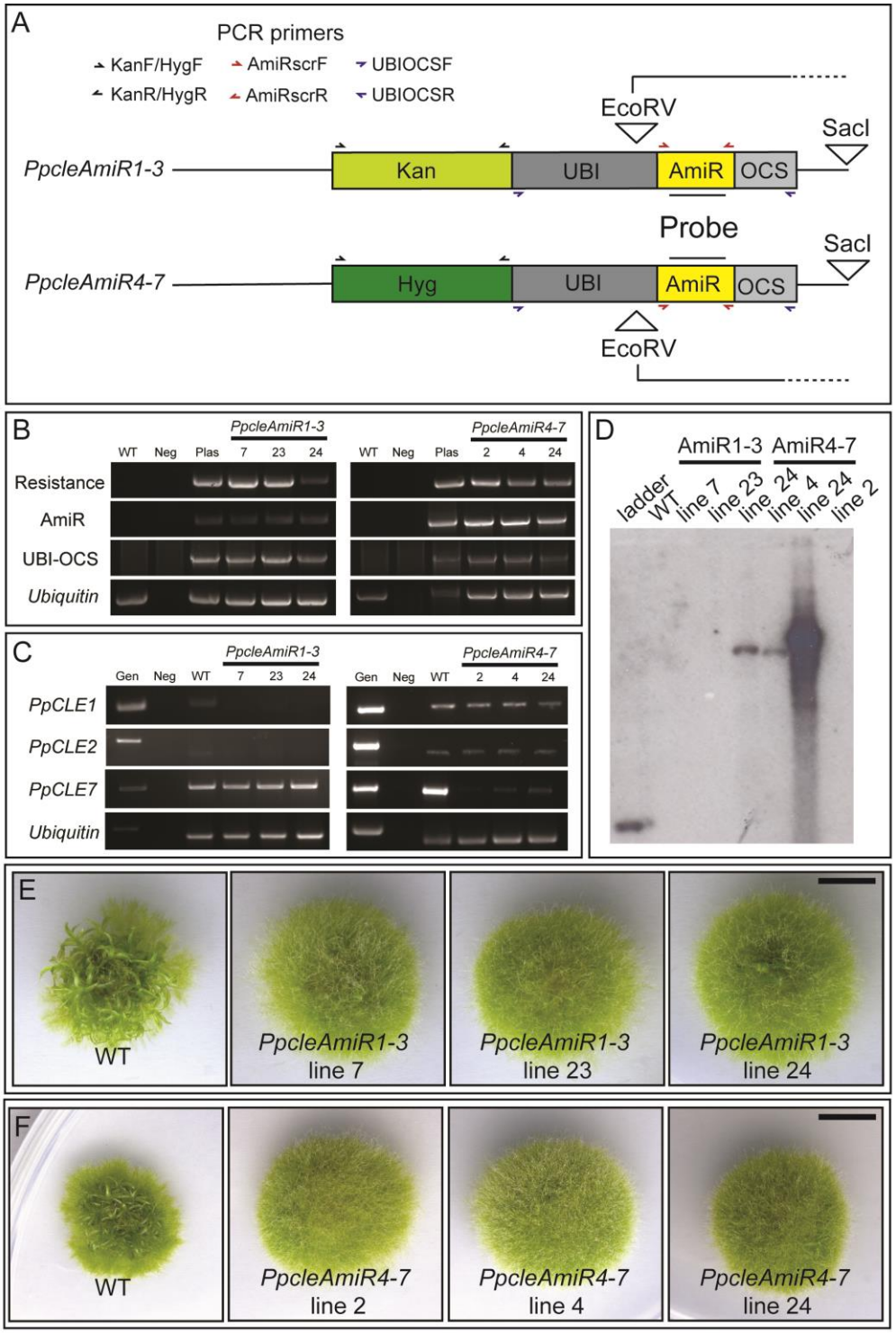

Methods Fig. 2 related to Fig. 3: Strategy for generating *PpcleAmiR* lines. (A) Plasmids were constructed as described in STAR Methods and linearized with SacI prior to transformation. (B) PCR analysis identified three positive lines for each AmiR construct. (C) RT-PCR showed that *PpCLE* expression was strongly reduced in transgenic lines. (D) Southern analysis showed that one *PpcleAmiR1-3* and two *PpcleAmiR4-7* lines were stable insertants. (E and F) Multiple *PpcleAmiR1-3* (E) and *PpcleAmiR4-7* (F) lines had similar mutant phenotypes. Scale bars = 1 cm.

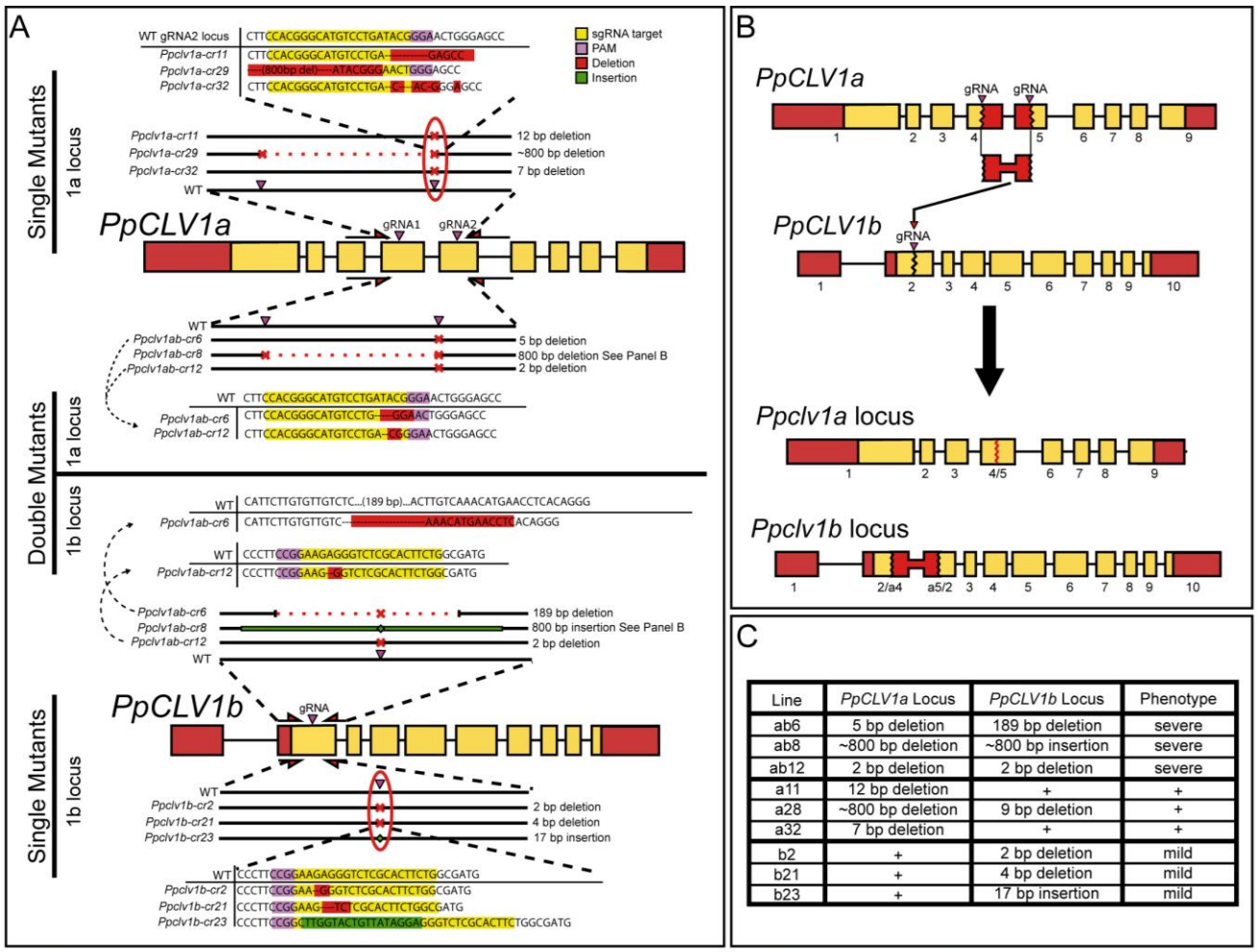

Methods Fig. 3 related to Fig. 3: CRISPR/Cas9 strategy for generating *Ppclv1* mutants. (A) Generation of *Ppclv1a* single mutants, *Ppclv1ab* double mutants, and *Ppclv1b* mutants. Guide RNAs were designed to target *PpCLV1a* or *PpCLV1b* as indicated by purple triangles, and plants were co-transformed as described in STAR Methods. Locus-specific PCR amplification used primers illustrated by red arrows with sequences listed in STAR Methods, and Sanger sequencing was used to identify the nature of mutation in three independent

disruptant lines. Sequences are colour coded to illustrate gRNA targets (yellow), protospacer adjacent motifs (PAM: purple), a deletion (green) and insertions (red). In gene models, UTRs are indicated in red and coding sequence is indicated in yellow. Exons are represented as boxes, and introns are represented as lines. (B) In *Ppclv1a1b-8* mutants, the region between two gRNAs targeting *PpCLV1a* translocated into the site cut by a gRNA targeting *PpCLV1b*. (C) Summary of mutations at each locus in nine *PpCLV1* mutant lines described in (A). + denotes wild type sequence or phenotype. (D-M) Multiple *Ppclv1a*, *Ppclv1b* and *Ppclv1a1b* mutant lines had similar mutant phenotypes. Whereas WT and single mutant plants had well-developed gametophores, double mutant plants comprising mainly protonemata, and few gametophores were visible. Scale bar = 1 mm.

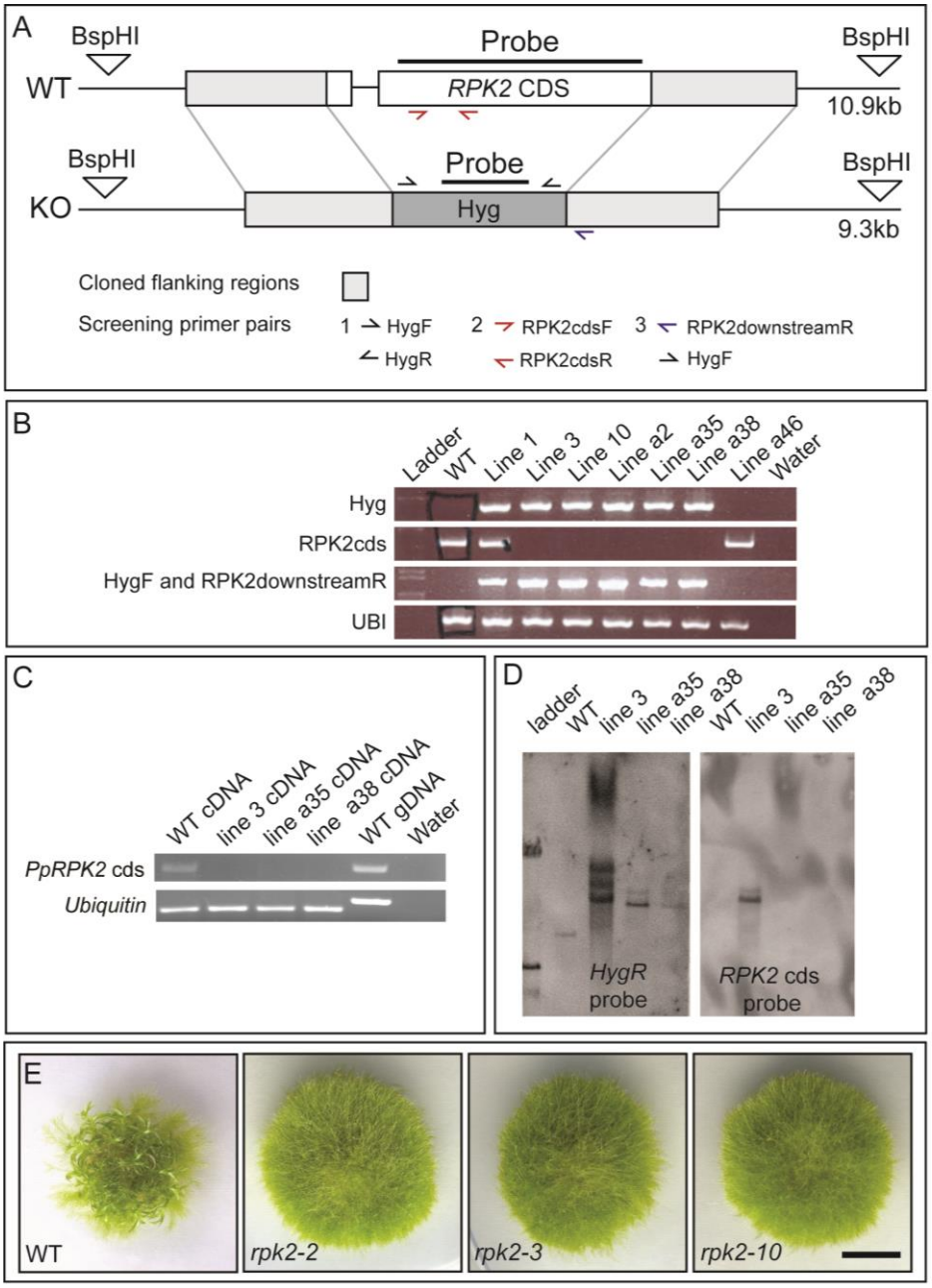

Methods Fig. 4 related to Fig 3: Strategy for generating *Pprpk2* KO lines. (A) To generate *Pprpk2* targeted deletion vectors, 5' and 3' *PpRPK2* flanking regions were PCR amplified and ligated into pGEM-TEASY™. The 5' flanking sequence was excised with SacI and PmeI and inserted in tandem with the 3' flanking sequence prior to insertion of a Hygromycin resistance casette from pBHRF108 [47] to generate the targeting vector. This was linearised with AflII for plant transformation. Stable insertants were screened by PCR with three primer pairs 1, 2 and 3. The *RPK2* locus is in a repeat rich genomic region, and we were unable to amplify fragments to screen for integration at the 5' end as Southern hybridization with several probes outside the insertion cassette gave smears. (B) PCR screening identified three candidate targeted deletion lines. (C) RT-PCR confirmed loss of *PpRPK2* expression in mutants. (D) Targeted deletion was confirmed by Southern analysis using sequential hybridization with *PpRPK2* and HygR probes at 42 ˚C. (E) Multiple knockout lines had similar mutant phenotypes. Scale bar = 1 cm.

SUPPLEMENTAL FIGURES

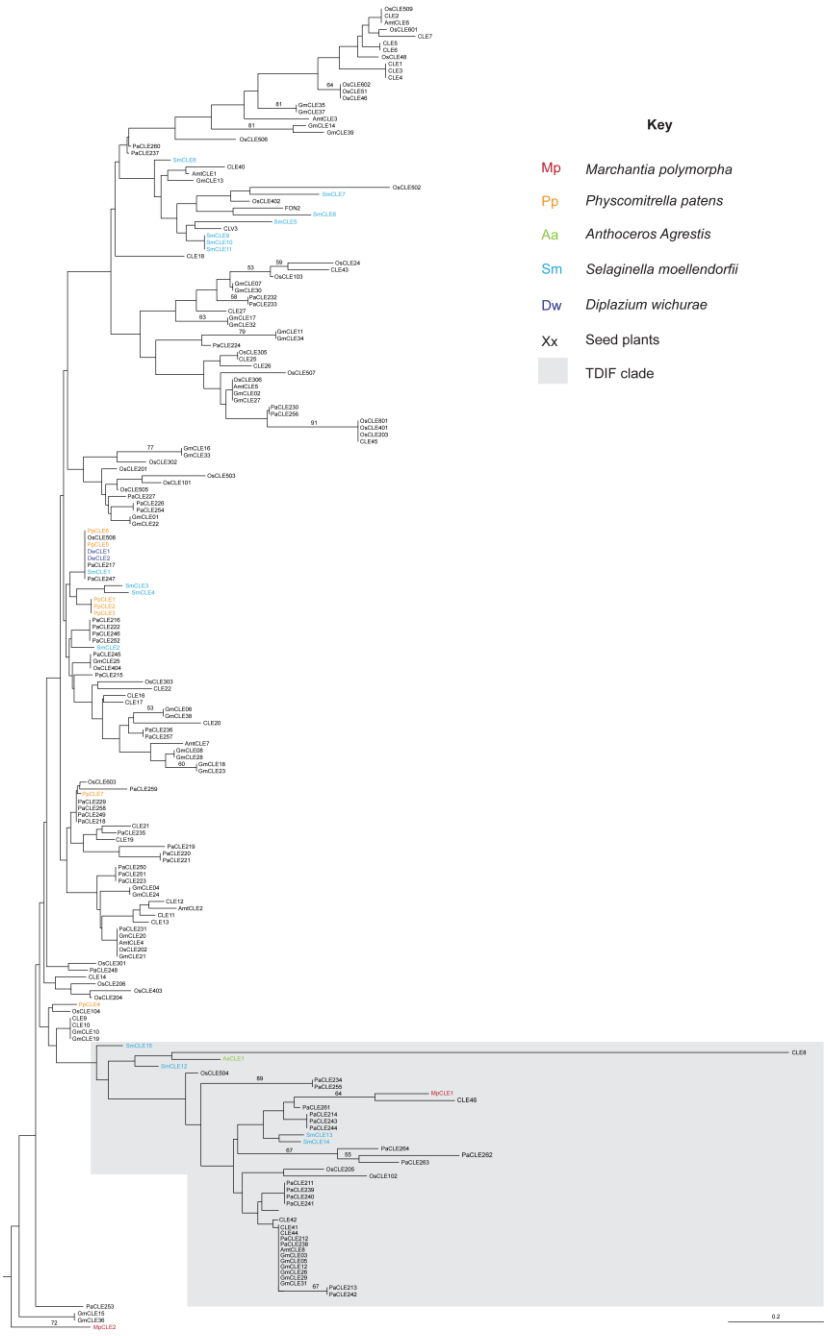

Fig. S1 related to Fig. 1: NJ tree showing relationships between land plant CLEs. 193 CLE motifs were aligned and a neighbour-joining analysis was undertaken as described in SI Methods. A *Marchantia polymorpha* CLE was used to root the tree, *Physcomitrella patens* was selected to represent mosses, *Anthoceros agrestis* was selected to represent hornworts, *Selaginella moellendorfii* was selected to represent lycophytes, *Diplazium wichurae* was selected to represent monilophytes, and seed plant sequences were retreived from *Picea abies*, *Amborella trichopoda*, *Glycine max*, *Oryza sativa* and *Arabidopsis thaliana*. 100 bootstrap replicates were performed, but bootstrap support was very low as there are few characters, and support values of > 50 are shown.

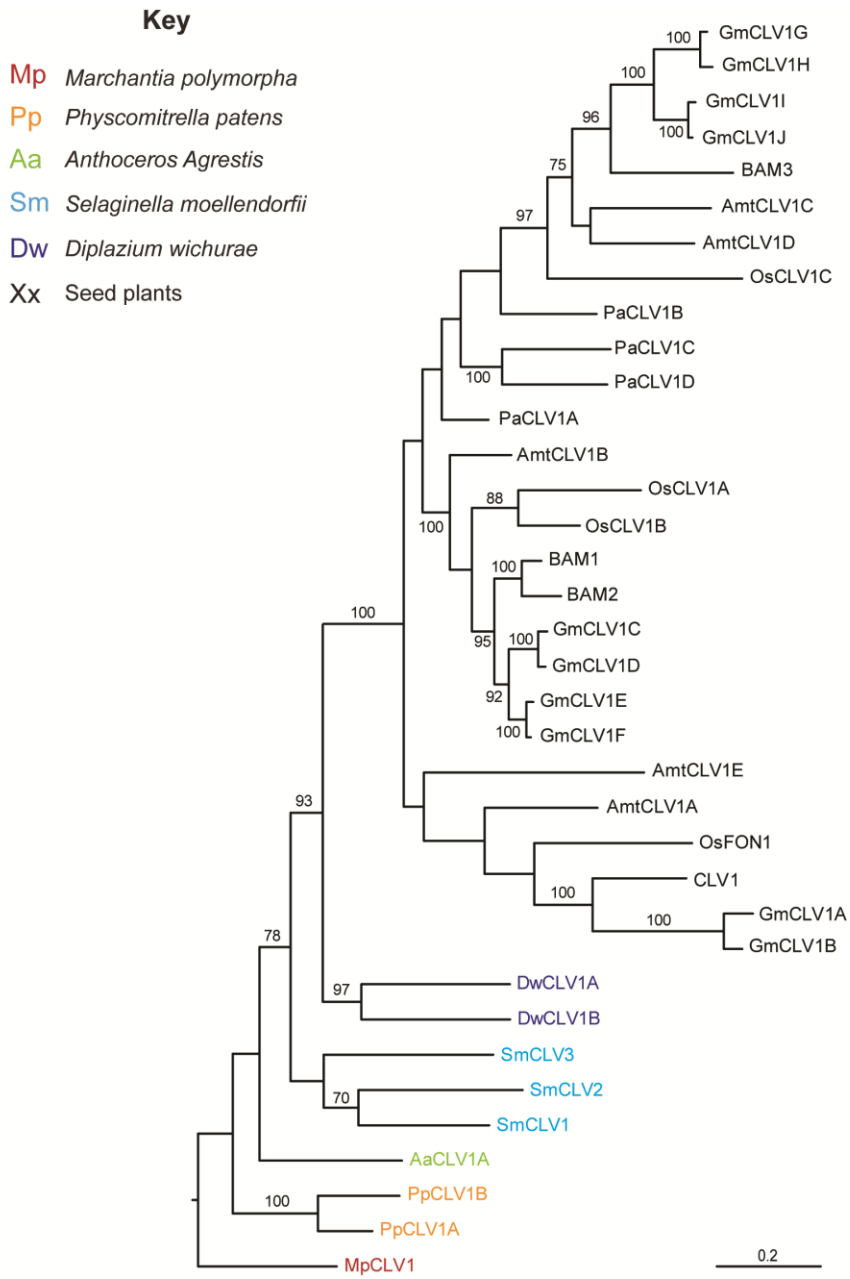

Fig. S2. Related to Fig. 1: ML tree showing relationships between land plant BAM/CLV1-like proteins. 36 BAM/CLV1-like receptor-like kinase sequences were aligned, and data were analysed using the maximum likelihood method with the JTT matrix-based model as described in SI Methods. All positions containing gaps and missing data were removed prior to analysis, leaving a total of 525 in the final dataset. The tree with the highest log likelihood is shown. *Marchantia polymorpha* was sampled to represent liverworts, *Physcomitrella patens* was sampled to represent mosses, *Anthoceros agrestis* was selected to represent hornworts, *Selaginella moellendorfii* was selected to represent lycophytes, *Diplazium wichurae* was selected to represent monilophytes, and seed plant sequences were retreived from *Picea abies*, *Amborella trichopoda*, *Glycine max*, *Oryza sativa* and *Arabidopsis thaliana*. The tree was rooted on MpCLV1 in line with current estimates of land plant phylogeny, and bootstrap values of > 70 from 100 replicates are shown next to branches. Branch lengths represent the number of substitutions per site.

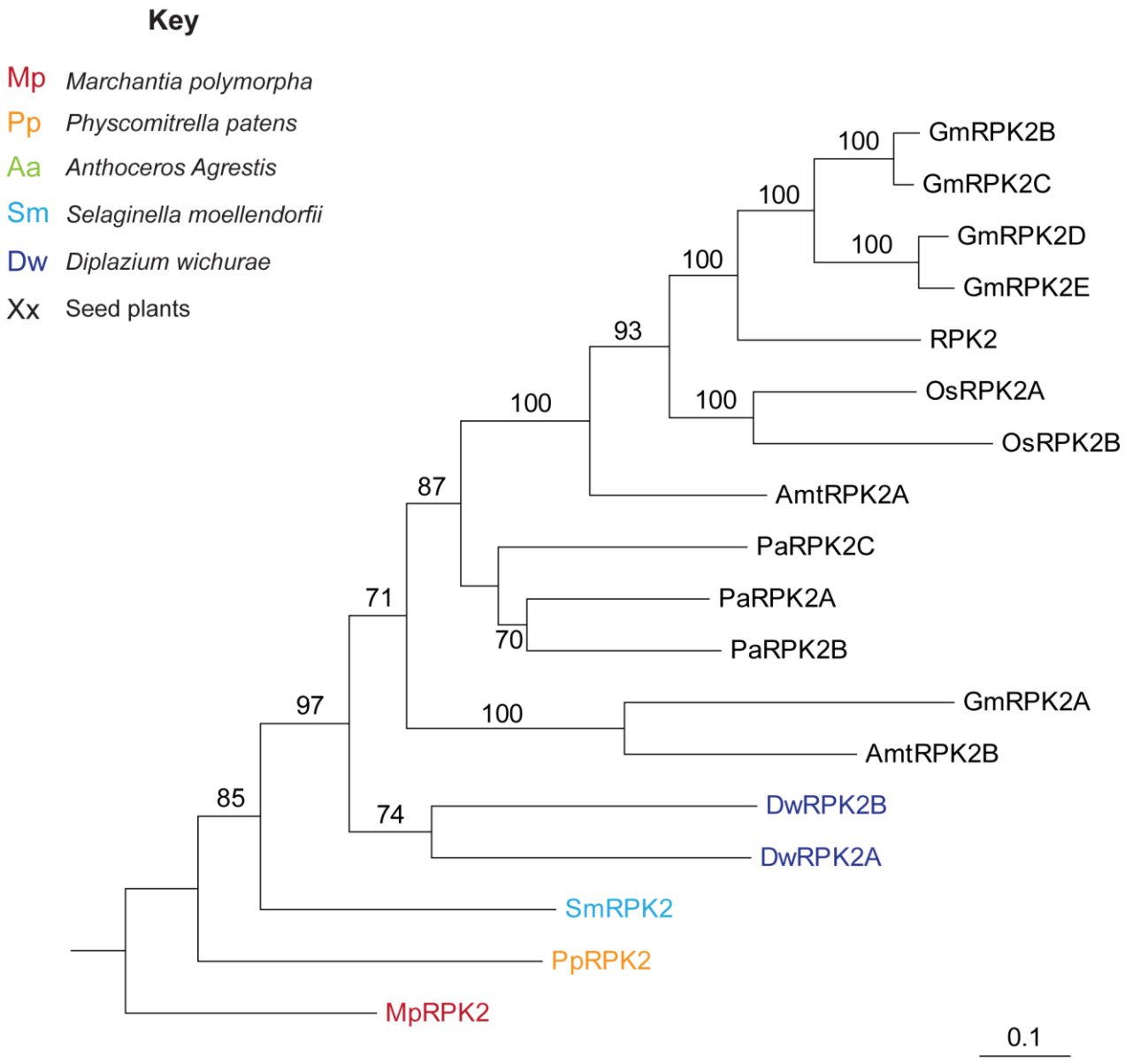

Fig. S3 related to Fig 1: ML tree showing relationships between land plant RPK2-like proteins. 18 RPK2-like receptor-like kinase sequences were aligned and the phylogenetic tree was reconstructed using the maximum likelihood method with the JTT matrix-based model as described in SI Methods. All positions containing gaps and missing data were removed prior to analysis, leaving a total of 782 in the final dataset. The tree with the highest log likelihood is shown. *Marchantia polymorpha* was sampled to represent liverworts, *Physcomitrella patens* was sampled to represent mosses, *Anthoceros agrestis* was selected to represent hornworts, *Selaginella moellendorfii* was selected to represent lycophytes, *Diplazium wichurae* was selected to represent monilophytes, and seed plant sequences were retreived from *Picea abies*, *Amborella trichopoda*, *Glycine max*, *Oryza sativa* and *Arabidopsis thaliana*. The tree was rooted on MpRPK2 in line with current estimates of land plant phylogeny, and bootstrap values of > 70 from 100 replicates are shown next to branches. Branch lengths represent the number of substitutions per site.

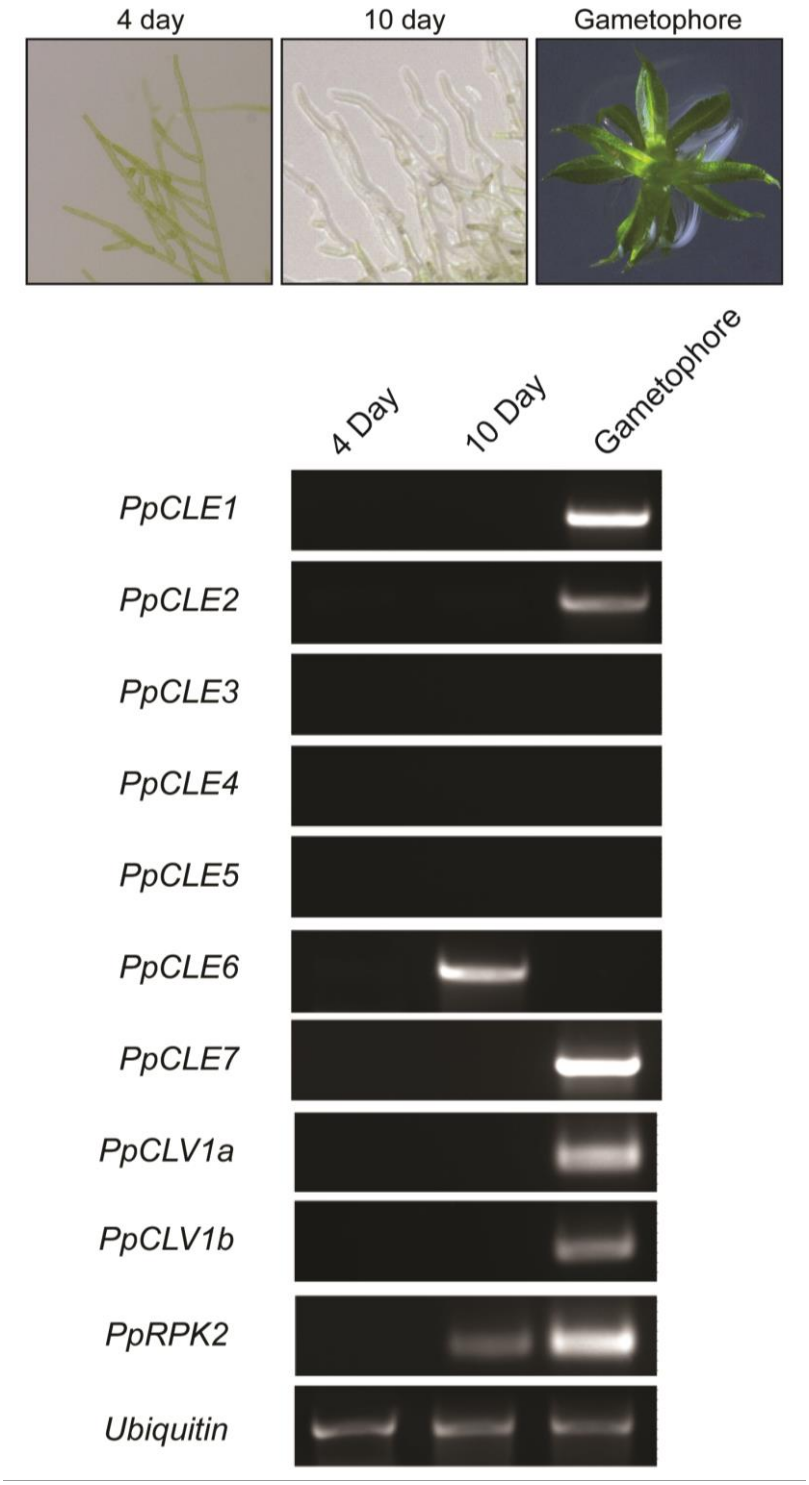

Fig. S4 related to Fig. 2: Expression of CLV signaling components in gametophytic *Physcomitrella* tissues as evaluated by RT-PCR. *PpCLEs 1*, *2* and *7* were expressed in gametophores. *PpCLV1a*, *PpCLV1b* and *PpRPK2* were also expressed in gametophores and *PpRPK2* expression was also detected in 10-day old protonemal tissues, which is when gametophores first start to initiate under our growth conditions.

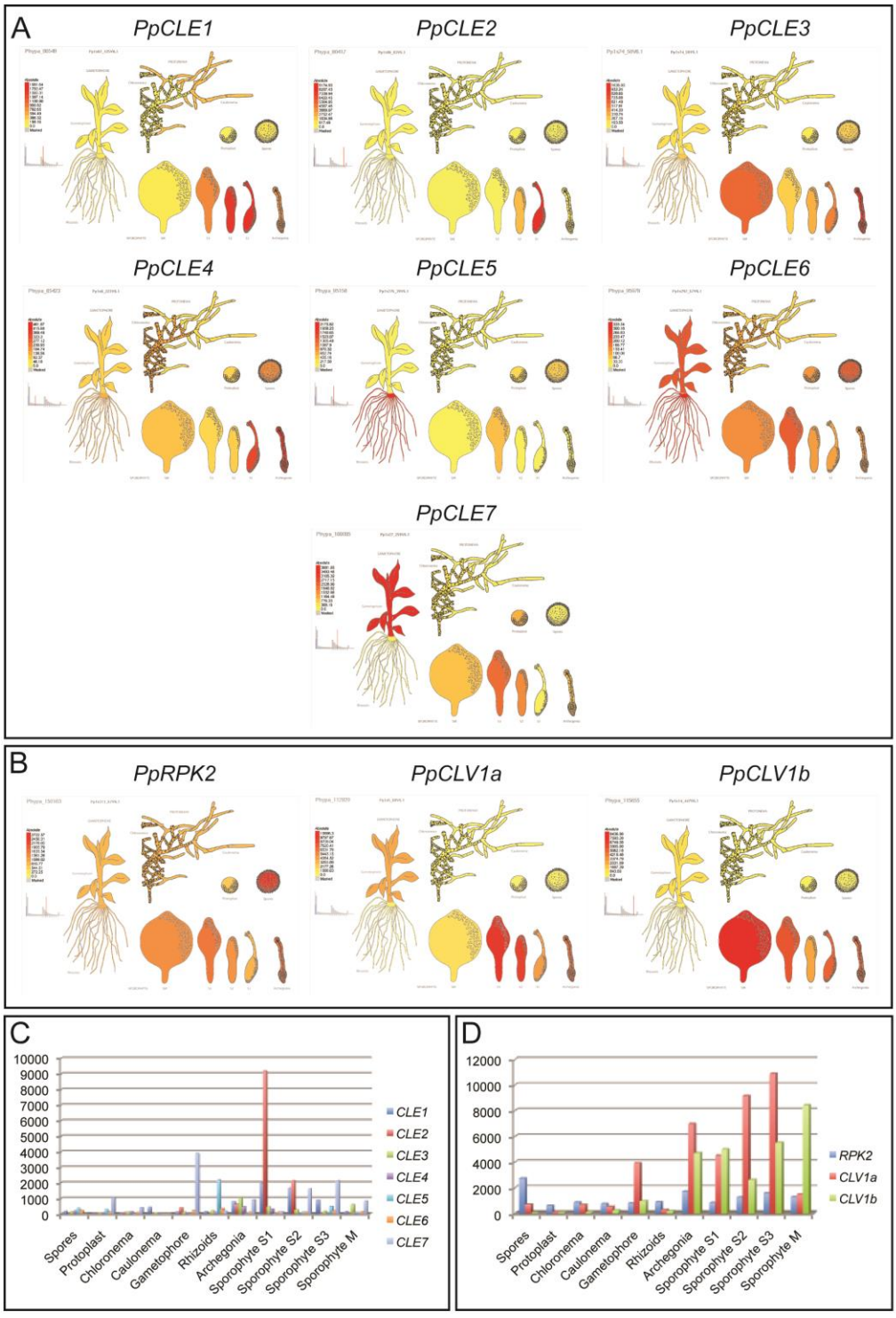

Fig. S5 related to Fig. 2: Expression of CLV signaling components in *Physcomitrella* tissues evaluated by eFP Browser data [1]. (A) Expression patterns of *PpCLEs 1-7*. (B) Expression patterns of receptor components. (C) Quantitative comparison of *PpCLE1-7* expression levels. (D) Quantitative comparison of *PpCLV1a, PpCLV1b* and *PpRPK2* expression levels.

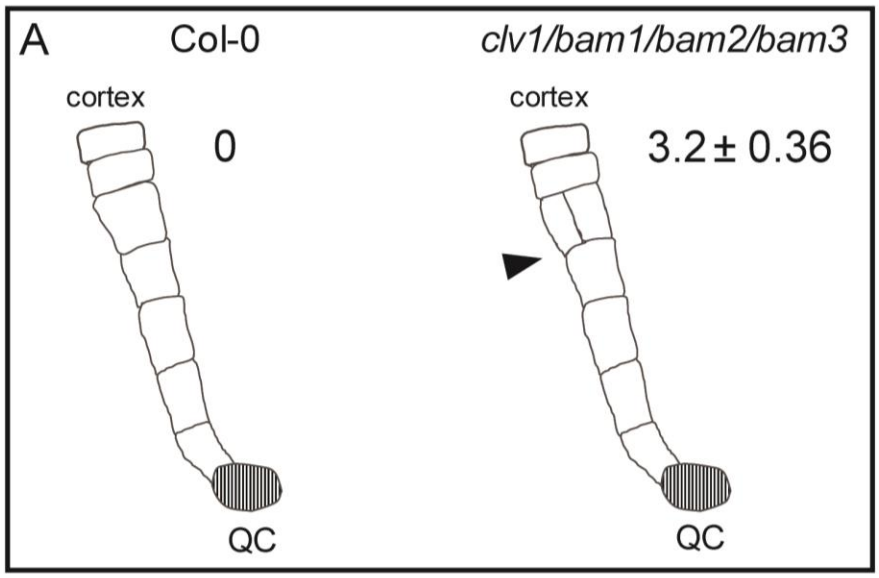

B

Root Length (cm) at time of imaging (stage-matched)		
Col-0		***clv1/bam1/bam2/bam3***
1.375	*Mean*	1.499
0.344	*SD*	0.33
0.661	*Min*	1.006
1.999	*Max*	2.165
19	*N*	13
0.078919012	*SE*	0.091525532

C

Col-0			***clv1/bam1/bam2/bam3***		
Label	*Meristematic zone Length (pixels)*	*Number of PCDs*	*Label*	*Meristematic zone Length (pixels)*	*Number of PCDs*
C3	650.308	0	Q1	636.572	3
C4	601.415	0	Q3	595.238	4
C5	584.411	0	Q6	586.276	1
C6	586.464	0	Q7	600.536	4
C7	609.908	0	Q8	635.437	3
C8	639.465	0	Q9	630.149	2
C10	558.516	0	Q10	586.464	4
C11	631.341	0	Q11	600.087	5
			Q12	619.681	3
			Q13	648.278	3
Mean	**607.729**	**0**	**Mean**	**613.872**	**3.2**
SD	31.26	**0**	SD	22.829	**1.135**

Fig. S6 related to Fig. 3: Quantification of cell division plane orientation defects in ground tissue layers in *Arabidopsis clv1/bam1/bam2/bam3* roots. (A) Diagram showing the nature of cell division plane orientation defects in wild-type versus *clv1*/*bam1*/*bam2*/*bam3* plants. (B) Equivalence of developmental stages used in comparisons between wild-type and mutant plants. (C) Quantitative data showing differences in the number of periclinal cell divisions (PCDs) in wild-type versus mutant plants.

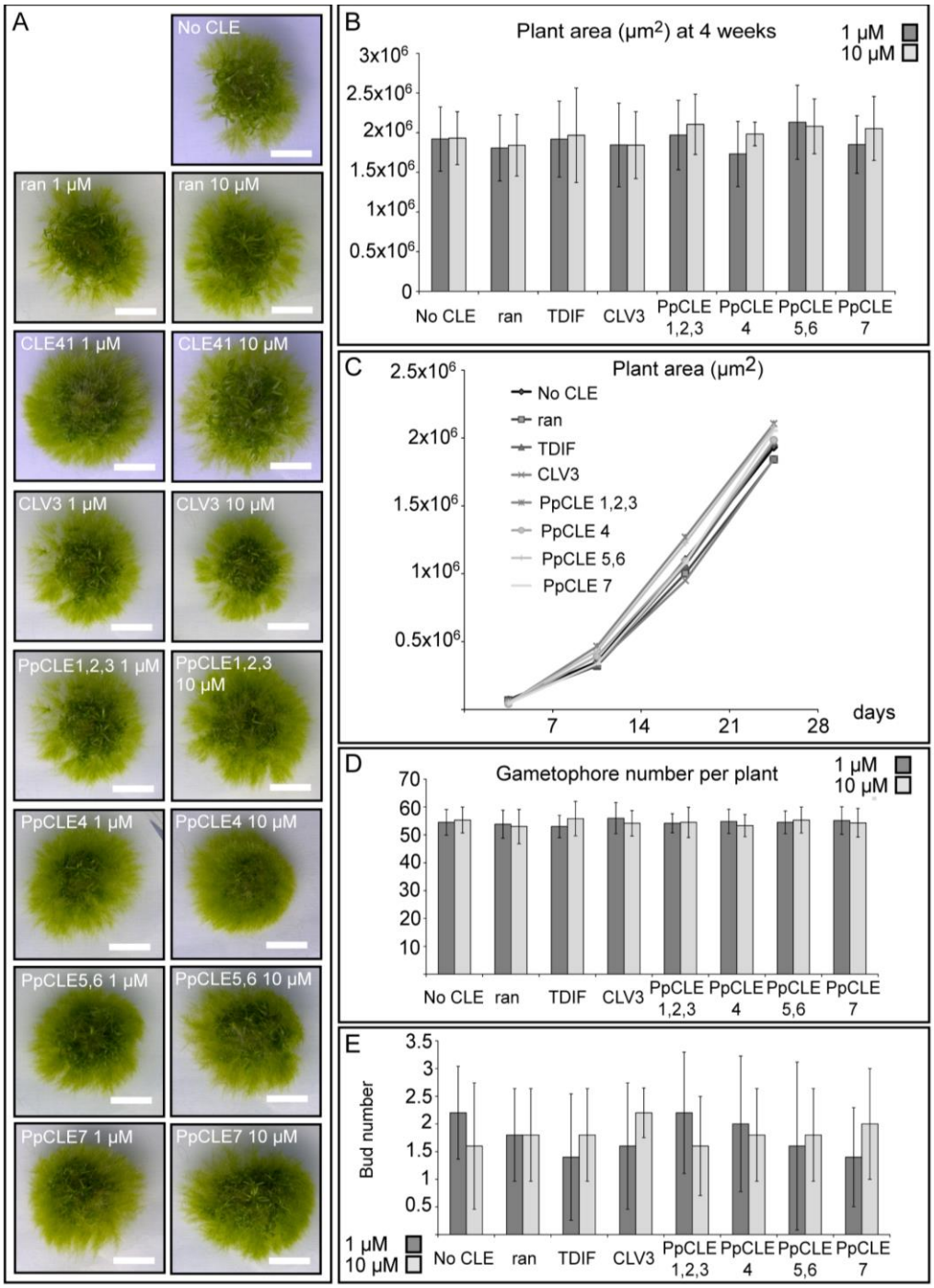

Fig. S7 related to Fig. 6: Treatment with CLE peptides had no appreciable effect on protonemal morphology. (A) Light micrographs of plants treated with a synthetic random peptide, CLE41, CLV3 or *Physcomitrella* CLEs showing morphology. Scale Bar = 1 cm. (B and C) The area of plants treated with 1 µM or 10 µM CLEs was no different from controls ($n \geq 20$). (D and E) CLE treatment did not effect gametophore initiation. For D, gametophores from 5 plants were counted for each treatment, and for E, a 5 mm square from the edge of 5 plants was counted for each treatment.

Table S1 related to Fig. 1: List of newly identified *CLE* genes, gene IDs and species of origin.

Gene name	Gene ID	Source
PpCLE1	Pp1s87_125V6.1	*Physcomitrella patens*
PpCLE2	Pp1s86_83V6.1	*Physcomitrella patens*
PpCLE3	Pp1s74_50V6.1	*Physcomitrella patens*
PpCLE4	Pp1s6_223V6.1	*Physcomitrella patens*
PpCLE5	Pp1s275_39V6.1	*Physcomitrella patens*
PpCLE6	Pp1s292_57V6.1	*Physcomitrella patens*
PpCLE7	Pp1s27_259V6.1	*Physcomitrella patens*
AaCLE1	MG571535	*Anthoceros agrestis*
DwCLE1	scaffold-UFJN-2003654-Diplazium_wichurae	*Diplazium wichurae*
DwCLE2	scaffold-UFJN-2087917-Diplazium_wichurae	*Diplazium wichurae*
AmtCLE1	>lcllevm_27.model.AmTr_v1.0_scaffold00022.262	*Amborella trichopoda*
AmtCLE2	>lcllevm_27.model.AmTr_v1.0_scaffold00030.123	*Amborella trichopoda*
AmtCLE3	>lcllevm_27.model.AmTr_v1.0_scaffold00021.96	*Amborella trichopoda*
AmtCLE4	>lcllevm_27.model.AmTr_v1.0_scaffold00007.246	*Amborella trichopoda*
AmtCLE5	>lcllevm_27.model.AmTr_v1.0_scaffold00002.301	*Amborella trichopoda*
AmtCLE6	>lcllevm_27.model.AmTr_v1.0_scaffold00021.106	*Amborella trichopoda*
AmtCLE7	>lcllevm_27.model.AmTr_v1.0_scaffold00010.83	*Amborella trichopoda*
AmtCLE8	>lcllevm_27.model.AmTr_v1.0_scaffold00067.109	*Amborella trichopoda*

Table S2 related to Fig. 1: List of newly identified *CLV1/BAM* genes, gene IDs and species of origin.

Gene name	Gene ID	Source
DwCLV1A	scaffold-UFJN-2012643	*Diplazium wichurae*
DwCLV1B	scaffold-UFJN-2014575	*Diplazium wichurae*
GmCLV1C	NP_001235065.1	*Glycine max*
GmCLV1D	NP_001237688.1	*Glycine max*
GmCLV1E	NP_001235080.1	*Glycine max*
GmCLV1F	NP_001237715.1	*Glycine max*
GmCLV1G	XP_003530709.1	*Glycine max*
GmCLV1H	XP_006602289.1	*Glycine max*
GmCLV1I	XP_003518489.2	*Glycine max*
GmCLV1J	XP_003545159.1	*Glycine max*
FON1	Os06g50340.1	*Oryza sativa*
OsCLV1A	Os03g0228800	*Oryza sativa*
OsCLV1B	Os07g0134200	*Oryza sativa*
OsCLV1C	Os05g0595950	*Oryza sativa*
PpCLV1A	Pp1s5_68V6.1	*Physcomitrella patens*
PpCLV1B	Pp1s14_447V6.1	*Physcomitrella patens*
PaCLV1A	MA_64117p0010	*Picea abies*
PaCLV1B	MA_943683p0010	*Picea abies*
PaCLV1C	MA_52165p0010	*Picea abies*
PaCLV1D	MA_120550p0010	*Picea abies*
SmCLV1	XP_002965214.1	*Selaginella moellendorffii*
SmCLV2	XP_002971751.1	*Selaginella moellendorffii*
SmCLV3	XP_002970036.1	*Selaginella moellendorffii*
AaCLV1A	MG571536	*Anthoceros agrestis*
AmtCLV1A	evm_27.model.AmTr_v1.0_scaffold00055.1	*Amborella trichopoda*
AmtCLV1B	evm_27.model.AmTr_v1.0_scaffold00033.36	*Amborella trichopoda*
AmtCLV1C	evm_27.model.AmTr_v1.0_scaffold00071.179	*Amborella trichopoda*
AmtCLV1D	evm_27.model.AmTr_v1.0_scaffold00068.165	*Amborella trichopoda*
AmtCLV1E	evm_27.model.AmTr_v1.0_scaffold00056.126	*Amborella trichopoda*

Table S3 related to Fig. 1: List of newly identified *RPK2* genes, gene IDs and species of origin.

Gene name	Gene ID	Source
DwRPK2A	scaffold-UFJN_2014694	*Diplazium wichurae*
DwRPK2B	scaffold-UFJN_2002858	*Diplazium wichurae*
GmRPK2A	XP_003548492.2	*Glycine max*
GmRPK2B	XP_003530440.2	*Glycine max*
GmRPK2C	XP_003551760.1	*Glycine max*
GmRPK2D	XP_003543956.1	*Glycine max*
GmRPK2E	XP_003554916.1	*Glycine max*
OsRPK2A	Os07g0602700	*Oryza sativa*
OsRPK2B	Os03g0756200	*Oryza sativa*
PaRPK2A	MA_13025p0010	*Picea abies*
PaRPK2B	MA_10427820p0020	*Picea abies*
PaRPK2C	MA_129592p0010	*Picea abies*
SmRPK2	XP_002982473	*Selaginella moellendorffii*
AmtRPK2A	evm_27.model.AmTr_v1.0_scaffold00154.29	*Amborella trichopoda*
AmtRPK2B	evm_27.model.AmTr_v1.0_scaffold00016.228	*Amborella trichopoda*

Table S4 related to Fig. 1: List of taxa, publications and databases searched for sequence data.

Class	Species	Publication	Database searched
Seed plant	*Arabidopsis thaliana*	[2] Strabala *et al.* (2006)	NCBI
Seed plant	*Oryza sativa*	[3] Yu *et al.* (2002)	NCBI
Seed plant	*Glycine max*	[4] Mortier *et al.* (2011)	NCBI
Seed plant	*Amborella trichopoda*	[5] Amborella Genome Project (2013)	Phytozome
Seed plant	*Picea abies*	[6] Strabala *et al.* (2014)	NCBI
Monilophyte	*Diplazium wichurae*	1kp project	1kp project
Lycophyte	*Selaginella moellendorffii*	[7] Miwa *et al.* (2009)	NCBI
Hornwort	*Anthoceros agrestis*	Draft genome assembly (Szövényi)	Draft genome assembly (Szövényi)
Moss	*Physcomitrella patens*	[7] Miwa *et al.* (2009)	COSMOSS
Liverwort	*Marchantia polymorpha*	[8] Bowman *et al.* (2017)	Phytozome
Charophyte alga	*Coleochaete nitellarum*	1kp project	1kp project
Charophyte alga	*Spirogyra* sp.	[9] Delaux *et al.* (2015)	Dunand lab
Charophyte alga	*Chara braunii*	Draft genome assembly (Rensing)	Draft genome assembly (Rensing)
Chlorophyte alga	*Ulva spp.*	1kp project	1kp project
Chlorophyte alga	*Chlamydomonas reinhardtii*	[10] Merchant *et al.* (2007)	Phytozome
Chlorophyte alga	*Volvox carteri*	[11] Prochnik *et al.* (2010)	Phytozome
Chlorophyte alga	*Ostreococcus tauri*	[12] Palenik *et al.* (2007)	Phytozome
Chlorophyte alga	*Chlorella vulgaris*	[13] Blanc *et al.* (2010)	Phytozome

Table S5 related to Fig. 1: List of *Physcomitrella* CLAVATA pathway V3 genome gene IDs.

Gene name	V1.6 genome	V3 genome	Peptide encoded
PpCLE1	Pp1s87_125V6.1	Pp3c7_11040V1.1	PpCLE 1/2/3
PpCLE2	Pp1s86_83V6.1	Pp3c1_13720V1.1	PpCLE 1/2/3
PpCLE3	Pp1s74_50V6.1	Pp3c3_10020V1.1	PpCLE 1/2/3
PpCLE4	Pp1s6_223V6.1	Pp3c26_11430V1.1	PpCLE 4
PpCLE5	Pp1s275_39V6.1	Pp3c22_4590V1.1	PpCLE 5/6
PpCLE6	Pp1s292_57V6.1	Pp3c19_6950V1.1	PpCLE 5/6
PpCLE7	Pp1s27_259V6.1	Pp3c21_5600V1.1	PpCLE 7
PpCLE8	not found	Pp3c11_15310V1.1	PpCLE 1/2/3
PpCLE9	not found	Pp3c4_31330V1.1	PpCLE 1/2/3
PpCLV1a	Pp1s5_68V6.1	Pp3c13_13360V1.1	PpCLV1a
PpCLV1b	Pp1s14_447V6.1	Pp3c6_21940V1.1	PpCLV1b
PpRPK2	Pp1s311_57V6.1	Pp3c7_5570V1.1	PpRPK2

Table S6 related to Figs. 2-4 and STAR methods: List of primers used in this study.

Primer name	Primer sequence
A. Primers for RT-PCR	
cDNA synthesis primer [30]	
Q_T	CCAGTGAGCAGAGTGACGAGGACTCGAGCT
PpCLE1	
PpCLE1F	GTAGCATTGAGGTTCACGACA
PpCLE1R	CACGGGAATATGACTTGAGA
PpCLE2	
PpCLE2F	CAGATGCGGTTGAGAAAGAGA
PpCLE2R	GACTTGAGACCGATTGCTGTT
PpCLE3	
PpCLE3F	GTAATCCTCGCCATTTTCCA
PpCLE3R	GGGTTTCGTGGATTCGTGAT
PpCLE4	
PpCLE4F	CGAAGGCAGACGACAGGTGA
PpCLE4R	GACCTGCGACCTGTTGCTATT
PpCLE5	
PpCLE5F	ACGTTGGTGCTGGATTGTGAT
PpCLE5R	TCTGCCTCCACATCCCAAAT
PpCLE6	
PpCLE6F	GTAGGAATGGTCGTCGTCGT
PpCLE6R	GAACCAAGCGCTTCGACAT
PpCLE7	
PpCLE7F	TGCTTGTCCATGGTGATTGT
PpCLE7R	CCCGACTGTGATCCAACTTT
PpCLV1a	
PpCLV1aF	CAACATCGCAATCCAGGCT
PpCLV1aR	CCACTCTCAGGACCAATACAA
PpCLV1b	
PpCLV1bF	GGCAATCTCCCCACCCT
PpCLV1bR	CTCCTCGTCCAAGCAGTCTA
PpRPK2	
PpRPK2F	GTGGACCCGTTTCGTGTGTT
PpRPK2R	GGCTGGTGGACCCTGATAA
PpUBI	
PpUbi-intF	GCCATGCAGATCTTCGTGAA
PpUbi-intR	CTACGCAGCCAAGAACCGA
B. Promoter::NGG construction	
PpCLE1	
CLE15'PF	gtttaaacGGCACCATCTCCATCACTATCT
CLE15'PR	gcgatcgccacgtgGGTAAGGCTCCATGCACCGT
PpCLE2	
CLE25'PF	CGCTGCTGATTCACCACCTCAA
CLE25'PR	GGCATAATGTGGGGAGAAGGA
PpCLE7	
CLE75'PF	CTTGTGACATTCTAATAAGTGCTTATCC
CLE75'PR	CCCTTCCGAAAAACTGATACCA
PpCLV1a	
CLV1aPF	tatggatccTCTGTCAAATTTATTACCACTT
CLV1aPR	tatggatccGAGGAAAGCATGAGCACTGA
PpCLV1b	
CLV1bPF	TTTTGGATCAGCCATCCCTATAAGGCTCAG
CLV1bPR	GGTTATTCATGTTTTCTAGACACTGTTGCT
PpRPK2	
RPK25'PF	cttaagATTATTTTTTGTTACCTTGTATTTT
RPK25'PR	gtttaaacTCTCCCCTAACTCCTCCTCA

C. Promoter::NGG screening primers

PIGF2	AGGACACCCTTTCCAAACACATT
PIGR1	AAAAACCAATCTGGGAATAGCTTG
G6TERM4F	TAGGGTTCTATAGGGTTTCGCTCA
CLE1SCREENR	ACAGATTGCAGTTCCGTATGCTC
CLE2SREENR	TAAGCATGCAGCTCTAGGAAACG
CLE7SCREENR	CCATTGGCTATTAAAATGGCTTGA
RPK2SCREENR	TCTCATTTGCAAGTATAATCCAAGC
CLV1ASCREENR	CGAGTGCAACGAGATTCAAA
CLV1BSCREENR	GCAATCGGACAGACCTTTGAGTA

D. PpcleAmiR *construction*

PpcleAmiR1-3	
123-I	gaTTGGGAACCATGCGGTCGGAGtctctcttttgtattcc
123-II	gaCTCCGACCGCATGGTTCCCAAtcaaagagaatcaatga
123-III	gaCTACGACCGCATGCTTCCCATtcacaggtcgtgatatg
123-IV	gaATGGGAAGCATGCGGTCGTAGtctacatatatattcct
amiR-A	CTGCAAGGCGATTAAGTTGGGTAAC
amiR-B	GCGGATAACAATTTCACACAGGAAACAG
PpcleAmiR4-7	
7-I	gaTTGAAGCGGATTAGGACCTGGtctctcttttgtattcc
7-II	gaCCAGGTCCTAATCCGCTTCAAtcaaagagaatcaatga
7-III	gaCCCGGTCCTAATCGGCTTCATtcacaggtcgtgatatg
7-IV	gaATGAAGCCGATTAGGACCGGGtctacatatatattcct
amiR-A	CTGCAAGGCGATTAAGTTGGGTAAC
amiR-B	GCGGATAACAATTTCACACAGGAAACAG

E. PpcleAmiR *screening*

Kanamycin resistance cassette	
Kan-F	GGCATGATTGAACAAGATGAT
Kan-R	TATCGGGAAACTACTCACACAT
Hygromycin resistance cassette	
Hyg-F	AGGGCGAAGAATCTCGTGCT
Hyg-R	GCTTAGCGAACTGTGGACGA
PpcleAmiR amplification	
AmiRscrF	CGGTCGGAGTCTCTCTTTTG
AmiRscrR	CGCTCGGTGTGTCGTAGATA
PpcleAmiR expression cassette	
UbiOCSF	GCCGAACCAGCTTTCTTGTA
UbiOCSR	GTTGAATGGTGCCCGTAACT
PpUBI CDS	
Pp-Ubi-intF	GCCATGCAGATCTTCGTGAA
Pp-Ubi-intR	CTACGCAGCCAAGAACCGA

F. Ppclv1a1b construction and sequencing

PpCLV1a sgRNA-1	GGCAGACAGTGCCCGAGGCTCTCT
PpCLV1a sgRNA-1*	AAACAGAGAGCCTCGGGCACTGTC
PpCLV1a sgRNA-2	GGCACCACGGGCATGTCCTGATAC
PpCLV1a sgRNA-2*	AAACGTATCAGGACATGCCCGTGG
PpCLV1b sgRNA	GGCAGAAGTGCGAGACCCTCTTC
PpCLV1b sgRNA*	AAACGAAGAGGGTCTCGCACTTC

G. Ppclv1a1b *screening*

PpCLV1a sgRNA targets fwd (exon 4)	AACGGCTCAATTCCTCCAGA
PpCLV1a sgRNA targets rev (exon 5)	TTAGACACTCCACCCTTGCG
PpCLV1b sgRNA target fwd	TGGAGAGACGCAACTTCCAT
PpCLV1b sgRNA target rev	TTAAGACGCCCCAAATCAGC

H. Pprpk2 *construction*	
5' flanking region	
PpRPK2-5'F	ATCGATGGCTCTGGAGGTGAGTGACA
PpRPK2-5'R	GTTTAAACAGTTCGAGACAACACAAGAATGC
3' flanking region	
PpRPK2-3'F	GTTTAAACGGCGCGCCGATGGTCGGCATAGTAAACG
PpRPK2-3'R	ATCGATCAGGACGACAAGGCGGA
I. Screening Pprpk2 *lines*	
Hygromycin resistance casette	
Hyg-F	AGGGCGAAGAATCTCGTGCT
Hyg-R	GCTTAGCGAACTGTGGACGA
3' integration site analysis	
Hygromycin-F	CGCACAATCCCACTATCCTT
PpRPK2downstream-R	CAAGAGTCAGCCAATGATGCA
PpRPK2 CDS	
PpRPK2F	GTGGACCCGTTTCGTGTGTT
PpRPK2R	GGCTGGTGGACCCTGATAA
PpUBI CDS	
PpUbi-intF	GCCATGCAGATCTTCGTGAA
PpUbi-intR	CTACGCAGCCAAGAACCGA
J. *Southern blot probes*	
PpRPK2 probe	
PpRPK2probe-F	GTGGACCCGTTTCGTGTGTT
PpRPK2probe-R	GGCTGGTGGACCCTGATAA
Hygromycin probe	
Hygprobe-F	CGCACAATCCCACTATCCTT
Hygprobe-R	GATGTTGGCGACCTCGTATT
K. Identification of Arabidopsis rpk-2 *homozygotes*	
dCAPS primers	
AtRPK2-BamHI-F	CACATCTTGAGAGATTTCTGCTTTGTAGGTGGATC
AtRPK2-BamHI-R	GAGAAGTCACTATGTTCATGGATAT

Supplemental references

1. Ortiz-Ramírez, C., Hernandez-Coronado, M., Thamm, A., Catarino, B., Wang, M., Dolan, L., Feijó, J.A., and Becker, J.D. (2016). A transcriptome atlas of *Physcomitrella patens* provides insights into the evolution and development of land plants. Molecular Plant *9*, 205-220.
2. Strabala, T.J., O'Donnell, P.J., Smit, A.-M., Ampomah-Dwamena, C., Martin, E.J., Netzler, N., Nieuwenhuizen, N.J., Quinn, B.D., Foote, H.C., and Hudson, K.R. (2006). Gain-of-function phenotypes of many CLAVATA3/ESR genes, including four new family members, correlate with tandem variations in the conserved CLAVATA3/ESR domain. Plant Physiology *140*, 1331-1344.
3. Yu, J., Hu, S., Wang, J., Wong, G.K.-S., Li, S., Liu, B., Deng, Y., Dai, L., Zhou, Y., and Zhang, X. (2002). A draft sequence of the rice genome (*Oryza sativa* L. ssp. *indica*). Science *296*, 79-92.
4. Mortier, V., Fenta, B.A., Martens, C., Rombauts, S., Holsters, M., Kunert, K., and Goormachtig, S. (2011). Search for nodulation-related CLE genes in the genome of *Glycine max*. Journal of Experimental Botany *62*, 2571-2583.

5. Chamala, S., Chanderbali, A.S., Der, J.P., Lan, T., Walts, B., Albert, V.A., Leebens-Mack, J., Rounsley, S., Schuster, S.C., and Wing, R.A. (2013). Assembly and validation of the genome of the nonmodel basal angiosperm *Amborella*. Science *342*, 1516-1517.
6. Strabala, T.J., Phillips, L., West, M., and Stanbra, L. (2014). Bioinformatic and phylogenetic analysis of the CLAVATA3/EMBRYO-SURROUNDING REGION (CLE) and the CLE-LIKE signal peptide genes in the Pinophyta. BMC plant biology *14*, 47.
7. Miwa, H., Tamaki, T., Fukuda, H., and Sawa, S. (2009). Evolution of CLE signaling: origins of the CLV1 and SOL2/CRN receptor diversity. Plant signaling & behavior *4*, 477-481.
8. Bowman, J.L., Kohchi, T., Yamato, K.T., Jenkins, J., Shu, S., Ishizaki, K., Yamaoka, S., Nishihama, R., Nakamura, Y., and Berger, F. et al. (2017). Insights into land plant evolution garnered from the *Marchantia polymorpha* genome. Cell *171*, 287-304. e215.
9. Delaux, P-M., Radhakrishnan, G.V., Jayaraman, D., Cheema, J., Malbreil, M., Volkening, J.D., Sekimoto, H., Nishiyama, T., Melkonian, M., and Pokorny, L. (2015). Algal ancestor of land plants was preadapted for symbiosis. *PNAS 112*, 13390-13395.
10. Merchant, S.S., Prochnik, S.E., Vallon, O., Harris, E.H., Karpowicz, S.J., Witman, G.B., Terry, A., Salamov, A., Fritz-Laylin, L.K., and Maréchal-Drouard, L. (2007). The *Chlamydomonas* genome reveals the evolution of key animal and plant functions. Science *318*, 245-250.
11. Prochnik, S.E., Umen, J., Nedelcu, A.M., Hallmann, A., Miller, S.M., Nishii, I., Ferris, P., Kuo, A., Mitros, T., and Fritz-Laylin, L.K. (2010). Genomic analysis of organismal complexity in the multicellular green alga *Volvox carteri*. Science *329*, 223-226.
12. Palenik, B., Grimwood, J., Aerts, A., Rouzé, P., Salamov, A., Putnam, N., Dupont, C., Jorgensen, R., Derelle, E., and Rombauts, S. (2007). The tiny eukaryote *Ostreococcus* provides genomic insights into the paradox of plankton speciation. PNAS *104*, 7705-7710.
13. Blanc, G., Duncan, G., Agarkova, I., Borodovsky, M., Gurnon, J., Kuo, A., Lindquist, E., Lucas, S., Pangilinan, J., and Polle, J. (2010). The *Chlorella variabilis* NC64A genome reveals adaptation to photosymbiosis, coevolution with viruses, and cryptic sex. The Plant Cell *22*, 2943-2955.

Chapter 3: Cytokinin-CLAVATA crosstalk regulates the function of a single-celled shoot apical meristem

Foreword

This chapter presents unpublished work probing the regulatory link between CLAVATA and cytokinin signaling proposed in chapters one and two.

Whereas the 2018 Current Biology publication was a culmination of work by many people, the work in Chapter 3 is mainly my own. Mike Scanlon and Adrienne Roeder were indispensable for helping me design and interpret the experiments presented here. Under my mentorship, Christopher Morales Farfan, a BTI summer intern, also provided a substantial contribution with his long days on the confocal, collecting hundreds of image stacks of moss shoots that were used for stem cell quantifications.

Cytokinin-CLAVATA crosstalk regulates the function of a single-celled shoot apical meristem

Abstract

Plant shoots grow from stem cells organized at the Shoot Apical Meristems (SAMs), which produce lateral organs while maintaining a pool of stem cells. In Arabidopsis shoots, signaling pathways downstream of CLAVATA3 (CLV3)-like peptides and the hormone cytokinin antagonistically control plant stem cell abundance by regulating the homeobox gene *WUSCHEL* (*WUS*). The moss *Physcomitrium patens* makes shoots that are derived from a single-celled SAM that performs the same functions as flowering plant SAMs but lacks a role for a *WUS*-like gene. Here we use *Physcomitrium patens* as a model to assess whether CLV3-cytokinin crosstalk is a feature of a stem cell regulatory pathway that lacks *WUS*. In moss shoots, new stem cells are specified on the epidermis, where they will form branches. We previously showed that moss mutants of the CLV3-like peptide receptor genes *CLAVATA1* (*CLV1*) and *RECEPTOR-LIKE PROTEIN KINASE2* (*RPK2*) produce ectopic stem cells, a phenotype associated with increased cytokinin response in both Arabidopsis and moss. We use genetics and cytokinin treatments to elucidate the crosstalk in the signaling network between CLV1, RPK2 and cytokinin in control of stem cell formation. *clv1* and *rpk2* double mutant stem cell phenotypes are additive, indicating they act through distinct mechanisms, and both mutants have weakened responses to cytokinin. Surprisingly, cytokinin receptor mutants have increased numbers of stem cells compared to wild type. Using mathematical modeling, we find that two simple networks can recapitulate the phenotypes of seven mutant genotypes and two dosage levels of exogenous cytokinin, including this novel and counter-intuitive effects of eliminating cytokinin signaling. In both models, CLV1 and RPK2 act through separate pathways where CLV1 represses cytokinin-mediated stem cell initiation and RPK2 inhibits stem cell initiation through a cytokinin-independent pathway. Our work elucidates *WUS*-independent crosstalk between CLV/RPK2 and cytokinin signaling in moss shoots and suggests that crosstalk between CLV and cytokinin signaling is an ancient feature of shoot stem cells.

Introduction

Plant shoot morphology is determined by groups of stem cells called Shoot Apical Meristems (SAMs) reserved at growing shoot tips. SAMs must perform two essential functions: first the patterning of lateral organ initiation, and second the rejuvenation of the stem cell population to replace cells recruited to form those lateral organs. Decades of study in the model flowering plant *Arabidopsis thaliana* have revealed a key role for a negative feedback loop in maintaining the SAM[1]. Stem cells at the apex of the meristem secrete the CLAVATA3/EMBRYO SURROUNDING REGION (CLE) peptide CLV3[2,3]. CLV3 acts through a suite of leucine-rich repeat receptor-like kinases (LRR-RLKs) including CLAVATA1 (CLV1) and RECEPTOR-LIKE PROTEIN KINASE2 (RPK2), to limit the expression of the stem cell organizing gene *WUSCHEL* (*WUS*) to several cell layers below the apex and delimit the size of the stem cell pool[4–8]. WUS protein moves apically to promote stem cell identity and activates expression of its repressor *CLV3*, completing the negative feedback loop[9,10]. In Arabidopsis, *wus* mutants fail to maintain a SAM[11,12]. In contrast, *clv3*, *clv1*, or *rpk2* loss-of-function mutants fail to downregulate *WUS* expression and produce too many stem cells, leading to increased organ numbers and eventual fasciation[1,4].

Stem cell homeostasis is important for determining shoot morphology. For example, changes to CLAVATA signaling can alter phyllotaxy, organ number, and organ size[13]. Despite its importance, we have a poor understanding of signaling pathways regulating stem cell homeostasis. This is in part because there is a large suite of LRR-RLKs and related proteins with complex interactions[14]. LRR-RLKs in the meristem often have multiple paralogs that can compensate for loss of function mutations[15]. Receptors from different gene families share the same set of co-receptors, and each respond to the same ligand (CLV3) through independent, unknown signaling pathways[16]. Meanwhile, receptors are not beholden to a single ligand; a single receptor complex was shown to produce different downstream signals elicited by two different CLE ligands[17]. Such a high degree of genetic complexity highlights the need for a simpler genetic system with which to dissect how CLE signaling regulates stem cell identity.

Physcomitrium patens (previously *Physcomitrella patens*) is a prominent bryophyte model system that is used to study the evolution of developmental mechanisms[18]. Physcomitrium produces haploid upright shoots (gametophores) that pattern leaves (phyllids) in a spiral phyllotactic pattern from a SAM. The Physcomitrium SAM comprises a single tetrahedral apical stem cell rather than a multicellular dome[20]. Despite this anatomical difference, the moss apical cell must accomplish the same two functions as the angiosperm SAM: self-renewal and lateral organ patterning. The transcriptome of the moss SAM shares a high degree of overlap with flowering plant SAMs, suggesting possible deep homology underlying control of the SAM in non-homologous shoots[21].

With only three known putative CLE receptors in its genome, Physcomitrium is an appealing model for understanding CLE signaling[19].

We previously characterized the role of *CLV1* and *RPK2* orthologs in Physcomitrium and found that these genes performed similar functions in moss and flowering plants[22]. We also discovered a novel role for CLV1 as a regulator of cell division plane orientation during shoot formation in moss and during root development in Arabidopsis. We also found that moss *clv1* and *rpk2* mutants produce ectopic stem cells along their shoots, establishing that the canonical function of CLV1 and RPK2 is conserved from Arabidopsis to Physcomitrium. Interestingly, whereas the Arabidopsis *clv1* and *rpk2* stem cell phenotypes are attributed to overaccumulation of WUS, *Physcomitrium patens* lacks closely related orthologs of *WUS*[23]. The Physcomitrium genome contains three *WUSCHEL-RELATED HOMEOBOX* (*WOX*) encoding genes, all of which are part of the ancient *WOX* clade that lack domains critical for the stem cell modulatory function of WUS[23–25]. Moss *wox* mutants are compromised in their ability to initiate tip growth in regenerating filamentous tissues; however, their shoot development is normal. Together, these data suggest an absence of *WOX* genes from the shoot stem cell regulatory network[26]. This raises the question: in the absence of WOX-mediated stem cell maintenance, how do CLV1 and RPK2 function as stem cell inhibitors in moss?

The hormone cytokinin plays an important role in promoting SAM formation in Arabidopsis[27,28]. Likewise in moss, cytokinin promotes the formation of SAMs from filamentous juvenile tissue and on existing shoots[29,30]. Several lines of evidence suggest an antagonistic relationship between CLE and cytokinin signaling in both

Arabidopsis and moss[22,31]. In moss shoots, cytokinin promotes the formation of new SAMs that initiate branches[30], while loss of CLE signaling causes ectopic stem cell formation[22]. Intriguingly, one of the best understood mechanisms by which cytokinin promotes SAM formation in Arabidopsis is by its induction of *WUS*[28,32]. This again begs the question of how a regulator of SAM function – in this case cytokinin – can perform the same function in moss and Arabidopsis despite the absence of a key *WOX* genes from the moss network. Given the antagonistic functions of CLV and cytokinin signaling, we ask whether there is ancient *WOX*-independent crosstalk between CLE and cytokinin signaling.

Here we continue our use of Physcomitrium as a model to understand stem cell signaling. We first investigated whether CLV1 and RPK2 act in common or separate pathways, which is also an open question in Arabidopsis. We found that CLV1 and RPK2 regulate cell differentiation via distinct pathways, with greater support for CLV1 acting upstream of cytokinin-induced stem cell formation. Surprisingly, we found that loss of cytokinin signaling increases the initiation of stem cells and associated branches. Our computational models provide several viable explanations for this unexpected phenotype, including a possible regulatory interaction where cytokinin promotes CLE signaling. Overall, our data support a network in which CLE signaling and cytokinin intersect in the regulation of moss SAM maintenance. This network is distinct from the canonical angiosperm network in that it lacks a role for a *WOX* gene as the hub where cytokinin and CLE signaling intersect.

RESULTS

CLV1 and RPK2 function through distinct pathways

Our previous research revealed a conserved role for the moss LRR-RLKs CLV1 and RPK2 in inhibiting stem cell specification in moss shoots[22]. Loss of function of the two *CLV1* paralogs (*CLV1a* and *CLV1b*) or of *RPK2* resulted in shoots with ectopic apical cells along the lengths of swollen stems[22]. In order to determine whether CLV1 and RPK2 function in the same pathway to regulate stem cell formation in moss, we used CRISPR-Cas9 mediated mutagenesis to target *RPK2* in a *clv1a;clv1b* mutant background and generated multiple, independent, triple mutant lines with similar phenotypes (Supplemental Figure 1). We examined wild type, *clv1a;clv1b*

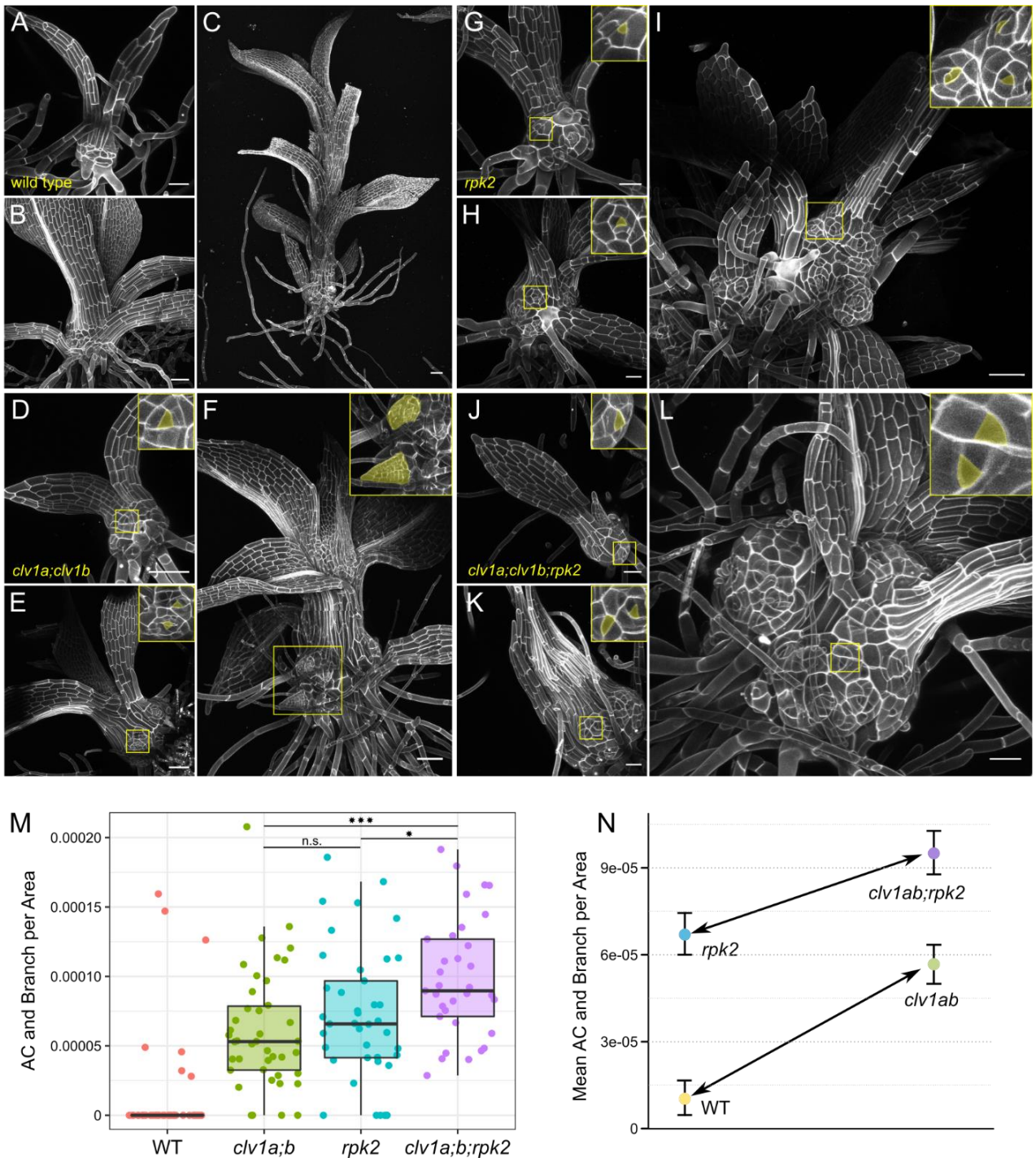

Figure 1: *clv1* and *rpk2* phenotypes are additive. Shoot development at approximately one week (A, D, G, J), two weeks (B, E, H, K) and at three to four weeks (C, F, I, L) in wild type (A-C), *clv1a;clv1b* (D-F), *rpk2* (G-I), and *clv1a;clv1b;rpk2* triple mutants (J-L). Ectopic stem cells and branches per square micron of visible stem tissue from 30-40 shoots of each genotype (M). An interaction plot showing the effects of *clv1* (left to right, arrow) and *rpk2* (top to bottom) on ectopic stem cell per square micron (N). The similar slopes of the two lines demonstrate that the effect of the *clv1* mutation is the same in the wild type or *rpk2* background.

double mutants, *rpk2* single mutants, and *clv1a;clv1b;rpk2* triple mutant shoots across developmental stages ranging from less than one week old to approximately four weeks old (Figure 1).

Wild type shoots were covered with leaves, leaving little exposed stem tissue (Figure 1 A, B, C). Where stem tissue was visible, we occasionally saw branches forming from newly specified apical cells (Figure 1 B). In contrast, *clv1a;clv1b, rp2k,* and triple mutant stems were swollen from the earliest stages of development (Figure 1D, G, K). Ectopic triangular apical cells were present on the rounded stems of these mutants at all stages of development. At later stages, *clv1, rpk2* and triple mutant shoots produced numerous ectopic branches, indicating that the ectopic apical cells observed at earlier stages were functional but dormant SAMs (Figure 1F, I).

Starting at approximately leaf four, wild type leaves developed midribs with long, densely staining cells (Figure 1B, C). Meanwhile, mutant leaves at often formed broad swaths of clear, midrib-like cells that sometimes spanned the width of the leaf-base (Figure 1 E, F, I, K, L). This novel phenotype was especially common in *clv1a;clv1b* and *clv1a;clv1b;rpk2* triple mutants, although it was sometimes observed in *rpk2* single mutants. Thus, *CLV1* and *RPK2* appear to have overlapping but non-identical roles regulating midrib development.

Finally, *clv1* and *rpk2* mutant shoots stopped elongating much earlier than wild type, often terminating in a swollen apex with abundant apical cells (Figure 2). After terminating longitudinal growth, *clv1a;clv1b, rpk2,* and triple mutant shoots continued to swell and initiate new growth axes from ectopic stem cells along the length of the stem (Figure 1 F, I, L, Figure 2 B). Stem swelling was especially prominent in *rpk2* and *clv1a;clv1b;rpk2* triple mutants, again highlighting different contributions of *CLV1* and *RPK2* to shoot development. Shoot termination in *clv1* and *rpk2* mutant stems was reminiscent of stem cell over-proliferation and disorganization of the SAM seen in Arabidopsis mutants with perturbed stem cell homeostasis, again highlighting the suitability of moss for studying stem cell specification[22].

The *clv1a;clv1b;rpk2* triple mutants appeared to combine aspects of the *clv1* and *rpk2* shoot phenotypes. Triple mutant shoots produced thick midribs like *clv1* mutants but terminated early and swelled like *rpk2* mutants.

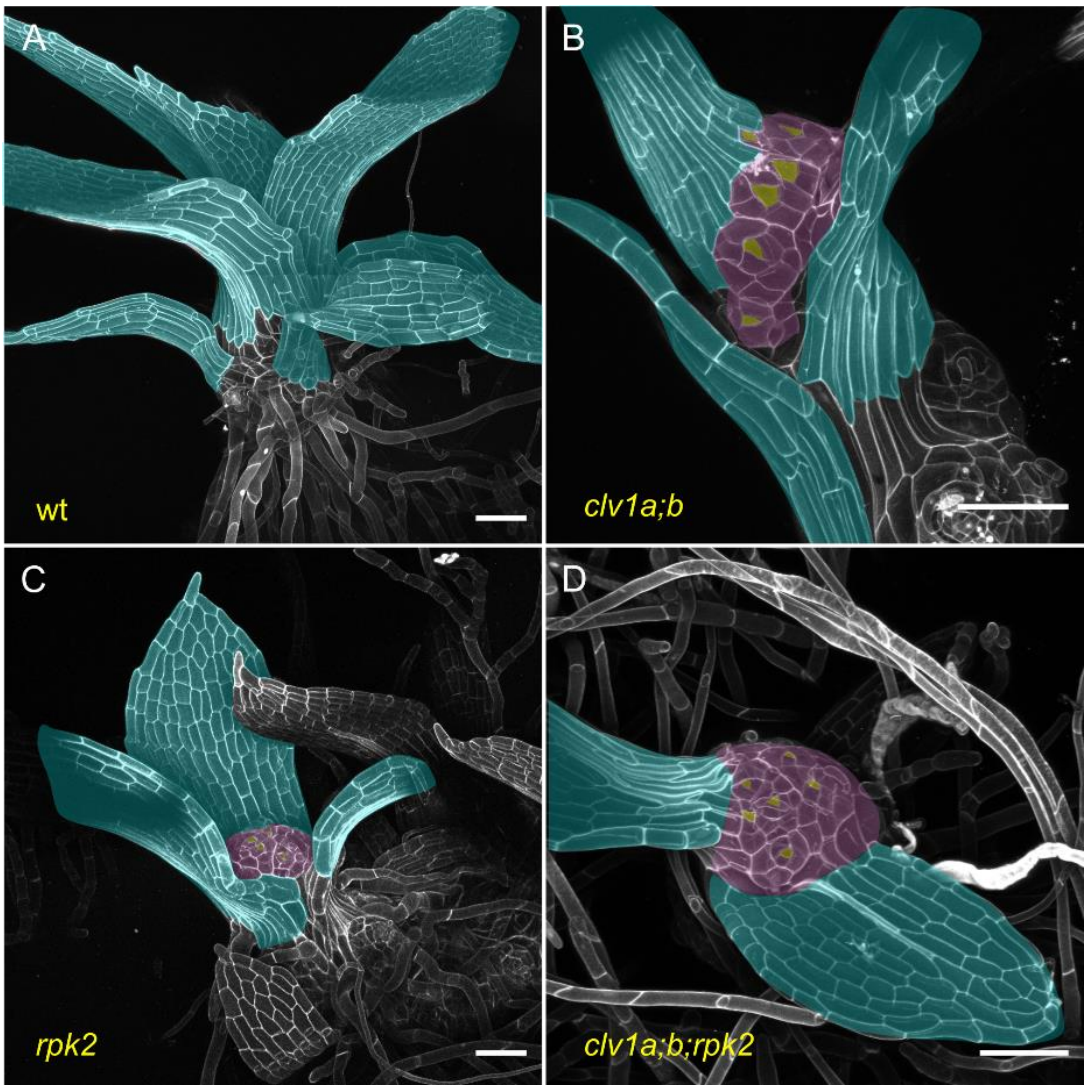

Figure 2: ***clv1* and *rpk2* shoots terminate in a mass of stem cells**. Approximately three-week-old wild type (A), *clv1a;clv1b* (B), *rpk2* (C), and *clv1a;clv1b;rpk2* triple mutant (D) shoots. Bare shoot apices replete with stem cells are visible in *clv1* and *rpk2* mutants, while the single apical cell at the apex of wild type shoots is well-covered by leaves. Leaves are pseudo colored blue, apices are pseudo colored magenta, and apical stem cells are pseudo colored yellow. Scalebars: 100 nm

However, it was not clear how CLV1 and RPK2 signaling interact to inhibit ectopic stem cell formation. In order to gain a deeper understanding of how CLV1 and RPK2 regulate stem cell specification, we quantified the number of ectopic stem cells visible by confocal microscopy on 30-40 shoots of each genotype. We normalized the number of ectopic stem cells to the size of the stem to control for any increase in stem cell count due to the swelling or variation in shoot developmental stage (Figure 1 M). If *CLV1* and *RPK2* act in a linear

genetic pathway, then one mutant should be epistatic to the other. If CLV1 and RPK2 have redundant functions but act in distinct complexes, we expected to see a synergistic increase in stem cell initiation in the *clv1a;clv1b;rpk2* triple mutant. Finally, if *CLV1* and *RPK2* act non-redundantly, i.e. in distinct signaling pathways, then we expected the mutations to have an additive effect on stem cell initiation.

While most wild type shoots produced no branch stem cells, we saw ectopic branch stem cells on almost all *clv1a;clv1b* and *rpk2* mutants. Every triple mutant gametophore we observed possessed at least one ectopic stem cell (Figure 1 M). Pairwise comparisons revealed no significant difference in ectopic stem cell formation between *clv1* and *rpk2* mutants, but each produced significantly fewer ectopic stem cells per square micron than the triple mutant. An interaction plot displaying the effects of mutating *clv1* (left to right) and *rpk2* (top to bottom) showed that the effect of mutating *clv1* (the slope of the arrow-headed line) was similar in both wild type and *rpk2* backgrounds, i.e. the effects were additive (Figure 1 N). Altogether, the data suggest that CLV1 and RPK2 do not function in the same linear pathway to regulate stem cell abundance in the moss shoot.

CLV1 and RPK2 signaling interacts with Cytokinin signaling

In moss, cytokinin induces stem swelling and the formation of new SAMs along the axis of the shoot[30], similar to the phenotypes seen in *clv1* and *rpk2* mutants (Figure 3A-C and Figure 1). We hypothesized two possible pathways to explain these data. First, *CLV1* and/or *RPK2* could function by inhibiting cytokinin-mediated stem cell specification, i.e. *CLV1/RPK2* function is upstream of cytokinin response. Alternatively, cytokinin signaling might be upstream and inhibit *CLV1/RPK2* such that cytokinin de-represses stem cell formation. To better understand how *CLV1* or *RPK2* signaling interact with cytokinin signaling, we characterized the response of *clv1a;clv1b*, *rpk2*, and *clv1a;clv1b;rpk2* mutants to 10nM and 100nM exogenous BAP, a synthetic cytokinin. If the first hypothetical pathway were true, we predicted that cytokinin treatment would induce stem cell formation in *clv1* and *rpk2* mutants. In the second scenario, *clv1* and *rpk2* loss of function would be epistatic to cytokinin and exogenous cytokinin would have no effect in *clv1* and *rpk2* mutants.

We quantified the number of ectopic stem cells and branches in each genotype grown on 10nM and 100nM cytokinin, and measured stem area as described above. Wild type shoots grown on a 10 nM BAP displayed

slight swelling, with more cells visible beneath where the first leaves attached than were visible on shoots grown without BAP (Figure 3A-B). These shoots also developed ectopic tetrahedral apical cells reminiscent of those seen in *clv1* and *rpk2* mutants. On a higher concentration of cytokinin, wild type stems were swollen and formed numerous ectopic branches (Figure 3C). 10 nM BAP only had a mild impact on stem swelling and ectopic apical cell formation in *clv1a;clv1b* and *rpk2* mutant shoots (Figure 3 E, H, M). However, *clv1* and *rpk2* shoots grown on 100 nM cytokinin displayed numerous ectopic branches and apical cells and a high degree of stem swelling (Figure 3F, I). Interestingly, growing *clv1a;clv1b;rpk2* triple mutants on 10 nM or 100 nM BAP resulted in a similar amount of stem cells per area (Figure 3 K, L, M). Overall, stem cell formation increased in *clv1a;clv1b, rpk2*, and *clv1a;clv1b;rpk2* triple mutants in response to cytokinin. These data support rejecting our second proposed pathway where cytokinin is an upstream inhibitor of *CLV1/RPK2* and instead support a role for *CLV1/RPK2* upstream of cytokinin response. Interestingly however, while cytokinin induced stem cell formation in all genotypes, this effect was weaker *clv1* and *rpk2* mutants (Figure3 M).

Given the possible reduced sensitivity of *clv1* and *rpk2* mutants to cytokinin, we wanted to statistically assess how *CLV1*, *RPK2*, and cytokinin interact to control stem cell specification. To do so, we analyzed our full dataset including each mutant off cytokinin and on 10 and 100 nM BAP using a Poisson regression suited for count data, including stem size as an offset in the model to account for any correlation between the size of the shoot and ectopic stem cell number. There was a significant increase in stem cells caused by loss of *CLV1* or *RPK2*, as well as by cytokinin treatment (p value and Poisson coefficient for *clv1*: $p = 0.0001$, coefficient = 0.64; *rpk2*: $p < 0.0001$, coefficient = 0.96; cytokinin treatment: $p < 0.0001$, coefficient = 0.0133, see materials and methods for details). There was no significant statistical interaction between the effects of *clv1* and *rpk2* loss of function, ($p = 0.240$) indicating that these mutant phenotypes were additive. Interestingly, each mutant showed a statistically significant, slight reduction in response to exogenous cytokinin (Figure 2I*; clv1*:cytokinin $p = 0.033$, coefficient = -0.003; *rpk2*:cytokinin $p < .0001$; coefficient = -0.009;).

In summary, the phenotypes of *clv1a;b* and *rpk2* were additive across a range of exogenous cytokinin concentration, suggesting that CLV1 and RPK2 act via distinct pathways regulating stem cell specification.

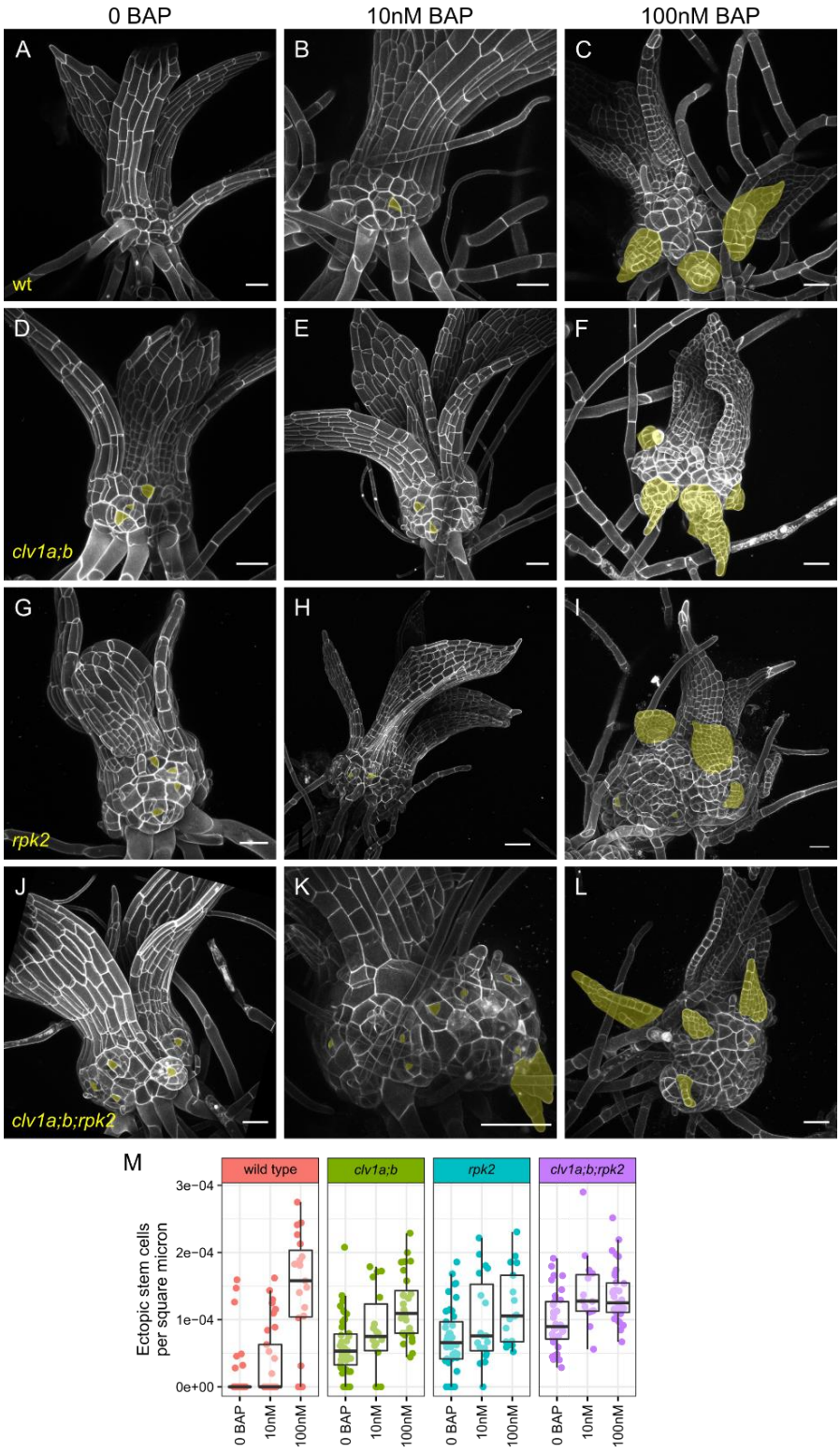

Figure 3: **Cytokinin induces phenotypes similar to *clv1/rpk2* and increases apical cell formation in *clv1/rpk2* mutants.** Two- to three-week-old shoots grown on media supplemented with low (10 nM, A, C, E, G) and high (100 nM, B, D, F, H) BAP. Quantification of ectopic stem cells per area of exposed stem (I). Note that (I) includes data from Figure 1M for clarity.

Stem cell initiation increased in *clv1* and *rpk2* mutants, supporting a role for *CLV1/RPK2* upstream or independent of cytokinin signaling. However, loss of *CLV1* or *RPK2* also slightly diminished the effect of exogenous cytokinin on stem cell production. These data suggest that cytokinin response could already be high in *clv1* and *rpk2* mutants such that exogenous cytokinin treatments represented a smaller relative increase in cytokinin signaling in the mutants than in wild type. Such a scenario would occur if CLV1 and/or RPK2 functioned by inhibiting cytokinin-mediated stem cell specification.

Mathematical modeling supports action by CLV1 and RPK2 through distinct pathways

To elucidate the regulatory network that integrates CLV1, RPK2, and cytokinin signaling to control stem cell identity in the moss shoot, we evaluated five hypothetical network models. Given that the data supported CLV1 and RPK2 signaling through separate pathways, we coded two variables, 'x' and 'y', to represent these pathways. It is important to note that x and y do not represent any specific genes, but rather are simplified representations of unknown but postulated signaling outputs. As cytokinin induces stem cell formation, we specified that x is induced by cytokinin, while y is synthesized according to a cytokinin-independent basal synthesis parameter; both x and y then induce stem cell formation.

In the first model, RPK2 and CLV1 are both capable of inhibiting stem cell initiation through both cytokinin-dependent and independent pathways, i.e. through both x and y (Figure 4 A). This model has the greatest flexibility and represents a scenario where CLV1 and RPK2 are partly redundant and partly independent. The second and third models simulate the cases where CLV1 and RPK2 act completely independently (Figure 4 B and C). In model two CLV1 inhibits cytokinin responsive stem cell induction (x) and RPK2 inhibits cytokinin-independent stem cell induction (y), while the roles for CLV1 and RPK2 are reversed in model three. Models four and five simulate completely redundant CLV1 and RPK2 activity: in model four both CLV1 and PPK2 inhibit x (Figure 4 D), while in model five both inhibit y (Figure 4 E).

The behavior and output of a model depends on the parameters selected. To find the optimal parameters for each model that allowed it to best fit the data, we used a random optimizer function. Given a set of parameters for the strength of interactions between variables (e.g. how potently cytokinin induces x), we used the model to

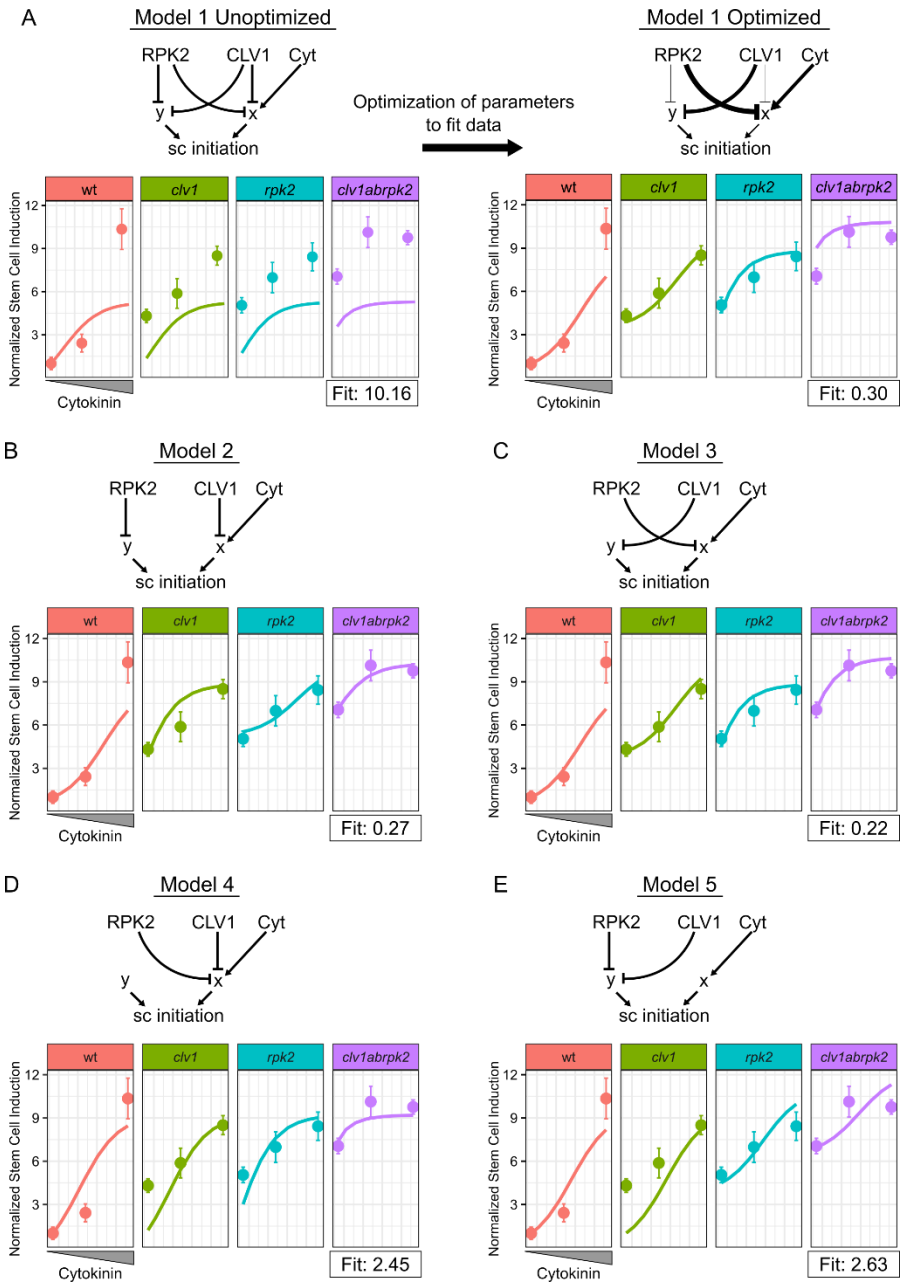

Figure 4: Dynamical model simulations of stem cell production by *clv1* and *rpk2* mutants over a range of cytokinin concentrations. Basic network depictions and simulation results of mathematical models formalizing five different hypotheses: CLV1 and RPK2 are partially redundant (A); CLV1 and RPK2 are independent with CLV1 upstream of cytokinin response (B); CLV1 and RPK2 are independent with RPK2 upstream of cytokinin response (C); CLV1 and RPK2 are redundant and upstream of cytokinin response (D); CLV1 and RPK2 are redundant and upstream of a cytokinin-independent pathway (E). On plots, Solid lines represent simulated data over a range of cytokinin concentrations. Dots with error bars represent the mean empirical stem cells per square micron data and standard errors. From left to right, dots represent values from moss grown on BCD, 10 nM BAP, and 1 nM BAP. The model on the right side of panel A has had the thickness of interactions changed proportional to the corresponding optimized parameters.

simulate each relevant genotype (wild type, *clv1a;b, rpk2, clv1a;b;rpk2*) at each level of cytokinin treatment (no BAP, 10nM BAP, 100nM BAP). For each model we thus simulated twelve scenarios that we compared with the corresponding mean values from the empirical data. We generated a single fit score that was proportional to the difference between the model and the empirical data, with larger differences penalized more heavily than smaller ones (See Model Methods). Once a score was generated, each model coefficient was randomly mutated (adjusted up or down) and a new fit score was calculated and compared to the previous one.

If the new fit score were better (lower), the new parameters for that run were adopted as the starting point for the next round of optimization. If the fit score proved worse, the previous parameters were kept as the starting point for the next round of optimization. We ran the optimizer for 300 iterations, allowing the fit score to plateau at an optimum value for each model (Supplemental model information).

Using this iterative optimizer, we tested our five competing hypotheses of how CLV1, RPK2, and cytokinin regulate stem cell identity. For model one, the optimizer selected parameters that separated the roles for CLV1 and RPK2, i.e. the optimizer minimized their redundant activity and emphasized their independent activity (Figure 4 A). Specifically, the optimizer strengthened the regulatory connection between RPK2 and cytokinin-dependent signaling while weakening the interaction between RPK2 and cytokinin-independent induction; the opposite was done for CLV1 (Figure 4 A). Thus, the optimized Model 1 was similar to Model 3 (Figure 4 C). Optimized Model 1 reasonably replicated the empirical data with a fit score of 0.3, but notably overestimated the number of ectopic stem cells in the *clv1a;b;rpk2* triple mutant grown in the absence of exogenous cytokinin (Figure 3 A). Models 2 and 3 produced nearly equivalent fits to Model 1 after optimization with fit scores of 0.27 and 0.23, respectively (Figure 5 B, C). Notably, Model 2 and Model 3 successfully simulated the level of stem cell initiation *clv1a;clv1b;rpk2* without exogenous cytokinin. These two models differed from one another predominately in the cytokinin response curves of *clv1* and *rpk2* mutants (Figure 3 B and C), but neither simulation was far from the empirical data. Finally, Model 4 (fit score = 2.45) and 5 (fit score = 2.63) produced very poor fits to the data (Figure 2 D and E). Altogether, the five models support CLV1 and RPK2 acting

through separate pathways. However, the models do not distinguish whether CLV1 or RPK2 functions upstream of the cytokinin response as either scenario could reproduce the empirical data.

We next used our models to predict how stem cell initiation would be affected by the absence of cytokinin signaling (Supplemental figure 2). Each model predicted that at zero cytokinin, every simulated genotype would produce even fewer apical cells than any other condition. This is consistent with data showing reduced branch stem cell initiation after increasing cytokinin degradation[30]. Informatively, the model predicted that at zero cytokinin perception, ectopic stem cell formation caused by the loss of whichever receptor (RPK2 or CLV1) that functioned upstream of cytokinin dependent stem cell initiation would be suppressed.

Loss of cytokinin signaling reveals a complex network controlling stem cell specification

The three *CYTOKININ HISTIDINE KINASE* (*CHK*) genes in Physcomitrella encode the cytokinin receptors, and *chk1;2;3* triple mutants lack the ability to perceive cytokinin[33,34]. Using CRISPR-Cas9 to mutate *CLV1a, CLV1b,* and *RPK2* in the *chk1;2;3* background, we generated multiple independent lines of *clv1a;clv1b;chk1;2;3* quintuple mutants, *rpk2;chk1;2;3* quadruple mutants, and *clv1a;clv1b;rpk2;chk1;2;3* sextuple mutants (Supplemental Figure 3). Our models predicted that if ectopic stem cell formation in *clv1* mutants resulted from increased cytokinin-mediated stem cell initiation, ectopic stem cell formation would be suppressed in the higher order *clv1;chk* mutants. Alternatively, if RPK2 signaling were upstream of the cytokinin response (x), the *rpk2* ectopic stem cell phenotype would be suppressed in *rpk2;chk1;2;3* mutants. To test our predictions of how loss of cytokinin signaling impact stem cell specification, we examined shoots from multiple independent lines of *chke1;2;3* and higher order mutants at cellular resolution.

Cytokinin induces the formation of branches on shoots[30] and promotes cell proliferation in leaves[35]. Consistent with these functions, the *chk1;2;3* mutants only form shoots after two weeks delay relative to wild type plants[34]. Once formed, *chk1;2;3* shoots produce long, slender leaves with highly elongated cells and fewer cell files. Surprisingly, confocal imaging of *chk1;2;3* shoots revealed the formation of supernumerary branches, indicating increased rather than decreased stem cell production. Higher order *clv1a;b;chk1;2;3, rpk2;chk1;2;3,* and *clv1a;clv1b;rpk2;chk1;2;3* and CLE-receptor mutants had variable phenotypes (Supplemental Figure 4),

but often produced swollen stems with ectopic apical cells (Figure 5). Thus, contrary to our predictions, loss of cytokinin signaling did not suppress stem cell initiation in general or the ectopic stem cell phenotypes of *clv1* or *rpk2* mutants. These data suggest that neither CLV1 nor RPK2 are upstream of cytokinin mediated stem cell specification in a simple pathway.

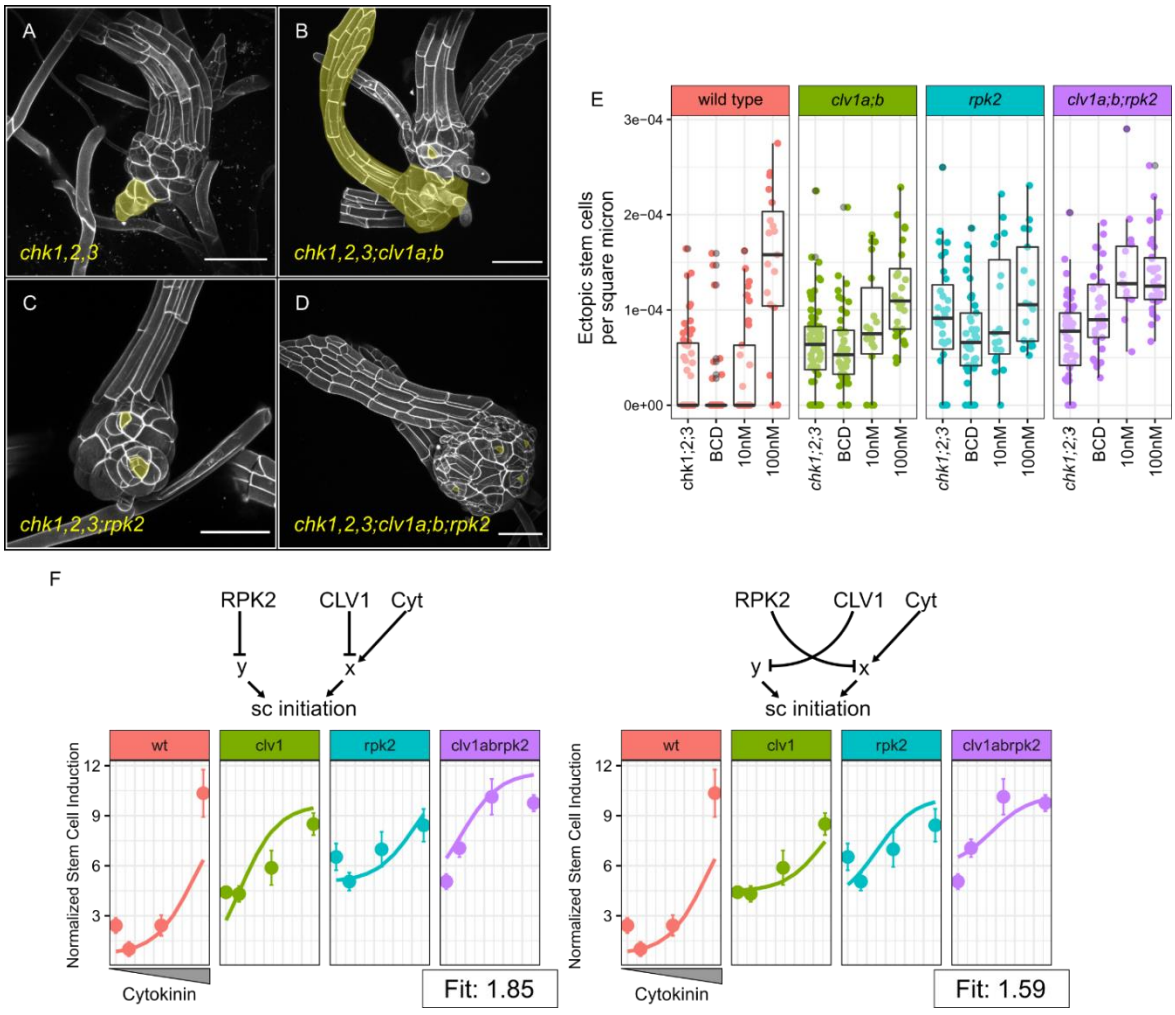

Figure 5: *chk1;2;3* mutants produce ectopic stem cells and have complex interactions with *clv1* and *rpk2* mutants. Shoots from five week old colonies (*chk* mutants are severely delayed in shoot production) of *chk1;2;3* (A), *clv1a;clv1b;chk1;2;3* quintuple mutants (B), *rpk2;chk1;2;3* quadruple mutants (C), and *clv1a;clv1b;rpk2;chk1;2;3* sextuple mutants (D). Quantification of ectopic stem cells per square micron of visible stem (E), including data from Figure 2 I to highlight trends in the data. Earlier models of stem cell regulation are unable to fit *chk* mutant data (F). For plots in panel F, solid lines represent optimized, simulated values while points with error bares represent empirical data. From left to right, dots reflect data from plants with mutated *CHK*, then moss grown on BCD, 10 nM BAP, and 100 nM BAP.

We tested whether the networks represented by our previous models could be optimized to fit the new *chk* mutant data. We quantified ectopic stem cell number and stem area in *chk* and in the quadruple, quintuple, and sextuple mutants. Using our random optimizer, we attempted to fit models two and three to the new, full data set that included the *chk* and higher order *chk*-CLE receptor mutants. Each model failed to recapitulate the data; specifically, the models failed to reproduce the increase in stem cell formation seen in the *chk* mutants (Figure 5 F). Altogether, our data falsified the hypotheses represented by our dynamical models and made clear that we are missing important features of the stem cell specification pathway.

Modulation of cytokinin-mediated stem cell specification and CLE signaling recapitulates *chk* mutant phenotypes

The production of ectopic branches in the *chk1;2;3* mutant could arise if cytokinin represses a pathway that induces branching, or if cytokinin promotes a pathway that represses branching. To test the plausibility of these hypotheses, we formalized each as a dynamical model (Model 6 and 7, respectively). For each model, we introduced a factor called z. In Model 6, z induced stem cell initiation and was inhibited by cytokinin (Figure 5 A), while in Model 7 z inhibited stem cell initiation and was itself induced by cytokinin (Figure 5 B). Several lines of evidence thus far suggested that CLV1, RPK2, or CLE signaling in general interact with cytokinin signaling: both *clv1* and *rpk2* mutants responded less strongly to exogenous cytokinin (Figure 3 M), and *clv1a;clv1b;rpk2* loss of function suppressed the *chk*-dependent increase in stem cell specification (Figure 5 E). Additionally, a growing body of evidence in Arabidopsis suggests that cytokinin upregulates *CLV3*[36,37]. Thus, we proposed Model 8, which represented a more specific case of model seven where instead of promoting an unknown inhibitor of stem cell specification (z), cytokinin promoted CLE expression (Figure 5 C). In Model 8 the CLEs formed complexes with CLV1 or RPK2, which were responsible for downstream signaling.

We attempted to fit each model to the full dataset and looked to see how well the models captured key trends in the empirical data. Because we were previously unable to determine whether CLV1 or RPK2 acted upstream of cytokinin signaling (x), we simulated both scenarios for each model. Model 6 simulated the data with high accuracy without any regulatory interaction between cytokinin and CLV1 or RPK2 (Figure 5 D). Interestingly, this model fit notably better if CLV1 were upstream of the cytokinin response (fit score = 0.53) than if RPK2

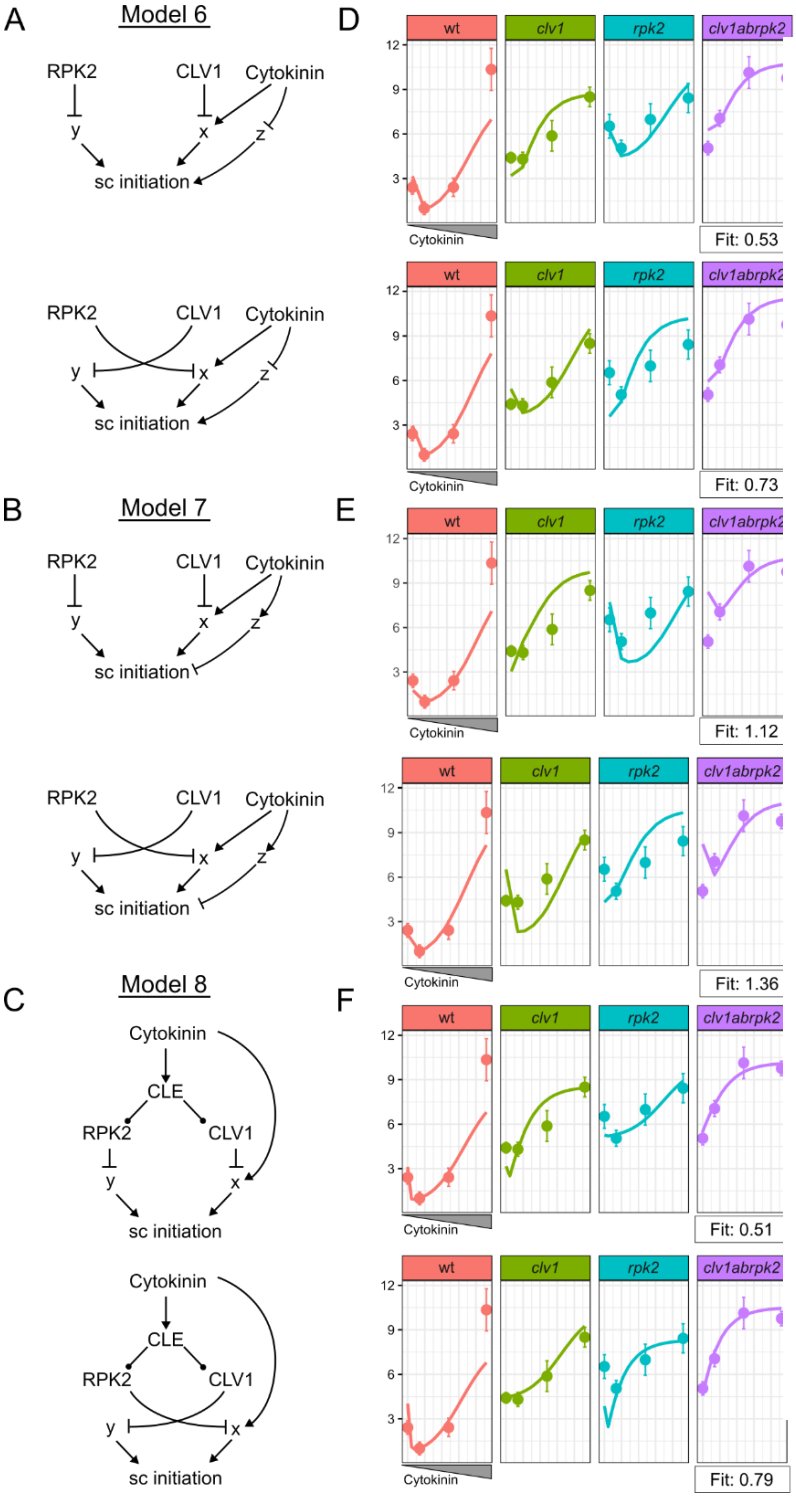

Figure 6: Additional input from cytokinin greatly improves simulations of stem cell initiation across. Model six posits that cytokinin inhibits an inducer of stem cell identity (A). In model seven, cytokinin promotes an inhibitor of stem cell specification (B). Model eight represents a specific case of model seven: instead of an unknown inhibitor of stem cell identity, we model that cytokinin promotes CLE signaling (C). Dots in (C) denote complex formation. Results for corresponding models on the left (D, E, F). Solid lines represent simulated data while dots represent mean stem cells per area from the empirical data. Error bars show the standard error. The x axis shows a log transformation of the cytokinin value input to the model. *chk* mutant data was aligned with the model simulating '0' cytokinin, while plants grown on BCD were aligned with cytokinin equal to 0.75.

were upstream of the cytokinin-dependent response (fit score = 0.73). Model 7 - in which cytokinin induced a stem-cell inhibitor – fit the data poorly in all cases (fit scores 1.86, 1.82) (Figure 5 E). While this model could replicate the *chk1;2;3* and wild type cytokinin treatment data, it was unable to recapitulate the effects of *chk* loss of function in *clv* and *rpk2* mutant backgrounds and simulated *clv1a;clv1b;rpk2;chk1;2;3* sextuple mutants especially poorly. Finally, Model 8 (with *CLE* expression downstream of cytokinin) successfully fit the data (Figure 5 F); like with Model 6, this model worked best when CLV1 was upstream of cytokinin response (fit score 0.51, as opposed to 0.79 with *RPK2* upstream). Thus, while either Model 6 or Model 8 could explain the data, both supported a role for *CLV1* as an inhibitor of cytokinin-mediated stem cell specification.

Discussion

There is evidence for crosstalk between CLV1, RPK2, and cytokinin signaling controlling cell differentiation throughout Arabidopsis development[31]. However, the complexities of CLE signaling and our poor understanding of it complicates these interpretations. Our previous work raised the possibility of an ancestral WOX-independent interaction between CLE and cytokinin signaling. Here we used a combination of genetics, hormone treatments, and mathematical modeling to demonstrate an ancient stem cell regulatory network with conserved roles for cytokinin and CLE signaling but without a role for a WOX gene. These data lead us to question the general centrality of WOX genes for meristem function, and instead indicate that WOX genes were later incorporated into stem cell regulatory networks.

CLV1 and RPK2 signal through distinct pathways

In Arabidopsis, it is unclear whether CLV1 and its paralogs function in the same pathway as RPK2. There is evidence of a signaling module of BARELY ANY MERISTEM1 (BAM1, a CLV1 paralog) and RPK2 regulating root meristem size[38], and *bam* and *rpk2* mutants have similar, non-identical anther phenotypes[39,40]. However, *rpk2* and *clv1* mutants additively increase expansion of the stem cell population in the Arabidopsis SAM, suggesting function through distinct pathways[4]. Thus, data from Arabidopsis is conflicting as to whether *CLV1* and *RPK2* function in the same or distinct pathways.

The suite of CLE receptors is much reduced in moss compared to Arabidopsis, making it a powerful system for studying the genetic interactions of these receptors[22]. We previously showed that *clv1a;clv1b* and *rpk2* have distinct filament phenotypes in moss, where *rpk2* colonies spread faster than wild type or *clv1* colonies[22]. This phenotypic distinction could arise from differences in expression patterns, rather than distinct molecular functions. However, *CLV1* and *RPK2* are co-expressed in buds, where they render distinct mutant phenotypes [22]. Here we showed that while *clv1* and *rpk2* mutants both produce ectopic stem cells, the higher order *clv1a;clv1b;rpk2* mutants displayed an additive increase in ectopic stem cells, suggesting that CLV1 and RPK2 act through distinct pathways to regulate stem cell specification. Altogether, phenotypic evidence from filaments, buds, and shoots all support distinct mechanisms of action for CLV1 and RPK2 in moss.

Crosstalk of CLV signaling with cytokinin is complex

In Arabidopsis, CLV1, RPK2, and cytokinin regulate stem cell identity as part of a network centered around the master regulator gene *WUSCHEL*. In moss, *WOX* genes are important for initiating tip growth and the regeneration of filaments, but do not otherwise regulate in shoot apical meristem function[26]. Both increased cytokinin and decreased CLV1/RPK2 cause similar phenotypes including stem swelling and ectopic stem cell formation, signaling led us to ask whether there is a *WOX*-independent CLV/RPK2-cytokinin network at play in moss. *clv1a;clv1b*, *rpk2*, and *clv1a;clv1b;rpk2* triple mutants produced fewer ectopic stem cells in response to cytokinin than wild type, indicating reduced sensitivity to cytokinin or that cytokinin response approached saturation in *clv1* and *rpk2* mutants. We used mathematical modeling to determine which of eight different hypothetical networks describing CLV1, RPK2, and cytokinin function could best recapitulate empirical stem cell specification data. Our data and modeling suggest that either *CLV1* or *RPK2* acts upstream of cytokinin-mediated stem cell induction, with greater support for CLV1 performing this role. Interestingly, this cytokinin-dependent pathway (x in the model, Figure 4, Figure 6) occupies the same position as *WUS* in models describing stem cell specification in the Arabidopsis SAM[1,41]. This suggests that in the absence of *WUS*, stem cell number in moss is regulated by similar mechanism as described in Arabidopsis but that the function of *WUS* is replaced by an unknown mechanism.

Cytokinin signaling both induces and inhibits SAM formation

Our analysis of *chk1;2;3* and higher order *clv;chk* and *rpk2;chk* mutants revealed several unexpected phenotypes. First, we observed that *chk1;2;3* mutants make ectopic branches, contrasting with our current understanding of cytokinin as a key factor promoting branch formation. We proposed several models to explain the counterintuitive *chk1;2;3* phenotype, and the higher order *clv1;chk* and *rpk2;chk* phenotypes. A model where cytokinin signaling inhibits an unknown factor (z) that promotes stem cell identity successfully replicated the trends seen in the empirical data, over a wide range of mutant genotypes and hormone treatments that perturb stem cell specification. Very little is known about genes promoting SAM formation in moss; the best understood pathways are downstream of auxin, not cytokinin[42,43]. It is possible that auxin signaling is de-regulated in *chk* mutants, leading to ectopic branch formation. However, while auxin promotes SAM formation on juvenile filamentous tissue, it inhibits branch formation on shoots[30,43]. Thus, it is unlikely that auxin signaling comprises 'z' in Model 6 . While still attractive, it is difficult to test this model without a better understanding of cytokinin-mediated stem cell induction.

Our statistical analyses revealed that *CLV1* and *RPK2* function through distinct downstream pathways. However, mutants of both genes were less sensitive to exogenous cytokinin, suggesting crosstalk from both receptors with cytokinin (Figure 3). Additionally, a growing body of work suggests that cytokinin promotes CLV3 signaling in the SAM and during shoot regeneration from callus, although these interactions are complex[36,37]. To assess whether such a regulatory interaction could explain the *chk1;2;3* and higher order *clv;rpk2;chk* mutant phenotypes, we generated a model where cytokinin induced CLE expression. This model (Model 8, Figure 6 successfully recapitulated empirical data, suggesting a cytokinin-CLE regulatory interaction could be an ancient feature of plant stem cell homeostasis.

It is important to note that although cytokinin signaling could be upstream of CLV signaling in the context of stem cell specification, this regulatory interaction does not apply to all developmental contexts. Aside from producing ectopic branches, the *chk1;2;3*, *clv1,* and *rpk2* phenotypes share little else in common. Other *chk* mutant phenotypes include increased cell length, fewer cell files, and loss of midribs from leaves. In contrast,

clv1 and *rpk2* mutant leaves have shorter cells and sometimes produce wide midribs that stretch the width of the leaf base. Higher order *clv1;chk1;2;3* and *rpk2;chk1;2;3* shoots also make thin leaves lacking midribs, phenotypes suggest that *chk1;2;3* mutant phenotypes are epistatic to *clv1*. Thus, with the exception of ectopic stem cell formation in *chk1;2;3*, most phenotypes suggest that CLE signaling functions upstream of cytokinin.

Common molecular mechanisms can underlie disparate developmental functions across plant evolution.

Similarities and differences in stem cell regulation between moss and Arabidopsis raise important questions about the evolution of this signaling network, especially in light of recent data from the liverwort *Marchantia polymorpha*. Current phylogenies support a monophyletic clade containing mosses and liverworts, such that mosses and liverworts are equally related to flowering plants. However unlike in moss and Arabidopsis, CLV function in Marchantia enhances stem cell specification[44].

Three hypotheses can explain the phenotypic differences between *clv1* mutants in Physcomitrium, flowering plants, and Marchantia. First, it is possible that Marchantia CLV1 possesses the ancestral function, while moss and Arabidopsis CLV1 have derived functions that are convergent. Second, the apparent reversal of CLV1 function in Marchantia could be derived. Finally, fundamental differences in the signaling networks controlling stem cell specification raise the possibility that CLV1 performs the same regulatory function in each species, but with a different developmental consequence. For example, in mosses auxin suppresses stem cell specification and activity while cytokinin promotes it. This pattern is reversed in Marchantia, where auxin promotes stem cell formation and branching while cytokinin reduces branching. According to this hypothesis, CLV1 could have the same network function in Marchantia as in Physcomitrium, for example inhibiting some subset of cytokinin signaling, and *clv* mutants in each species would produce the reported, seemingly opposite phenotypes. Notably, the Marchantia stem cells in question produce a thallus, whereas Moss and Arabidopsis SAMs make upright shoots with multiple, successively iterated leaves in a phyllotactic pattern. This fundamental difference in shoot architecture may be correlated with differences in CLV function between Marchantia, Physcomitrium, and Arabidopsis.

Elucidation of the intervening, stem cell specification pathways may enable tests of these hypotheses. Interestingly, CLE-mediated control of the meristem in Marchantia is also independent of *WOX* genes, supporting the later recruitment of *WOX* genes to regulation of the SAM[44]. However, several critical questions remain. First, the function of RPK2 is unknown in Marchantia and poorly understood in Arabidopsis. Second, little is known about the molecular pathway through which cytokinin promotes SAM formation at any stage of moss development. Third, if SAM specification occurs in a *WOX*-independent pathway in bryophytes, is there also a *WOX* independent pathway in angiosperms? Interestingly, several studies now in maize have failed to detect a *WUS* paralog in the vegetative SAM[45]. Finally, it is curious how the moss SAM transcriptome is highly enriched for orthologs of genes that function in angiosperm SAMs, but lacks a role for *KNOX* and *WOX* genes, two central and necessary gene families for SAM function in Arabidopsis[26,46,47]. Intriguingly, *Physcomitrium* encodes a single gene of the *HAIRY MERISTEM* (HAM) clade of GRAS transcription factors. In the Arabidopsis SAM, HAM genes are critical for many functions of WUS [48]. It is appealing to ask whether of *WOX*, *KNOX*, and *HAM* genes, it is the *HAMs* that lie central to stem cell regulation in moss.

References

1. Brand, U., Fletcher, J.C., Hobe, M., Meyerowitz, E.M., and Simon, R. (2000). Dependence of Stem Cell Fate in Arabidopsis on a Feedback Loop Regulated by CLV3 Activity. Science (80-.). *289*, 617–619.

2. Fletcher, J.C., Brand, U., Running, M.P., Simon, R., and Meyerowitz, E.M. (1999). Signaling of cell fate decisions by CLAVATA3 in Arabidopsis shoot meristems. Science *283*, 1911–1914.

3. Rojo, E., Sharma, V.K., Kovaleva, V., Raikhel, N. V, and Fletcher, J.C. (2002). CLV3 is localized to the extracellular space, where it activates the Arabidopsis CLAVATA stem cell signaling pathway. Plant Cell *14*, 969–977.

4. Kinoshita, A., Betsuyaku, S., Osakabe, Y., Mizuno, S., Nagawa, S., Stahl, Y., Simon, R., Yamaguchi-Shinozaki, K., Fukuda, H., and Sawa, S. (2010). RPK2 is an essential receptor-like kinase that transmits the CLV3 signal in Arabidopsis. Development *137*, 3911–3920.

5. Kayes, J.M., and Clark, S.E. (1998). CLAVATA2, a regulator of meristem and organ development in Arabidopsis. Development *125*, 3843–3851.

6. Clark, S.E., Running, M.P., and Meyerowitz, E.M. (1995). CLAVATA3 is a specific regulator of shoot and floral meristem development affecting the same processes as CLAVATA1. Development *121*.

7. Riedel-Kruse, I.H., Müller, C., and Oates, A.C. (2007). Synchrony dynamics during initiation, failure, and rescue of the segmentation clock. Science *317*, 1911–1915.

8. Müller, R., Bleckmann, A., and Simon, R. (2008). The receptor kinase CORYNE of Arabidopsis transmits the stem cell-limiting signal CLAVATA3 independently of CLAVATA1. Plant Cell *20*, 934–946.

9. Yadav, R.K., Perales, M., Gruel, J., Girke, T., Jönsson, H., and Venugopala Reddy, G. (2011). WUSCHEL protein movement mediates stem cell homeostasis in the Arabidopsis shoot apex. Genes Dev. *25*, 2025–2030.

10. Daum, G., Medzihradszky, A., Suzaki, T., and Lohmann, J.U. (2014). A mechanistic framework for noncell autonomous stem cell induction in Arabidopsis. Proc. Natl. Acad. Sci. *111*, 14619–14624.

11. Laux, T., Mayer, K.F.X., Berger, J., and Jürgens, G. (1996). The WUSCHEL gene is required for shoot and floral meristem integrity in Arabidopsis. Development *122*, 87–96.

12. Mayer, K.F.X., Schoof, H., Haecker, A., Lenhard, M., Jürgens, G., and Laux, T. (1998). Role of WUSCHEL in Regulating Stem Cell Fate in the Arabidopsis Shoot Meristem. Cell *95*, 805–815.

13. Leyser, H.M.O., and Furner, I.J. (1992). Characterisation of three shoot apical meristem mutants of Arabidopsis thaliana. Development *116*, 397–403.

14. Somssich, M., Je, B. Il, Simon, R., and Jackson, D. (2016). CLAVATA-WUSCHEL signaling in the shoot meristem. Development *143*, 3238–3248.

15. Nimchuk, Z.L. (2017). CLAVATA1 controls distinct signaling outputs that buffer shoot stem cell

proliferation through a two-step transcriptional compensation loop. PLoS Genet. *13*.

16. Hu, C., Zhu, Y., Cui, Y., Cheng, K., Liang, W., Wei, Z., Zhu, M., Yin, H., Zeng, L., Xiao, Y., et al. (2018). A group of receptor kinases are essential for CLAVATA signalling to maintain stem cell homeostasis. Nat. Plants *4*, 205–211.

17. Je, B. Il, Xu, F., Wu, Q., Liu, L., Meeley, R., Gallagher, J.P., Corcilius, L., Payne, R.J., Bartlett, M.E., and Jackson, D. (2018). The CLAVATA receptor FASCIATED EAR2 responds to distinct CLE peptides by signaling through two downstream effectors. Elife *7*.

18. Rensing, S.A., Goffinet, B., Meyberg, R., Wu, S.Z., and Bezanilla, M. (2020). The moss physcomitrium (Physcomitrella) patens: A model organism for non-seed plants. Plant Cell *32*, 1361–1376.

19. Cammarata, J., and Scanlon, M.J. (2020). A functionally informed evolutionary framework for the study of LRR-RLKs during stem cell maintenance. J. Plant Res. *133*, 331–342.

20. Harrison, C.J., Roeder, A.H.K., Meyerowitz, E.M., and Langdale, J. a. (2009). Local Cues and Asymmetric Cell Divisions Underpin Body Plan Transitions in the Moss Physcomitrella patens. Curr. Biol. *19*, 461–471.

21. Frank, M.H., and Scanlon, M.J. (2014). Transcriptomic Evidence for the Evolution of Shoot Meristem Function in Sporophyte-Dominant Land Plants through Concerted Selection of Ancestral Gametophytic and Sporophytic Genetic Programs. Mol. Biol. Evol. *32*, 355–367.

22. Whitewoods, C.D., Cammarata, J., Nemec Venza, Z., Sang, S., Crook, A.D., Aoyama, T., Wang, X.Y., Waller, M., Kamisugi, Y., Cuming, A.C., et al. (2018). CLAVATA Was a Genetic Novelty for the Morphological Innovation of 3D Growth in Land Plants. Curr. Biol. *28*, 1–12.

23. Nardmann, J., and Werr, W. (2012). The invention of WUS-like stem cell-promoting functions in plants predates leptosporangiate ferns. Plant Mol. Biol. *78*, 123–134.

24. Ikeda, M., Mitsuda, N., and Ohme-Takagi, M. (2009). Arabidopsis wuschel is a bifunctional transcription factor that acts as a repressor in stem cell regulation and as an activator in floral patterning. Plant Cell *21*, 3493–3505.

25. Lin, H., Niu, L., McHale, N. a, Ohme-Takagi, M., Mysore, K.S., and Tadege, M. (2013). Evolutionarily conserved repressive activity of WOX proteins mediates leaf blade outgrowth and floral organ development in plants. Proc. Natl. Acad. Sci. U. S. A. *110*, 366–71.

26. Sakakibara, K., Reisewitz, P., Aoyama, T., Friedrich, T., Ando, S., Sato, Y., Tamada, Y., Nishiyama, T., Hiwatashi, Y., Kurata, T., et al. (2014). WOX13-like genes are required for reprogramming of leaf and protoplast cells into stem cells in the moss Physcomitrella patens. Development *141*, 1660–1670.

27. Skoog, F., Miller, C.O., and Folke K. Skoog and Carlos O. Miller (1957). Chemical regulation of growth and organ formation in plant tissue cultured in vitro. Symp Soc exp Biol.

28. Gordon, S.P., Heisler, M.G., Reddy, G. V., Ohno, C., Das, P., and Meyerowitz, E.M. (2007). Pattern formation during de novo assembly of the Arabidopsis shoot meristem. Development *134*, 3539–3548.

29. Reski, R., and Abel, W.O. (1985). Induction of budding on chloronemata and caulonemata of the moss,Physcomitrella patens,using isopentenyladenine. Planta *165*, 354-358.

30. Coudert, Y., Palubicki, W., Ljung, K., Novak, O., Leyser, O., and Harrison, C.J. (2015). Three ancient hormonal cues co-ordinate shoot branching in a moss. Elife, 1–26.

31. Cammarata, J., Roeder, A.H., and Scanlon, M.J. (2019). Cytokinin and CLE signaling are highly intertwined developmental regulators across tissues and species. Curr. Opin. Plant Biol. *51*.

32. Meng, W.J., Cheng, Z.J., Sang, Y.L., Zhang, M.M., Rong, X.F., Wang, Z.W., Tang, Y.Y., and Zhang, X.S. (2017). Type-B ARABIDOPSIS RESPONSE REGULATORs Is Critical to the Specification of Shoot Stem Cell Niche by Dual Regulation of WUSCHEL. Plant Cell *29*, tpc.00640.2016.

33. Ishida, K., Yamashino, T., Nakanishi, H., and Mizuno, T. (2010). Classification of the genes involved in the two-component system of the moss Physcomitrella patens. Biosci. Biotechnol. Biochem. *74*, 2542–2545.

34. von Schwartzenberg, K., Lindner, A., Gruhn, N., Šimura, J., Novák, O., Strnad, M., Gonneau, M., Nogué, F., Heyl, A., Schwartzenberg, K. Von, et al. (2015). CHASE domain-containing receptors play an essential role in the cytokinin response of the moss Physcomitrella patens. J. Exp. Bot. *67*, 667–679.

35. Barker, E.I., and Ashton, N.W. (2013). Heteroblasty in the moss, *Aphanoregma patens* (*Physcomitrella patens*), results from progressive modulation of a single fundamental leaf developmental programme. J. Bryol. *35*, 185–196.

36. Zhao, Z., Andersen, S.U., Ljung, K., Dolezal, K., Miotk, A., Schultheiss, S.J., and Lohmann, J.U. (2010). Hormonal control of the shoot stem-cell niche. Nature *465*, 1089–1092.

37. Liu, Z., Dai, X., Li, J., Liu, N., Liu, X., Li, S., and Xiang, F. (2020). The Type-B cytokinin response regulator ARR1 inhibits shoot regeneration in an ARR12-dependent manner in Arabidopsis. Plant Cell *32*, 2271–2291.

38. Shimizu, N., Ishida, T., Yamada, M., Shigenobu, S., Tabata, R., Kinoshita, A., Yamaguchi, K., Hasebe, M., Mitsumasu, K., and Sawa, S. (2015). BAM 1 and RECEPTOR-LIKE PROTEIN KINASE 2 constitute a signaling pathway and modulate CLE peptide-triggered growth inhibition in Arabidopsis root. New Phytol. *3*, 1104–1113.

39. Hord, C.L.H., Chen, C., DeYoung, B.J., Clark, S.E., and Ma, H. (2006). The BAM1/BAM2 receptor-like kinases are important regulators of Arabidopsis early anther development. Plant Cell *18*, 1667–80.

40. Cui, Y., Hu, C., Zhu, Y., Cheng, K., Li, X., Wei, Z., Xue, L., Lin, F., Shi, H., Yi, J., et al. (2018). CIK Receptor Kinases Determine Cell Fate Specification during Early Anther Development in Arabidopsis. Plant Cell *30*, 2383–2401.

41. Gordon, S.P., Chickarmane, V.S., Ohno, C., and Meyerowitz, E.M. (2009). Multiple feedback loops through cytokinin signaling control stem cell number within the Arabidopsis shoot meristem. Proc. Natl. Acad. Sci. U. S. A. *106*, 16529–16534.

42. Moody, L.A., Kelly, S., Rabbinowitsch, E., and Langdale, J.A. (2018). Genetic Regulation of the 2D

to 3D Growth Transition in the Moss Physcomitrella patens. Curr. Biol. *28*, 473-478.e5.

43. Aoyama, T., Hiwatashi, Y., Shigyo, M., Kofuji, R., Kubo, M., Ito, M., and Hasebe, M. (2012). AP2-type transcription factors determine stem cell identity in the moss Physcomitrella patens. Development *139*, 3120–3129.

44. Hirakawa, Y., Fujimoto, T., Ishida, S., Uchida, N., Sawa, S., Kiyosue, T., Ishizaki, K., Nishihama, R., Kohchi, T., and Bowman, J.L. (2020). Induction of Multichotomous Branching by CLAVATA Peptide in Marchantia polymorpha. Curr. Biol. *30*, 3833-3840.e4.

45. Satterlee, J.W., Strable, J., and Scanlon, M.J. (2020). Plant stem cell organization and differentiation at single-cell resolution. bioRxiv.

46. Frank, M.H., and Scanlon, M.J. (2015). Cell-Specific Transcriptomic Analyses of 3-Dimensional Shoot Development in the moss Physcomitrella patens. Plant J. *83*, 743–51.

47. Sakakibara, K., Nishiyama, T., Deguchi, H., and Hasebe, M. (2008). Class 1 KNOX genes are not involved in shoot development in the moss Physcomitrella patens but do function in sporophyte development. Evol. Dev. *10*, 555–566.

48. Zhou, Y., Liu, X., Engstrom, E.M., Nimchuk, Z.L., Pruneda-Paz, J.L., Tarr, P.T., Yan, A., Kay, S.A., and Meyerowitz, E.M. (2015). Control of plant stem cell function by conserved interacting transcriptional regulators. Nature *517*, 377–380.

Supplemental Figures

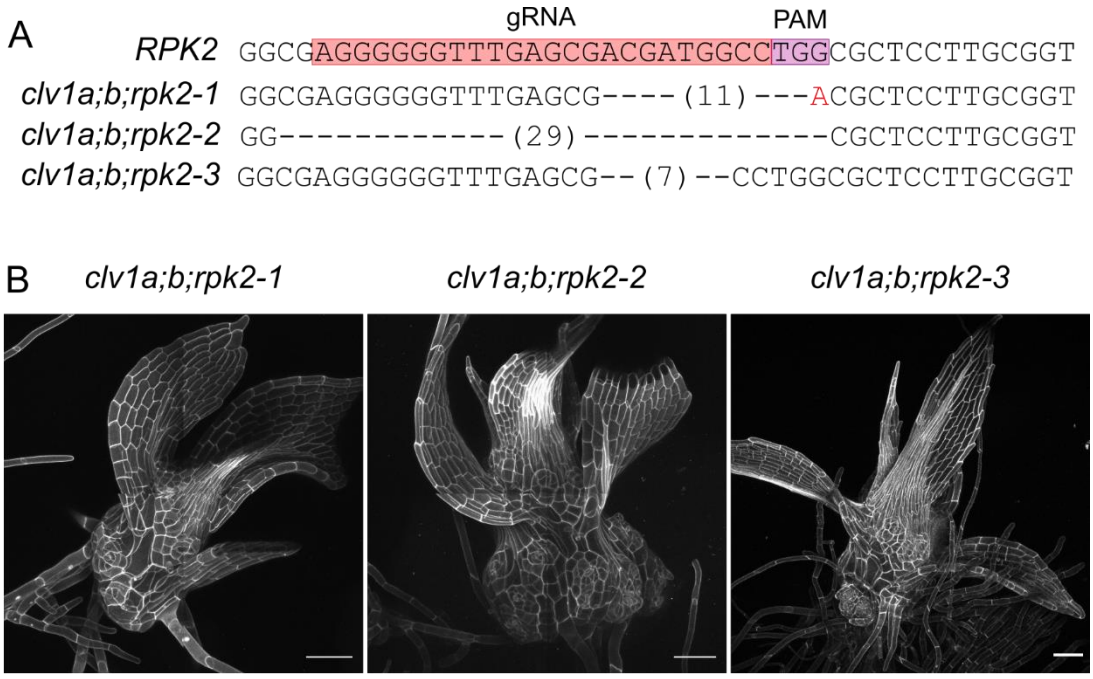

Supplemental Figure 1: Sequence of three *clv1a;clv1b;rpk2* triple mutant lines. We transformed *clv1a;clv1b-8* double mutants (Whitewoods, Cammarata et al.) with plasmids expressing an *RPK2*-targeting gRNA, Cas9, and a selectable marker. We generated seven independent lines with *rpk2*-like colony phenotypes (not shown), and selected three for in-depth phenotyping of shoot morphogenesis, shown here. **A)** Portion of *RPK2* exon 1 with gRNA target sequence and PAM highlighted. Below, aligned sequences of the *rpk2* mutant loci from three *clv1a;clv1b;rpk2* lines. **B)** All *clv1a;clv1b;rpk2* mutants display the short stature, ectopic stem cell phenotypes, and ectopic midrib specification representative of a combination of *clv1* and *rpk2* phenotypes.

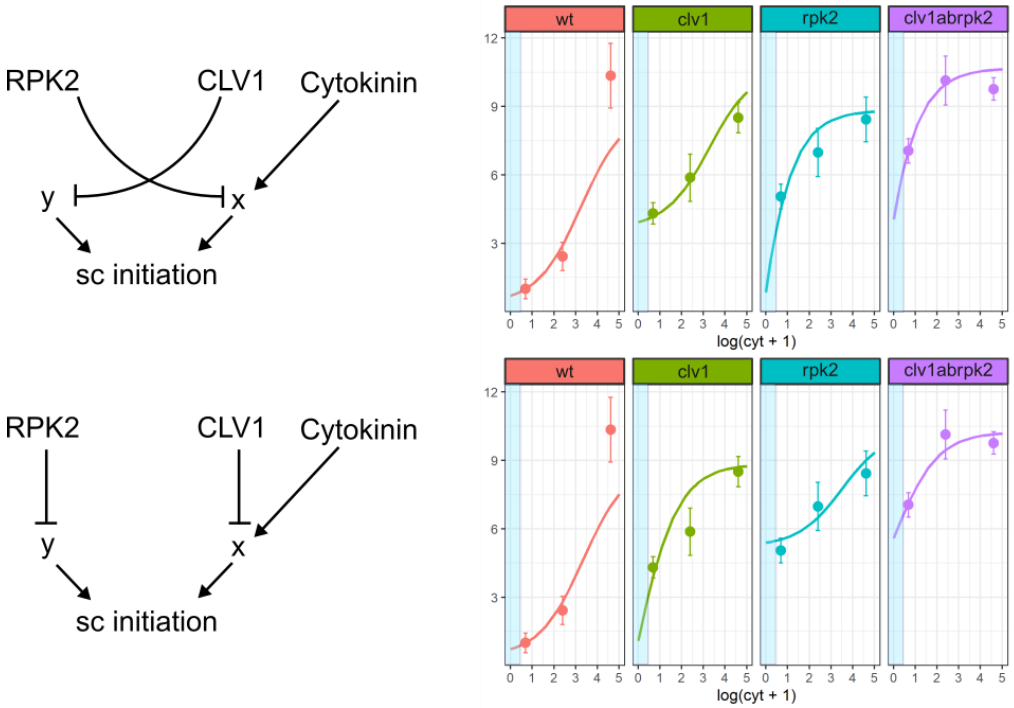

Supplemental Figure 2: Predictions of stem cell initiation at zero cytokinin. The best performing models of stem cell initiation in wild type, *clv1*, *rpk2,* and *clv1;rpk2* higher order mutants with and without exogenous cytokinin were used to predict stem cell initiation levels if cytokinin levels were reduced (highlighted blue). Each model predicted a reduction in stem cell initiation. More informatively, mutants of whichever gene that acts upstream of *x* would see their stem cell initiation phenotypes fully suppressed upon reduced cytokinin (*RPK2* above, *CLV1* below). Data points and error bars represent empirical stem cell per area values normalized to wild type grown on BCD. From left to right: BCD, 10nM BAP, 100nM BAP. Solid lines represent model simulations after optimization of parameters to the data.

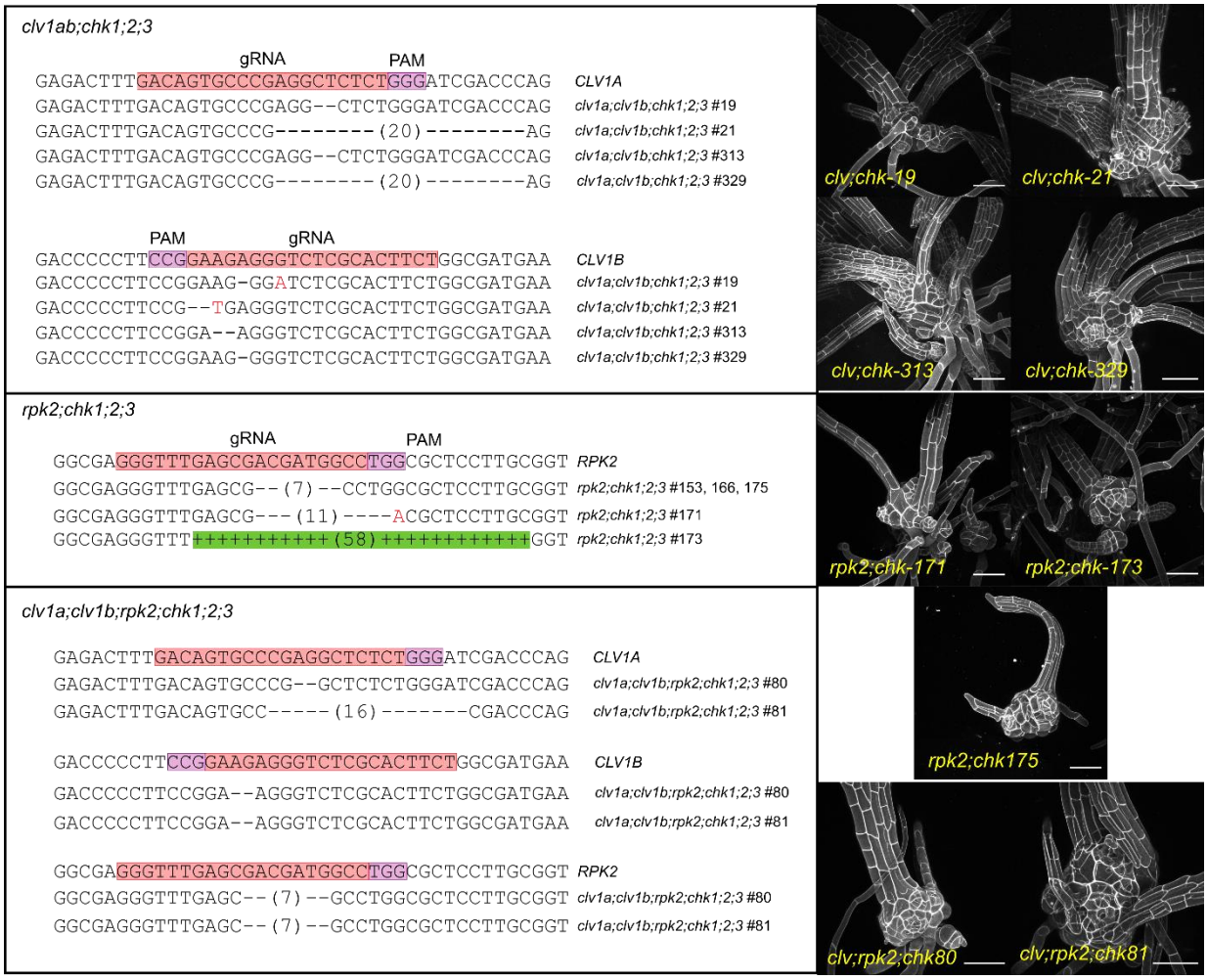

Supplemental Figure 3: genotyping higher order *chk1;2;3* and *clv1/rpk2* mutants. *chk1;2;3-1* plants were transformed with gRNAs targeting *CLV1a* and *CLV1b*, *RPK2*, or all three. Three independent lines for *clv1a;clv1b;chk1;2;3* sextuple mutants (upper panel) and *rpk2;chk1;2;3* quadruple mutants were obtained (middle panel). *clv1b;rpk2;chk1;2;3* quintuple mutants were recovered and re-transformed with *CLV1a*-specific gRNAs to generate two sextuple mutant lines (lower panel). On the right, examples of shoot phenotypes for each of these lines show a combination of *clv1, rpk2*, and *chk1;2;3* phenotypes.

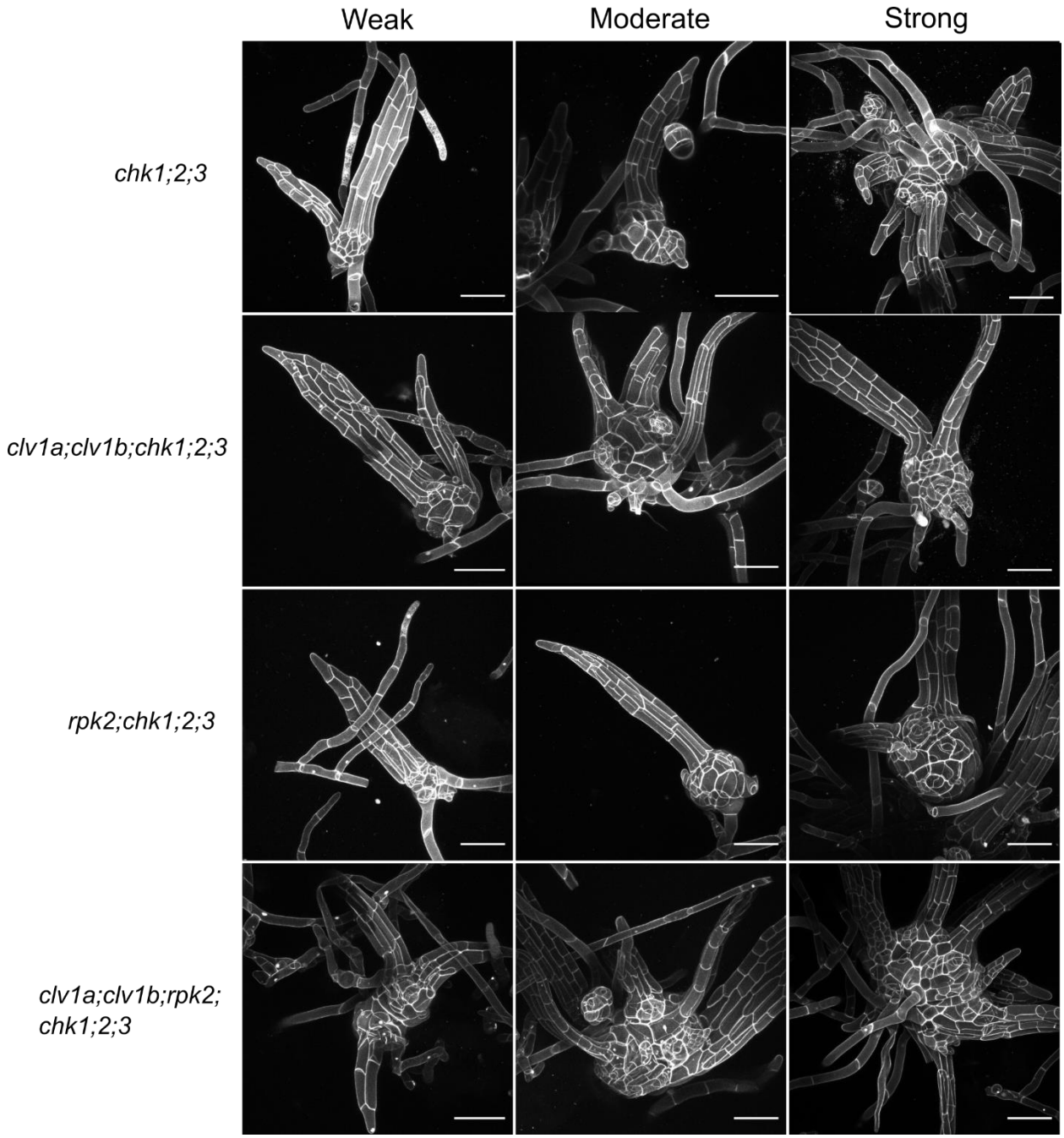

Supplemental Figure 4: higher order *lrr-rlk;chk1;2;3* phenotypes are variable. Examples of weak, moderate, and strong phenotypes observed for *chk1;2;3* mutants and each higher order *lrr-rlk;chk* mutant. *rpk2;chk1;2;3* mutant phenotypes were particularly variable. However, when quantified these lines still presented an increased initiation of stem cells per area (Figure 5 E).

Methods

Moss Culture

The Gransden 04 strain of *Physcometrium patens* (formerly *Physcomitrella patens*) was used for all experiments[1]. Fresh, actively growing protonema tissue was propagated on BCDAT (minimal media supplemented with Ammonium Tartrate) plates overlain with autoclaved cellophane under continuous light at 25 degrees Celsius. For BCD and BCDAT media components, see Media section. To propagate moss, tissue was blended in 5-7 ml sterile Water using a Dremel with a custom-made propeller blade attachment, and 1-2 ml of blended moss was pipetted to inoculate fresh plates. For phenotyping gametophores, small samples of freshly blended protonema were placed onto BCD media supplemented with the specified amount of filter sterilized BAP. These tufts of tissue grew for the specified time before gametophores were dissected for imaging.

Moss Transformation

The moss transformation protocol was adapted for smaller amounts of DNA and tissue. Protonema grown for 5-7 days on BCDAT plates overlain with cellophane was collected and placed into 15 ml 8% Mannitol solution in a petri dish. 5 ml of 2% Drisilase solution (see solutions table) was then added, and the dish was placed on a shaker set to 80 RPM for one hour. After this time, the solution was gently pipetted through a 70 µm mesh into a 50 ml conical tube. Filtered protoplasts were spun at 250 g for five minutes with low brake. The liquid was then poured off and replaced with 20 ml 8% mannitol, and this wash step was repeated two more times. Upon being resuspended in mannitol solution a third time, a sample of protoplasts were was measured using a hemocytometer. Cells were then pelleted one final time and resuspended in a volume of 3M solution to yield $2*10^6$ protoplasts/ml. 16. 300 ul of the protoplast/3M solution was transferred to a 2 ml tube with a maximum of 10 ug DNA (with equimolar ratios of each plasmid, including each gRNA-encoding plasmid, the Cas9 expression plasmid, and selectable marker), stir gently. The DNA, 3M, and protoplast mixture was then transferred to a 15 ml conical tube 300 ul PEG solution already inside it; these were mixed gently by pipetting. The DNA and protoplast solution was heat shocked at 45 degrees Celsius for three minutes and then left to cool in a bath of room temperature water for 10 minutes. The solution was slowly

diluted to a final volume of 5 ml with 8% mannitol, and then spun down to pellet the protoplasts. During the previous step, PRMT was melted, supplanted with $CaCl_2$ to a final concentration of 10 mM and left to keep warm in a 45 degree water bath. PRMB plates were overlain with sterile cellophane, pelleted protoplasts were resuspended in PRMT, and then 1 ml of the PRMT and protoplast mixture was plated onto each PRMB plate.

Moss Selection

Seven days after transformation, the cellophane on which the protoplasts were growing was transferred off the PRMB plates and onto BCDAT plates supplemented with 20 mg/L G418. After one week to ten days on selection, regenerating colonies were transferred to new BCDAT plates and left to grow until individual colonies were visible by eye (two-to-three weeks). Individual colonies were transferred to BCDAT plates without cellophane, and left to grow for three more weeks. After this time, these colonies were split and samples were taken for DNA extractions and genotyping by PCR and Sanger sequencing.

Plasmid Construction

For routine cloning of gRNAs into a transient expression vector suitable for use in P. patens, we ordered synthesized DNA (gblock from IDT) containing the moss U3 or U6 promoter, a cloning site containing two BSAI cut sites, and the gRNA scaffold all flanked by ATTL gateway sites. We cloned these DNA fragments into pDONR using LR clonase reactions to generate pENT U3 sgRNA and pENT U6 sgRNA. to generate pENT:U3::sgRNA and pENT:U6::sgRNA plasmids. P. U6 and U3 promoter sequences were adapted from Lopez-Obando et al[2].

To clone gRNA expression vectors, oligonucleotides with overhangs complementary to the BSAI cut sites (GGC and CAT for U3 and U6 promoters, and aaac to ligate on the 3' end with and were annealed. pENT U3 sgRNA or pENT U6 sgRNA were then digested with BSAI, and linear plasmid was purified by gel extraction. Annealed oligonucleotides were then ligated into the linearized gRNA vectors using T4 DNA ligase. Ligated DNA constructs were transformed into DH5-alpha competent cells grown in the presence of 50 µg/ml kanamycin. Clones were screened by colony PCR using the forward oriented gRNA oligonucleotide and pJCm208 (in the gRNA scaffold) as primers followed by Sanger sequencing using the pJCm208 primer.

gRNA sequences were selected using the CRISPOR online service[3]. we minimized off target effects and where possible chose gRNAs that cleaved in the first exon. We tried four gRNAs for the *CLV1a* gene before finding one that cleaved effectively (not shown); otherwise the first gRNAs designed for each gene successfully induced mutations.

Genotyping

For few moss samples, tissue was ground by hand, while for large numbers of samples we purified DNA in 96 well plates. For small DNA preps and some 96 well-plate preps, tissue was ground in water, to which an equal volume of 2x Shorty Extraction buffer (0.4 M Tris, pH 9.0; 0.8 M LiCl; 50 mM EDTA; 2% SDS) was added. The debris were then pelleted, and the supernatant removed to a new tube to which an equal volume of isopropanol was added. The solution was then mixed by inversion and placed on ice or at -20 degrees Celsius for 15-30 minutes and then spun at maximum speed to pellet the DNA (10 minutes in a microcentrifuge, 40 minutes in a swinging-bucket centrifuge). The pellet was then rinsed with 70% ethanol and then left to air dry before being resuspended in 200 ul nuclease-free water. For higher throughput 96-well plate DNA extractions, we extracted DNA from three to four week old colonies using a filter-plate prep as described in Strable et al[4].

For genotyping PCRs, 1-2 ul of genomic DNA was used to PCR a small (200-300 bp) region flanking the gRNA target site. A subset of PCR products were checked on a gel, and PCR products were purified using ExoSap-IT (https://www.thermofisher.com/order/catalog/product/78205.10.ML#/78205.10.ML) PCR cleanup reagent before being sent for Sangar sequencing. Large sets of Sangar sequencing results were converted into FASTA format and aligned with the wild type sequence using MUSCLE[5].

Staining and Imaging

Slides were prepared by extruding a ring of vacuum grease through a syringe to onto glass slides. These rings would retain a pool of staining solution and prevent gametophores from being crushed by the coverslip. The area within the vacuum grease was filled with 5 µg/ml Propidium Iodide (PI). Tufts of moss grown on BCD were flooded with water and vigorously tapped to remove as many air bubbles as possible. Gametophores

were then dissected from the periphery of tufts and placed into the PI solution on the slides. Moss was allowed to stain for at least 15 minutes in the PI solution before imaging. Imaging was conducted using a Zeiss 710 laser scanning confocal microscope. We used a 514 nm laser for excitation and collected an emission spectrum from 566 to 650 nM. Images were captured using either a 20x 1.0 NA water immersion or 10x objective.

Ectopic Apical Cell Quantification

Areas of stem visible on maximum intensity projections (not including leaves) were manually measured using FIJI[6]. Ectopic apical cells were identified by eye as tetrahedral cells sometimes surrounded by short, curled hair cells. Apical cells were distinguished from illusory tetrahedral cells seen in maximum intensity projections by manually looking through z-stacks. Ectopic branches were defined as an ectopic feature that was producing visible leaves. Counting was done primarily on maximum intensity projections, but for features where the shape was unclear, the Z-stack was referred to.

Statistical analysis

Statistical analysis was performed using the R statistical programming language. Genotypes were coded as two loci (*CLV1* and *RPK2*) for the purposes of our analysis, since *clv1a* and *clv1b* single mutants were not analyzed separately. The effects of mutating CLV1 and RPK2 and of growth on 10nM and 100nM BAP as well as the interactions between these three factors (the two loci and the media) were modeled using a Poisson general linear model that included stem area as an offset (model: glm(total_ectopic ~ clv1L + rpk2L + exock + clv1L:rpk2L + clv1L:exock + rpk2L:exock + (log(area)), family = 'poisson'). BAP concentrations were treated as a continuous variable with levels of zero, ten, and one hundred.

Poisson coefficients are akin to Beta values reported by linear regressions, in that they are proportional to the expected change in the dependent variable given the change in independent variable associated with the coefficient. In the case of a Poisson coefficient, the exponentiation of the coefficient tells you the predicted effect due to the change in factor level. For instance, with a Poisson coefficient of 0.64, the estimated change in apical cell number due to the *clv1* mutation is ~1.9 (= e^0.64). It is important to note that our models make

use of both categorical and continuous variables, which makes the coefficients appear deceptively different in magnitude. For example, the coefficient associated with exogenous cytokinin is small because cytokinin is coded as a continuous variable. The coefficient is 0.013 and it's exponent is 1.013, which appears much lower than the expected change due to *clv1* of 1.9. However, the cytokinin coefficient of 1.013 shows the predicted change per unit cytokinin. The predicted change for 10nM BAP is the exponentiation of 10*the coefficient, so e^(10*.013) = 1.14. Going on to predict the change for 100nM bap is e^(1.3) = 3.67. Finally, these numbers represent the fold change from the 'intercept' value also reported by the model.

Primers and gRNA sequences

Name	Sequence	Function
oJCm278	GAGTTAGGGGAGATGACGCG	rpk2_gRNA target locus genotyping
oJCm279	CTTGGAGGACTCACCAACCC	rpk2_gRNA target locus genotyping
oJCm379	cacctaaacggctcaattcc	PpClv1aE4 gRNA target site genotyping
oJCm380	tgatgatctccgatggtatgg	PpClv1aE4 gRNA target site genotyping
oJCm181	tggagagacgcaacttccat	CLV1b gRNA target site genotyping
oJCm182	ttaagacgccccaaatcagc	CLL1b gRNA target site genotyping
oJCm175	gcttcGAGCTCGAATTCAGA	PpU3_promoter_fwd
oJCm176	ggtcGACGAGCTCAAAAAAAG	sgRNA_scaffold_reverse
oJCm208	GAGCTCGAATTCGTCCATTGA	U6 promoter fwd pcr primer

sgRNA Oligo	Sequence	Target	In Vector
sgJTC5	GGCAgacagtgcccgaggctctct	CLL1a_exon4_cds	U3_BSAI-sgRNA
sgJTC6	AAACagagagcctcgggcactgtc	CLL1a_exon4_cds*	U3_BSAI-sgRNA
sgJTC9	GGCagaagtgcgagaccctcttc	CLL1b_exon1_cds_sgRNA1	U3_BSAI-sgRNA
sgJTC10	AAACgaagagggtctcgcacttc	CLL1b_exon1_cds_sgRNA1*	U3_BSAI-sgRNA
sgJTC105	catGGGTTTGAGCGACGATGGCC	PpRPK2cds	U6_sgRNA
sgJTC106	aaacGGCCATCGTCGCTCAAACCC	PpRPK2cds	U6_sgRNA

Genes referenced in this study

Full Gene Name	Alias	Version 1.6	Version 3
CLAVATA1a	*CLV1a*	Pp1s14_447V6	Pp3c6_21940
CLAVATA1b	*CLV1B*	Pp1s5_68V6	Pp3c13_13360
RECEPTOR-LIKE PROTEIN KINASE 2	*RPK2*	Pp1s311_57V6	Pp3c7_5570
CYTOKININ HISTIDINE KINASE 1	*CHK1*	Pp1s50_141V6	Pp3c25_8540
CYTOKININ HISTIDINE KINASE 2	*CHK2*	Pp1s194_72V6	Pp3c16_7610
CYTOKININ HISTIDINE KINASE 3	*CHK3*	Pp1s252_49V6	Pp3c6_7030

Dynamical Model Methods

Each model was solved using the LSODA solver for Ordinary Differential Equations (ODEs) and the R statistical programming language Version 4.0.2[7,8]. Models were confirmed to converge to steady state values before and after each run of the optimizer, as determined by each variable reaching a plateau by the end of the modeled time period. All plotting used the ggplot2 package[9].

Model Variables

The set of differential equations that constitutes a model describes the change in a set of interrelated variables through time. The variables used in this work are summarized here:

Variable	Describes
x	Cytokinin-dependent pathway that induces stem cell formation
y	Cytokinin-independent pathway inducing stem cell formation
init	Level of stem cell initiation
clv	Abundance of CLV1. In Models 1-7, this is a static, non-dynamical parameter set to 2; Dynamical in model 8 only
rpk2	Abundance of CLV1. In Models 1-7, this is a static, non-dynamical parameter set to 2; Dynamical in model 8 only
cle	Abundance of CLE signal. Used in model 8 only
clvsig	Signaling strength through CLV1 used for model 8. Variable increases to reflect binding of CLV1 to CLE signal
rpk2sig	Signaling strength through RPK2 used for model 8. Variable increases to reflect binding of RPK2 to CLE signal

Model parameters

Each equation in the model describes how one of the above variables accumulates over time. The change over time is proportional to the current value of the parameters and other variables in the model. Each of the other variables in an equation is associated with a proportionality constant that describes how that variable affects the accumulation rate described by that equation. Additionally, a differential equation might include a term to describe accumulation independent of the other variables as well as degradation rates. These constants were assigned to the following categories:

- p = production; describes basal accumulation rates
- d = degradation; describes degradation rates, or in the case of CLE-CLV or CLE-RPK2 complexes, the rate of complex dissolution into its components
- k = interaction coefficient/proportionality constant

Each model also used a set of initial conditions, which we named 'base' values, and a time vector that we named times0. Models were run for 3000 time points distributed over 300 'seconds'. Finally, cytokinin was coded as a static parameter and altered in the following ways to simulate different conditions from our experimental datasets:

Cytokinin value	**Simulates the condition**
0	*chk1;2;3* mutant
1*	growth on minimal media (BCD) with wild type *CHK* genes
10	10 nM BAP
100	100 nM BAP

* As '1' here is somewhat arbitrary, we also tried values of 0.5 and 0.75 in its stead, to no significant change to the model outputs (not shown).

Running a model

Each system of differential equations was solved using the LSODA solver for Ordinary Differential Equations (ODEs) in the R statistical programming language (REF, REF). Models were confirmed to converge to steady state values before and after each run of the optimizer, as determined by each variable reaching a plateau by the end of the modeled time period. Models were run for 3000 time points distributed over 300 'seconds', as depicted by the sample model run below:

lsoda(func = MODEL8, y = base0, times = times0, parms = cytokinin)

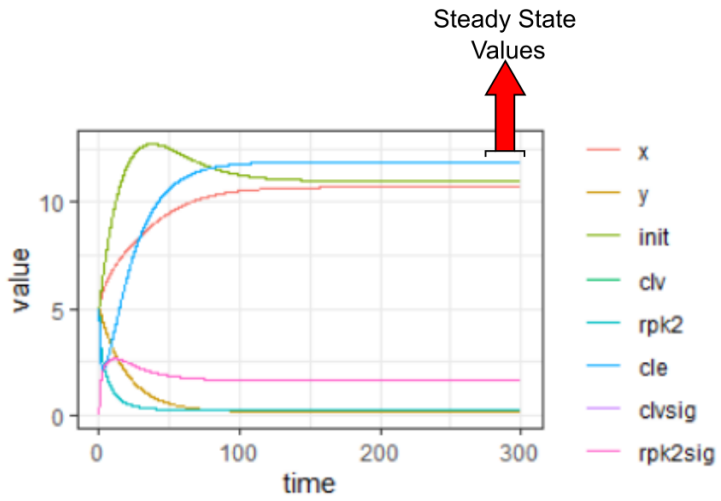

Variables change through time and converge at steady state values (above figure). The final values, at time 300 (the 3,000th time point used for integration) were taken and stored as the output of the model.

Criteria for selection in the optimizer

Comparing the simulated data to the empirical data required that the two datasets be normalized to a unified scale. To achieve this, each data set was normalized to the ectopic stem cell per area value of wild type moss grown on minimal media. This allowed us to compare the trends in the data, for instance if *clv1a;b* mutants on minimal media made four times as many stem cells per area as wild type on minimal media, we assigned a value of four to this condition in the dataset. The model would then attempt to generate a value for *clv1a;b* at the minimal media cytokinin input parameter that was four times higher than wild type at the same cytokinin level.

Each simulated value was compared to its corresponding empirical data value to generate a score. These scores were used to penalize a model with a given set of parameters; higher scores were worse than lower scores. The score was intended to accomplish the following:

1) Equally penalize simulated values that overshot or undershot the data

2) Weigh all datapoints equally. To do this, the score had to minimize fold changes in the data. Otherwise, a change from 1->2 would be penalized less than a change from 10 to 14, despite constituting a much larger relative change.
3) Penalize larger deviations from the data more severely than smaller ones. Otherwise, a model might be 'optimized' to have good fits to some data points but terrible fits to others. Since the intention of the model is to capture the trends in the data across all conditions, such a scenario was unacceptable.

We used the log of the fold change between the simulated and empirical data to accomplish the above aims one and two, and then squared to accomplish aim 3. The sum of these penalty scores at each data point then yielded the total fit score *F*

$$P_i = \ln\left(\frac{m_i}{d_i}\right)$$

$$F = \sum {P_i}^2$$

Mutating parameter values

Each model was run initially with semi-arbitrary parameters that allowed the model to converge within the given time frame. When comparing models, each model used similar starting parameters before optimization.

Model parameters k, p, d, and base were randomly mutated and then the model was run again. The Fit Score *F* for the new model was compared with the previous *F*. If the new *F* proved lower than the previous, then the new model parameters were saved and mutated again for the next run. If instead the new *F* was not lower than the previous, the original parameter set was randomly mutated again.

To mutate the parameters, a vector of values following a normal distribution and centered on 1 was generated.

```
mutator = rnorm(mean = 1, n = number_parameters, sd = 0.1)
```

The vector was the same length as the number of parameters to be mutated.

This vector was multiplied by the parameters to generate the new parameter set.

Simulating mutant genotypes

To simulate mutant genotypes in models 1-7 where CLV1 and RPK2 were non-dynamical, we simply set CLV1 or RPK2 to 0 instead of 2. In model 8, CLV1 and RPK2 initial (base) values, synthesis parameters, and interaction terms were set to 0 to simulate mutants.

Summary of workflow

1) Run the model and confirm that it converges to a steady-state value within the allotted time.
2) Simulate each mutant genotype at each cytokinin level of interest with the initial parameters to generate a starting fit score.
3) Begin the optimizer: randomly mutate parameters, compare fit score, repeat
4) After 300 runs of the optimizer, extract parameters from optimal run and plot simulations vs. empirical data

Model functions

Each of the models described here simulated the accumulation of gene products through time, simultaneously modeling transcription and translation. The equations are modified from Gordon et al. 2009, where the authors use similar systems of differential equations to test predictions about CLV43, CLV1, WUS, and cytokinin interactions[10].

Model 1-5

Models 1-5 consist of the following equations. Edges in the network (such as RPK2 inhibition of y) were changed by setting corresponding *k* values (in this case, *k*[5], to 0).

```
nofb = function(t = times0, s = base0, parms = parmsb){
   Cyt = parms[1]; clv = parms[2]; rpk2 = parms[3]
#Assign initial conditions
  x = s[1]; y = s[2]; init = s[3]
#Begin system of equations
  dx = (p[1] + Cyt*k[1])/(1+p[1]+Cyt*k[1]+k[2]*clv + k[3]*rpk2) - d[1]*x
  dy = (p[2])/(1+p[2]+k[4]*clv + k[5]*rpk2) - d[2]*y
  dinit = (p[3]+k[6]*x + k[7] * y)/(1+p[3]+k[6]*x + k[7] * y) - d[3]*init
  #return outputs
  dR = c(x = dx, y = dy, init = dinit)
  return(list(dR))
}
```

Model 6

```
endfb4 = function(t = times0, s = base0, parms = parmsb){
   Cyt = parms[1]; clv = parms[2]; rpk2 = parms[3]
 x = s[1]; y = s[2];init = s[3]; z = s[4]
 #differentials
        dx = (pb[1] + Cyt*kb[1])/(1+pb[1]+Cyt*kb[1]+kb[2]*clv + kb[3]*rpk2 + kb[9] * z)- db[1]*x
        dz = (pb[4])/(1 + pb[4] + kb[8]*Cyt) - db[4]*z
        dy = (pb[2])/(1+pb[2]+kb[4]*clv + kb[5]*rpk2) - db[2]*y
        dinit = (pb[3]+kb[6]*x + kb[7] * y + kb[9]*z)/(1+pb[3]+kb[6]*x + kb[7] * y + kb[9]*z) -
db[3]*init
dR = c(x = dx, y = dy, init = dinit, z = dz)
 return(list(dR))
}
```

Model 7

```
endfb3 = function(t = times0, s = base0, parms = parmsb){
   Cyt = parms[1]; clv = parms[2]; rpk2 = parms[3]
 x = s[1]; y = s[2];init = s[3]; z = s[4]
 #differentials
        dx = (pb[1] + Cyt*kb[1])/(1+pb[1]+Cyt*kb[1]+kb[2]*clv + kb[3]*rpk2 + kb[9] * z)- db[1]*x
        dz = (pb[4] + kb[8]*Cyt)/(1 + pb[4] + kb[8]*Cyt) - db[4]*z
        dy = (pb[2])/(1+pb[2]+kb[4]*clv + kb[5]*rpk2) - db[2]*y
        dinit = (pb[3]+kb[6]*x + kb[7] * y)/(1+pb[3]+kb[6]*x + kb[7] * y + kb[9]*z) - db[3]*init
dR = c(x = dx, y = dy, init = dinit, z = dz)
return(list(dR))
}
```

Model 8

```
feedbacks6 = function(t = times0, s = base0, parms = parmsb){#no auxing
  Cyt = parms[1];
  x = s[1]; y = s[2]; init = s[3]; clv = s[4]; rpk2 = s[5]; cle = s[6]; clvsig = s[7]; rpk2sig = s[8]
  #differentials
          dx = (pb[1] + Cyt*kb[1])/(1+pb[1]+Cyt*kb[1]+clvsig*kb[2]+rpk2sig*kb[3])- db[1]*x
          dy = pb[2]/(1+pb[2] + rpk2sig*kb[4] + clvsig *kb[5]) - db[2]*y
          dinit = (pb[3] + x * kb[6] + y * kb[7]) / (1 + pb[3] + x * kb[6] + y * kb[7]) -  db[3]*init
          dclv = (pb[4] + kb[8] * Cyt)/(1 + pb[4] + kb[8] * Cyt)- db[4] * clv - kb[9]*clv*cle + db[5]*clvsig
          drpk2 = (pb[5]+kb[10]*Cyt)/(1 + pb[5]+kb[10]*Cyt) - db[6]*rpk2 - kb[11]*rpk2*cle +
db[7]*rpk2sig
          dcle = (pb[6] + Cyt*kb[12])/(1 + pb[6]+ Cyt*kb[12]) - db[8]*cle - clv*cle*kb[9] - rpk2*cle*kb[11]
+db[7]*rpk2sig+db[5]*clvsig
          dclvsig = clv*cle*kb[9] - db[5]*clvsig - db[9]*clvsig
          drpk2sig = rpk2*cle*kb[11] - db[7]*rpk2sig - db[10] * rpk2sig

  dR = c(x = dx, y = dy, init = dinit, clv = dclv, rpk2 = drpk2, cle = dcle, clvsig = dclvsig, rpk2sig =
drpk2sig)
  return(list(dR))
}
```

List of parameters, starting values, and finishing values

Model 1 (Figure 4 A)

Parameter	Description	Starting Value	Finishing Value
k_1	cytokinin ↑ x	1	1.500644
k_2	clv ↓ x	1	0.525365
k_3	rpk2 ↓ x	1	20.8025
k_4	clv ↓ y	1	4.652118
k_5	rpk2 ↓ y	1	0.190285
k_6	x ↑ init	0.1	0.019766
k_7	y ↑ init	0.1	0.319337
p_1	basal x synthesis	.01	0.00365
p_2	basal y synthesis	0.01	0.02994
p_3	basal init synthesis	0.01	0.008979
d_1	x degradation	0.05	0.035265
d_2	y degradation	0.05	0.035136
d_3	init degradation	0.05	0.02294
$base_1$	initial x	1	1.165125
$base_2$	initial y	1	0.84229
$base_3$	initial init	1	0.402657

Model 2 (Figure 4 B)

Parameter	Description	Starting Value	Finishing Value
k_1	cytokinin ↑ x	1	0.304867
k_2	clv ↓ x	1	5.506337
k_3	rpk2 ↓ x	0	0
k_4	clv ↓ y	0	0
k_5	rpk2 ↓ y	1	3.955426
k_6	x ↑ init	0.1	0.048441
k_7	y ↑ init	0.1	0.209578
p_1	basal x synthesis	0.1	0.025085
p_2	basal y synthesis	0.1	0.0416
p_3	basal init synthesis	.01	0.003168
d_1	x degradation	0.01	0.047735

d_2	y degradation	0.01	0.017703
d_3	init degradation	0.05	0.041424
$base_1$	initial x	0.05	0.452641
$base_2$	initial y	0.05	0.333642
$base_3$	initial init	1	0.351427

Model 3 (Figure 4 C)

Parameter	**Description**	**Starting Value**	**Finishing Value**
k_1	cytokinin ↑ x	1	0.655062
k_2	clv ↓ x	0	0
k_3	rpk2 ↓ x	1	7.480788
k_4	clv ↓ y	1	2.17663
k_5	rpk2 ↓ y	0	0
k_6	x ↑ init	0.1	0.055229
k_7	y ↑ init	0.1	0.27232
p_1	basal x synthesis	0.1	0.014258
p_2	basal y synthesis	0.1	0.015025
p_3	basal init synthesis	.01	0.002324
d_1	x degradation	0.01	0.159216
d_2	y degradation	0.01	0.03027
d_3	init degradation	0.05	0.04435
$base_1$	initial x	0.05	1.239331
$base_2$	initial y	0.05	0.899113
$base_3$	initial init	1	0.540307

Model 4 (Figure 4 D)

Parameter	**Description**	**Starting Value**	**Finishing Value**
k_1	cytokinin ↑ x	1	0.841983
k_2	clv ↓ x	1	2.50779

k_3	rpk2 ↓ x	1	9.162987
k_4	clv ↓ y	0	0
k_5	rpk2 ↓ y	0	0
k_6	x ↑ init	0.1	0.218686
k_7	y ↑ init	0.1	0.070918
p_1	basal x synthesis	0.1	0.009767
p_2	basal y synthesis	0.1	0.004626
p_3	basal init synthesis	.01	0.003158
d_1	x degradation	0.01	0.057663
d_2	y degradation	0.01	0.106677
d_3	init degradation	0.05	0.019892
$base_1$	initial x	0.05	0.072355
$base_2$	initial y	0.05	0.866898
$base_3$	initial init	1	0.740589

Model 5 (Figure 4 E)

Parameter	Description	Starting Value	Finishing Value
k_1	cytokinin ↑ x	1	0.035789
k_2	clv ↓ x	0	0
k_3	rpk2 ↓ x	0	0
k_4	clv ↓ y	1	0.296071
k_5	rpk2 ↓ y	1	6.576975
k_6	x ↑ init	0.1	0.027982
k_7	y ↑ init	0.1	0.359106
p_1	basal x synthesis	0.1	0.004176
p_2	basal y synthesis	0.1	0.03289
p_3	basal init synthesis	.01	0.000394
d_1	x degradation	0.01	0.045523
d_2	y degradation	0.01	0.030657
d_3	init degradation	0.05	0.045014
$base_1$	initial x	0.05	0.551109
$base_2$	initial y	0.05	0.300094
$base_3$	initial init	1	0.702136

Models 6 and 7

Models 6 and 7 are similar in topology with the inclusion of the variable *z* downstream of cytokinin. In Model 6, *z* is inhibited by cytokinin, and induces *init*. In model 7, *z* is induced by cytokinin, and inhibits *init*. Two versions of each model were run: one with CLV1 inhibiting *x* and RPK2 inhibiting *y*, and one RPK2 inhibits *x* and CLV1 inhibits *y*.

Model 6 (Figure 6 A, upper panel)

Parameter	Description	Starting Value	Finishing Value
k_1	cytokinin ↑ x	1	0.435963
k_2	clv ↓ x	1	5.048187
k_3	rpk2 ↓ x	0	0

k_4	clv ↓ y	0	0
k_5	rpk2 ↓ y	1	8.082593
k_6	x ↑ init	0.1	0.017249
k_7	y ↑ init	0.1	0.169828
k_8	cytokinin ↓ z	0.5	8.181178
k_9	z ↑ init	0.5	0.768938
p_1	basal x synthesis	0.01	0.004266
p_2	basal y synthesis	0.03	0.023539
p_3	basal init synthesis	.01	0.004809
p_4	basal z synthesis	0.01	0.008215
d_1	x degradation	0.05	0.04629
d_2	y degradation	0.05	0.027294
d_3	init degradation	0.05	0.032801
d_4	z degradation	0.05	0.063203
$base_1$	initial x	1	1.927968
$base_2$	initial y	1	0.232216
$base_3$	initial init	1	0.379397
$base_4$	initial z	1	0.656615

Model 6 (Figure 6 A, lower panel)

Parameter	**Description**	**Starting Value**	**Finishing Value**
k_1	cytokinin ↑ x	1	0.380677
k_2	clv ↓ x	0	0
k_3	rpk2 ↓ x	1	6.363934
k_4	clv ↓ y	1	2.772667
k_5	rpk2 ↓ y	0	0
k_6	x ↑ init	0.1	0.053368
k_7	y ↑ init	0.1	0.205299
k_8	cytokinin ↓ z	0.5	12.45164

k_9	z ↑ init	0.5	0.854566
p_1	basal x synthesis	0.01	0.059793
p_2	basal y synthesis	0.03	0.032342
p_3	basal init synthesis	.01	0.002267
p_4	basal z synthesis	0.01	0.008643
d_1	x degradation	0.05	0.097205
d_2	y degradation	0.05	0.048109
d_3	init degradation	0.05	0.052553
d_4	z degradation	0.05	0.074966
$base_1$	initial x	1	0.933395
$base_2$	initial y	1	1.584061
$base_3$	initial init	1	0.876901
$base_4$	initial z	1	0.579399

Model 7 (Figure 6 B, upper panel)

Parameter	**Description**	**Starting Value**	**Finishing Value**
k_1	cytokinin ↑ x	1	0.863826
k_2	clv ↓ x	1	19.77114
k_3	rpk2 ↓ x	0	0
k_4	clv ↓ y	0	0
k_5	rpk2 ↓ y	1	1.999533
k_6	x ↑ init	0.1	0.040456
k_7	y ↑ init	0.1	0.173769
k_8	cytokinin ↑ z	0.5	1.685863
k_9	z ↓ init	0.5	0.311607
p_1	basal x synthesis	0.01	0.028438
p_2	basal y synthesis	0.03	0.056778
p_3	basal init synthesis	.01	0.004693
p_4	basal z synthesis	0.01	0.005662

d_1	x degradation	0.05	0.014775
d_2	y degradation	0.05	0.018722
d_3	init degradation	0.05	0.038537
d_4	z degradation	0.05	0.118948
$base_1$	initial x	1	0.654166
$base_2$	initial y	1	0.251628
$base_3$	initial init	1	2.202736
$base_4$	initial z	1	0.992124

Model 7 (Figure 6 B, lower panel)

Parameter	**Description**	**Starting Value**	**Finishing Value**
k_1	cytokinin ↑ x	1	1.463869
k_2	clv ↓ x	0	0
k_3	rpk2 ↓ x	1	19.17415
k_4	clv ↓ y	1	1.013134
k_5	rpk2 ↓ y	0	0
k_6	x ↑ init	0.1	0.027886
k_7	y ↑ init	0.1	0.087528
k_8	cytokinin ↑ z	0.5	2.157959
k_9	z ↓ init	0.5	0.190479
p_1	basal x synthesis	0.01	0.039586
p_2	basal y synthesis	0.03	0.061077
p_3	basal init synthesis	.01	0.00435
p_4	basal z synthesis	0.01	0.012878
d_1	x degradation	0.05	0.012762
d_2	y degradation	0.05	0.024692
d_3	init degradation	0.05	0.055329
d_4	z degradation	0.05	0.042331
$base_1$	initial x	1	0.432841

$base_2$	initial y	1	1.570673
$base_3$	initial init	1	0.574236
$base_4$	initial z	1	0.270798

Model 8

Model 8 introduces a new mechanism, including complex formation and dissolution. Binding coefficients and dissolution rates are incorporated into new *k* and *d* parameters. 'CLVsig' and 'RPK2sig' represent actively signaling CLE-CLV1 and CLE-RPK2 complexes, respectively. This model included coefficients for cytokinin-mediated induction of CLV1 and RPK2. However, these interactions were left out of the final version of the model by setting these parameter values to 0. Including them did not change the outcome of the model (not shown).

Model 8 (Figure 6 C, upper panel)

Parameter	Description	Starting Value	Finishing Value
k_1	cytokinin ↑ x	1	0.434556
k_2	clv ↓ x	1	3.634155
k_3	rpk2 ↓ x	0	0
k_4	clv ↓ y	0	0
k_5	rpk2 ↓ y	1	2.258783
k_6	x ↑ init	0.1	0.049658
k_7	y ↑ init	1	0.660561
k_8	cytokinin ↑ CLV1	0	0
k_9	CLE:CLV1 binding	0.1	0.106173
k_{10}	cytokinin ↑ RPK2	0	0
k_{11}	CLE:RPK2 binding	0.1	0.275352
k_{12}	cytokinin ↑ CLE	1	2.731367
p_1	basal x synthesis	0.01	0.054615
p_2	basal y synthesis	0.02	0.019844
p_3	basal init synthesis	0	0

p_4	basal CLV1 synthesis	0.1	0.199788
p_5	basal RPK2 synthesis	0.1	0.111586
p_6	basal CLE synthesis	0.1	0.036183
d_1	x degradation	0.05	0.061757
d_2	y degradation	0.05	0.03428
d_3	init degradation	0.05	0.230952
d_4	CLV1 degradation	0.05	0.067365
d_5	CLE:CLV complex dissolution	0.1	0.071258
d_6	RPK2 degradation	0.05	0.113099
d_7	CLE:RPK2 complex dissolution	0.1	0.048117
d_8	CLE degradation	0.05	0.140781
d_9	CLE:CLV complex degradation	0.05	0.019153
d_{10}	CLE:RPK2 complex degradation	0.05	0.016996
$base_1$	initial x	5	1.137288
$base_2$	initial y	5	11.37192
$base_3$	initial init	5	7.199671
$base_4$	initial CLV1	5	2.289835
$base_5$	initial RPK2	5	8.035224
$base_6$	initial CLE	5	7.77699
$base_7$	initial CLE:CLV1 complex	0	0
$base_8$	initial CLE:RPK2 complex	0	0

Model 8 (Figure 6, lower panel)

Parameter	Description	Starting Value	Finishing Value
k_1	cytokinin ↑ x	1	0.7673
k_2	clv ↓ x	0	0
k_3	rpk2 ↓ x	1	2.766442
k_4	clv ↓ y	1	1.359283
k_5	rpk2 ↓ y	0	0
k_6	x ↑ init	0.1	0.025157
k_7	y ↑ init	1	1.885248
k_8	cytokinin ↑ CLV1	0	0
k_9	CLE:CLV1 binding	0.1	0.066278
k_{10}	cytokinin ↑ RPK2	0	0
k_{11}	CLE:RPK2 binding	0.1	0.064306
k_{12}	cytokinin ↑ CLE	1	1.37944
p_1	basal x synthesis	0.01	0.019233
p_2	basal y synthesis	0.02	0.005913
p_3	basal init synthesis	0	0
p_4	basal CLV1 synthesis	0.1	0.327789
p_5	basal RPK2 synthesis	0.1	0.18695
p_6	basal CLE synthesis	0.1	0.008464
d_1	x degradation	0.05	0.072154
d_2	y degradation	0.05	0.066177
d_3	init degradation	0.05	0.032721
d_4	CLV1 degradation	0.05	0.031734
d_5	CLE:CLV complex dissolution	0.1	0.157496
d_6	RPK2 degradation	0.05	0.032288

d_7	CLE:RPK2 complex dissolution	0.1	0.054447
d_8	CLE degradation	0.05	0.014541
d_9	CLE:CLV complex degradation	0.05	0.044547
d_{10}	CLE:RPK2 complex degradation	0.05	0.01662
$base_1$	initial x	5	1.360174
$base_2$	initial y	5	1.365039
$base_3$	initial init	5	3.108931
$base_4$	initial CLV1	5	11.19204
$base_5$	initial RPK2	5	2.068501
$base_6$	initial CLE	5	6.102137
$base_7$	initial CLE:CLV1 complex	0	0
$base_8$	initial CLE:RPK2 complex	0	0

References

1. Ashton, N.W., and Cove, D.J. (1977). The isolation and preliminary characterisation of auxotrophic and analogue resistant mutants of the moss, Physcomitrella patens. MGG Mol. Gen. Genet.

2. Lopez-Obando, M., Hoffmann, B., Gery, C., Guyon-Debast, A., Teoule, E., Rameau, C., Bonhomme, S., and Nogue, F. (2016). Simple and Efficient Targeting of Multiple Genes Through CRISPR-Cas9 in Physcomitrella patens. G3: Genes|Genomes|Genetics *6*, 3647–3653.

3. Haeussler, M., Schönig, K., Eckert, H., Eschstruth, A., Mianné, J., Renaud, J.B., Schneider-Maunoury, S., Shkumatava, A., Teboul, L., Kent, J., et al. (2016). Evaluation of off-target and on-target scoring algorithms and integration into the guide RNA selection tool CRISPOR. Genome Biol. *17*, 1–12.

4. Strable, J., Wallace, J.G., Unger-Wallace, E., Briggs, S., Bradbury, P.J., Buckler, E.S., and Vollbrecht, E. (2017). Maize YABBY genes drooping leaf1 and drooping leaf2 regulate plant architecture. Plant Cell.

5. Edgar, R.C. (2004). MUSCLE: multiple sequence alignment with high accuracy and high throughput. Nucleic Acids Res. *32*, 1792–1797.

6. Schindelin, J., Arganda-Carreras, I., Frise, E., Kaynig, V., Longair, M., Pietzsch, T., Preibisch, S., Rueden, C., Saalfeld, S., Schmid, B., et al. (2012). Fiji: An open-source platform for biological-image analysis. Nat. Methods.

7. Soetaert, K., Petzoldt, T., and Setzer, R.W. (2010). Solving differential equations in R: Package deSolve. J. Stat. Softw.

8. Team, R.C. (2016). R: A Language and Environment for Statistical Computing. R Found. Stat. Comput.

9. Hadley, W., Winston, C., Lionel, H., Thomas, Lin, P., Kohske, T., Claus, W., Kara, W., Hiroaki, Y., and Dewey, D. (2016). ggplot2 - Elegant Graphics for Data Analysis (Springer-Verlag New York).

10. Gordon, S.P., Chickarmane, V.S., Ohno, C., and Meyerowitz, E.M. (2009). Multiple feedback loops through cytokinin signaling control stem cell number within the Arabidopsis shoot meristem. Proc. Natl. Acad. Sci. U. S. A. *106*, 16529–16534.

Chapter 4: Auxin-Cytokinin interactions regulate shoot development in moss

Foreword

Regulation of the shoot apical meristem is complicated, and I could not stop myself from investigating the role of the ever-present hormone auxin in moss stem cell signaling. This chapter presents a collection of unpublished work on auxin-cytokinin interactions. The work has been assembled into a manuscript format for publication.

The work presented here was conducted by me, with many crucial intellectual contributions from Mike Scanlon and Adrienne Roeder.

Auxin-Cytokinin interactions regulate shoot development in moss

Abstract

Crosstalk between auxin and cytokinin contributes to widespread developmental processes, including root and shoot meristem maintenance, phyllotaxy, and vascular patterning. However, while auxin and cytokinin are potent regulators of plant development across land plants, our understanding of crosstalk between these hormones is relatively limited to few model systems. The moss *Physcomitrium patens* is a powerful model system for studying plant hormone function. Auxin and cytokinin play similar roles in regulating moss shoot architecture as they do in flowering plants. However, auxin-cytokinin crosstalk has yet to be investigated in moss shoots. Here we find that the ratio of auxin to cytokinin is an important determinant of shoot development in moss, especially for leaves. Our data suggests a role for cytokinin in modulating auxin transport and possibly auxin signaling. Auxin is necessary for the prevention of ectopic stem cell initiation, and likely does so by inhibiting signals downstream of cytokinin. However, our data supports that the counter-intuitive ectopic stem cell initiation due to loss of cytokinin signaling is auxin-independent and occurs through an unknown pathway. Overall, our work demonstrates that complex and tissue-specific crosstalk between auxin and cytokinin plays an important role in determining moss shoot architecture.

Introduction

The hormones auxin and cytokinin are potent regulators of plant development. Their ability to specify root and shoot identity has long been utilized to regenerate plants in culture[1], and in recent decades auxin and cytokinin have been repeatedly found to play critical roles in widespread developmental processes[2,3]. Each hormone elicits manifold responses that depend on cell type and developmental stage. For example, auxin can induce cell elongation, cell differentiation (shoots), or the maintenance of an undifferentiated state (roots), while cytokinin promotes cell division, stem cell maintenance (shoots), or cell differentiation (roots). Understanding how these phytohormones perform such diverse, context-dependent functions is one of the most substantial challenges of plant developmental biology.

The functional diversity of hormone responses relies on crosstalk between hormone signaling pathways. In particular, crosstalk between auxin and cytokinin is widespread, and is critical for varied developmental processes such as root meristem maintenance[4], root branching architecture[5], and shoot stem cell maintenance[6]. Crosstalk can comprise many phenomena; one hormone can modulate the transport[7–9], synthesis[10,11], and signaling pathway of the other[8]. Several of these mechanisms can be at play simultaneously; for example, during root vascular patterning, auxin promotes cytokinin biosynthesis as well as inducing a cytokinin signaling inhibitor, thereby increasing cytokinin signaling in neighboring cells but not in cells with high auxin response[11]. In most instances we are just beginning to understand how auxin and cytokinin interact to regulate development, and our understanding is fairly limited to the angiosperm model plant *Arabidopsis thaliana*.

The moss *Physcomitrium patens* is a powerful model system for studying plant evolution and development[12]. Although the gametophytic moss shoot (gametophore) and sporophytic angiosperm shoot evolved independently, mounting evidence indicates that many developmental functions are accomplished by similar sets of genes in each group of plants[13]. For example, both mosses and angiosperms rely on signaling through CLAVATA3-like peptides to regulate the abundance of stem cells in the shoot, and *ROOT HAIR DEFECTIVE* genes direct the development of filamentous cells with rooting function (rhizoids and root hairs)[14].

Physcomitrium has also proven a useful model in the study of plant hormones due to reduced gene family sizes of hormone receptors and downstream signaling components[15]. As in Arabidopsis, auxin and cytokinin are important regulators of cell fate and of various developmental transitions[16], and it is clear that auxin-cytokinin crosstalk is a critical factor in development in both species. Physcomitrium begins development as a spore, from which grows a network of branched, photosynthetic filaments called chloronemata. After about one week in culture, a second type of filament forms called caulonema, which is faster growing, has oblique crosswalls, and lower chloroplast density. A small proportion of side branches from these caulonema form buds that establish a tetrahedral apical stem cell, from which will develop an entire, three-dimensional, leafy shoot called a gametophore.

In our best understood instance of auxin-cytokinin crosstalk from moss, auxin and cytokinin synergistically promote bud formation. Auxin induces the expression of the *AINTEGUMENTA, PLETHORA* and *BABY BOOM* (*APB*) orthologous genes[17]. Cytokinin and APBs together promote the formation of buds through unknown downstream mechanisms. Exogenous auxin or over expression of *APB* genes alone causes a moderate increase in bud production, and while cytokinin has a stronger effect on budding, *apb* quadruple mutants make no buds in response to cytokinin[17].

Once the shoot is formed, auxin and cytokinin perform antagonistic functions. With regard to branch formation, auxin and cytokinin function in moss shoots is analogous to angiosperms: auxin inhibits branch outgrowth, while cytokinin promotes branching[18]. Each hormone also substantially impacts leaf development: cytokinin increases leaf width via promoting cell division, whereas auxin promotes cell elongation and inhibits cell division, leading to the formation of long, narrow leaves[19]. Despite the importance of auxin and cytokinin in moss shoots, the mechanisms by which they control branching and leaf development are poorly understood and crosstalk has not been investigated.

Here we examine the contributions of auxin, cytokinin, and their interaction to moss shoot development. Overall, auxin and cytokinin antagonistically regulate leaf cell differentiation and branch outgrowth, and the ratio between these two hormones is critical during shoot development. Auxin prevents branch initiation and outgrowth, and reduced auxin synthesis phenocopies increased cytokinin signaling. Meanwhile, mutants unable to perceive cytokinin have increased auxin sensitivity, possibly altered auxin transport, and several phenotypes indicative of altered auxin response. Our data suggest that auxin inhibits cytokinin-mediated branch formation, whereas loss of cytokinin signaling activates branching via a separate pathway. Overall, our work reaffirms the importance of the ratio of auxin to cytokinin signaling during shoot development and provides a foundation for exploring auxin and cytokinin function and crosstalk during moss morphogenesis.

Results:

Cytokinin and auxin antagonistically regulate leaf outgrowth and development

To test how auxin and cytokinin interact to regulate shoot morphogenesis, we grew wild type moss on a range of concentrations of auxin and cytokinin and observed the morphology of three-week-old shoots. We wanted to subject moss to low and high concentrations of exogenous auxin, and so we chose 100 nM and 2.5 µM. On the other hand, moss shoots are sensitive to low concentrations of cytokinin, which can induce mild increases in stem cell specification at 10nM and severe stem cell and swelling phenotypes at 100 nM[20]. In order to elicit moderate and strong cytokinin phenotypes, we grew moss on concentrations of 25 nM and 250 nM of the synthetic cytokinin 6-*Benzylaminopurine (BAP)*. Moss was also grown on each combination of high and/or low auxin and cytokinin concentrations described above, to assess how changes in auxin/cytokinin ratios contribute to moss shoot morphology.

Low doses of auxin (100 nM NAA) mildly impacted shoot development, causing the formation of slightly narrow, elongated stems and leaves (Figure 1 B). Meanwhile, increased auxin concentration (2.5 µM NAA) had severe effects on development, inhibiting leaf outgrowth and stem elongation while promoting rhizoid formation (Figure 1 C)[16,21]. In contrast, growth on low doses of cytokinin (25 nM BAP) generated wider leaves (Figure 1 D, Supplemental Figure 1) and ectopic branch formation on the stem (Figure 1 D, E). Intriguingly, shoots grown on 25 nM BAP produced ectopic buds on rhizoids, whereas cytokinin has previously been reported to induce shoot formation on caulonema and chloronema (Supplemental Figure 1). Shoots grown on high doses of cytokinin (250 nM BAP) produced wide leaves with many small cells and ectopic stem cells that produced actively growing branches, consistent with a previously-described role for cytokinin in promoting cell proliferation and apical meristem identity[19,22].

Combined applications of exogenous auxin and cytokinin indicated that the ratio of these two hormones is a critical determinant of shoot development in moss. Auxin and cytokinin antagonistically regulate branch outgrowth, however a low dose of auxin (100 nM NAA) was not sufficient to inhibit branch outgrowth stimulated by the combined presence of either 25 nM or 250 nM BAP (Figure 1 E, I). Increasing the

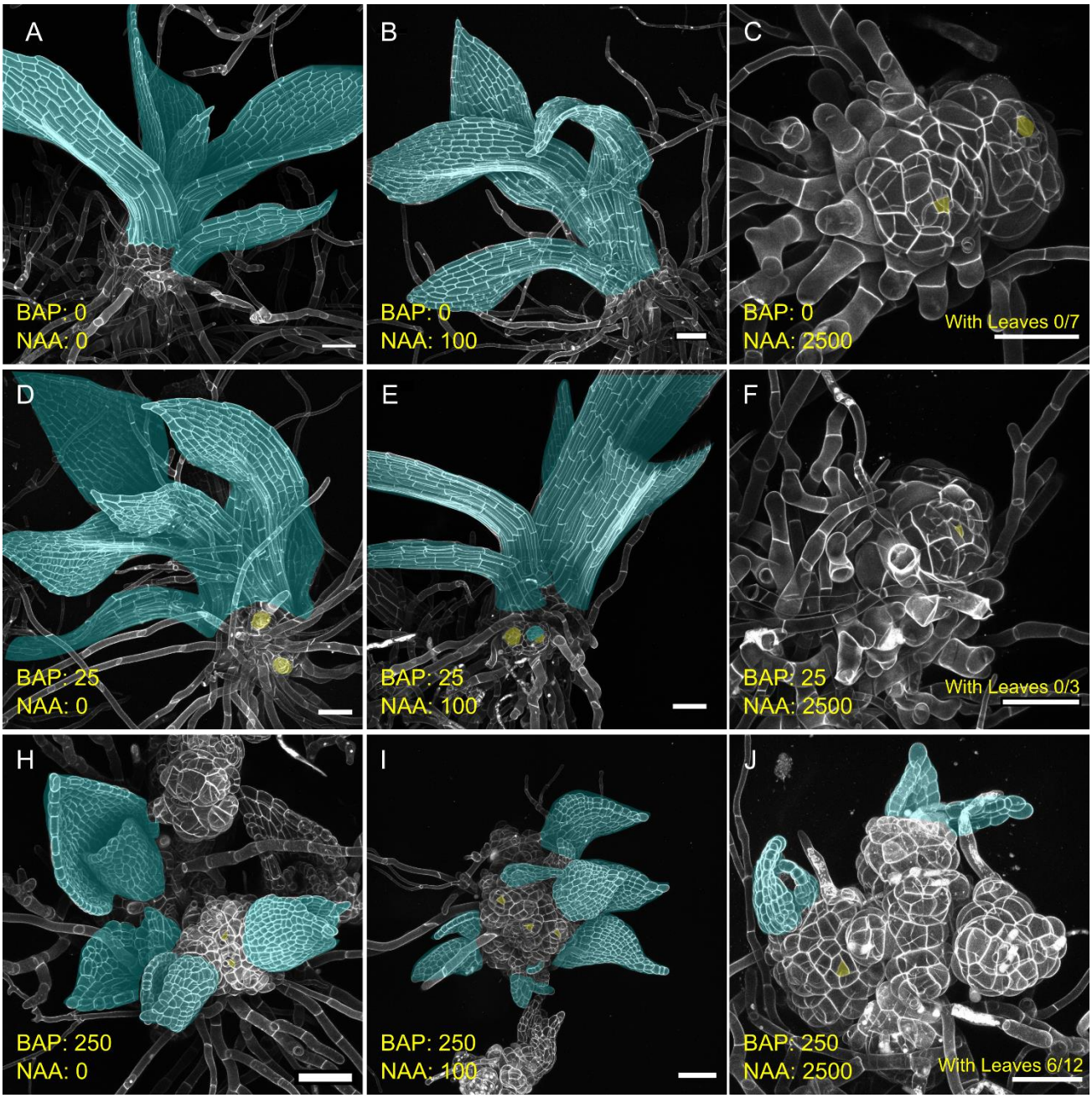

Figure 1: Effects of auxin and cytokinin on moss shoot morphology. Wild type moss grown on a range of concentrations of the auxin NAA and cytokinin BAP. From left to right: 0, 100, and 2500 nM NAA. From top to bottom: 0, 25, and 250 nM BAP. Leaves are highlighted blue and visible or ectopic stem cells or nascent ectopic branches are highlighted yellow. Scalebars: 100 nm

concentration of auxin to 2.5 µM NAA in combination with low doses of cytokinin (25 nM BAP) phenocopied shoots grown on 2.5 µM NAA alone; 25 nM BAP was insufficient to rescue the leaf outgrowth, stem elongation, or rhizoid overproduction phenotypes caused by 2.5 µM NAA (Figure 1F).

In contrast, high concentrations of cytokinin were sufficient to partly restore leaf outgrowth overcoming the inhibition of leaf outgrowth by high concentrations of auxin. Shoots grown on high doses of both cytokinin and auxin (250 nM BAP and 2.5 µM NAA) displayed increased cell proliferation and partially suppressed inhibition of leaf outgrowth compared to high auxin alone (Figure 1 J, Supplemental Figure 2). Leaf outgrowth was rescued on half of the imaged shoots (6/12), although most leaves were small and triangular, resembling juvenile leaves[23]. We observed one leaf comprising two files of elongated cells, representing a case where auxin-mediated repression was barely escaped (Supplemental Figure 2). Therefore, rescue of auxin-mediated leaf outgrowth by cytokinin was partial and analogue. Overall, these data demonstrate that a high concentration of exogenous cytokinin can rescue phenotypes caused by high concentrations auxin, suggesting the two pathways antagonistically control shoot development and that the ratio of auxin to cytokinin signaling is critical.

Reducing auxin synthesis phenocopies cytokinin treatment

If the ratio of auxin/cytokinin, rather than their absolute concentrations, is the determinant factor in moss shoot development, we hypothesize that reduced auxin concentrations should produce plants resembling those treated with cytokinin. To assess the impact of reduced auxin abundance on apical stem cell development, we grew wild type moss on media supplemented with the auxin synthesis inhibitor L-Kynurinine (L-Kyn).

Wild type moss grown on 10uM L-Kyn produced dense, bushy colonies with smaller shoots than plants grown on minimal media, similar to moss grown on low concentrations of BAP (Figure 2 A, B). Young L-Kyn-grown shoots had broad leaves with reduced cell elongation, reminiscent of cytokinin-treated shoots (Figure 2C, Figure 1). At later stages of development, L-Kyn-grown leaf cells were less abnormally short, suggesting that older plants either overcame L-Kyn-mediated auxin inhibition, or that cell elongation at later stages occurs by an auxin-independent mechanism (Figure 2 D).

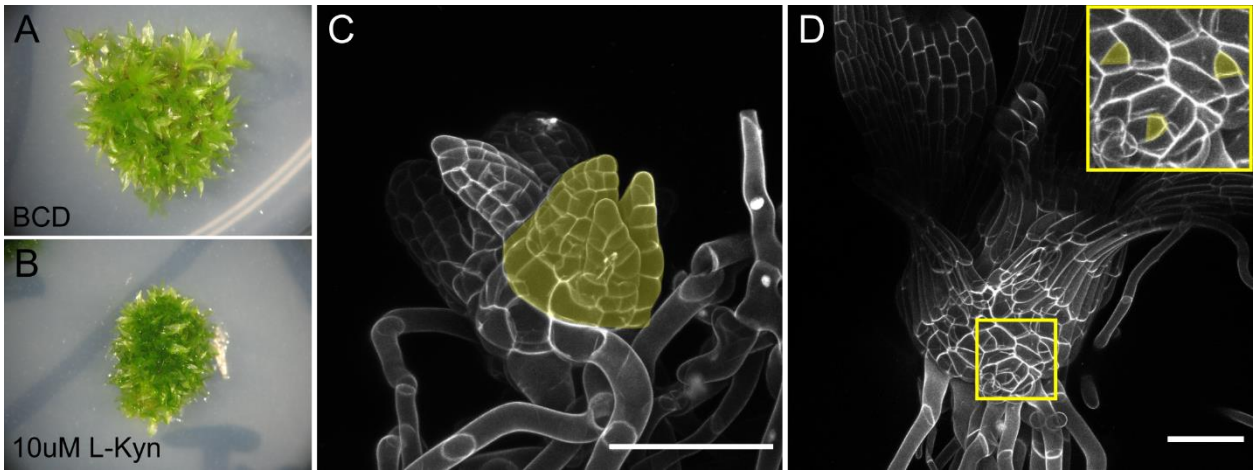

Figure 2: Inhibition of auxin synthesis phenocopies cytokinin treatment. Three-week-old wild type moss colonies grown in the absence of the auxin synthesis inhibitor L-Kyn (A) or on 10 µM L-Kyn (B). A young shoot from a moss colony grown in the presence of L-Kyn, with leaves from an ectopic branch highlighted in yellow (C). An older shoot from moss grown with L-Kyn, with inset highlighting the presence of ectopic apical stem cells (highlighted yellow) (D). Scalebars: 100 nm.

L-Kyn also caused stem swelling, and in some cases, shoots developed ectopic stem cells or branches, phenocopying the effects of cytokinin (Figure 2 C, D, Figure 1 D, E). It was previously shown that reductions in auxin abundance increase branch number on mature gametophores[18]. However, it was unclear whether reduced auxin caused the initiation of more axillary meristems, or in contrast, existing meristems were de-repressed. The formation of ectopic branches at early developmental stages, i.e. before branch initials normally form, suggests that auxin is required to inhibit axillary meristem initiation. Both the production of wide leaves with short cells and the formation of ectopic SAMs are phenotypes also caused by exogenous cytokinin (Figure 1 D, H). Thus, plants with reduced auxin abundance phenocopy shoots grown in high cytokinin concentration, further demonstrating the developmental importance of these hormone ratios.

Loss of cytokinin perception partially phenocopies increased auxin signaling

While the effects of exogenous cytokinin on moss shoot development have been tested, shoot development of mutants with impaired cytokinin perception is poorly understood. Loss of function mutants of the three *CYTOKININ HISTIDINE KINASE* (*CHK*) genes are completely insensitive to exogenous cytokinin and produce small shoots after a two week-long delay, consistent with a role for cytokinin in promoting cell division and bud initiation[16,18,24]. In order to determine whether plants lacking cytokinin perception resembled

plants with increased auxin signaling, we re-examined *chk1;2;3* triple knockout shoots. Buds from *chk1;2;3* colonies had normal division planes, but smaller cells compared to wild type buds (Figure 3 A, D). *chk1;2;3* shoots produced narrow leaves with few cell files and long cells (Figure 3 E, F). The production of leaves with long, narrow cells and fewer cell files is associated with increased auxin signaling[19,21] (Figure 1B). As reported previously, we noticed a counter-intuitive increase in branch production, contrary to expectations based on cytokinin's role in promoting branching[20]. We previously proposed that ectopic branch formation in

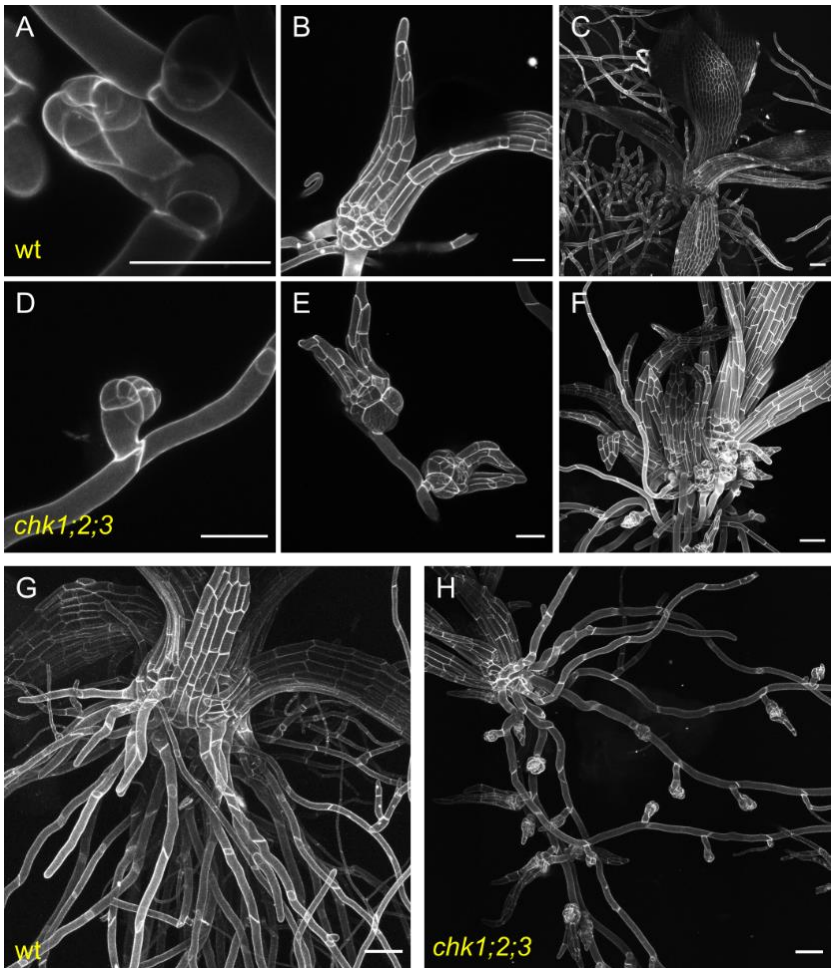

Figure 3: Loss of cytokinin signaling resembles altered auxin signaling, suggesting complex crosstalk. Wild type shoot initial (A), one-week old shoot (B), and approximately four week old shoot (C). *chk1;2;3* mutant bud (D). *chk1;2;3* mutant shoots have narrow leaves and often form adjacent one another (E). *chk1;2;3* shoots make ectopic branches, making them very bushy at later stages (F). Approximately four-week-old wild type (G) and *chk1;2;3* (H) shoots with rhizoids, showing ectopic bud formation on *chk1;2;3* rhizoids. Scalebars in A, B, D, E are 50 nm. Scalebars in C, F, G, and H are 100 nm.

chk1;2;3 might occur if cytokinin signaling inhibited stem cell formation through an unknown pathway[20]. Auxin represses branch outgrowth, and the increased branch formation in *chk1;2;3* triple mutants phenocopies plants with increased auxin degradation[18]. Thus, *chk1;2;3* phenotypes suggest increased auxin signaling in the mutant leaves and decreased auxin signaling in stems. Surprisingly, we observed a novel moss phenotype: whereas wild type rhizoids rarely initiate branches (Figure 3 G), *chk1;2;3* mutant rhizoids initiated numerous branches, almost all of which differentiated into shoots (Figure 3 H). Ectopic bud formation on rhizoids has not been described in any plant where auxin synthesis, transport, or signaling are perturbed, suggesting this phenotype arises from the misregulation of an auxin-independent pathway[20]. However, auxin does promote bud formation[16,17], such that ectopic bud formation in *chk1;2;3* may also arise from loss of interaction between auxin and cytokinin signaling. Overall, while the leaf phenotype of *chk1;2;3* mutants supports the importance of the auxin-cytokinin ratio in moss shoot development, ectopic branching, and bud formation in *chk1;2;3* points to a more complex interaction between auxin and cytokinin in stems and rhizoids.

PIN1 polarity is altered in *chk1;2;3* mutant leaves

Because aspects of the *chk1;2;3* phenotype suggested non-uniform changes to auxin signaling, we asked whether auxin transport is altered in *chk1;2;3* mutants. To test this, we conducted whole-mount immunofluorescence staining of the auxin efflux carrier PINFORMED (PIN) transporters using an Arabidopsis PIN1 antibody on shoots from five-to-six-week-old wild type and *chk1;2;3* colonies (Figure 4).

Immunofluorescence staining revealed polarized localization of PIN within young leaf cells. Staining was often diffuse in larger leaves, possibly demonstrating poor penetrance into mature leaf cells (not shown). However, polarity crescents were more tightly localized in younger leaves (Figure 4 A), and fluorescence was completely absent from negative controls lacking the PIN1 antibody (Figure 4 C). Cells with PIN polarity crescents oriented both apically and basally were observed in wild type (Figure 4 A) and *chk1;2;3* mutant (Figure 4 B) leaves, as had been previously reported for PIN1-GFP localization in moss[25]. We could not discern the localization of PIN in stems.

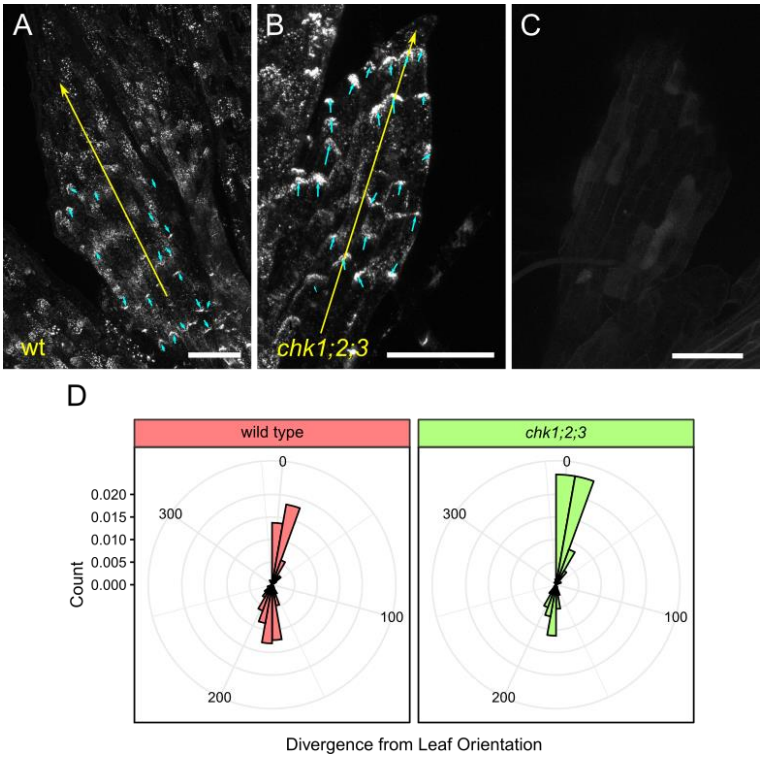

Figure 4: Auxin transport is altered in *chk1;2;3* leaves. Whole mount immunolocalization using the maize PIN1A antibody. Leaf from a five week-old wild type (A) and *chk1;2;3* mutant shoots (B). Control lacking primary antibody (C). Radial histograms showing altered distribution of PIN polarity crescents in wild type vs. *chk1;2;3* leaves. Polarity crescent angles (Blue arrows in A, B) were measured relative to the angles of the leaves on which they were found (yellow lines in A, B). On histograms in D, 0 degrees represents perfect alignment with the leaf. Scalebars: 100 nm

There were no readily observable differences in PIN localization between wild type and *chk* shoots. To test whether more subtle, differences in PIN1 localization could underly the *chk1;2;3* phenotype, we quantified the orientation of PIN1 polarity crescents relative to the apical-basal axis of the leaf (Figure 4 D). We categorized crescents as being either acropetally oriented or basipetally oriented and tested for a change in the proportion of crescents that fell into each category. We found that PIN crescents were more often oriented acropetally in *chk1;23* (105 acropetal, 63 basipetal)*;* than in wild type (170 acropetal, 170 basipetal; Fisher's exact test, $p = 0.008$). Thus, there is increased transport away from stems and toward leaf tips in *chk1;2;3*, consistent with more branching and leaf cell elongation in the mutants. However, drastically altered development in *chk1;2;3* prohibits the comparison of equivalent 'stages' with wild type shoots. We thus cannot rule out that differences in PIN localization are indirectly caused by developmental differences and are not causative of them.

chk1;2;3 mutants are hypersensitive to auxin

Our results thus far demonstrated that reducing auxin signaling mimicked the phenotypic effects of increasing cytokinin, while reducing cytokinin mimicked the effect of increasing auxin. To test whether loss of cytokinin

signaling in the *chk1,2,3* mutant affects responsiveness to auxin, we grew wild type and *chk1;2;3* mutants on moderate (500 nM) and high (5 µM) concentrations of NAA. Wild type shoots on 500 nM NAA had slightly enlarged stems with rounded cells (Figure 5 A). Later staged shoots produced a greater number of rhizoids, elongated stem and leaf cells, and narrow leaves (Figure 5 C). While 500 nM NAA was insufficient to suppress leaf outgrowth in wild type shoots, 500 nM NAA robustly suppressed leaf outgrowth in chk1,2,3 and resulted in the formation of small shoots with a bare apical meristem and supernumerary rhizoids (Figure 5 E). These auxin treated *chk1,2,3* shoots resembled wild type shoots grown on much higher concentrations of auxin (5 µM NAA; Figure 5 B, D). Moreover, increasing the concentration of NAA to 5 µM only slightly increased the severity of the defects in shoot development compared to *chk1;2;3* grown on 500 nM NAA. Specifically, we sometimes observed small cellular projections that suggested leaf initial identity was attained, but subsequent development was rapidly terminated on 500 nM NAA. These small leaf initials were absent on 5 µM NAA (Supplemental Figure 3, Figure 5 F). Therefore, *chk1;2;3* mutants are hypersensitive to NAA with regard to leaf development. These findings are consistent with the ratiometric model of auxin-cytokinin interaction: in *chk1;2;3* bereft of cytokinin signaling, a lower concentration of auxin is required to tip the scales to inhibit leaf outgrowth than in wild type shoots.

Whereas the ratio of auxin to cytokinin signaling appeared critical for leaf development, the regulation of branching by auxin and cytokinin appeared more complex. We often observed multiple SAMs on *chk1;2;3* mutants grown on auxin, suggesting that 500nM NAA is sufficient to inhibit leaf outgrowth but not the formation of ectopic stem cells in *chk1;2;3*. However, *chk1;2;3* mutant shoots still formed multiple SAMs on 5 µM NAA (Figure 5 F). Thus, even a very high auxin concentration was insufficient to prevent ectopic SAM formation in *chk1;2;3*. These data suggest that the mechanism(s) whereby auxin inhibits stem cell formation is impaired in *chk* mutants and that the control of branch development did not hinge on the ratio of auxin to cytokinin signaling as was the case for leaf development.

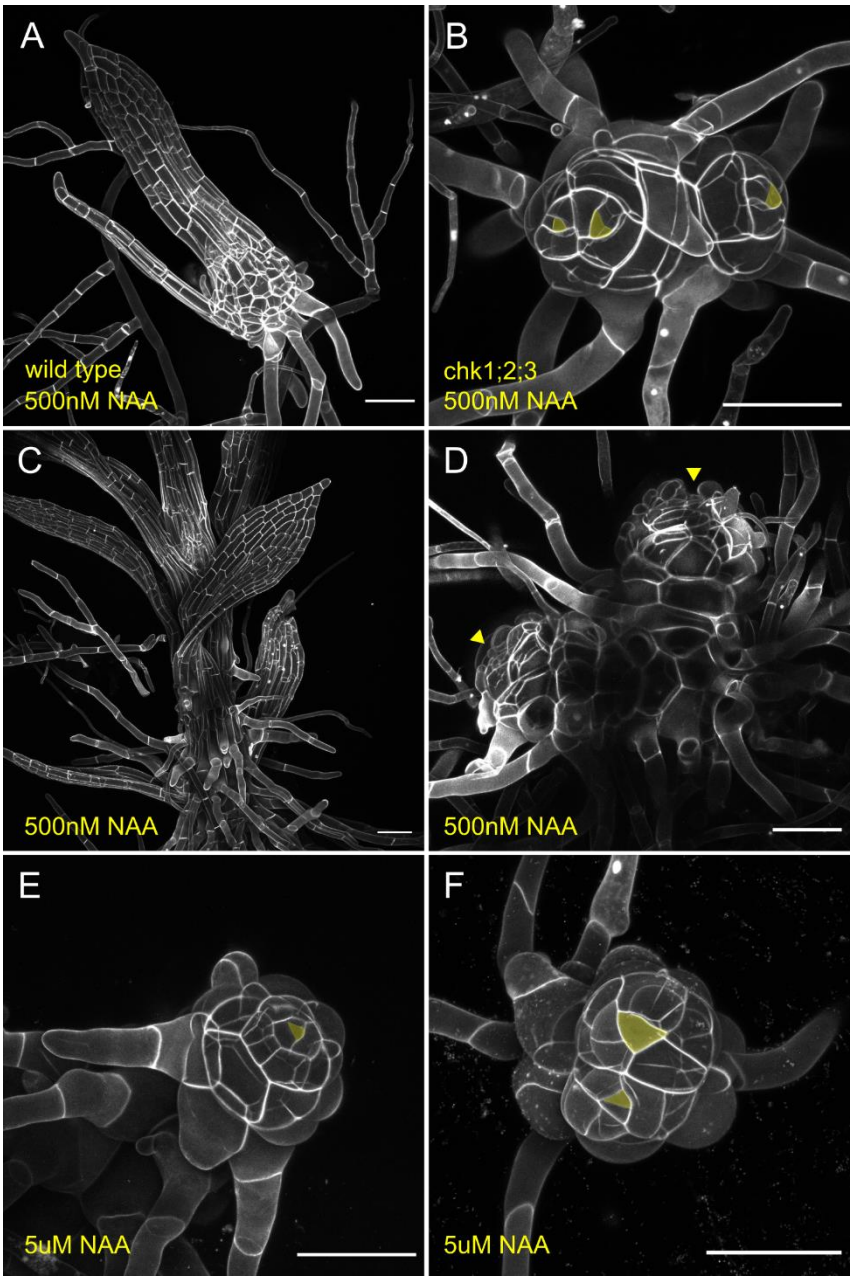

Figure 5: *chk1;2;3* mutants are hypersensitive to auxin. Early (A, B) and late (C, D) stage wild type (A, C) and *chk1;2;3* (B, D) plants grown on 500 nM NAA. Whereas 500nM NAA causes cell expansion and the formation of elongated stems and leaves in wild type moss, *chk1;2;3* mutants on 500nM NAA resemble wild type moss grown on 5 µM NAA. Wild type (E) and *chk1;2;*3 (F) shoots grown on 5 µM NAA have bare apices with no leaf emergence and increased rhizoid production. Scalebars: 100 nm.

Discussion

Antagonistic control of leaf development

High concentrations of exogenous auxin can inhibit leaf outgrowth, and the dose of auxin at which leaf outgrowth is robustly inhibited has previously been used as a gauge of auxin sensitivity[21]. We found that leaf outgrowth in *chk1;2;3* mutants was hypersensitive to auxin. A moderate concentration of NAA (500 nM) suppressed leaf outgrowth in *chk* mutant shoots but not wild type shoots. Inversely, supplementing plants with a high concentration of cytokinin rescued auxin-mediated leaf outgrowth inhibition. Therefore, auxin and cytokinin act antagonistically to regulate leaf development.

We propose two, non-exclusive mechanisms to explain the antagonistic regulation of leaf outgrowth. Both explanations are consistent with the ratio of auxin to cytokinin signaling being critical for directing leaf development. First, auxin and cytokinin might independently regulate the potential of the leaf initial cell to divide. After the asymmetric division that forms it, the leaf initial undergoes repeated, self-renewing cell divisions that produce cells for early leaf development[23]. In *chk* mutants, leaves are composed of fewer files of longer cells, indicating a reduced capacity to divide (Figure 1)[31]. Similar phenotypes have been shown for plants treated with auxin[16,19,21]. Thus, the inhibition of leaves on *chk* shoots grown on auxin could represent the cumulation of two independent effects reducing cell division competency. Likewise, rescued leaf outgrowth observed by the combination of 250 nM BAP with 2.5 µM NAA would result from cytokinin promoting division of the leaf initial for long enough to generate a few files of leaf cells before division terminates. In support of this idea, not all shoots on 250 nM BAP and 2.5 µM NAA escape leaf suppression, and some that do still form small leaves with as few as two cell files (Supplemental Figure 1).

A second possibility is that cytokinin might alter auxin signaling and response at the cellular level, and vice versa. A similar interaction between cytokinin and auxin regulates the size of the root meristem, where cytokinin induces the expression of *AUX/IAA* genes, which encode transcriptional repressors of auxin signaling[4]. In moss filaments, cytokinin similarly promotes *AUX/IAA* expression[32]. However, the transcriptional response of moss shoots to cytokinin has yet to be assessed. Our data demonstrating the

antagonistic effects of auxin and cytokinin on leaf outgrowth and development is consistent with cytokinin reducing the sensitivity of a cells to auxin. In this scenario, *chk* mutant cells would be hypersensitive to auxin, explaining the high-auxin phenotype when grown on minimal media and the full repression of leaf outgrowth at 500 nM NAA. Exogenous BAP would then be expected to reduce sensitivity of cells to auxin, explaining the re-emergence of leaves on shoots grown on both high cytokinin and high auxin.

Auxin modulates stem cell formation in a cytokinin-dependent manner

Auxin and cytokinin antagonistically regulate branch formation in moss. However, it was previously unknown whether auxin is necessary for repressing the initiation and/or outgrowth of axillary meristems. Growth of moss on the auxin synthesis inhibitor L-Kyn resulted in shoots with ectopic branches and meristems even at early developmental stages, demonstrating the importance of auxin during inhibition of axillary SAM initiation and outgrowth.

Meanwhile, although cytokinin promotes axillary branch formation, *chk1;2;3* mutants that are devoid of cytokinin perception counter-intuitively form more branches. We have previously shown that a network where cytokinin promotes stem cell formation via one pathway but inhibits it via another can explain stem cell specification rates in wild type and stem cell specification mutants moss grown on a range of cytokinin concentrations[20]. However, the role of auxin in this proposed pathway is unclear. Reducing auxin synthesis with L-Kyn led to the formation of ectopic stem cells, swollen stems, and broad leaves, phenocopying plants treated with cytokinin. These data suggest that auxin and cytokinin interact antagonistically to regulate axillary meristem specification in moss. Because reduced auxin signaling and exogenous cytokinin elicit similar effects, it appears that the ratio and not the absolute amount of signaling through each pathway is important.

Because *chk1;2;3* mutants make long, narrow leaves in addition to ectopic branching, we proposed that altered auxin signaling due to reduced auxin flux from leaves to stems may account for some of the *chk1;2;3* phenotypes. Our findings that PIN transporters were more often acropetally oriented in *chk1;2;3* mutants supported this idea. However, very high concentrations of auxin were unable to suppress ectopic branch

formation in *chk1;2;3* mutants, suggesting that redistributed auxin alone does not explain ectopic branch formation in *chk1;2;3*. We interpret these findings altogether to suggest that auxin inhibits cytokinin-mediated branch initiation, and that a different, auxin-independent mechanism is at play during ectopic stem cell production in *chk1;2;3*.

chk mutants resemble plants with loss of polycomb group function

We found a novel phenotype where *chk1;2;3* rhizoids produce a high number of buds, such that buds are formed from almost every rhizoid cell. This phenotype has not been described for any other mutant or treatment perturbing cytokinin or auxin synthesis, transport, or signaling, suggesting that, like ectopic branch formation in *chk*, ectopic bud formation results from the disruption of a distinct mechanism.

Interestingly, several lines of evidence link cytokinin signaling to the function of POLYCOMB REPRESSIVE COMPLEX 2 (PRC2) in moss. PRC2 functions in the stabilizing of cell identity by adding and maintaining the repressive H3K27me3 chromatin modification[26]. The expression domains of *CYTOKININ OXIDASE* (*CKX*) genes, which are strong markers of cytokinin signaling[27], tightly overlaps at the bud and shoot apical meristem with the expression of *FERTILIZATION-INDEPENDENT ENDOSPERM* (*FIE*)[28], an essential PRC2 component. *fie* knockout mutants make supernumerary buds, and once initiated, these nascent shoots reiteratively produce more and more stem cells. Intriguingly, complementing the *fie* mutant with the Arabidopsis *FIE* partly rescues this severe *fie* phenotype, resulting in shoots with short internodes, narrow leaves, and ectopic branches. These partly rescued shoots that strikingly resemble *chk1;2;3*, suggesting that aspects of the *chk1;2;3* phenotype could result from the inability to maintain cell identity.

Likewise, the moss *CURLY LEAF* gene that encodes another PRC2 component, is also co-expressed with *CKX* and *FIE* at apical and axillary meristems. Moss *clf* mutants initiate ectopic three-dimensional shoots from filaments to the same degree as *chk1;2;3* rhizoids. Although these ectopic *clf* shoots form juvenile sporophyte-like bodies rather than normal gametophytic moss shoots, Okano et al. elegantly used heat shock induction of CLF to rescue the *clf* phenotype at different points in development[29]. In doing so, the authors demonstrated that CLF is both necessary to prevent the conversion of gametophytic shoots into indeterminate sporophytic ones,

and to prevent the formation of any shoots in place of filament initials at side branches[29]. Finally, moss knockouts of the *LIKE HETEROCHROMATIN PROTEIN1*/*TERMINAL FLOWER2* (*LHP1/TFL2*), components of the PRC1 complex that supports transcriptional repression established by PRC2, also have increased branching, reduced caulonema, and increased bud formation[30]. Overall, based on these expression patterns and mutant phenotypes, we speculate that *chk* mutants are partially impaired in polycomb complex function.

Final overview

We examined the contributions of auxin, cytokinin, and their interaction to moss shoot development. In general, auxin and cytokinin antagonistically regulate leaf cell proliferation, shoot length, and branch formation. Reducing auxin synthesis phenocopies cytokinin treatment, while cytokinin receptor mutants partly phenocopy auxin treatment. Thus, the ratio of auxin to cytokinin signaling is critical for directing shoot development. However, high concentrations of auxin were not sufficient to inhibit ectopic meristem initiation in *chk* mutants, which are defective in cytokinin signaling. These data suggest that auxin modulates stem cell formation in a cytokinin-dependent manner and supports our previous hypothesis that cytokinin is upstream of a separate pathway regulating SAM initiation. Overall, we provide a foundation for the study of the interaction of auxin and cytokinin in moss shoots.

References

1. Skoog, F., Miller, C.O., and Folke K. Skoog and Carlos O. Miller (1957). Chemical regulation of growth and organ formation in plant tissue cultured in vitro. Symp Soc exp Biol.
2. Wybouw, B., and De Rybel, B. (2019). Cytokinin – A Developing Story. Trends Plant Sci. *24*, 177–185.
3. Leyser, O. (2018). Auxin signaling. Plant Physiol. *176*, 465–479.
4. Dello Ioio, R., Nakamura, K., Moubayidin, L., Perilli, S., Taniguchi, M., Morita, M.T., Aoyama, T., Costantino, P., and Sabatini, S. (2008). A genetic framework for the control of cell division and differentiation in the root meristem. Science *322*, 1380–1384.
5. Jing, H., and Strader, L.C. (2019). Interplay of auxin and cytokinin in lateral root development. Int. J. Mol. Sci. *20*, 486.
6. Zhao, Z., Andersen, S.U., Ljung, K., Dolezal, K., Miotk, A., Schultheiss, S.J., and Lohmann, J.U. (2010). Hormonal control of the shoot stem-cell niche. Nature *465*, 1089–1092.
7. Laplaze, L., Benkova, E., Casimiro, I., Maes, L., Vanneste, S., Swarup, R., Weijers, D., Calvo, V.,

Parizot, B., Herrera-Rodriguez, M.B., et al. (2007). Cytokinins act directly on lateral root founder cells to inhibit root initiation. Plant Cell *19*, 3889–3900.

8. Bishopp, A., Help, H., El-Showk, S., Weijers, D., Scheres, B., Friml, J., Benková, E., Mähönen, A.P., and Helariutta, Y. (2011). A mutually inhibitory interaction between auxin and cytokinin specifies vascular pattern in roots. Curr. Biol. *21*, 917–26.

9. Marhavý, P., Bielach, A., Abas, L., Abuzeineh, A., Duclercq, J., Tanaka, H., Pařezová, M., Petrášek, J., Friml, J., Kleine-Vehn, J., et al. (2011). Cytokinin Modulates Endocytic Trafficking of PIN1 Auxin Efflux Carrier to Control Plant Organogenesis. Dev. Cell *21*, 796–804.

10. Nordström, A., Tarkowski, P., Tarkowska, D., Norbaek, R., Åstot, C., Dolezal, K., and Sandberg, G. (2004). Auxin regulation of cytokinin biosynthesis in Arabidopsis thaliana: A factor of potential importance for auxin-cytokinin-regulated development. Proc. Natl. Acad. Sci. U. S. A. *101*, 8039–8044.

11. De Rybel, B., Adibi, M., Breda, A.S., Wendrich, J.R., Smit, M.E., Novak, O., Yamaguchi, N., Yoshida, S., Van Isterdael, G., Palovaara, J., et al. (2014). Integration of growth and patterning during vascular tissue formation in Arabidopsis. Science (80-.). *345*, 1255215–1255215.

12. Rensing, S.A., Goffinet, B., Meyberg, R., Wu, S.Z., and Bezanilla, M. (2020). The moss physcomitrium (Physcomitrella) patens: A model organism for non-seed plants. Plant Cell *32*, 1361–1376.

13. Frank, M.H., and Scanlon, M.J. (2014). Transcriptomic Evidence for the Evolution of Shoot Meristem Function in Sporophyte-Dominant Land Plants through Concerted Selection of Ancestral Gametophytic and Sporophytic Genetic Programs. Mol. Biol. Evol. *32*, 355–367.

14. Menand, B., Yi, K., Jouannic, S., Hoffmann, L., Ryan, E., Linstead, P., Schaefer, D.G., and Dolan, L. (2013). An Ancient Mechanism Controlls the Development of Cells with a Rooting Function in Land Plants. Science (80-.). *339*, 1335–1338.

15. Rensing, S.A., Lang, D., Zimmer, A.D., Terry, A., Salamov, A., Shapiro, H., Nishiyama, T., Perroud, P.F., Lindquist, E.A., Kamisugi, Y., et al. (2008). The Physcomitrella genome reveals evolutionary insights into the conquest of land by plants. Science (80-.).

16. Ashton, N.W., Grimsley, N., and Cove, D.J. (1979). Analysis of gametopytic development in the moss, Physcomitrella patens, using auxin and cytokinn resistants mutants. Planta *144*, 427–435.

17. Aoyama, T., Hiwatashi, Y., Shigyo, M., Kofuji, R., Kubo, M., Ito, M., and Hasebe, M. (2012). AP2-type transcription factors determine stem cell identity in the moss Physcomitrella patens. Development *139*, 3120–3129.

18. Coudert, Y., Palubicki, W., Ljung, K., Novak, O., Leyser, O., and Harrison, C.J. (2015). Three ancient hormonal cues co-ordinate shoot branching in a moss. Elife, 1–26.

19. Barker, E.I. (2011). A examination of leaf morphogenesis in the moss, *Physcomitrella patens*. PhD thesis, Univ. Regina.

20. Cammarata, J., Morales Farfan, C., Scanlon, M.J., and Roeder, A.H.K. (2020). Cytokinin-CLAVATA

crosstalk regulates the function of a single-celled shoot apical meristem. prep.

21. Bennett, T.A., Liu, M.M., Aoyama, T., Bierfreund, N.M., Braun, M., Coudert, Y., Dennis, R.J., O'Connor, D., Wang, X.Y., White, C.D., et al. (2014). Plasma Membrane-Targeted PIN Proteins Drive Shoot Development in a Moss. Curr. Biol. *24*, 2776–2785.

22. Barker, E.I., and Ashton, N.W. (2013). Heteroblasty in the moss, *Aphanoregma patens* (*Physcomitrella patens*), results from progressive modulation of a single fundamental leaf developmental programme. J. Bryol. *35*, 185–196.

23. Harrison, C.J., Roeder, A.H.K., Meyerowitz, E.M., and Langdale, J. a. (2009). Local Cues and Asymmetric Cell Divisions Underpin Body Plan Transitions in the Moss Physcomitrella patens. Curr. Biol. *19*, 461–471.

24. von Schwartzenberg, K., Lindner, A.-C., Gruhn, N., Šimura, J., Novák, O., Strnad, M., Gonneau, M., Nogué, F., and Heyl, A. (2015). CHASE domain-containing receptors play an essential role in the cytokinin response of the moss Physcomitrella patens. J. Exp. Bot., erv479.

25. Viaene, T., Landberg, K., Thelander, M., Medvecka, E., Pederson, E., Feraru, E., Cooper, E.D.D., Karimi, M., Delwiche, C.F.F., Ljung, K., et al. (2014). Directional Auxin Transport Mechanisms in Early Diverging Land Plants. Curr. Biol. *24*, 2786–2791.

26. Pengelly, A.R., Copur, Ö., Jäckle, H., Herzig, A., and Müller, J. (2013). A histone mutant reproduces the phenotype caused by loss of histone-modifying factor polycomb. Science (80-.).

27. Nishiyama, T., Fujita, T., Shin-i, T., Seki, M., Nishide, H., Uchiyama, I., Kamiya, A., Carninci, P., Hayashizaki, Y., Shinozaki, K., et al. (2003). Comparative genomics of Physcomitrella patens gametophytic transcriptome and Arabidopsis thaliana : Implication for land plant evolution. PNAS *100*, 8007–8012.

28. Mosquna, A., Katz, A., Decker, E.L., Rensing, S.A., Reski, R., and Ohad, N. (2009). Regulation of stem cell maintenance by the Polycomb protein FIE has been conserved during land plant evolution. Development *2444*, 2433–2444.

29. Okano, Y., Aono, N., Hiwatashi, Y., Murata, T., Nishiyama, T., Ishikawa, T., Kubo, M., and Hasebe, M. (2009). A Polycomb Repressive Complex 2 gene regulates apogamy and gives evolutionary insights into early land plant evolution A polycomb repressive complex 2 gene regulates apogamy and gives evolutionary insights into early land plant evolution. PNAS.

30. Parihar, V., Arya, D., Walia, A., Tyagi, V., Dangwal, M., Verma, V., Khurana, R., Boora, N., Kapoor, S., and Kapoor, M. (2019). Functional characterization of LIKE HETEROCHROMATIN PROTEIN 1 in the moss Physcomitrella patens: its conserved protein interactions in land plants. Plant J.

31. Schwartzenberg, K. Von, Lindner, A., Gruhn, N., and Šimura, J. (2016). CHASE domain-containing receptors play an essential role in the cytokinin response of the moss Physcomitrella patens. *67*, 667–679.

32. Prigge, M.J., Lavy, M., Ashton, N.W., and Estelle, M. (2010). Physcomitrella patens auxin-resistant mutants affect conserved elements of an auxin-signaling pathway. Curr. Biol. *20*, 1907–1912.

Supplemental Figures

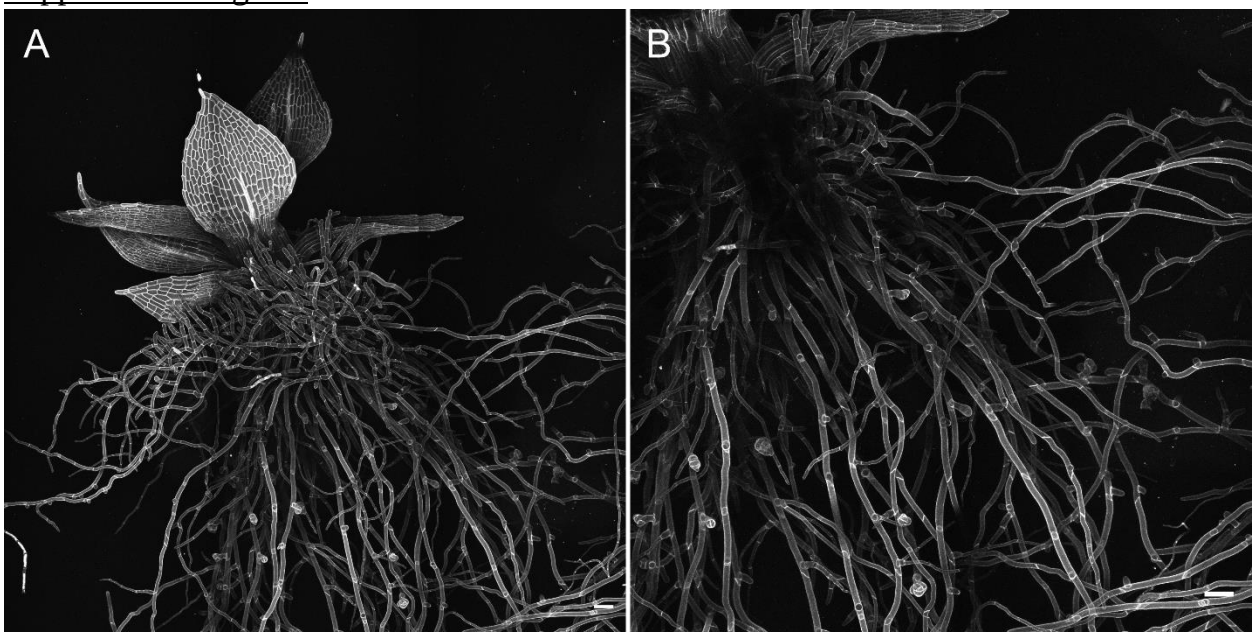

Supplemental Figure 1: Treatment with 25 nM BAP causes leaf widening and ectopic bud formation on rhizoids. A) Z-projection of a shoot grown on 25 nM BAP. B) projection of a smaller area and fewer Z-slices of the image in panel A to better show rhizoids and ectopic buds. Scale bars: 100 nm

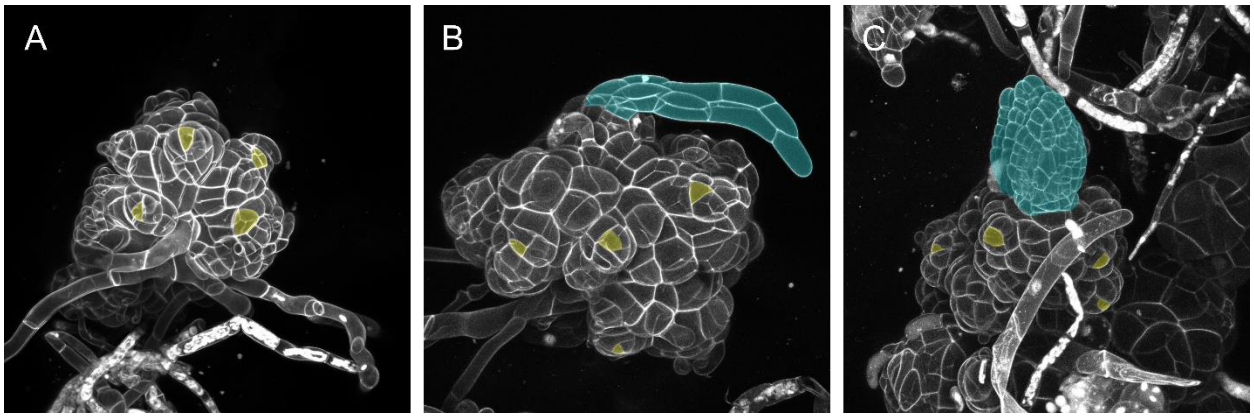

Supplemental Figure 2: High concentrations of cytokinin variably rescue leaf-suppression caused by high concentrations of auxin. Each image depicts shoots grown on 250 nM BAP and 2.5 µM NAA. Suppression of leaves can be complete (A), partial (B), or abrogated (C). Leaves pseudo colored blue and visible apical stem cells pseudo colored yellow.

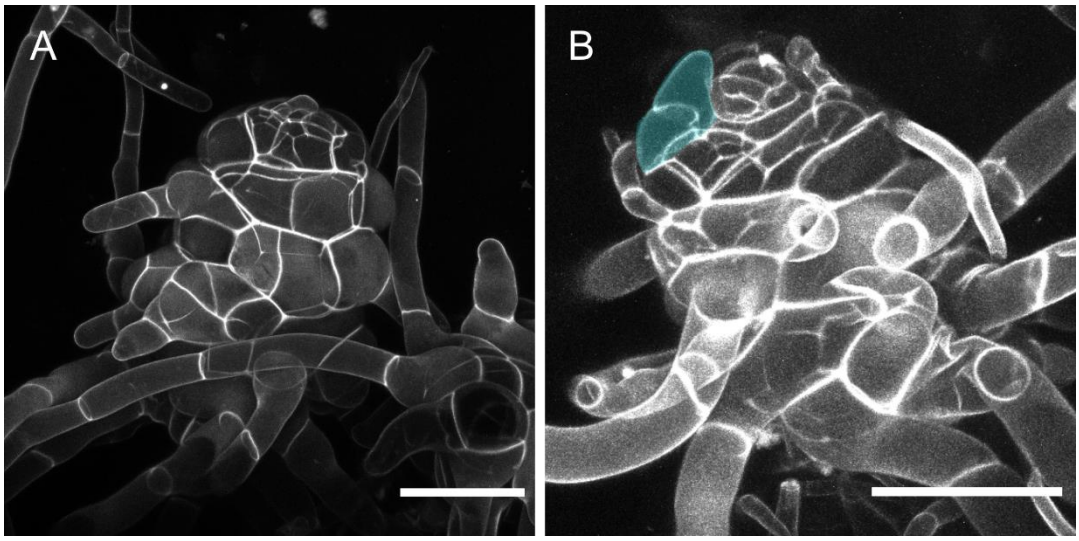

Supplemental Figure 3: *chk1;2;3* mutants are hypersensitive to exogenous NAA. Two shoots grown on 500 nM NAA, a concentration insufficient to inhibit shoot elongation or leaf emergence in wild type. Leaf formation is completely inhibited in *chk1;2;3* shoots grown on 500 nM NAA (A). Sometimes, small projections resembling one or two leaf cells can be seen (B).

Materials and methods

Moss culture and hormone treatment

Routine moss culture was conducted on minimal media supplemented with ammonium tartrate (BCDAT, see Media section) and overlain with cellophane. To propagate moss, tissue was blended in 5-7 ml sterile Water using a Dremel with a custom-made propeller blade attachment. 1-2 ml of blended moss was pipetted to inoculate fresh plates. All experiments and lines were of the Gransden strain of *Physcomitrium patens* (previously *Physcomitrella patens*)[1]. For phenotyping, small tufts of moss filaments growing on BCDAT were placed on agar BCD plates and grown for three to five weeks. All moss was grown under continuous light at 25 degrees Celsius

Confocal Microscopy

Moss shoots for imaging were dissected from three-to-five week old colonies grown on minimal media (BCD). Colonies were flooded with water prior to dissection and tapped vigorously to liberate air bubbles. Dissected shoots were placed on a slide with a well made of vacuum grease and filled with 5 µg/ml propidium iodide (PI). Slides were then sealed with a coverslip and incubated for at least fifteen minutes before imaging. All confocal imaging was conducted using a Zeiss LSM-710 laser scanning microscope. PI-stained tissues were imaged using a 514 nm laser for excitation. Emission wavelengths between 566 and 650 nm were collected. For PIN immunolocalization, slides were imaged using a 488 nm laser for excitation, and emission wavelengths from 493 to 630 nm were collected.

Immunofluorescence

The whole-mount immunofluorescence followed the protocol in Pasternak et al. that used methanol fixation[2]. We made slight modifications to this protocol: namely the placement of tissue under vacuum while shaking for the fixation steps. Subsequent washes and steps, with the exception of the antibody incubation, were performed while shaking at 37 degrees Celsius. Tissue was mounted in Fluoromount G and cover slips were sealed around the edges with clear nail polish. Secondary antibodies were conjugated to Alexa Fluor 488.

Analysis of PIN polarity

Diffuse crescents or crescents without clearly discernable polarity were excluded from the analysis. To determine the angle relative to the leaf, using the FIJI image processing software[3] we drew a line from the base to the tip of the leaf. We then drew lines from the approximate center of each cell to that cell's polarity crescent. We exported a csv file for each leaf that contained the angle of each line (leaf and crescent) relative to default coordinates of the image (vertical lines in FIJI have an angle of 90 degrees). Using a custom R-script, we read each csv and determined whether each polarity crescent was apically or basally oriented by taking the absolute value of the difference between the angle of the polarity crescent and the angle of the leaf reference line. If the absolute value was greater than 90 degrees, we assigned the tip to the basally oriented class; if less than 90 degrees we assigned the apical class. Radial histograms were generated using the ggplot2 package[4]. For statistical analysis, generated a contingency table and then conducted a Fisher's exact test on the data in the table.

Media

BCDAT

- 250mg/L $MgSO_4.7H_2O$
- 250mg/L KH_2PO_4 (pH6.5)
- 1010mg/L KNO_3, 12.5mg/L
- $FeSO_4.7H_2O$
- 0.001% Trace Element Solution*
- 0.92 g/L $C_4H_{12}N_2O_6$ (ammonium tartrate)
- 8g/L agar
- $CaCl_2$ added to a 1mM concentration after autoclaving.

Minimal Media (BCD) is BCDAT without the ammonium tartrate

*Trace Element Solution

- 0.614mg/L H_3BO_3
- 0.055mg/L $AlK(SO_4)2.12H_2O$
- 0.055mg/L $CuSO_4.5H_2O$
- 0.028mg/L KBr
- 0.028mg/L LiCl
- 0.389mg/L $MnCl_2.4H_2O$

- 0.055mg/L $CoCl_2.6H_2O$
- 0.055mg/L $ZnSO_4.7H_2O$
- 0.028mg/L KI
- 0.028mg/L $SnCl_2.2H_2O$

References for Materials and Methods

1. Ashton, N.W., and Cove, D.J. (1977). The isolation and preliminary characterisation of auxotrophic and analogue resistant mutants of the moss, Physcomitrella patens. MGG Mol. Gen. Genet.

2. Pasternak, T., Tietz, O., Rapp, K., Begheldo, M., Nitschke, R., Ruperti, B., and Palme, K. (2015). Protocol: An improved and universal procedure for whole-mount immunolocalization in plants. Plant Methods *11*, 50.

3. Schindelin, J., Arganda-Carreras, I., Frise, E., Kaynig, V., Longair, M., Pietzsch, T., Preibisch, S., Rueden, C., Saalfeld, S., Schmid, B., et al. (2012). Fiji: An open-source platform for biological-image analysis. Nat. Methods.

4. Hadley, W., Winston, C., Lionel, H., Thomas, Lin, P., Kohske, T., Claus, W., Kara, W., Hiroaki, Y., and Dewey, D. (2016). ggplot2 - Elegant Graphics for Data Analysis (Springer-Verlag New York).

Chapter 5: A functionally informed evolutionary framework for the study of LRR-RLKs during stem cell maintenance

Foreword

In my first year as a graduate student, I learned how to construct phylogenetic trees from Kevin Nixon in a core lab class. I was immediately hooked. I loved learning to handle large amounts of data, how to run various scripts and processes, and most of all how to glean evolutionary insights from trees. It has always felt like, upon learning something from a tree I constructed, I discovered a secret piece of information that only I knew and had to share with the world.

I am however no expert in these methodologies. In this chapter is my attempt to leverage my enthusiasm about the evolution of gene families to gain meaningful insights about stem cell regulation. The work here was published in a special issue of Journal of Plant Research in April 2020.

Adapted by permission from the Licensor: Springer Nature, Journal of Plant Research, Cammarata, J., Scanlon, M.J. A functionally informed evolutionary framework for the study of LRR-RLKs during stem cell maintenance. *J Plant Res* **133,** 331–342 (2020). https://doi.org/10.1007/s10265-020-01197-w

A Functionally Informed Evolutionary Framework for the Study of LRR-RLKs during Stem Cell Maintenance

Joseph Cammarata[1,2], Michael J. Scanlon*[1]

1. School of Integrative Plant Sciences, Plant Biology Section, Cornell University
2. Weill Institute for Cell and Molecular Biology, Cornell University

Introduction

New plant tissues develop from reserves of stem cells called meristems that are found at the tips of roots and shoots and at the sites of vasculature formation. Maintenance of stable stem cell populations poses a challenge during development: if the stem cell population grows too large then development becomes disorganized, whereas under-proliferation of the stem cell pool can lead to meristem consumption and the termination of development. Signaling pathways dedicated to meristem maintenance are thus critical for maintaining indeterminate growth, a hallmark of plant development and a strategic source of morphological diversity.

Decades of research have revealed widespread functions for a suite of LEUCINE-RICH RECEPTOR-LIKE KINASES (LRR-RLK), RECEPTOR-LIKE PROTEINS (LRR-RLP), and pseudokinases in the regulation of plant meristem maintenance. These include the LRR-RLKs CLAVATA1 (CLV1) (Clark et al. 1997), PHLOEM INTERCALATED WITH XYLEM (PXY) (Fisher and Turner 2007), and RECEPTOR-LIKE PROTEIN KINASE 2/TOADSTOOL 2 (RPK2)(Kinoshita et al. 2010), the LRR-RLPs CLAVATA2 (CLV2) (Kayes and Clark 1998) and FASCIATED EAR 3 (FEA3) (Wu et al. 2016), the pseudokinase CORYNE (CRN) (Miwa et al. 2008), and the CLAVATA INSENSITIVE KINASE (CIK) co-receptors (Hu et al. 2018). Each of these cell-surface proteins are thought to act in signal perception and transduction that is elicited by mobile CLAVATA3/EMBRYO SURROUNDING REGION (CLE) peptide ligands.

LRR RLKs and related proteins have been studied predominately in the model plant *Arabidopsis thaliana*. While much progress has been made, we are still far from understanding the downstream signaling pathways

or how these signaling components are employed in different developmental contexts. More recently, research on crop and bryophyte species has revealed that many of these signaling components have conserved functions, and that these pathways can be altered for agronomic benefit (Bommert et al. 2013; Je et al., 2016; Rodríguez-Leal et al. 2017; Whitewoods et al. 2018). These results demonstrate the insights gleaned from and the benefits of studying stem cell maintenance in diverse model species.

This work promotes a strategy of using a framework of combined phylogenetic and functional data to facilitate future analyses of meristem regulatory LRR RLKs from diverse species. We assess how stem cell regulating LRR-RLKs and related proteins have evolved across several plant model organisms, namely Arabidopsis, Tomato, Maize, Rice, the moss *Physcomitrella patens*, and the liverwort *Marchantia polymorpha*. We extend our analysis to include the lycophyte *Selaginella moellendorfii* and the moss *Sphagnum fallax* in order to shed light on gene duplications associated with the evolution of vasculature, and to gain a broader understanding of bryophyte stem cell signaling. We also propose a cogent, functionally and phylogenetically based nomenclature for heretofore unannotated orthologs of these meristem signaling components (supplemental table 1). Finally, we use our phylogenetic analysis to highlight trends and propose testable hypotheses about the evolution of stem cell signaling in land plants.

Materials and Methods:

Starting with *Arabidopsis thaliana* gene of interest (i.e. CLV1), except in the case of FEA3 where the maize ortholog was used, we performed pBLAST in Phytozome 11 against: *Arabidopsis thaliana* TAIR10, *Solanum lycopersicum* iTAG2.4, *Zea mays* Ensembl-18, *Oryza sativa* v7_JGI, *Selaginella moellendorfii* v1.0, *Physcomitrella Patens* v3.3, *Marchantia polymorpha* v3.1, and *Sphagnum fallax* v 0.5 proteomes. Peptide sequences for the top 250 blast hits were selected and then filtered so that only peptides encoded by primary transcripts remained.

We used the CIPRES portal to run mafft set to the slowest but most accurate mode (linsi) (Katoh 2005). We then trimmed multiple sequence alignments of positions high in gaps using trimal (Capella-Gutiérrez et al. 2009), removing any position comprised of over 50% gaps. Using these trimmed multiple sequence

alignments, we then constructed phylogenetic trees using RaXML (Stamatakis 2014) set to the PROTCATDAYHOFF model with 1,000 rapid bootstrap via the CIPRES server (Miller et al. 2010). We viewed trees with the highest likelihood score with bootstrap values represented on bipartitions using MEGAX. From these larger trees, we found the most basal bipartition with a support value over 90% that contained our gene family of interest and selected that subtree for representation here.

Trees were visualized and annotated in MEGAX or using ete3 (Huerta-Cepas et al. 2016). Alignments juxtaposed to trees were alignments only of the sequences referenced on that tree (not the whole set of 200) aligned using Muscle (Edgar 2004) visualized in Aliview.

Results

CLV1 and BAM: dynamic gene gain and loss

CLV1 encodes an LRR/RLK that regulates stem cell identity in the SAM by acting in a negative feedback loop wherein the homeobox transcription factor WUSCHEL (WUS), expressed in the middle of the shoot apical meristem (SAM), diffuses to overlying cells to activate the expression of the CLE peptide-encoding gene *CLAVATA3 (CLV3)* (Schoof et al. 2000). CLV3 is secreted and diffuses back down to the middle of the meristem, where it acts through the CLV1 receptor to repress *WUS* expression, completing the negative feedback loop. Angiosperm genomes contain a suite of paralogs of *CLV1* called *BARELY ANY MERISTEM* (*BAM*). Our analysis of the *CLV1/BAM* clade of *LRR-RLK* genes suggests that Arabidopsis *BAM1* and *BAM2* were generated following a recent gene duplication (Figure 1). We also detected a clade of *BAM* genes absent from the Arabidopsis genome that includes the recently characterized tomato gene *SlBAM4* (Rodriguez-Leal et al. 2019). Meanwhile, maize lacks a member of the *BAM3* clade, but contains two copies of *BAM4*. Overall, there is evidence for frequent gain and loss of *BAM* genes, while *CLV1* was maintained as a single copy in each angiosperm sampled.

Our analysis also shows that *CLV1* and *BAM* genes diverged after the separation of the lycophyte and flowering plant lineages (Figure 1). Thus, lycophyte and bryophyte genes presented here are co-orthologous

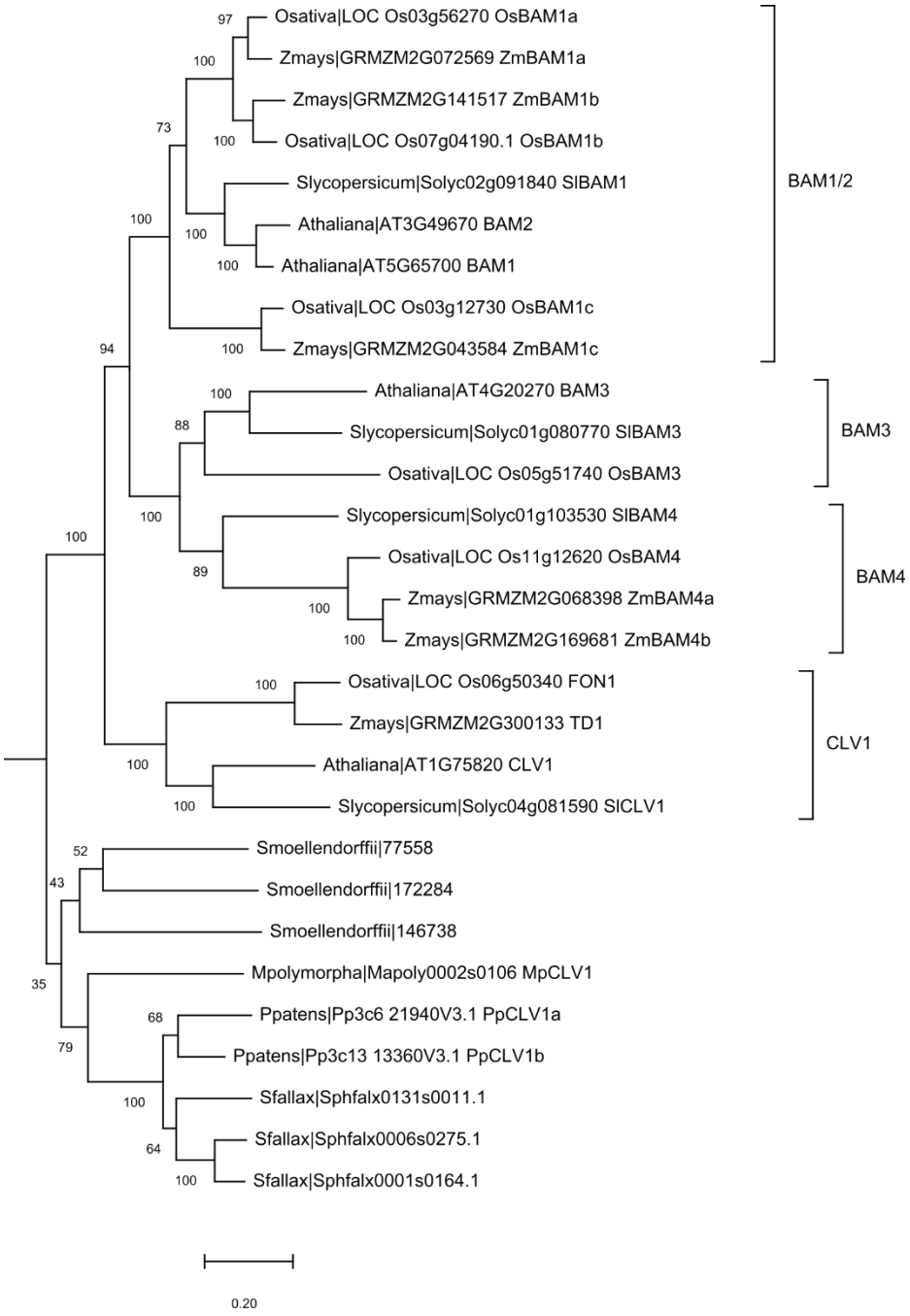

Figure 1. Maximum Likelihood tree of CLV1/BAM LRR-RLKs based on full length peptide sequences. Subtree shown here is taken from a larger maximum likelihood tree; bootstrap support at the base of this tree was 100%. *CLAVATA1* and *BAM* genes are paralogs that evolved after the split between lycophytes and angiosperms, while Selaginella and bryophyte orthologs underwent lineage-specific duplications.

to the *CLV1* and *BAM* clades. Recent work demonstrated a conserved role for the moss genes *PpCLV1a* and *PpCLV1b* in inhibiting meristem identity and uncovered a previously undescribed function in the regulation

of cell division plane orientation (Whitewoods et al. 2018). Intriguingly, a role for CLV1/BAM in the control of cell division plane orientation was also found to be conserved in Arabidopsis, wherein *clv1, bam1, bam2, bam3* quadruple mutations resulted in cell division plane defects in the root (Whitewoods et al. 2018). It is likely that historical challenges in generating higher order mutants had obscured the role of CLV1/BAM during cell division plane orientation in Arabidopsis. Moreover, these reverse genetic challenges had previously rendered cross-species comparisons of 'loss of clade' rather than 'loss of gene' function untenable. However, with the advent of facile genome editing technologies and a wealth of genomic information, we can, informed by phylogenies, test and gain a general understanding of gene family function.

Many developmental functions for *BAM1* and *BAM2* have been demonstrated, including CLE perception and regulation of cell fate and periclinal divisions in root vasculature and in anther development, and buffering of CLE signaling in the SAM (Hord et al. 2006; DeYoung and Clark 2008; Shimizu et al. 2015a; Cui et al. 2018; Qian et al. 2018). Despite these distinct roles for *CLV1* and *BAM1/BAM2*, *BAM1* also compensates for *clv1* loss of function in shoot meristems (Nimchuk et al. 2015). These data suggest that BAM1/BAM2 can perform the same biochemical function as CLV1, and that differences in mutant phenotypes between these related LRR-RLKs are due to differences in gene expression.

PXY: an ancient LRR-RLK recruited to vascular development

Within the broader LRR-RLK phylogeny, the clade containing *PHLOEM INTERCELATED WITH XYLEM* (*PXY*) is sister to the *CLV1* and *BAM* clade of receptor kinases (Liu et al. 2017). Like *CLV1*, *PXY* encodes a CLE receptor and regulates the activity of a *WUSCHEL-like HOMEOBOX* (*WOX)* gene, here *WOX4* in the stem cell niche comprising the vascular procambium (Hirakawa et al. 2010; Etchells et al. 2013). The PXY ligand is TDIF/CLE41, a different class of CLE from CLV3 (Goad et al. 2017). Whereas *PXY* is conserved across flowering plants and Selaginella, the moss genomes sampled here lack both *PXY* (Figure 2) and TDIF orthologs (Whitewoods et al. 2018). However, the genome of the liverwort *Marchantia polymorpha* harbors a *PXY* ortholog, as well as TDIF peptide encoding gene, which together reduce cell proliferation near the apical

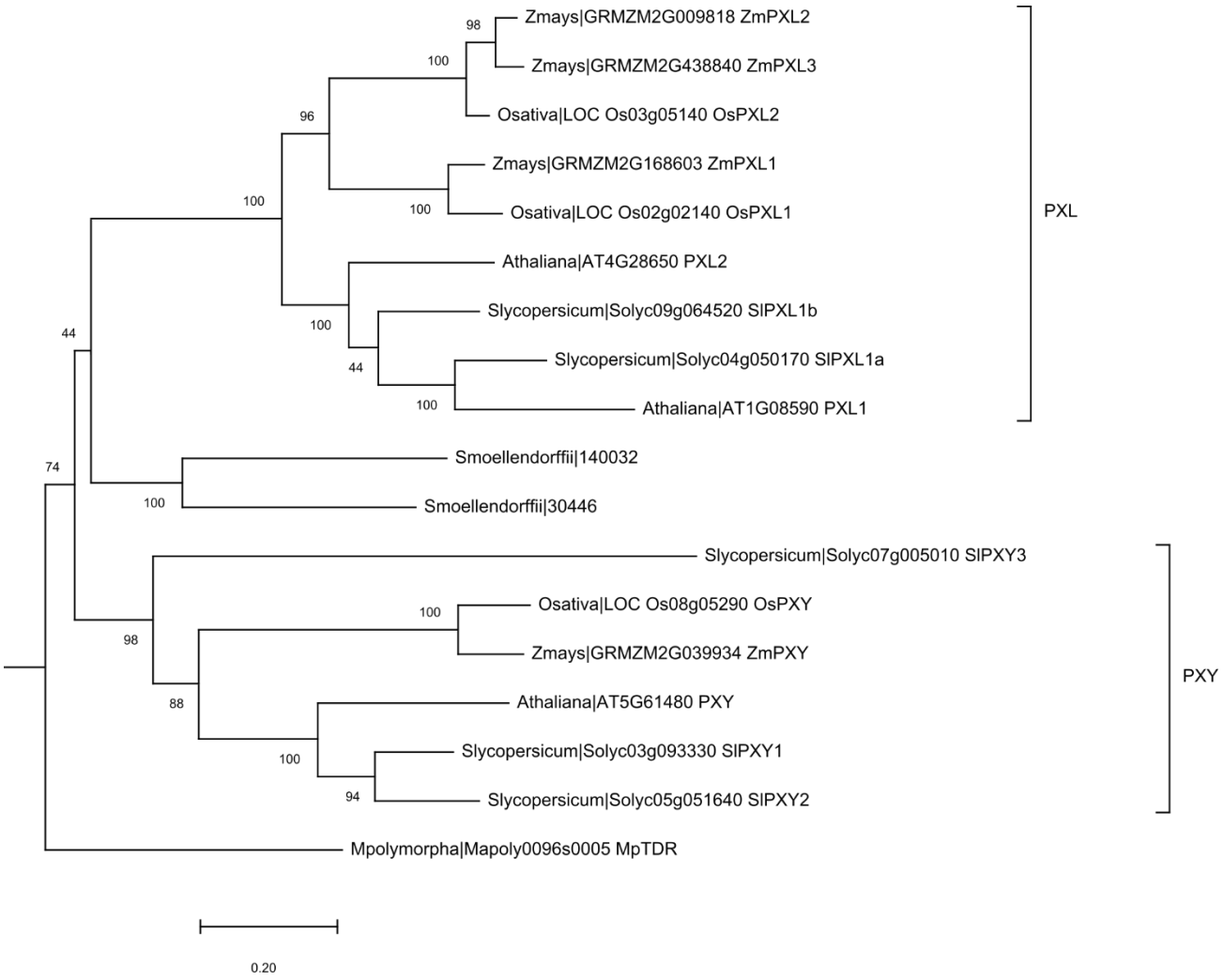

Figure 2. Maximum Likelihood tree of PXY LRR-RLKs based on full length peptide sequences. Subtree shown here is taken from a larger maximum likelihood tree that also included the CLV1/BAM clade; bootstrap support at the base of this subtree was 100%. PXY is typically associated with vascular development, but the non-vascular liverwort Marchantia polymorpha possesses one PXY ortholog.

notch of the thallus (Hirakawa et al. 2019). This topology and the functional characterization of TDIF signaling in Marchantia suggests that PXY function predates the evolution of vasculature, and that a function during vascular formation was co-opted later in land plant evolution.

CLAVATA2 and CORYNE: pieces of a whole

Conclusive evidence for protein-protein interactions among LRR-RLKs is scarce, owing to the inherent difficulties in studying low-abundance membrane-associated proteins. However, data supporting the

formation of a CLV2:CRN complex is compelling (Bleckmann et al. 2010; Guo et al. 2011; Somssich et al. 2015). CLV2 possesses an LRR-ectodomain while CRN possesses a cytoplasmic domain but no ectodomain; it is attractive to think that together these two proteins constitute a complete LRR-RLK. However, the CRN cytoplasmic domain possesses a pseudokinase that is important for its function, although the mechanism is unclear. Like other LRR-RLK complexes that maintain stem cell populations in the SAM, *CLV2* and *CRN* have roles in diverse developmental processes including phloem development (Hazak et al. 2017). The function of *CLV2* and *CRN* appear to be conserved in grasses, as mutants of the maize *CLV2* ortholog *FASCIATED EAR 2* (*FEA2*) also develop enlarged and fasciated inflorescence meristems (Taguchi-Shiobara et al. 2001). In both models, the effects of *clv1* and *clv2/crn* loss of function are additive, suggesting that CLV1 and CV2/CRN comprise distinct CLE signaling pathways (Müller et al. 2008).

In our phylogenetic analysis, we find that *CLV2* exists as a single-copy gene in the four angiosperm genomes sampled, and we did not detect *CLV2* orthologs in *Selaginella moellendorffii* or bryophytes (Supplemental Figure 1). Further analysis, however, is limited by very low support values for relationships along the backbone of the phylogenetic tree, hindering our ability to draw further conclusions about the evolution of *CLV2* within land plants.

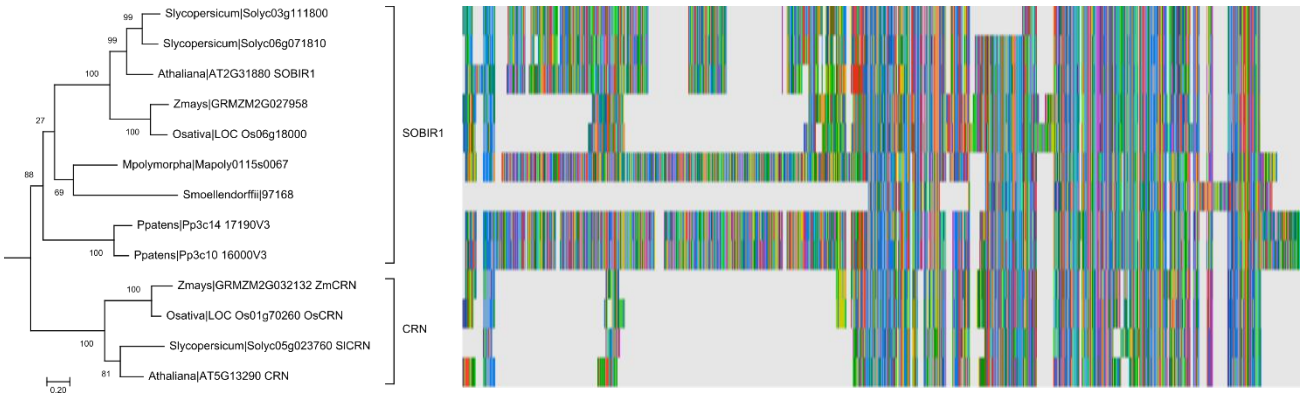

Figure 3. Maximum Likelihood tree of the CRN pseudokinase and the related LRR-RLK SOBIR1 based on full length peptide sequences. Appended to the right is a realignment of the full-length peptide sequences from the genes represented in the tree. Subtree shown here is taken from a larger maximum likelihood tree; bootstrap support at the base of this subtree was 100%. CRN and SOBIR1 family members have distinct functions, but repeated domain loss has led to the convergent evolution of similar protein structures between the clades with truncated ectodomains.

Similar to *CLV2*, each angiosperm genome assayed here possesses one ortholog of *CRN* (Figure3). In the case of *CRN* however, we were able to identify a well-supported sister clade containing the Arabidopsis receptor kinase gene *SUPPRESSOR OF BIR1* (*SOBIR1*). Unlike CRN, SOBIR1 possesses an extracellular domain with LRRs and has been described to function in immunity-induced and developmentally programmed cell death (Gao et al. 2009; Leslie et al. 2010). We identified orthologs of *SOBIR1* in Marchantia, Physcomitrella, and Selaginella; the Marchantia and Physcomitrella genes are predicted to encode proteins containing the longest extracellular domains of any in the clade (Figure 3). Interestingly, the maize and rice orthologs of SOBIR1 have short extracellular domains, similar to CRN. These disparities raise questions as to whether these grass SOBIR1 orthologs functionally resemble *SOBIR1* or *CRN*, or whether they possess separate functions entirely. These phylogenetic data support a model wherein CRN is evolutionarily derived from a full-length LRR-RLK, raising the appealing hypothesis that *CLV2* is similarly derived from a gene encoding a full length LRR-RLK but lost its cytoplasmic domain. However, whereas conservation of the kinase domain enables phylogenetic analyses of *CRN*, discerning the evolution of *CLV2* will prove much more difficult given that the sequence is largely composed of repeat domains.

RPK1/RPK2: Structural changes and possible neofunctionalization

RPK2 acts downstream of CLE signaling in multiple developmental contexts. In the SAM, *RPK2* performs a similar function as *CLV1* and *CLV2*, but via a separate pathway (Kinoshita et al. 2010). During anther development, *RPK2* acts with *BAM1* and *BAM2* to coordinate cell division plane orientation and cell identity (Mizuno et al. 2007; Cui et al. 2018). As a final example of overlapping function with CLV1/BAM type LRR-RLKs, RPK2 and BAM1 interact to inhibit cell proliferation in the root (Shimizu et al. 2015b). Interestingly, and despite the repeated discovery of overlap between *RPK2* and *CLV1/BAM* genes, the Arabidopsis *RPK2* paralog *RPK1* appears to function in a completely distinct pathway. RPK1 is required for ABA response (Osakabe et al. 2005) and is essential for shoot regeneration (Motte et al. 2014). However, there is an exception to this separation of *RPK2* and *RPK1* pathways, as these genes appear to have redundant functions in the embryo where they are implicated in organizing auxin efflux carriers during embryonic patterning (Nodine et al. 2007). While this impact on auxin efflux is the most mechanistic description of

RPK1 or RPK2 function, whether such changes in auxin transport could account for other *rpk1* or *rpk2* mutant phenotypes has not been explored.

As *RPK1* and *RPK2* have distinct functions in most developmental contexts, we used our phylogenetic analyses to determine whether *RPK2* or *RPK1* is more likely to carry out the ancestral *RPK1/RPK2* function, and whether one gene's activity is likely the result of neofunctionalization. Given that Selaginella, Physcomitrella, and Marchantia each have a single *RPK1*/*RPK2* homolog, tree topology alone provides little useful information toward answering this question (Figure 4). Comparing the structures of the bryophyte and angiosperm *RPK1*/*RPK2* homologs (Figure 4) reveals that *RPK1* and several angiosperm orthologs are truncated, with shorter extracellular domains, whereas *RPK2* resembles the ancestral, full-length form. Together with recent functional data from Physcomitrella showing that *PpRPK2* is a regulator of stem cell number and cell division plane similar to *RPK2* (Whitewoods et al. 2018), this evidence suggests that *RPK1's* role in ABA signaling might represent neofunctionalization of the ancestral *RPK1/RPK2* gene, concurrent with a loss of LRR domains.

Like *RPK1*, several other genes in this clade encode proteins that are truncated or appear to be missing internal LRR domains (Figure 4). While one of these short-ectodomain variants includes the tomato gene

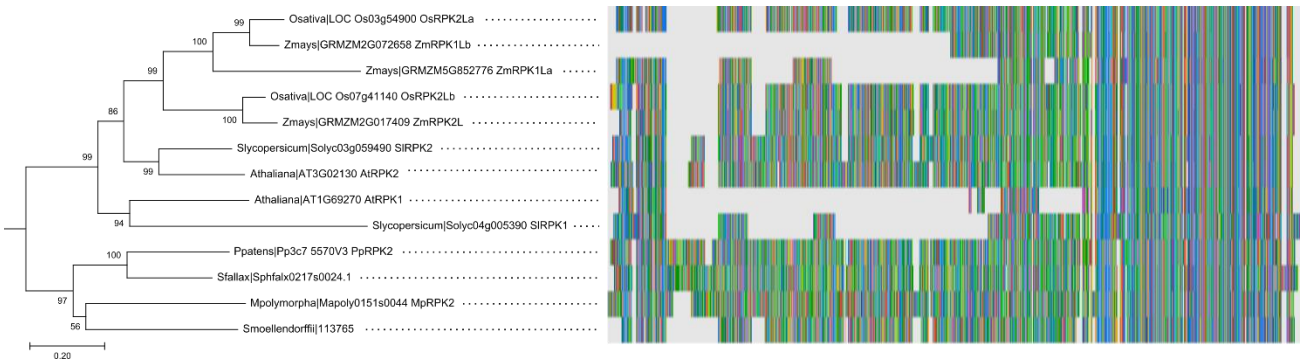

Figure 4. Maximum Likelihood tree of the RPK1 and RPK2 LRR-RLKs based on full length peptide sequences. Subtree shown here is taken from a larger maximum likelihood tree; bootstrap support at the base of this subtree was 100%. Adjacent to the phylogeny are the realigned, full-length peptide sequences encoded by the genes depicted on this subtree. AtRPK2 more closely resembles the bryophyte ortholog of RPK1/RPK2. Truncations of genes in this clade appear to be common derived features.

most closely related to *RPK1*, in several cases the number of LRR domains is unrelated to the position of the gene on the tree. This suggests, as others have shown (Liu et al. 2017), that LRR domain number is highly dynamic. In the case of *RPK1/RPK2*, it would be interesting to see whether, as appears to be the case for moss and Arabidopsis *RPK2*, functional conservation can be predicted based on conserved LRR domain structure more than by relatedness as depicted by the gene tree (determined by sequence). In accordance with this hypothesis, we named short-ectodomain homologs of *RPK1/RPK2* as *RPK1 LIKE* and long-ectodomain homologs *RPK2 LIKE* (Supplemental Table 1).

FEA3 and TMM: close relatives with distinctive ligands

The RLP-encoding gene *FEA3* was discovered in maize as a single copy gene regulating meristem size, akin to *CLV1* (Wu et al. 2016). FEA3 is hypothesized to binds to and transduce signals from the CLE peptide FON2-LIKE CLE PROTEIN 1 (FCP1). The discovery of *FEA3* led to the hypothesis that different LRR-RLKs contribute to the regulation of meristem size by controlling the expression of *WUS* in different meristematic domains. In this model, *FEA3* represses *ZmWUS1* in the center of the SAM toward the stem in response to FCP1, whereas in Arabidopsis CLV1 responds to CLV3 to repress *WUS* nearer the apex of the shoot meristem. While FEA3 was originally hypothesized to regulate SAM size based on leaf-derived FCP1 (Wu et al. 2016), more recent data conflicts with the originally reported expression domains for *FCP1*, indicating that the model of FCP1-FEA3 activity should be revisited (Knauer et al. 2019).

Unexpectedly, our phylogenetic analysis revealed that the clade sister to *FEA3* contains the Arabidopsis gene *AT4G28560*, which is annotated as *ROP-INTERACTIVE CRIB MOTIF-CONTAINING PROTEIN 7* (*RIC7*) that contains a CRIB (Cdc42/Rac-interactive binding) domain (Figure5). This annotation led us to question the close position of *AT4G28560* to *FEA3* in our maximum likelihood analysis. After subjecting AT4G28560 to a conserved protein domain search, we found that this gene encodes a protein predicted to contain 9 LRR domains and no CRIB domain (Supplemental Figure 2). Additionally, the highest scoring pBLAST hits against the Arabidopsis thaliana genome are the Arabidopsis orthologs of *FEA3*, but not other *RIC* gene family members (pBLAST data not shown). Finally, another gene model, *AT4G28556*, is annotated as *RIC7*

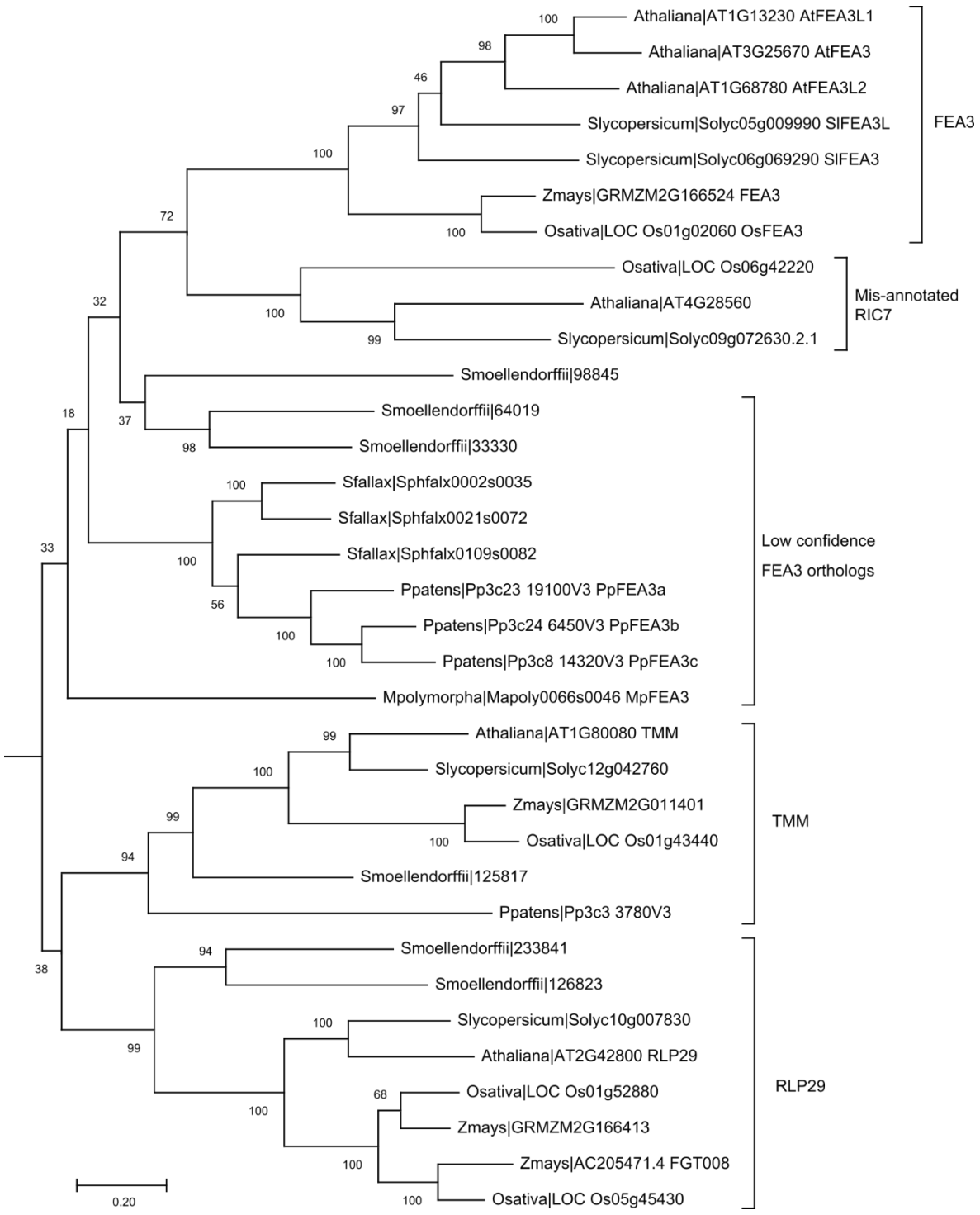

Figure 5. Maximum Likelihood tree of the FEA3 and TMM LRR-RLPs based on full length peptide sequences. Subtree shown here is taken from a larger maximum likelihood tree; bootstrap support at the base of this subtree was 94%. Whereas FEA3 is a putative CLE receptor, TMM binds a distinct class of ligands. Support for placement of bryophyte orthologs of FEA3 is low.

in the paper where RIC7 function was originally characterized (Jeon et al. 2008).Altogether, these results suggest that *AT4G28560* is currently misannotated as *RIC7*. Furthermore, the clade containing *AT4G28560* also contains one rice and one tomato gene, but no maize genes, suggesting that the maize ortholog may have been lost and that the current closest maize ortholog is *FEA3.*

We next tried to determine whether *FEA3* is conserved in bryophytes and Selaginella. Although the tree topology with the highest likelihood places a set of Selaginella and bryophyte genes sister to the clade containing *FEA3*, bootstrap support for these relationships are low (Figure 5). It is thus difficult to tell conclusively whether the lycophyte and bryophyte clades are more closely related to *FEA3,* or to the gene family sister to *FEA3* containing the *ERECTA* (*ER*) co-receptor *TOO MANY MOUTHS* (*TMM*) (Lee et al. 2012). Given that *TMM* has a well-supported moss ortholog (*Pp3c3 3780V3.1*) separate from the putative bryophyte *FEA3* orthologs, we propose that the bryophyte clade sister to the *FEA3* clade likely comprises true orthologs of *FEA3*. Interestingly, while *Physcomitrella patens* contains a high-confidence ortholog of *TMM* with a demonstrated conserved function (Caine et al. 2016), the peat moss *Sphagnum fallax* and the liverwort *Marchantia polymorpha* do not. Thus, as neither Sphagnum nor Marchantia possess stomata and Physcomitrella does, the presence/absence of *TMM* tracks well with the evolution of stomata. These analyses suggest that TMM functions specifically in stomatagenesis as far back as the earliest land plants.

Unlike the *CRN* and *RPK1/RPK2* gene families, the RLPs comprising the FEA3 and TMM clades vary little in their protein length and overall domain structure, at least in the taxa sampled (Supplemental Figure 3)**.** These data suggest that while dynamic LRR-domain gain and loss is common in many LRR-RLK gene families, it is not the case universally.

CIK: co-receptors at the crossroads of immune and stem cell signaling

CLAVATA insensitive kinases (CIKs) are recently discovered LRR-RLKs that act as co-receptors within diverse developmental contexts. CIKs form co-receptor complexes with many of the signaling proteins discussed above, including CLV1, BAM1/2, RPK2, CLV2, and CRN (Anne et al. 2018; Hu et al. 2018; Cui et al. 2018). CIK receptors are closely related to the NSP-INTERACTING KINASE (NIK) LRR-RLKs that

function in plant immunity (Fontes et al. 2004; Zorzatto et al. 2015). Expansion and diversification of CIK and NIK receptors occurred following the speciation events that separated bryophytes and lycophytes from vascular plants (Figure 6). We thus resolve a well-supported clade of bryophyte genes co-orthologous to all angiosperm CIK and NIK LRR-RLKs.

The CIK/NIK clade thus presents us with a family of receptors that function in both immunity and development. Expression of *NIK* genes in Arabidopsis under *CIK* promoters can complement *cik* mutant phenotype (Anne et al. 2018), indicating that while the function of these genes has diverged, the biochemical operations they can conduct have not. Immune and developmental pathways consistently exhibit substantial crosstalk, and how similar signaling pathways are parsed differently during development and immune response is an open question in plant biology. Given that CIK1/2 and NIK1/2 are such similar proteins with quite distinct functions, we propose that comparison of all *CIK/NIK* genes to their bryophyte orthologs will prove a fertile ground for experiments seeking to understand how subfunctionalization of LRR-RLKs occurs, how different receptor protein complexes evolve, and the crosstalk between immune and developmental signaling.

Discussion

Many of the LRR-RLKs discussed herein are have distinct functions across many tissues but are unified in their regulation of stem cell specification. Within a clade, the ability of various homologs to complement one another is widespread, despite differences in mutant phenotypes among these homologs. Often times these differences in loss-of-function phenotype are ascribed to variations in expression domain. However, given that a protein accumulates within a new domain, two distinct outcomes are possible. First, the protein can perform the same biochemical operation it did in its original domain (i.e. subfunctionalization); which can lead to unexpected mutant phenotypes for the subfunctionalized paralog. For example, a mutation that reduces proliferation in leaf initial cells will have quite distinct developmental consequences from a mutation of a paralogous gene functioning in SAM stem cell proliferation even though both regulate the same process, i.e. proliferation. Second, the protein may evolve new biochemical functions in its new domain (i.e.

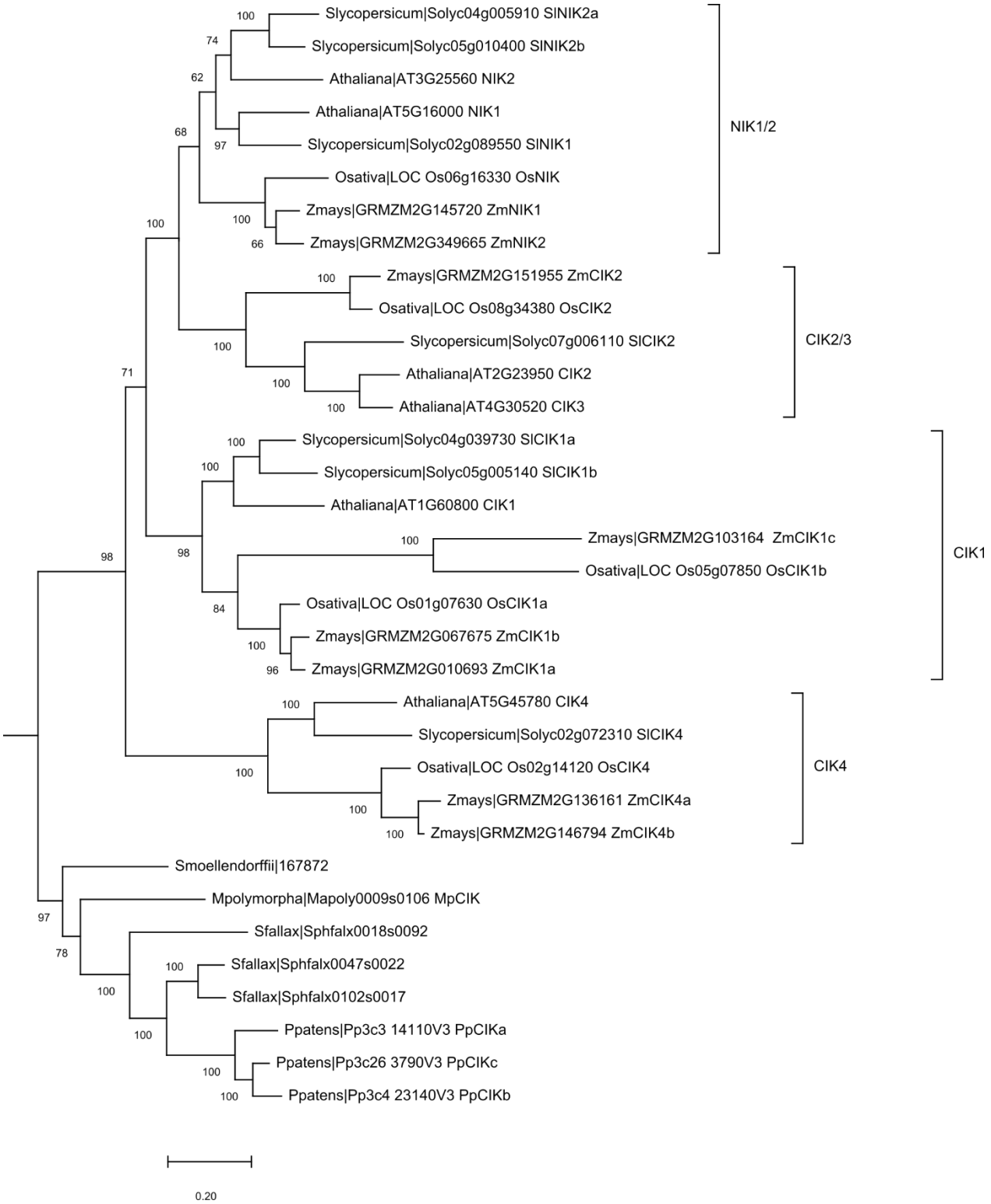

Figure 6: Maximum Likelihood tree of CLAVATA insensitive kinases (CIKs) based on full length peptide sequences. Moss contains a clade of genes co-orthologous to the CIK coreceptors of stem cell maintenance LRR-RLKs/RLPs and the NIK immunity-related coreceptors.

neofunctionalization), which might involve new binding new partners, phosphorylating novel downstream targets, or binding to different ligands. Such neofunctionalization may stem from structural changes to the protein itself that arise after gene duplication or might be entirely dependent on novel interactions in the new context. Uncovering which of the above scenarios are operating during the diversification of the LRR-RLKs and related proteins will lead to a better understanding of stem cell maintenance pathways in land plants. Working within a functionally informed phylogenetic framework like the one provided here will expedite such studies.

Given the degree of redundancy, apparent promiscuity in complex formation, and diversity of downstream responses possible even from the same receptors (Je et al. 2018), understanding LRR-RLK function will require experiments with high spatial and temporal resolution. This pursuit will be aided by the advent of single-cell technologies; high-throughput experiments providing a set of plausible protein-protein interactions (Smakowska-Luzan et al. 2018) can be combined with single-cell RNAseq data to generate hypotheses about which receptors might be forming a complex in a given cell type during development.

Here we presented an evolutionary framework for analyses of signaling genes involved in stem cell maintenance. We identified orthologs of these signaling components in diverse plant model systems and propose a nomenclature for unannotated genes based on functional and phylogenetic (Supplemental Table 1). We see, as has been previously reported (Liu et al. 2017), that LRR domain number is highly dynamic within some (*RPK1/RPK2*) but not all (*FEA3*) gene families. We identify bryophyte orthologs for most *LRR-RLK*-like genes examined, reaffirming that LRR-RLK gene families diversified early in land plant evolution. Interestingly, even in clades with frequent truncations in extracellular protein domains such as *CRN*/*SOBIR1* or *RPK1*/*RPK2*, bryophyte extracellular domains were always the longest and exhibited no evidence of domain loss. It will be interesting to see whether this is a general trend that extends beyond the taxa and gene families sampled here, and will require the assembly of a greater number of bryophyte genomes.

Within clades, we find evidence that the pseudokinase CRN evolved from a full-length LRR-RLK that is the likely ancestor of *CRN* and *SOBIR1*. In the case of *CRN* and *SOBIR1* as well for *CIK* and *NIK* genes, we find

that many of these regulators of stem cell signaling are closely related to genes that function in plant immunity. Intriguingly, *cik* mutations can be complemented by *NIK* genes, which suggests that the context within which a protein functions is determined not only by cell type, but also by that the biotic and abiotic stimuli perceived by that cell. Moreover, a gene closely related to *FEA3* was identified to be mis-annotated, and we found that *FEA3* is closely related to the *ER* co-receptor encoding gene *TMM*. This relationship is interesting, as the TMM/ER complex binds a distinct class of ligands from FEA3, adding another level of promiscuity to these LRR-RLK gene families that will need to be untangled.

In this work we sought to provide a useful reference to facilitate research on stem cell signaling pathways in diverse model and crop species. As plant transformation and genome editing technologies improve, the number of systems available for functional genetic studies will expand, and analyses like the one conducted here will need to be replicated. Altogether, increasing the number of model systems and performing clade to clade rather than gene to gene comparisons will provide us with a deeper and more general understanding of plant stem cell signaling.

Acknowledgements

The authors would like to acknowledge Jesus Martínez-Gómez for stimulating conversation on the topics discussed here. Joseph Cammarata would also like to thank the Provost Diversity Fellowship for Advanced Doctoral Students for funding.

References

Anne P, Amiguet-Vercher A, Brandt B, et al (2018) CLERK is a novel receptor kinase required for sensing of root-active CLE peptides in *Arabidopsis*. Development 145:dev162354. https://doi.org/10.1242/dev.162354

Bleckmann A, Weidtkamp-Peters S, Seidel CAM, Simon R (2010) Stem Cell Signaling in Arabidopsis Requires CRN to Localize CLV2 to the Plasma Membrane. Plant Physiol 152:166–176. https://doi.org/10.1104/pp.109.149930

Bommert P, Nagasawa NS, Jackson D (2013) Quantitative variation in maize kernel row number is controlled by the FASCIATED EAR2 locus. Nat Genet 45:334–7. https://doi.org/10.1038/ng.2534

Caine RS, Chater CC, Kamisugi Y, et al (2016) An ancestral stomatal patterning module revealed in the non-vascular land plant *Physcomitrella patens*. Development 143:3306–3314. https://doi.org/10.1242/dev.135038

Capella-Gutiérrez S, Silla-Martínez JM, Gabaldón T (2009) trimAl: A tool for automated alignment trimming in large-scale phylogenetic analyses. Bioinformatics 25:1972–1973. https://doi.org/10.1093/bioinformatics/btp348

Clark SE, Williams RW, Meyerowitz EM (1997) The CLAVATA1 gene encodes a putative receptor kinase that controls shoot and floral meristem size in Arabidopsis. Cell 89:575–585. https://doi.org/10.1016/S0092-8674(00)80239-1

Cui Y, Hu C, Zhu Y, et al (2018) CIK Receptor Kinases Determine Cell Fate Specification during Early Anther Development in Arabidopsis. Plant Cell 30:2383–2401. https://doi.org/10.1105/TPC.17.00586

DeYoung BJ, Clark SE (2008) BAM receptors regulate stem cell specification and organ development through complex interactions with CLAVATA signaling. Genetics 180:895–904. https://doi.org/10.1534/genetics.108.091108

Edgar RC (2004) MUSCLE: multiple sequence alignment with high accuracy and high throughput. Nucleic Acids Res 32:1792–1797. https://doi.org/10.1093/nar/gkh340

Etchells JP, Provost CM, Mishra L, Turner SR (2013) WOX4 and WOX14 act downstream of the PXY receptor kinase to regulate plant vascular proliferation independently of any role in vascular organisation. Development 140:2224–34. https://doi.org/10.1242/dev.091314

Fisher K, Turner SR (2007) PXY, a Receptor-like Kinase Essential for Maintaining Polarity during Plant Vascular-Tissue Development. Curr Biol 17:1061–1066. https://doi.org/10.1016/j.cub.2007.05.049

Fontes EPB, Santos AA, Luz DF, et al (2004) The geminivirus nuclear shuttle protein is a virulence factor that suppresses transmembrane receptor kinase activity. Genes Dev 18:2545–2556. https://doi.org/10.1101/gad.1245904

Gao M, Wang X, Wang D, et al (2009) Regulation of Cell Death and Innate Immunity by Two Receptor-like Kinases in Arabidopsis. Cell Host Microbe 6:34–44. https://doi.org/10.1016/j.chom.2009.05.019

Goad DM, Zhu C, Kellogg EA (2017) Comprehensive identification and clustering of CLV3/ESR-related (CLE) genes in plants finds groups with potentially shared function. New Phytol 216:605–616. https://doi.org/10.1111/nph.14348

Guo Y, Han L, Hymes M, et al (2011) CLAVATA2 forms a distinct CLE-binding receptor complex regulating Arabidopsis stem cell specification. Plant J 63:734–747. https://doi.org/10.1111/j.1365-313X.2010.04295.x.CLAVATA2

Hazak O, Brandt B, Cattaneo P, et al (2017) Perception of root-active CLE peptides requires CORYNE function in the phloem vasculature. EMBO Rep 18:1367–1381. https://doi.org/10.15252/EMBR.201643535

Hirakawa Y, Kondo Y, Fukuda H (2010) TDIF peptide signaling regulates vascular stem cell proliferation via the WOX4 homeobox gene in Arabidopsis. Plant Cell 22:2618–2629. https://doi.org/10.1105/tpc.110.076083

Hirakawa Y, Uchida N, Yamaguchi YL, et al (2019) Control of proliferation in the haploid meristem by CLE peptide signaling in Marchantia polymorpha. PLOS Genet 15:1–20.

https://doi.org/10.1371/journal.pgen.1007997

Hord CLH, Chen C, DeYoung BJ, et al (2006) The BAM1/BAM2 receptor-like kinases are important regulators of Arabidopsis early anther development. Plant Cell 18:1667–80. https://doi.org/10.1105/tpc.105.036871

Hu C, Zhu Y, Cui Y, et al (2018) A group of receptor kinases are essential for CLAVATA signalling to maintain stem cell homeostasis. Nat Plants 4:205–211. https://doi.org/10.1038/s41477-018-0123-z

Huerta-Cepas J, Serra F, Bork P (2016) ETE 3: Reconstruction, Analysis, and Visualization of Phylogenomic Data. Mol Biol Evol 33:1635–1638. https://doi.org/10.1093/molbev/msw046

Je B Il, Xu F, Wu Q, et al (2018) The CLAVATA receptor FASCIATED EAR2 responds to distinct CLE peptides by signaling through two downstream effectors. Elife 7:. https://doi.org/10.7554/eLife.35673

Jeon BW, Hwang J-U, Hwang Y, et al (2008) The Arabidopsis small G protein ROP2 is activated by light in guard cells and inhibits light-induced stomatal opening. Plant Cell 20:75–87. https://doi.org/10.1105/tpc.107.054544

Katoh K (2005) MAFFT version 5: improvement in accuracy of multiple sequence alignment. Nucleic Acids Res 33:511–518. https://doi.org/10.1093/nar/gki198

Kayes JM, Clark SE (1998) CLAVATA2, a regulator of meristem and organ development in Arabidopsis. Development 125:3843–3851

Kinoshita A, Betsuyaku S, Osakabe Y, et al (2010) RPK2 is an essential receptor-like kinase that transmits the CLV3 signal in Arabidopsis. Development 137:3911–3920. https://doi.org/10.1242/dev.061747

Knauer S, Javelle M, Li L, et al (2019) A high-resolution gene expression atlas links dedicated meristem genes to key architectural traits. Genome Res 29:1962–1973. https://doi.org/10.1101/gr.250878.119

Lee JS, Kuroha T, Hnilova M, et al (2012) Direct interaction of ligand-receptor pairs specifying stomatal patterning. Genes Dev 26:126–136. https://doi.org/10.1101/gad.179895.111

Leslie ME, Lewis MW, Youn JY, et al (2010) The EVERSHED receptor-like kinase modulates floral organ shedding in Arabidopsis. Development 137:467–476. https://doi.org/10.1242/dev.041335

Liu P-L, Du L, Huang Y, et al (2017) Origin and diversification of leucine-rich repeat receptor-like protein kinase (LRR-RLK) genes in plants. BMC Evol Biol 17:47. https://doi.org/10.1186/s12862-017-0891-5

Miller MA, Pfeiffer W, Schwartz T (2010) Creating the CIPRES Science Gateway for inference of large phylogenetic trees. In: 2010 Gateway Computing Environments Workshop, GCE 2010

Miwa H, Betsuyaku S, Iwamoto K, et al (2008) The receptor-like kinase SOL2 mediates CLE signaling in Arabidopsis. Plant Cell Physiol 49:1752–1757. https://doi.org/10.1093/pcp/pcn148

Mizuno S, Osakabe Y, Maruyama K, et al (2007) Receptor-like protein kinase 2 (RPK 2) is a novel factor controlling anther development in Arabidopsis thaliana. Plant J 50:751–766. https://doi.org/10.1111/j.1365-313X.2007.03083.x

Motte H, Vercauteren A, Depuydt S, et al (2014) Combining linkage and association mapping identifies

RECEPTOR-LIKE PROTEIN KINASE1 as an essential Arabidopsis shoot regeneration gene. Proc Natl Acad Sci U S A 111:8305–10. https://doi.org/10.1073/pnas.1404978111

Müller R, Bleckmann A, Simon R (2008) The receptor kinase CORYNE of Arabidopsis transmits the stem cell-limiting signal CLAVATA3 independently of CLAVATA1. Plant Cell 20:934–946. https://doi.org/10.1105/tpc.107.057547

Nimchuk ZL, Zhou Y, Tarr PT, et al (2015) Plant stem cell maintenance by transcriptional cross-regulation of related receptor kinases. Development 142:1043–1049. https://doi.org/10.1242/dev.119677

Nodine MD, Yadegari R, Tax FE (2007) RPK1 and TOAD2 Are Two Receptor-like Kinases Redundantly Required for Arabidopsis Embryonic Pattern Formation. Dev Cell 12:943–956. https://doi.org/10.1016/j.devcel.2007.04.003

Osakabe Y, Maruyama K, Seki M, et al (2005) Leucine-rich repeat receptor-like kinase1 is a key membrane-bound regulator of abscisic acid early signaling in Arabidopsis. Plant Cell 17:1105–19. https://doi.org/10.1105/tpc.104.027474

Qian P, Song W, Yokoo T, et al (2018) The CLE9/10 secretory peptide regulates stomatal and vascular development through distinct receptors. Nat Plants 4:1071–1081. https://doi.org/10.1038/s41477-018-0317-4

Rodríguez-Leal D, Lemmon ZH, Man J, et al (2017) Engineering Quantitative Trait Variation for Crop Improvement by Genome Editing. Cell 470–480. https://doi.org/10.1016/j.cell.2017.08.030

Rodriguez-Leal D, Xu C, Kwon CT, et al (2019) Evolution of buffering in a genetic circuit controlling plant stem cell proliferation. Nat. Genet. 51:786–792

Schoof H, Lenhard M, Haecker a, et al (2000) The stem cell population of Arabidopsis shoot meristems in maintained by a regulatory loop between the CLAVATA and WUSCHEL genes. Cell 100:635–644. https://doi.org/10.1016/S0092-8674(00)80700-X

Shimizu N, Ishida T, Yamada M, et al (2015a) BAM 1 and RECEPTOR-LIKE PROTEIN KINASE 2 constitute a signaling pathway and modulate CLE peptide-triggered growth inhibition in Arabidopsis root. 3:1104–1113

Shimizu N, Ishida T, Yamada M, et al (2015b) BAM 1 and RECEPTOR-LIKE PROTEIN KINASE 2 constitute a signaling pathway and modulate CLE peptide-triggered growth inhibition in Arabidopsis root. New Phytol 3:1104–1113. https://doi.org/10.1111/nph.13520

Smakowska-Luzan E, Mott GA, Parys K, et al (2018) An extracellular network of Arabidopsis leucine-rich repeat receptor kinases. Nature 553:342–346. https://doi.org/10.1038/nature25184

Somssich M, Ma Q, Weidtkamp-Peters S, et al (2015) Real-time dynamics of peptide ligand-dependent receptor complex formation in planta. Sci Signal 8:ra76–ra76. https://doi.org/10.1126/scisignal.aab0598

Stamatakis A (2014) RAxML version 8: A tool for phylogenetic analysis and post-analysis of large phylogenies. Bioinformatics 30:1312–1313. https://doi.org/10.1093/bioinformatics/btu033

Taguchi-Shiobara F, Yuan Z, Hake S, Jackson D (2001) The fasciated ear2 gene encodes a leucine-rich repeat

receptor-like protein that regulates shoot meristem proliferation in maize. Genes Dev 15:2755–2766. https://doi.org/10.1101/gad.208501

Whitewoods CD, Cammarata J, Nemec Venza Z, et al (2018) CLAVATA Was a Genetic Novelty for the Morphological Innovation of 3D Growth in Land Plants. Curr Biol 1–12. https://doi.org/10.1016/j.cub.2018.05.068

Wu Q, Gruel J, Lee YK, Bommert P (2016) Signaling from maize organ primordial via FASCIATED EAR3 regulates stem cell proliferation and yield traits. Nat Genet. https://doi.org/http://www.nature.com/ng/journal/vaop/ncurrent/full/ng.3567.html

Zorzatto C, MacHado JPB, Lopes KVG, et al (2015) NIK1-mediated translation suppression functions as a plant antiviral immunity mechanism. Nature 520:679–682. https://doi.org/10.1038/nature14171

Supplemental Figures and Tables

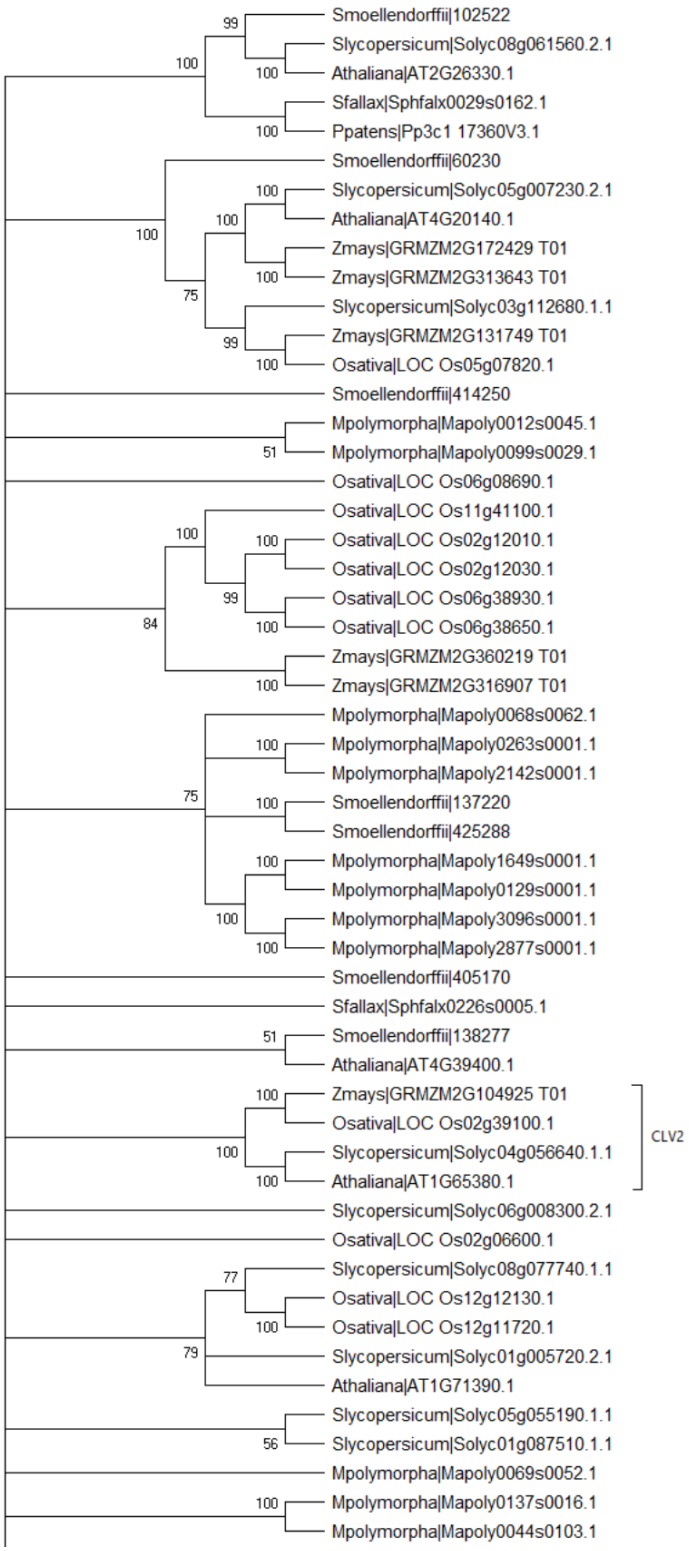

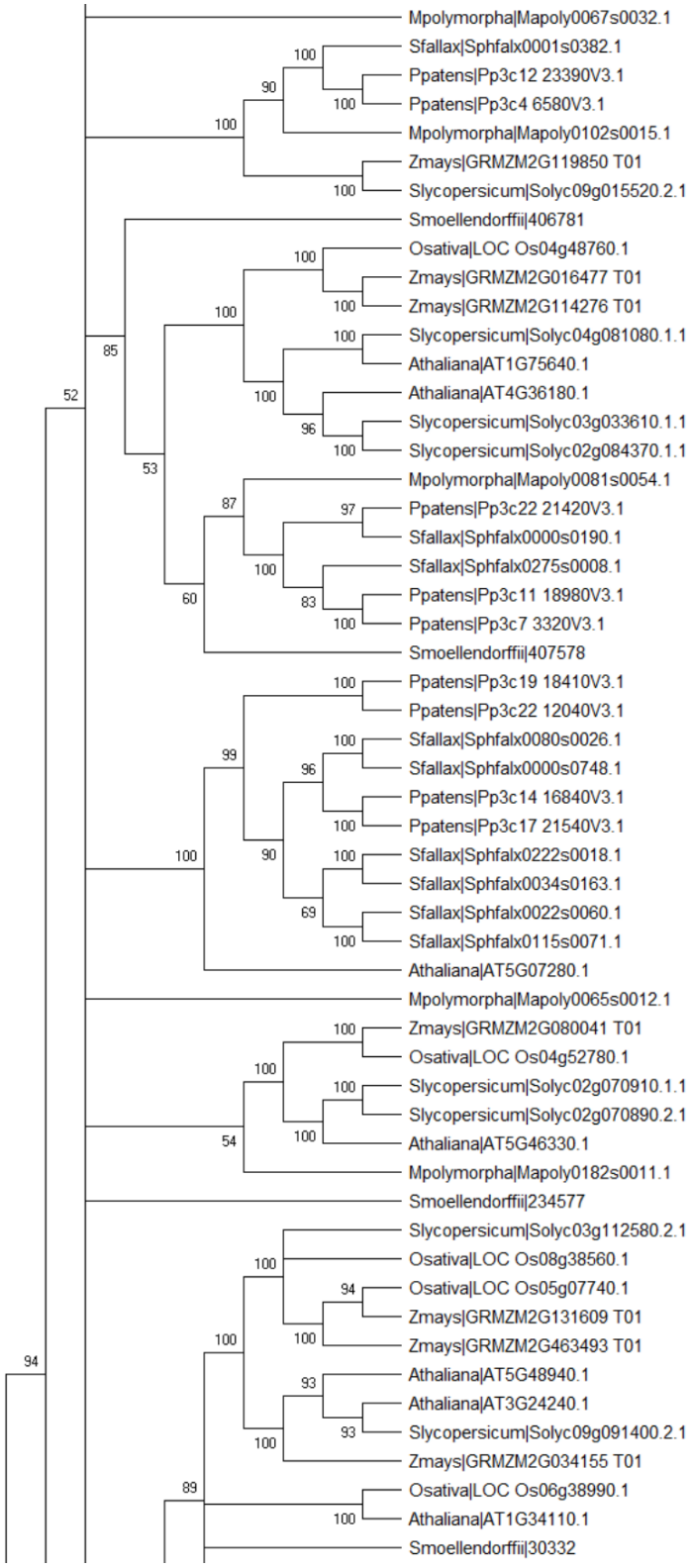
Mpolymorpha|Mapoly0067s0032.1
Sfallax|Sphfalx0001s0382.1
Ppatens|Pp3c12 23390V3.1
Ppatens|Pp3c4 6580V3.1
Mpolymorpha|Mapoly0102s0015.1
Zmays|GRMZM2G119850 T01
Slycopersicum|Solyc09g015520.2.1
Smoellendorffii|406781
Osativa|LOC Os04g48760.1
Zmays|GRMZM2G016477 T01
Zmays|GRMZM2G114276 T01
Slycopersicum|Solyc04g081080.1.1
Athaliana|AT1G75640.1
Athaliana|AT4G36180.1
Slycopersicum|Solyc03g033610.1.1
Slycopersicum|Solyc02g084370.1.1
Mpolymorpha|Mapoly0081s0054.1
Ppatens|Pp3c22 21420V3.1
Sfallax|Sphfalx0000s0190.1
Sfallax|Sphfalx0275s0008.1
Ppatens|Pp3c11 18980V3.1
Ppatens|Pp3c7 3320V3.1
Smoellendorffii|407578
Ppatens|Pp3c19 18410V3.1
Ppatens|Pp3c22 12040V3.1
Sfallax|Sphfalx0080s0026.1
Sfallax|Sphfalx0000s0748.1
Ppatens|Pp3c14 16840V3.1
Ppatens|Pp3c17 21540V3.1
Sfallax|Sphfalx0222s0018.1
Sfallax|Sphfalx0034s0163.1
Sfallax|Sphfalx0022s0060.1
Sfallax|Sphfalx0115s0071.1
Athaliana|AT5G07280.1
Mpolymorpha|Mapoly0065s0012.1
Zmays|GRMZM2G080041 T01
Osativa|LOC Os04g52780.1
Slycopersicum|Solyc02g070910.1.1
Slycopersicum|Solyc02g070890.2.1
Athaliana|AT5G46330.1
Mpolymorpha|Mapoly0182s0011.1
Smoellendorffii|234577
Slycopersicum|Solyc03g112580.2.1
Osativa|LOC Os08g38560.1
Osativa|LOC Os05g07740.1
Zmays|GRMZM2G131609 T01
Zmays|GRMZM2G463493 T01
Athaliana|AT5G48940.1
Athaliana|AT3G24240.1
Slycopersicum|Solyc09g091400.2.1
Zmays|GRMZM2G034155 T01
Osativa|LOC Os06g38990.1
Athaliana|AT1G34110.1
Smoellendorffii|30332

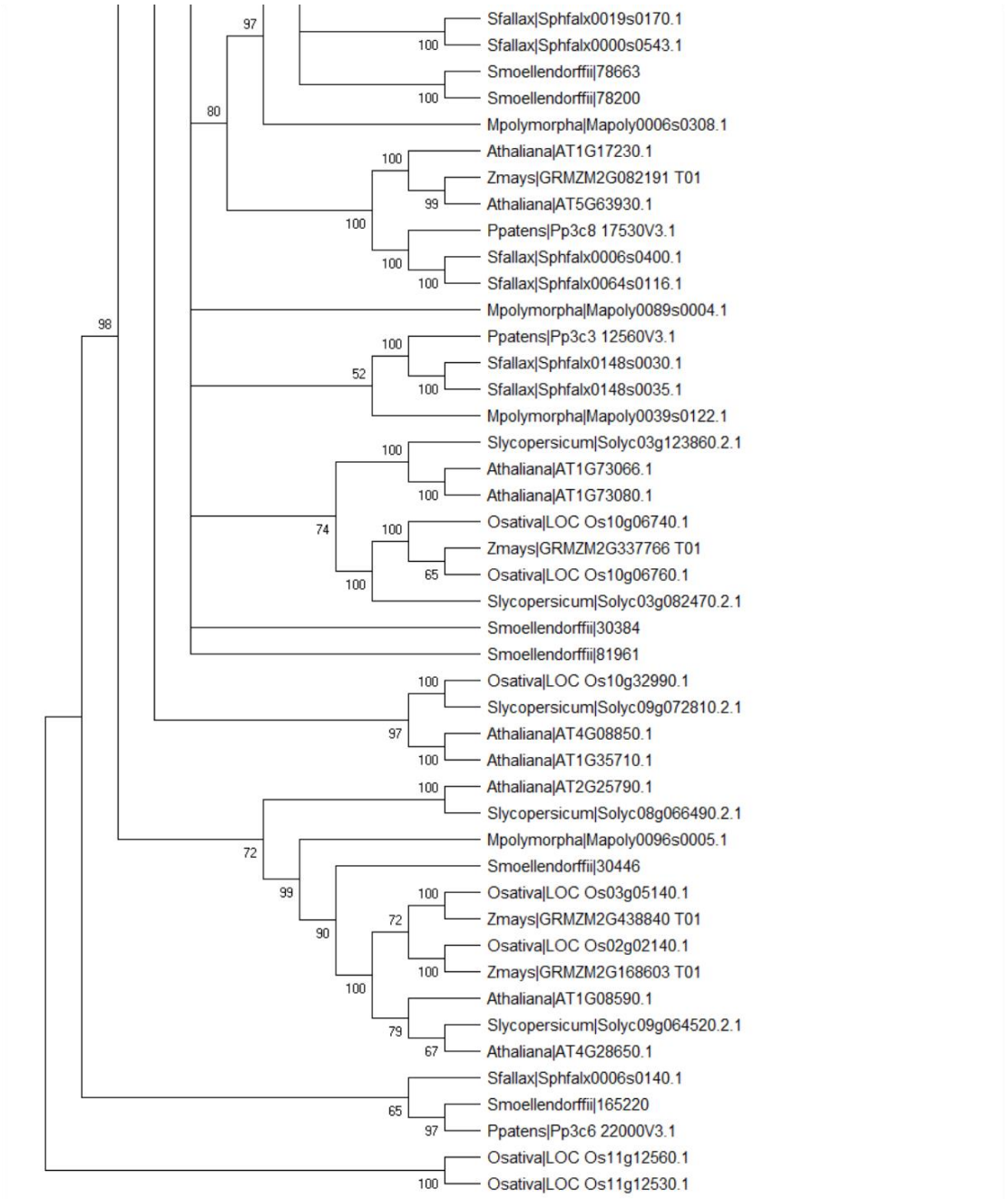

Fig. S1. Maximum likelihood tree of constructed using aligned peptide sequencs from best pBLAST hits of CLV2. Many clades have strong support and date as far back as bryophytes, but branch support (percent of bootstrap runs with 1000 runs) is very low along the backbone. Relationships between clades are thus difficult to resolve.

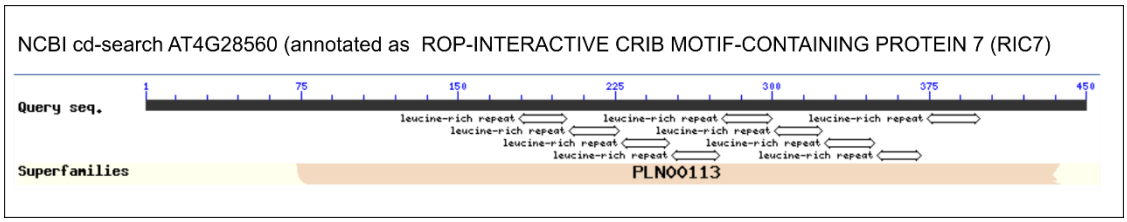

Fig. S2. Protein domain search using cd-search within the peptide sequence of AT4G28560. This gene model encodes an LRR-RLP and is mis-annotated as *RIC7*.

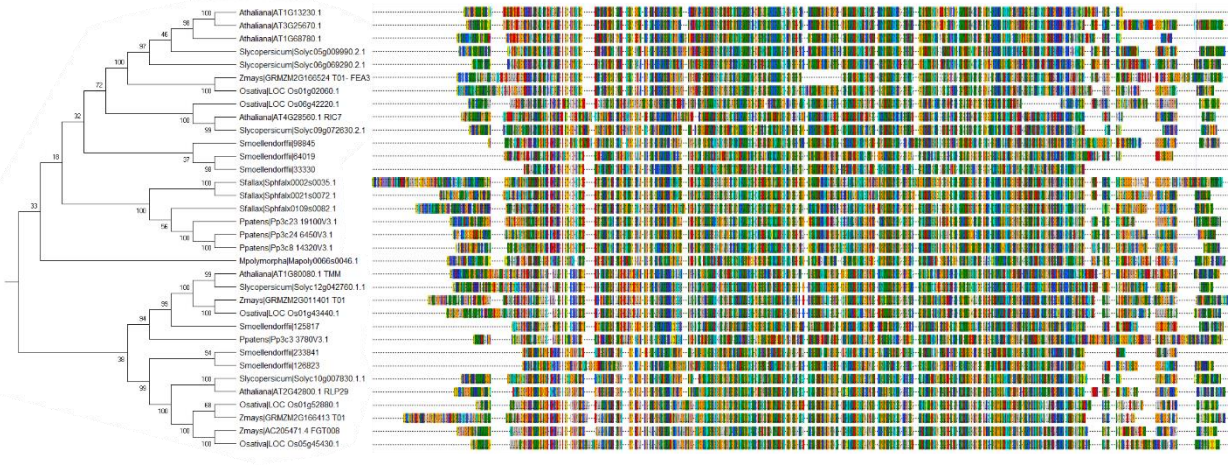

Fig. S3. Maximum likelihood tree and protein alignment for LRR-RLP encoding *FEA3* and *TMM* gene families. Unlike some other LRR gene families (e.g. *RPK2/RPK1*), the length of TMM and FEA3 peptides has remained consistent throughout land plant evolution.

Supplemental table with suggested LRR-RLK nomenclature

Receptor Family	Arabidopsis		Tomato			Maize			Oryza Sativa			Physcomitrella			Marchantia		
	Gene ID	Annotation	Gene ID	Annotation	Orthologous to	Gene ID	Annotation	orthologous to	Gene ID	Annotation	Orthologous to	Gene ID	Annotation	Orthologous to			
CLV1	AT1G75820	CLV1	Solyc04g081590	SlCLV1	CLV1	GRMZM2G300133	TD1	CLV1	Os06g50340	FON1	CLV1						
BAM	AT5G65700	BAM1	Solyc02g091840	SlBAM1	BAM1, BAM2	GRMZM2G072569	ZmBAM1a	BAM1, BAM2	Os03g56270	*OsBAM1a*	BAM1, BAM2	Pp3c13 13360	PpCLV1b	CLV1, BAM1,BAM2,BAM3, BAM4	Mapoly0002s0106	MpCLV1	CLV1, BAM1,BAM2, BAM3, BAM4
						GRMZM2G141517	ZmBAM1b	BAM1, BAM2	Os07g04190	OsBAM1b	BAM1, BAM2						
	AT3G49670	BAM2				GRMZM2G043584	ZmBAM1c	BAM1, BAM2	Os03g12730	OsBAM1c	BAM1, BAM2						
	AT4G20270	BAM3	Solyc01g080770	SlBAM3	BAM3	X	X	X	Os05g51740	OsBAM3	BAM3	Pp3c6 21940	PpCLV1a	CLV1, BAM1,BAM2,BAM3, BAM4			
	X	X	Solyc01g103530	SlBAM4	BAM4	GRMZM2G068398	ZmBAM4a	BAM4	Os11g12620	OsBAM4	BAM4						
						GRMZM2G169681	ZmBAM4b	BAM4									
CLV2	AT1G65380	CLV2	Solyc04g056640	SlCLV2	CLV2	GRMZM2G104925	FEA2	CLV2	Os02g39100	OsCLV2	CLV2	X	X	X	X	X	X
CRN	AT5G13290	CRN	Solyc05g023760	SlCRN	CRN	GRMZM2G032132	ZmCRN	CRN	Os01g70260	OsCRN	CRN	X	X	s	X	X	X
FEA3*	AT3G25670	FEA3	Solyc06g069290	SlFEA3	FEA3, FEA3L1, FEA3L2	GRMZM2G166524	FEA3	FEA3, FEA3L1, FEA3L2	Os01g02060	OsFEA3	FEA3, FEA3L1, FEA3L2	Pp3c23 19100**	*PpFEA3a*	FEA3	Mapoly0066s0046**	MpFEA3	FEA3
	AT1G13230	FEA3L1	Solyc05g009990	SlFEA3L1	FEA3, FEA3L1, FEA3L2							Pp3c24 6450**	PpFEA3b	FEA3			
	AT1G68780	FEA3L2*										Pp3c8 14320**	PpFEA3c	FEA3			
RPK1/RPK2*	AT1G69270	RPK1	Solyc04g005390	SlRPK1	RPK1	GRMZM5G852776	ZmRPK1a	RPK1, RPK2	Os03g54900	OsRPK2a	RPK1, RPK2						
	AT3G02130	RPK2	Solyc03g059490	SlRPK2	RPK2	GRMZM2G017409	ZmRPK2L	RPK1, RPK2	Os07g41140	OsRPK2b	RPK1, RPK2	Pp3c7 5570	PpRPK2	RPK1, RPK2	Mapoly0151s0044	MpRPK2	RPK1, RPK2
						GRMZM2G072658	ZmRPK1b	RPK1, RPK2									
CIK*	AT1G60800	CIK1	Solyc04g039730	SlCIK1a	CIK1	GRMZM2G010693	ZmCIK1a	CIK1	Os01g07630	OsCIK1a	CIK1						
			Solyc05g005140	SlCIK1b	CIK1	GRMZM2G067675	ZmCIK1b	CIK1	Os05g07850	OsCIK1b	CIK1	Pp3c3 14110	PpCIKa	CIK1, CIK2, CIK3, CIK4 NIK1, NIK2	Mapoly0009s0106	MpCIK	CIK1, CIK2, NIK1, NIK2, CIK3, CIK4
						GRMZM2G103164	ZmCIK1c	CIK1									
	AT5G16000	NIK1	Solyc02g089550	SlNIK1	NIK1	GRMZM2G145720	ZmNIK1	NIK1	Os06g16330	OsNIK	NIK1,NIK2						
	AT3G25560	NIK2	Solyc04g005910	SlNIK2a	NIK2	GRMZM2G349665	ZmNIK2	NIK2				Pp3c4 23140	PpCIKb	CIK1, CIK2, CIK3, CIK4 NIK1, NIK2			
			Solyc05g010400	SlNIK2b	NIK2												
	AT2G23950	CIK2	Solyc07g006110	SlCIK2	CIK2, CIK3	GRMZM2G151955	ZmCIK2	CIK2, CIK3	Os08g34380	OsCIK2	CIK2, CIK3						
	AT4G30520	CIK3															
	AT5G45780	CIK4	Solyc02g072310	SlCIK4	CIK4	GRMZM2G136161	ZmCIK4a	CIK4	Os02g14120	OsCIK4	CIK4	Pp3c26 3790	PpCIKc	CIK1, CIK2, CIK3, CIK4 NIK1, NIK2			
						GRMZM2G146794	ZmCIK4b	CIK4									
PXY	AT5G61480	PXY	Solyc03g093330	SlPXY1	PXY	GRMZM2G039934	ZmPXY	PXY	Os08g05290	OsPXY	PXY	X	X	X	Mapoly0096s0005	MpTDR	PXY/PXL1/PXL2
			Solyc05g051640	SlPXY2	PXY												
			Solyc07g005010	SlPXY3	PXY												
	AT1G08590	PXL1	Solyc04g050170	SlPXL1a	PXL1	GRMZM2G168603	ZmPXL1	PXL1/PXL2	Os02g02140	OsPXL1	PXL1/PXL2						
			Solyc09g064520	SlPXL1b	PXL1	GRMZM2G009818	ZmPXL2	PXL1/PXL2	Os03g05140	OsPXL2	PXL1/PXL2						
	AT4G28650	PXL2	X	X	X	GRMZM2G438840	ZmPXL3	PXL1/PXL2									

Table notes

FEA3: A clade containing AT4G28560, Solyc09g072630, and Os06g42220 is closely related to FEA3. AT4G28560 is possibly misannotated as RIC7.

FEA3: Orthology supported by maximum likelihood topology, but with poor bootstrap support

RPK1/RPK2: Organization in table based on tree topology, but naming takes structure into account. RPK1-LIKE (RPK1L) have short ectodomains, while RPK2-like have long ectodomains.

NIK: Clade of NSP-INTERACTING KINASE (NIK) Immune co-receptors is nested within CIK genes. NIK proteins are implicated in immune signaling, but NIK genes can complement cik2 loss of function when expressed under the CIK2 promoter.

Concluding Remarks

Shoot Apical Meristems (SAMs) produce the entire shoot of every plant we see. Every SAM must accomplish the basic functions of self-maintenance and the production of lateral organs. Morphological diversity across plants heralds largely from the modulation of these two functions, with tremendous consequences for evolution and agriculture.

The SAM is a complex structure. After decades of research, scientists are still driven to understand how the SAM functions. As a field, we have discovered complex crosstalk between hormones and receptor kinase pathways. This network exists in a state of exquisite tension. Layers of control of hormone and signal sensitivity result in the establishment of molecular thresholds controlling gene expression, which in turn establish tightly bounded populations of cells with distinct developmental functions. Disrupt this tense network, and the boundaries between cells with different identities snap, causing disorganization of the SAM and potentially shoot termination or fasciation.

Apical meristems underwent a dramatic change during the evolution of upright plant shoots the earliest land plants. It was at this moment that the SAM gained the function of patterning lateral organs in a phyllotactic pattern. Previously, filamentous or thalloid bodies were derived from SAMs that had only to self-replicate, and even this task was made simpler by cell geometry. These early SAMs evolved in the haploid gametophytic phase of the plant lifecycle, in contrast to the diploid sporophytic SAMs prevalent in vascular plants. Thus, not evolving from a shared ancestral structure, the SAMs of bryophytes and of vascular plants are non-homologous.

Convergent structures can however, repeatedly arise by coopting the same underlying components. This phenomenon, called deep homology, is the foundation for much of my thesis work. Throughout this dissertation I asked, with the help of others, whether the single celled SAM of the moss *Physcomitrium patens* was regulated by the same mechanisms as multicellular flowering plants.

By and large, I found that the answer seems to be yes. Mutants of the *CLV1* and *RPK2* genes generate an overabundance of stem cells in both moss and flowering plants. The networks too appear to be similar: cytokinin promotes stem cell formation through a pathway inhibited by *CLV1* in both plant groups. Meanwhile, the formation of new SAMs through this pathway is inhibited by auxin. Thus, this complex network with crosstalk between CLV signaling, cytokinin, and auxin appears to be intact in moss.

There are also interesting differences. That the loss of cytokinin signaling somewhat phenocopies cytokinin treatment is a puzzling phenomenon that does not occur in Arabidopsis. Also notable is the apparent absence of a *WUSCHEL-RELATED HOMEOBOX* (*WOX*) gene from the stem cell signaling network in moss, whereas *WOX* genes are central to SAM function in flowering plants. It is not clear whether something else performs the function of *WOX* genes in moss, or whether the SAM signaling network can simply do without that function in a single-celled SAM.

Overall, there are more similarities between the regulation of stem cell function in moss and flowering plants than there are differences. It is possible that the sporophyte coopted developmental mechanisms from the gametophytic phase, such that shoot morphogenesis evolved in the gametophyte and was transferred to the sporophyte. Alternatively, these genetic components served another function in a thalloid ancestor of bryophytes and vascular plants, and shoots evolved concurrently in different phases of the life cycle using a common set of building blocks. These and many other interesting evolutionary and developmental questions spawn from this work.